Student Poster Book of Abstracts

2012 IEEE Power and Energy Society General Meeting

Sand Diego, California July 22-26 2012

Welcome Message from the Chair –

IEEE PES Student Activities Subcommittee

On behalf of the Student Activities Subcommittee, I welcome you to the Student Poster Contest at the 2012 IEEE Power & Energy Society General Meeting held at San Diego, CA, USA on July 24, 2012.

At the time of printing this book, we have 172 extended abstracts from students from different parts of the world confirmed to participate in the 2012 IEEE PES GM student poster contest. This book of extended abstracts is aimed at documenting the many outstanding research projects, some at their early stages, and providing a glimpse of some of the activities of interest to our society at various educational institutions around the world which is presented at this meeting in form of posters by students. The research topics of these posters fall into 15 categories, namely:

1. Advanced computational methods for power systems planning
2. Asset management
3. Cyber and physical security of the smart grid
4. Dynamic performance and control of power systems
5. Electric machines and drives
6. Flexible AC transmission systems
7. Integrating renewable energy into the grid
8. Intelligent monitoring and outage management
9. Market interactions in power systems
10. Power electronics
11. Power system modeling and simulation
12. Smart grid technology
13. Smart sensors
14. Substation and distribution automation
15. System-wide events and analysis methods

All students are invited to attend the Student/Faculty/Industry (SFI) luncheon to be held on July 25 from 1200 pm to 1 pm. A job fair that is co-located with the SFI luncheon follows this. The student poster contest winners will be announced at the SFI luncheon.

Support from the Grainger Foundation, and the IEEE Power & Energy Society, especially the Power and Energy Education Committee (PEEC), for the student activities is gratefully acknowledged.

The subcommittee acknowledges the services of Prof. Aaron St. Leger, Assistant Professor, in the Dept. of Electrical Engineering and Computer Science at the United States Military Academy, West Point, NY, and Prof. Chee-Woi Ten, Assistant Professor, in the Dept. of Electrical and Computer Engineering at Michigan Tech University, Haughton, MI, in the compilation of this book of extended abstracts.

Siddharth (Sid) Suryanarayanan
Fort Collins, Colorado, USA.

IEEE PES Student Activities Subcommittee

Chair
Dr. Siddharth Suryanarayanan
Assistant Professor, Electrical and Computer Engineering
Colorado State University
Fort Collins, CO 80523-1373, USA
sid.suryanarayanan@ieee.org

Vice-Chair
Dr. Anurag K Srivastava
Assistant Professor
School of Electrical Engineering and Computer Science
Washington State University
PO Box 642752
EME 102
Spokane St Pullman
Washington 99164-2752, USA
asrivast@eecs.wsu.edu

Secretary
Dr. Hamidreza (Hamid) Zareipour,
Associate Professor,
Department of Electrical and Computer Engineering,
Schulich School of Engineering, University of Calgary,
2500 University Drive NW, Calgary,
Alberta, T2N 1N4, Canada
h.zareipour@ucalgary.ca

Webmaster
Dr. Jignesh M. Solanki
Assistant Research Professor
Lane Department of Computer Science and Electrical Engineering
West Virginia University
395 Evansdale Drive,
Morgantown, WV 26506-6109, USA
jmsolanki@csee.wvu.edu

LIST OF PARTICIPANTS AND POSTER TITLES

Advanced Computational Methods for Power Systems Planning

Page #	Student Reg. No.	Title of Poster	Student Name
16	1031	Wade Area Voltage Monitoring and Optimization	Haoen Li
17	1037	Economic Dispatch Considering Integration of Wind Power Generation and Mixed-mode Electric Vehicles	Haojun Yu
18	1062	Assessment of TTC for Simultaneous Transactions in Decentralized MAPS	Ali Ahmadi Khatir
19	1067	Probabilistic Load Flow Computation Using First-order Second-moment Method	Can Wan
20	1124	Extremal Optimization for Unit Commitment Problem for Power Systems	Jin Ding
21	1126	A Graph Theory Approach For Detecting Loops In Wide-Area Transmission Networks	Manish Mohanpurkar
22	1132	Risk-oriented preventive control of transmission lines overload	Yunfeng Wen
23	1146	Optimal Incremental Placement of PMUs for Power System Observability	Fei Wang
24	1165	Application of MIQCP Based SVC Allocation Method to a Complex Real-World Grid	Robert Chang
25	1167	Daily Generation Scheduling for Reducing Unit Regulating Frequency Using Multi-Population Genetic Algorithm	Yiming Li
26	1214	Synchrophasor State Estimation and Parameter Estimation on the New York Power System	Scott G. Ghiocel
27	1247	Measurement-Based Non-Iterative Direct State Calculation for Power Networks	Xinyu Tony Jiang
28	1262	Quantify Spinning Reserve in Systems With Significant Wind Power Penetration	Guodong Liu
29	1271	Security-Constrained Unit Commitment with Wind Power Generation by Using Interval Linear Programming	Boran Zhou
30	1285	Robust and flexible power system expansion planning under two levels of multiple uncertainties	Diego Mejia-Giraldo
31	1286	A Simultaneous Perturbation Approach of the Lagrange Relaxation Method for Solving Hydro-thermal Coordination Problems	Yu Xia
32	1301	Application f Non-linear Programming for Large-Scale AC-DC Power Flow Analysis	Zhijun Qin
33	1350	Hierarchical two-level Voltage Controller for Large Power Systems (Central Coordinator Level Approach)	Javier Guerrero
34	1366	Transmission Planning under Uncertainties of Wind and Load: Sequential Approximation Approach	Heejung Park
35	1370	Novel methodology for determining the location for the Battery Storage in a Microgrid	Luis F. Montoya

Asset Management

Page #	Student Reg. No.	Title of Poster	Student Name
36	1066	Multivariate Analysis for Correlations among Different Transformer Oil Parameters to Determine Transformer Health Index	Atefeh Dehghani Ashkezari
37	1072	A Study on Suitability of Different Transformer Winding Models for Frequency Response Analysis	Mohd Fairouz Mohd Yousof
38	1203	Optimal Maintenance Strategy for Wind Turbines with Markov Decision Processes	Salman Kahrobaee
39	1248	Expanding the Global Reach of IEEE PES: What the organization has done and where it should go	Laurie Stewart

Cyber and Physical Security of the Smart Grid

Page #	Student Reg. No.	Title of Poster	Student Name
40	1136	Cyber-Physical Security in a Substation	Junho Hong
41	1258	A New Reliability Model of Direct Cyber-Power Interdependencies	Bamdad Falahati
42	1345	Defend-Attack-Defend in Power Grid: Global Optimality with transmission line switching	Wei Yuan
43	1363	Power Systems Operations Planning with Coordinated Cyber Attacks	Siddharth Sridhar
44	1365	A Secure and Privacy-Preserving Communication Scheme for AMI Network	Pan Deng
45	1371	Risk Assessment Based on Information Entropy of Cascading Failure in Power Systems	Youwei Jia

Dynamic Performance and Control of Power Systems

Page #	Student Reg. No.	Title of Poster	Student Name
46	1022	Hybrid Multi-terminal LCC HVDC with a VSC converter: A case study of Simplified South East Australian System	Mai H. Nguyen
47	1060	Design of Robust Power Oscillation Damping Controller for Large-scale PV Plant	Rakibuzzaman Shah
48	1081	Design Considerations in Development of Active Mobile Substations	Nima Yousefpoor
49	1170	ATP Modeling of Internal Transformer Faults for Relay Performance Testing	Elizaveta Egorova
50	1193	Calculation of Available Transfer Capability under Transient Stability Constraints for Tie-lines Considering N-1 Contingencies	Masashi Hitosugi
51	1196	Electromechanical Mode Estimation Using Instrumental Variable Method	Yong Jia
52	1206	Improvement of Available Transfer Capability	Masaya Takiguchi
53	1218	Phasor State Estimation from PMU Measurements with Bad Data	Dongliang Duan
54	1250	A Model Predictive based Emergency Control Scheme using TCSC to Improve Power System Transient Stability	Xiaochen Du
55	1251	Subsynchronous Oscillation Analysis in Conventional Power Plants and Wind Farms	Hamed Khalilinia
56	1254	Improving Power System Dynamic Stability via Operating Condition Adjustment Using PMU Data	Goodarz Ghanavati
57	1293	Modal Analysis of grid connected Photovoltaic	Yashodhan Agalgaonkar
58	1299	Multi-Agent based Controller for Multi-Terminal VSC HVDC Transmission System	Mohammad Nazari
59	1322	Electric Vehicle Smart Charging to Mitigate Distribution System Overloads	Pooya Rezaei
60	1341	A DFT-Based Frequency Estimator for Three-Phase Power Systems	Luoyang Fang
61	1372	A New Control Strategy for Electromechanical Disturbances In Power Networks	Meimanat Mahmoudi

Electric Machines and Drives

Page #	Student Reg. No.	Title of Poster	Student Name
62	1265	Non Linear Harmonic Domain Analysis of an Induction Machine in DQ Reference	Pablo Rodriguez

Flexible AC Transmission Systems

Page #	Student Reg. No.	Title of Poster	Student Name
63	1056	Appropriate Placement of Series Compensators to Improve Transient and Small Signal Stability	Amin Nasri
64	1212	System Identification based VSC-HVDC DC Voltage Controller Design	Ling Xu
65	1232	Novel approach for Transmission Line Loss Minimization Using Power Flow Controllers	Gopiram Maddela

Integrating Renewable Energy into the Grid

Page #	Student Reg. No.	Title of Poster	Student Name
66	1001	Sustainable Energy and Distributed Generation Scenario in the Brazilian Electricity Sector	Tiago R. Ricciardi
67	1011	Review of International Guides for the Interconnection of Distributed Generation into Low Voltage Distribution Networks	Ricardo Torquato
68	1033	Enhancement of Distribution Systems Stability by Proper Placement of Renewable Energy Sources (RES)	Naruttam Kumar Roy
69	1053	Revisiting Damping Performance of the Queensland Network under Wind Power Penetration	Nilesh Modi
70	1055	Inertial response capability of DFIG wind turbine	Stefanie Kuenzel
71	1073	Analysis and Mitigation of Transient Overvoltage with Integration of Small Scale Power-Electronic Interfaced DG	Tareq Aziz
72	1090	Probabilistic Power Flow for Transmission Systems with Photovoltaic Generation Considering Power Dispatching Operation	Miao Fan
73	1091	Transient Stability Assessment of the Systems with High Penetration of Photovoltaic Generation	Sara Eftekharnejad
74	1145	Cascading Tripping out of Numerous Wind Turbines in China: Fault Evolution Analysis and Simulation Study	Xi Ye
75	1149	Reliability Quantification and Visualization for Optimal Asset Dispatch in Electric Microgrids	Mayank Panwar
76	1150	Targeted Conversion of AC lines to DC lines for Improved Power System Dispatch	Omar A. Urquidez
77	1154	Optimal Incentive Design to Facilitate Solar PV Investments	Indrajit Das
78	1179	Evaluation of Islanding Detection Techniques for Inverter-Based Distributed Generation	Omar N. Faqhruldin
79	1184	An Enhanced Fault-Ride-Through Capability of Doubly-Fed Induction Generators during Grid Faults	Maher Abdelkhalek Azzouz
80	1190	Increasing Renewable Energy Utilization through Nonlinear Load Frequency Control Model	Toshiki Takayama
81	1222	PQ and PV control of photovoltaic generators in three-phase distribution system	Sarina Adhikari
82	1225	Solar Panel DC-DC Converter Configuration for Optimizing Output Power	Carl B. Westerby
83	1227	MW Resource Assessment Model for a Hybrid Energy	Subhadarshi

		Conversion System With Wind and Solar Resources	Sarkar
84	1231	Multi-objective Stochastic Distribution Feeder Reconfiguration in Systems with Wind Power Generators and Fuel Cells Using Point Estimate Method	Ahmad Reza Malekpour
85	1237	Probabilistic Optimal Sizing of Stand-Alone PV Systems with Modeling of Variable Solar Radiation and Load Demand	Simon K. K. Ng
86	1282	Battery Switch Station Modeling and its Economic Evaluation in Microgrid	Yiqun Miao
87	1287	Flatness-Based Automatic Generation Control with Wind Units	Maryam Hassani Variani
88	1289	Dynamic Models of Wind Turbines for Stability Studies	Felipe Wilches
89	1291	Power System Transient Stability Enhancement Using Direct Drive Wind Generators	Hasmina Tari Mokui
90	1292	Impact Study of Multiple Source Harmonic Interactions with Distributed Energy Resources	Reza Arghandeh
91	1302	Methodology for Monitoring Control and Operation of Power Systems with Wind Farms	Evangelos Farantatos
92	1304	Solar Irradiance Estimations for Solar Panels of Varying Tilt and Azimuth Angles Using Global and Diffuse Horizontal Radiation Measurements	Yazmin Najera
93	1313	Novel Control Strategies for DFIG Wind Turbines During Grid Disturbances that Comply With Strictly Grid Codes	Santos Kihwele
94	1325	Optimal Penetration of Three Types of Wind Turbine Generators	Baohua Dong
95	1335	Modeling of Tidal Energy Conversion Systems for Primary Response Testing	Maren Kuschke
96	1340	Quantifying Variability in Power Systems: Comparison of Four Metrics	M. Lwin
97	1361	Hardware and Software Testing Platform for Battery Management Systems in the Presence of Renewables	Jesse Hill
98	1373	Protection Coordination Between HVDC Offshore Wind System and AC Grid	Lina He
99	1374	Transient Stability Assessment with Large Scale Wind penetration	Prem Kumar Naik

Intelligent Monitoring and Outage Management

Page #	Student Reg. No.	Title of Poster	Student Name
100	1082	Distributed Online Monitoring of Quasi-Static Voltage Collapse in Multi-area Power Systems	Yang Chen
101	1085	External Data Exchange Issues for State Estimation in Power Systems	Kai Yin Kenny Poon
102	1088	Measurement-based Coherency Identification Technique via Independent Component Analysis	Mohd Aifaa Mohd Ariff
103	1111	Reliability Modeling of Dynamic Thermal Rating	Hamid Shakerardakani
104	1129	An Online Intelligent Alarm-Processing System Based on Abductive Reasoning Network	Jianan Mu
105	1280	The effect of parameter and measurement uncertainties on hybrid state estimation	Markos Asprou
106	1323	Power Quality Monitoring for Microgrids	Patricio Mendoza-Araya
107	1333	Statistical and predictive modeling of automated meter reading system outages	Prasad Shinde
108	1344	Event Analysis Engine for Oscillation Monitoring using Synchrophasors	Zaid Tashman

Market Interactions in Power Systems

Page #	Student Reg. No.	Title of Poster	Student Name
109	1029	Coupon Incentive-based Demand Response in Smart Grid	Haiwang Zhong
110	1054	Emission Pricing and Locational Signal Impact on Generation Portfolio in Large Scale Queensland Network	Kazi Nazmul Hasan
111	1127	A Balance Between Stochastic and Deterministic Unit Commitment Formulations	Garret LaBove
112	1200	Day-Ahead electricity price forecasting using a hybrid non-linear model	Christian Geidel
113	1257	Multiobjective Based Energy and Ancillary Service Markets Clearing	Amin Kargarian
114	1283	Optimal Investment Decisions in a Smart Grid	Chin Yen Tee
115	1303	Maintenance Management of Wind Turbines	Pramod Bangalore
116	1317	A Review of ERCOTês Nodal Market	Sruti Nuthalapati
117	1319	Scheduling of Plug-in Electric Vehicle Charging and Effects on Day-ahead Market Price	Pavan Balram
118	1332	Distribution-class Locational Marginal Pricing Index	Oluwaseyi Akinbode
119	1348	Zonal Supply Curve Estimation in Transmission-Constrained Electricity Markets	Mostafa Sahraei-Ardakani
120	9280	Using Demand Response to Reduce Price Variations	Ailin Asadinejad

Power Electronics

Page #	Student Reg. No.	Title of Poster	Student Name
121	1097	A Novel Power Management Control Strategy for a Renewable Stand-Alone Power System	Abu Mohammad Osman Haruni
122	1339	Controllers Parameter Variation Effects on a Multi-Converter based Microgrid	Juan C. Jimenez
123	1355	Application of Stochastic Differential Equations to Feasibility Studies of Converter Systems in the Presence of Communication Network Delay	Sachi Jayasuriya
124	1356	Predictive Control of a Modular Multilevel Converter for a Back-to-Back HVDC System	Jiangchao Qin

Power System Modeling and Simulation

Page #	Student Reg. No.	Title of Poster	Student Name
125	1107	Real-Time Parameter Identification of DFIG Using Online Measurement	Shaotong Guo
126	1108	Stochastic Optimization of a Microgrid with Solar Power Generation	Robin Broder Hytowitz
127	1112	Interval Arithmetic for Short-Circuit Computation in MV Radial Networks with Distributed Generation	Wendy Carolina Briceno Vicente
128	1113	Online Risk-based Security-Constrained OPF in Power System and Market Operation	Qin Wang
129	1131	Sensitivity Analysis of Load-Damping Characteristic in Power System Frequency Control	Hao Huang
130	1151	Short Circuit Modeling of Wind Turbine Generators	Sriram Chandrasekar
131	1152	Transient Stability Studies on Large Power System	Parikshit Sharma
132	1159	Reserve Zone Determination and Analysis	Fengyu Wang
133	1164	Multi-level state estimation utilizing synchronized phasor measurements	Lin Zhang
134	1168	Modeling and Stability Analysis of Distributed Generation	Ehsan Nasr Azadani
135	1183	Experience of Implementing Controller-in-the-Loop with Over-current Relay Example by Using cRIO PXI and RTDS	Hung-Ming Chou
136	1236	Long-term effect of relay protection operation on cascading failures in growing scale-free small-world power grid	Yudong Zhang
137	1242	A Novel Method for Solving the Divergence of Power Flow and Controlling Voltage in Integrated Distributed Generators Network	Hung Nguyen Dinh
138	1253	Automated Topology Processing for Conventional Phasor-Assisted and Phasor-Only State Estimators	Mostafa Farrokhabadi
139	1263	A Statistical Study on Impact of PHEVs Charging on Power grid	Zahra Darabi
140	1266	Effect of Shield Thickness on Braided-Shield Cables Crosstalk	Miguel Penagos
141	1267	A Dynamic Equivalent Model for Wind Power Plants with Type-4 Units	Dalia N. Hussein
142	1270	Towards Sustainable Intra-Dispatch Real Power Balancing	Nipun Popli
143	1316	Identification of Power System Inter-area Oscillation by Analytic Wavelet Transforms	Daham Min
144	1328	Comprehensive Evaluation of Power Reversal Action of	Hee Jin Kim

		LCC- and VSC-HVDC Transmission	
145	1343	Multistage Stochastic Optimal Operation of Energy-Efficiency Building with CHP Systems	Ping Liu
146	1349	Stochastic Economic Dispatching for Wind Penetrated Power System	Amir Shahirinia
147	1364	Capturing Electro-Thermal Dynamics in Power System Models with Building Loads	Mohammed Muthalib
148	1369	Quantifying Economic Operational and Environmental Impacts of Adoption of Plug-in Hybrid Electric Vehicle on California Electricity Grid	Jingjie Xiao
149	1375	Modeling an Islanded Microgrid Addressing Power Quality Assessment	Qiang Fu
150	1371	Network Capacity Assessment of Distributed Generation Based on Urban Infrastructures	Xianjun Zhang
151	1189	An Affine Arithmetic Method to Solve the Stochastic Power Flow Problem Based on a Mixed Complementarity Formulation	Mehrdad Pirnia

Smart Grid Technology

Page #	Student Reg. No.	Title of Poster	Student Name
152	1036	Assigning Weights for PMU Measurements: Two Alternative Methods	Liuxi Zhang
153	1043	Development of an Agent-Based Distribution Test Feeder with Smart-Grid Functionality	Pedram Jahangiri
154	1061	Modeling and Planning of EV Fast Charging Station in Power Grid	Champa Hemamali Dharmakeerthi
155	1068	Topology Comparison of 3-Phase Solid State Transformers based on Efficiency and Control	Sachin Madhusoodhanan
156	1092	Effects of Price-Responsive Residential Demand on Retail and Wholesale Power Market Operations	Auswin Thomas
157	1191	Different Classes of Oscillation Monitoring systems: Advantages and Disadvantages	S. Arash Nezam Sarmadi
158	1192	Real-Time Intelligent Operation of Hybrid AC/DC Smart Grids	Ahmed Mohamed
159	1215	Voltage Unbalance Analysis of Distribution Systems Using a Three-Phase Power Flow and a Genetic Algorithm for PEV Fleets Scheduling	Alejandra Jimenez-Vega
160	1216	Developing Smart Grid Demonstrations and Experiments	Abderrahmane Elandaloussi
161	1249	Air Conditioner Optimal Scheduling Using Best Response Techniques	Jie Dang
162	1261	DC Fault Interruption Using Reactor-Assisted AC Circuit Breaker	Saurabh Kulkarni
163	1288	Integrating Distribution System Operational Constraints into Demand Side Management	Benyamin Moradzadeh
164	1318	Exploiting the Flexibility of Controllable Residential Loads for Energy and Peak Demand Savings	Kyungsung An
165	1321	A Stochastic Dynamic Programming Method for Optimizing Vehicle-to-Grid Frequency Regulation	Jonathan Donadee
166	1326	A Novel Wireless Power Supply and Charging for Appliances in Smart Houses	Jinchi Han
167	1353	Residential Energy Management using multi-resolution Moving Window Algorithm	Marc Beaudin
168	1357	Synchrophasor Data Quality	Karl Reinhard
169	1360	Comparison of Interval-Specific Building Load Forecasting Models for Demand Resource Planning	Jonathan Berardino
170	1376	Measurement-based Load Modeling at Distribution Level with Complete Model Structure	Jia Hou

171	1377	Zinc-Bromine Flow Batteries in Residential Electricity Supply: Two Case Studies	Mio Nakatsuji-Mather
172	1378	Modeling and Impacts of Smart Charging PEVs in Residential Distribution Systems	Isha Sharma
173	1379	Control and Operation of Multiple Microsources in a Microgrid	M. Rasheduzzaman

Smart Sensors

Page #	Student Reg. No.	Title of Poster	Student Name
174	1024	Detection, Identification, and Correction of Bad Sensor Measurements for Fault Location	Mert Korkali
175	1084	Monitoring the Energy Consumptions of Home Appliances using Smart Meter Data	Ming Dong
178	1103	Effect of Network Packet-Dropout on the Control Performance of Power Systems	Abhinav Kumar Singh
179	1296	Vulnerabilities in Coupled Control and Communication Systems with Power Grids and Their Effects on Cascading Failures	Mahshid Rahnamay-Naeini
180	1330	A Partitioning Method for Distributed Capacitor Control of Electric Power Distribution Systems	Michael Kleinberg
181	1380	A Reliability Analysis for the Smart Grid Distribution Communications	Babak Karimi

Substation and Distribution Automation

Page #	Student Reg. No.	Title of Poster	Student Name
183	1354	Hierarchical two-level Voltage controller for Large Power Systems(Local Substation Level)	Hong Chun

System-Wide Events and Analysis Methods

Page #	Student Reg. No.	Title of Poster	Student Name
184	1014	Improved Harmonic Estimation of Time-Varying Signals using RBFNN and ESPRIT	Sachin K. Jain
185	1172	Look-ahead Dispatch with Forecast Uncertainty and Infeasibility Management	Yingzhong Gu
186	1208	Robust Corrective Transmission Switching Schemes for System Reliability	Akshay S. Korad
187	1223	Uncoordinated Charging Impacts of Electric Vehicles on Electric Distribution Grids: Normal and Fast Charging Comparison	Elham Akhavan-Rezai
188	1346	Screening Algorithm for Event Detection in PMU Data	Alicia Allen
189	1381	A Gaussian Mixture Model Based Prediction for Weather-Related Outages by EM Algorithm	Padmavathy Kankanala
190	1382	Stochastic Determination of PHEV Load Profiles with Recommendations for Charging Strategies	Maigha Fnu

Wade Area Voltage Monitoring and Optimization

Haoen Li and Anjan Bose
Department of Electrical Engineering and Computer Science, Washington State University, Pullman, WA 99163, USA,
Email: *lihaoen@gmail.com* and *bose@wsu.edu*

Abstract—**As the power demand becomes higher all over the world, transmission lines are often carrying electric power near their limits, which will course power system being operated under serious stress. Where voltage collapse is one of the most critical problems that impacts power system operational security. Many of the recent major blackouts are all coursed by voltage collapse. Therefore, a fast and accurate voltage stability monitor approach is necessarily needed for the modern system. The development and applications of wide area measurement system (WAMS) established the foundation of on-line assessment of voltage stability in large scale power system. A voltage stability Index based on Phasor Measurement Units (PMU) is introduced here and the comparison with the Q margin shows good result.**

I. KEY EQUATIONS

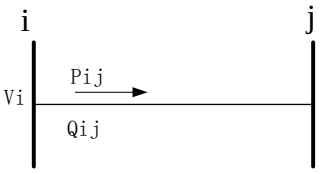

$$P_{ij} = V_i^2(G_{ij} + G_{i0}) - V_iV_j(G_{ij}\cos\delta_{ij} + B_{ij}\sin\delta_{ij})$$

$$Q_{ij} = -V_i^2(B_{ij} + B_{i0}) - V_iV_j(G_{ij}\sin\delta_{ij} - B_{ij}\cos\delta_{ij})$$

$$\Delta P_{ij} = \Delta P_{ij}(\Delta\delta_i, \Delta\delta_j) = \frac{\partial P_{ij}}{\partial \delta_i}\Delta\delta_i + \frac{\partial P_{ij}}{\partial \delta_j}\Delta\delta_j + O(\delta_i, \delta_j)$$

$$\Delta Q_{ij} = \Delta Q_{ij}(\Delta V_i, \Delta V_j) = \frac{\partial Q_{ij}}{\partial V_i}\Delta V_i + \frac{\partial Q_{ij}}{\partial V_j}\Delta V_j + O(V_i, V_j)$$

$$\begin{bmatrix}\Delta P \\ \Delta Q\end{bmatrix} = \begin{bmatrix}J_{P\delta} & J_{PV} \\ J_{Q\delta} & J_{QV}\end{bmatrix}\begin{bmatrix}\Delta\delta \\ \Delta V\end{bmatrix}$$

If $\Delta P = 0$

$$\Delta Q = [J_{QV} - J_{Q\delta}J_{P\delta}^{-1}J_{PV}]\Delta V = J_R\Delta V$$

$$\frac{\Delta Q_i}{\Delta V_i} = \frac{\det(J_R)}{[\text{adj}(J_R)]_{ii}} = \Gamma_{QVi}$$

If $\Delta Q = 0$

$$\Delta P = [J_{P\delta} - J_{PV}J_{QV}^{-1}J_{Q\delta}]\Delta\delta = J_R\Delta\delta$$

$$\frac{\Delta P_i}{\Delta \delta_i} = \frac{\det(J_R)}{[\text{adj}(J_R)]_{ii}} = \Gamma_{P\delta i}$$

II. KEY RESULT

IEEE 14-bus system

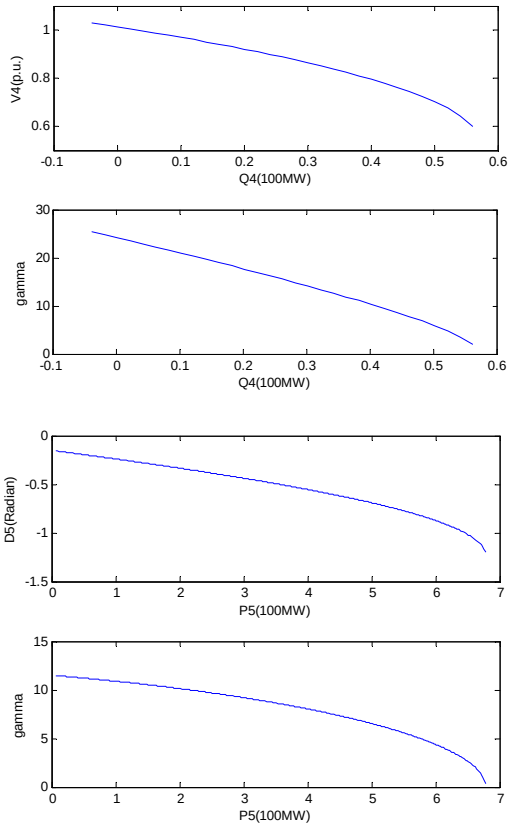

IEEE 118-bus system (bottom 20 Γ_{QV} buses)

	Γ_{QV}	$\Gamma_{P\delta}$		Γ_{QV}	$\Gamma_{P\delta}$
bus 117	6.231121	3.065712	bus 115	13.52197	4.739412
bus 21	7.417637	4.047214	bus 114	13.87229	4.78423
bus 43	7.916137	4.744205	bus 52	13.97283	5.516753
bus 22	8.624364	4.247125	bus 98	15.39899	8.247718
bus 20	8.930231	4.408601	bus 16	15.60155	4.793931
bus 86	12.44016	3.351821	bus 50	15.75845	8.287604
bus 44	12.75531	4.958411	bus 67	16.06825	9.343576
bus 101	13.42263	5.542053	bus 13	16.13228	4.554155
bus 57	13.43175	6.613067	bus 2	16.60265	4.458887
bus 28	13.43547	4.32947	bus 45	17.91815	6.395136

Economic Dispatch Considering Integration of Wind Power Generation and Mixed-mode Electric Vehicles

H.J. Yu, W. Gu, *Member, IEEE*, N. Zhang and D. Q. Lin

School of Electric Engineering, Southeast University, Nanjing 210096, China

***Abstract*— The anticipation of high penetration of electric vehicles (EV) and renewable energy sources into future power grid brings up many technological problems that need to be addressed. This paper deals with the economic dispatch problem (EDP) for distribution systems with wind power and mixed-mode EVs. The developed stochastic models of different interactive modes between EVs and power systems are incorporated into EDP studies. A continuous action learning automata (CALA) was applied and verified in a modified IEEE 30 bus system which includes two wind farms, two battery exchange stations for EVs and distributed EVs penetration. The simulation results indicated the interaction between mixed-mode EVs and power systems can significantly reduce the gap between demand and power generation in different periods of time with optimal dispatch schedule.**

***Index Terms*—EV, stochastic modeling and optimization, economic dispatch, wind power, learning automata**

I. KEY EQUATIONS

EDP with integration of wind power generation and mixed-mode EV is formulated as a constrained minimization problem as shown as (1):

$$
\begin{aligned}
&C_{total} = T\sum_{t=start}^{end}(f_1(t)+f_2(t)+f_3(t))\\
&f_1(t)=\sum_{j\in n}(\alpha^j P_n^{j2}(t)+\beta^j P_n^j(t)+\gamma^j)\\
&f_2(t)=\sum_{i\in w}C_w P_w^i(t)+\sum_{m\in exev}C_{exev}P_{exev}^m(t)\\
&f_3(t)=\sum_{m\in exev}C_{un}E_{un}^m(t)+C_{pv}(P_{peak}-P_{valley})\\
&s.t.\sum_{i\in w}P_w^i(t)+\sum_{j\in n}P_n^j(t)+\sum_{k\in sev}P_{sev}^k(t)+\sum_{m\in exev}P_{exev}^m(t)+P_{loss}(t)=\sum_{r\in l}P_l^r(t)\\
&P_{\min}^j \le P_n^j(t)\le P_{\max}^j\\
&P_{e\min}\le P_{exev}(t)\le P_{e\max}\\
&\left|P^i(t)-P^j(t)\right|<P_{\max}^{ij}\\
&U_{\min}^i<U^i(t)<U_{\max}^i\\
&E(t)\le E_{\max}\\
&E(end)\ge 0.9E_{\max}\\
&E(start)\ge 0.9E_{\max}
\end{aligned}
\qquad (1)
$$

II. KEY FIGURES

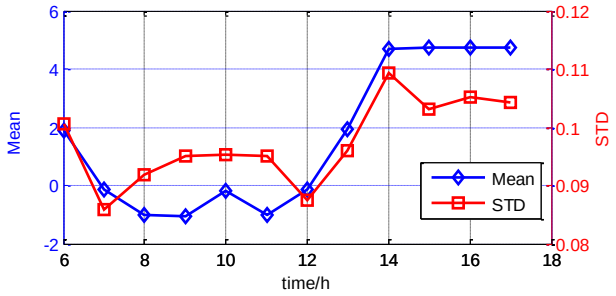

Figure 1 Power demand/supply of NI EVs of bus 7

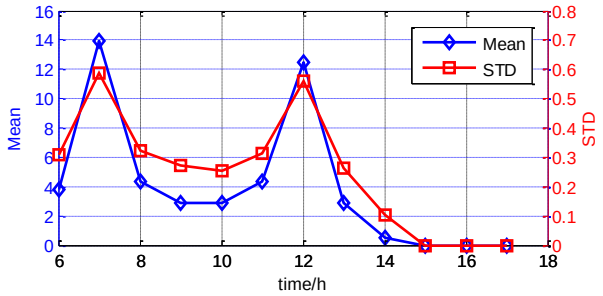

Figure 2 BE demand of bus 2

III. KEY RESULTS

Table 1 Results of case 1, Std is Standard deviation, diff is difference.

Cost(￥)	Mean peak (MW)	Std peak	Mean valley (MW)	Std valley	Diff (MW)
2.3674e5	156.21	5.46	75.46	4.31	80.75

Table 2 Results of case 2

Cost(￥)	Mean peak (MW)	Std peak	Mean valley (MW)	Std valley	Diff (MW)
4.9596e5	147.77	5.53	93.88	4.19	53.89

Table 3 Results of case 3

Cost(￥)	Mean peak (MW)	Std peak	Mean valley (MW)	Std valley	Diff (MW)
3.08e05	156.99	5.33	84.07	4.43	72.93

Table 4 Results of case 4

Cost(￥)	Mean peak (MW)	Std peak	Mean valley (MW)	Std valley	Diff (MW)
5.964e6	147.87	5.40	103.49	3.87	44.38

Assessment of TTC for Simultaneous Transactions in Decentralized MAPS

A. Ahmadi Khatir, V. Etard and R. Cherkaoui
Power Systems Laboratory, EPFL, Lausanne, Switzerland, Email: ali.khatir@epfl.ch

***Abstract*—With the liberalization of the electricity market, the cross-border transactions have become more common but set up new problems due to the non-existence of a super TSO which would have a whole knowledge of such electrical system. In reality, the cross-border transactions can be performed at the same time and this reality has brought into focus the practical limitations of interconnections and the associated problem of simultaneous or multiple Total Transfer Capability (TTC). This paper proposes a new efficient model to take into account the simultaneous transactions over large Multi-area Power System (MAPS), which are operated by different TSOs in a decentralized manner. The proposed model relies on a decomposition algorithm to compute PTDFs for each area over the whole network by running a decentralized load flow problem. The solution of different areas is coordinated through the information exchanged among TSOs to converge to the global solution. Afterward, each TSO uses the right PTDFs corresponding to its own area and computes the multiple TTC's by solving an integrated LP problem. These values are then used to assess the ultimate multiple TTC's using an appropriate cooperation among adjacent areas. The numerical results for a four area test system demonstrate the performance of the proposed model.**

I. Key Equations

The decentralized DC load flow equation is formulated as

$$\min \sum_{a\in\mathbb{A}} \sum_{\substack{i\in\mathbb{B}^a \\ b\in\mathbb{F}^a}} \left\{ \frac{1}{2}\gamma_\theta \left(\theta_i^a - \theta_i^b\right)^2 + \frac{1}{2}\gamma_T \left(T_i^a + T_i^b\right)^2 \right\} \quad (1)$$

$$\mathbf{B}^a\theta^a = \mathbf{P^a} - \mathbf{D^a} - \mathbf{T^a}, \quad \forall \mathbf{a} \in \mathbb{A} \quad (2)$$

$$\theta_i^a = \theta_i^b, \quad T_i^a = -T_i^b, \forall a \in \mathbb{A} \;\; and \;\; \forall b \in \mathbb{F}^a \quad (3)$$

The multiple TTC's computation for a given area:

$$\max \sum_{t\in\mathbb{T}} TTC_t^a \quad (4)$$

$$pf_l = \sum_{t\in\mathbb{T}} ptf_l^{a,t} * TTC_t^a, \texttt{for all lines } l \in \mathbb{L}^a \quad (5)$$

$$|pf_l| \leq pf_l^{max}, \texttt{for all lines } l \in \mathbb{L}^a \quad (6)$$

II. Key Figurers

Convex hull computation of multiple TTC's for a given area is illustrated in Fig.1.

III. Key Results

According to Fig.2, the ultimate value of multiple TTC's is 98 MW for the first transaction t_1 and 34 MW for the second transaction t_2 (see the vertex of converged convex hull).

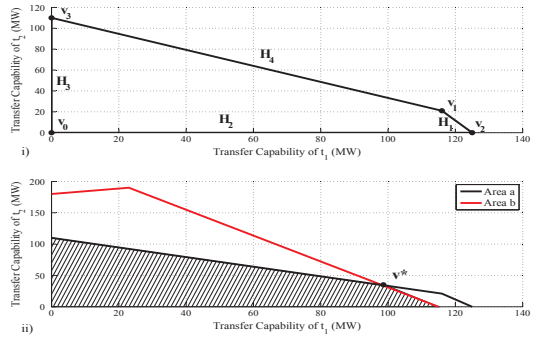

Figure 1. i) convex hull of multiple TTC's of area a; ii) intersection of convex hulls of area a and area b.

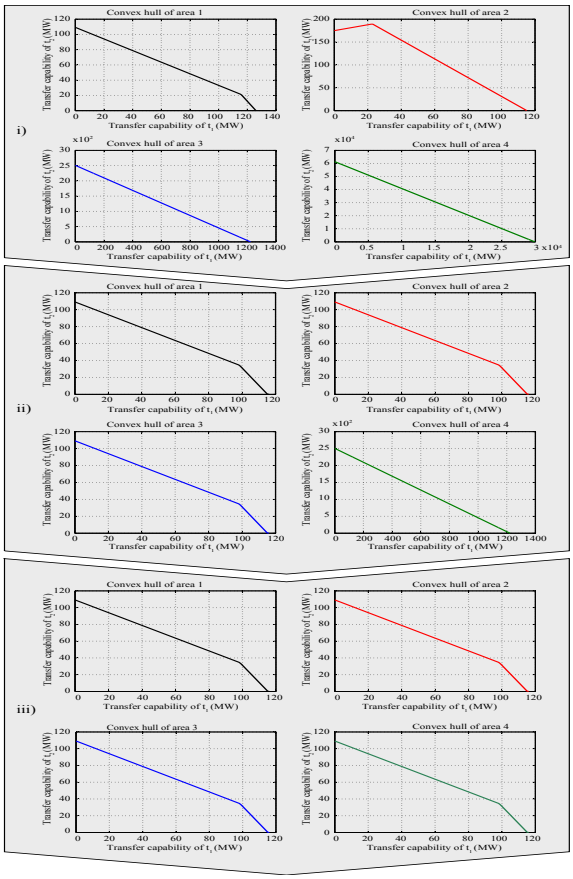

Figure 2. Final cooperation procedure. i) convex hulls of multiple TTC's of all areas; ii) Intersection of convex hulls of areas- first iteration; iii) Intersection of convex hulls of areas- second iteration.

Probabilistic Load Flow Computation Using First-order Second-moment Method

Can Wan[1], *Student Member*, *IEEE*, Zhao Xu[1], *Member*, *IEEE*, Zhao Yang Dong[2], *Senior Member*, *IEEE*, and Kit Po Wong[3], *Fellow*, *IEEE*

[1] Department of Electrical Engineering, The Hong Kong Polytechnic University, Kowloon, Hong Kong
[2] Centre for Intelligent Electricity Networks, The University of Newcastle, Newcastle, NSW 2308, Australia
[3] School of Electrical, Electronic and Computer Engineering, The University of Western Australia, Perth, WA 6009, Australia
Email: can.wan@polyu.edu.hk, eezhaoxu@polyu.edu.hk, joe.dong@newcastle.edu.au, kitpo@ieee.org

***Abstract*—This paper proposes a new probabilistic load flow method based on the first-order second-moment method. The proposed method aims to obtain the mean and standard deviation of load flow solution distributions considering various uncertainties in system operation. Power injection uncertainties including fluctuation of loads and unit outages are considered in the probabilistic load flow calculation. The performance of the proposed method is examined by comparing the results with those from Monte Carlo simulation using IEEE 9-bus and 118-bus test systems. A normalized accuracy and efficiency based procedure is developed for result analyses. Numerical tests demonstrate that the proposed method can obtain accurate results while reducing the computation time significantly.**

I. Key Equations

Linearized load flow equation:

$$\mathbf{X} = \mathbf{X}_0 + \mathbf{J}_0^{-1}\Delta\mathbf{S} \tag{1}$$

$$\mathbf{Z} = \mathbf{Z}_0 + \mathbf{H}_0\Delta\mathbf{X} \tag{2}$$

First-order second-moment method:

$$Y = f(x_1, x_2, \ldots, x_n) \tag{3}$$

$$Y \approx f(\mu_{x_1}, \mu_{x_2}, \ldots, \mu_{x_n}) + \sum_{i=1}^{n}(x_i - \mu_{x_i})\left.\frac{\partial f}{\partial x_i}\right|_{\boldsymbol{\mu}_\mathbf{X}} \tag{4}$$

$$E(Y) = f(\mu_{x_1}, \mu_{x_2}, \ldots, \mu_{x_n}) \tag{5}$$

$$\mathrm{var}(Y) = E\left[\left(\sum_{i=1}^{n}(x_i - \mu_{x_i})\left.\frac{\partial f}{\partial x_i}\right|_{\boldsymbol{\mu}_\mathbf{X}}\right)^2\right] = \sum_{i=1}^{n}\left(\left.\frac{\partial f}{\partial x_i}\right|_{\boldsymbol{\mu}_\mathbf{X}}\right)^2 \mathrm{var}(x_i)$$
$$+ 2\sum_{i=1}^{n}\sum_{j\neq i}^{n}\left(\left.\frac{\partial f}{\partial x_i}\right|_{\boldsymbol{\mu}_\mathbf{X}}\right)\left(\left.\frac{\partial f}{\partial x_j}\right|_{\boldsymbol{\mu}_\mathbf{X}}\right)\mathrm{cov}(x_i, x_j) \tag{6}$$

II. Key Results

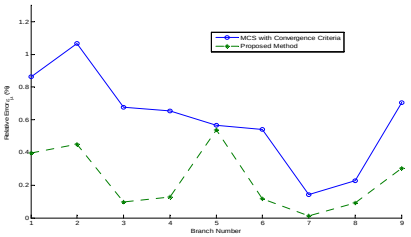

Fig. 1. Relative error of active power mean for 9-bus system.

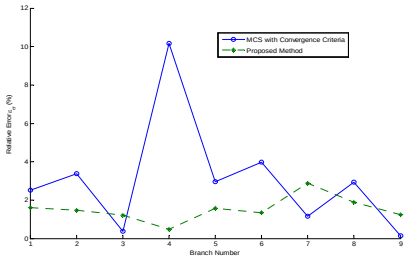

Fig. 2. Relative error of active power standard deviation for 9-bus system.

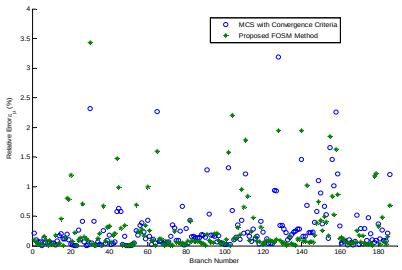

Fig. 3. Relative error of active power mean for 118-bus system.

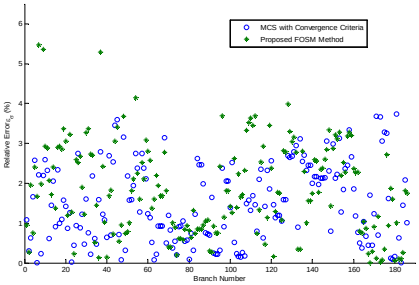

Fig. 4. Relative error of active power standard deviation for 118-bus system.

Extremal Optimization for Unit Commitment Problem for Power Systems

Jin Ding, Yong-Zai Lu, *Fellow, IEEE*, Jian Chu

State Key Laboratory of Industrial Control Technology, Institute of Cyber-System and Control, Zhejiang University, Hangzhou, 310027, China.

E-Mail: jding@zju.edu.cn, y.lu@ieee.org and chj@csc.zju.edu.cn

***Abstract*--This paper introduces extremal optimization (EO) method to solve unit commitment problem for power systems. EO is a local-search heuristic algorithm and originally developed from the fundamentals of statistical physics. In the implementation of EO for unit commitment (UC) problem, a novel problem-specific mutation operator is introduced and rule-based heuristic constraint-repairing techniques are devised. Simulation results on power systems which are composed of up to 100-units over a scheduling horizon of 24-hours demonstrate competitive performance with EO method compared with other existing methods for UC problem.**

I. Problem Formulation

- *Objective Function:*

$$\min \sum_{t=1}^{T}\sum_{j=1}^{N}[u_{j,t} f_j(p_{j,t}) + u_{j,t}(1-u_{j,t-1})SU_{j,t} + (1-u_{j,t})u_{j,t-1}SD_{j,t}] \quad (1)$$

- *System and Unit Constraints:*

Load Balance Constraint:

$$\sum_{j=1}^{N} p_{j,t}u_{j,t} = PD_t \quad (2)$$

Generation Limit Constraint:

$$u_{j,t}p_j^{\min} \le p_{j,t} \le p_j^{\max}u_{j,t} \quad (3)$$

Spinning Reserve Constraint:

$$\sum_{j=1}^{N} u_{j,t}p_j^{\max} \ge PD_t + SR_t \quad (4)$$

Generation Ramping Constraint:

$$RD_j \le p_{j,t+1} - p_{j,t} \le RU_j \quad (5)$$

Minimum Up/down Time Constraint:

$$u_{j,t} = \begin{cases} 1, & if\ 1 \le T_{j,t}^{on} < MUT_j \\ 0, & if\ 1 \le T_{j,t}^{off} < MDT_j \\ 0\ or\ 1, & otherwise \end{cases} \quad (6)$$

II. EO For UC Problem

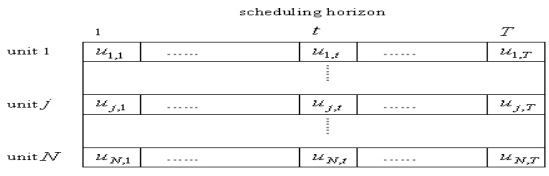

Fig. 1. Structure of chromosome of EO for UC problem

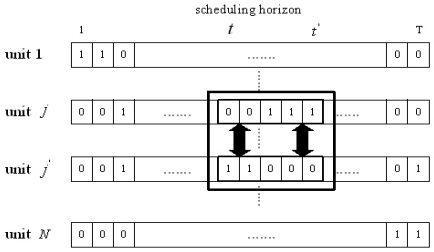

Fig. 2. mutation operator of EO

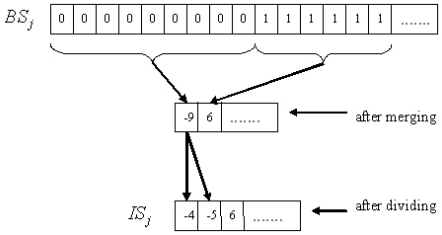

Fig. 3. process of obtaining interval string of unit j

- repairing minimum up/down violation
- repairing spinning reserve violation
- de-commit units for excessive spinning reserve

III. Numeric Tests

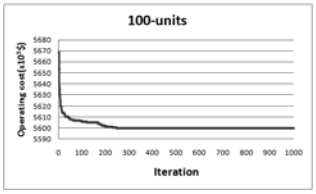

Fig. 4. Convergence characteristics of EO on 100-units test case.

TABLE I
COMPARISON OF SIMULATION RESULTS OF METHODS

Method	Best Cost($)	Average Cost($)	Worst Cost($)	Difference (%)
GA[13]	5,627,437	-	5,637,914	0.19
EP[15]	5,623,885	5,633,800	5,639,148	0.27
SA[20]	5,617,876	5,624,301	5,628,506	0.19
QEA-UC[18]	5,609,550	5,611,797	5,613,220	0.07
QBPSO[21]	5,602,486	5,604,275	5,606,178	0.07
EO	**5,599,969**	5,600,959	5,602,118	0.04

A GRAPH THEORY APPROACH FOR DETECTING LOOPS IN WIDE-AREA TRANSMISSION NETWORKS

Manish Mohanpurkar, *Student Member IEEE*,
Advanced Power Engineering Laboratory, Department of Electrical and Computer Engineering,
Colorado State University, Fort Collins, CO 80523, USA,
Email: *manishm@rams.colostate.edu*

***Abstract*—Transmission lines act as corridors for power transportation from bulk generation to the distribution systems. A mesh type graph is formed by the transmission lines rated at different voltage and power levels. In graph theory terms, a power system network is an equivalent of a multi-planar graph with Hamiltonian cycles. A cycle in graph theory terms is similar to a loop in power system networks; however, a loop in graph theory implies an isolated cycle with the same start and end nodes and any other nodes within the loop isolated from rest of the network. For practical power system networks, visual aid fails to recognize the loops accurately. Objective of the study is to develop a framework to detect loops in a given network.**

The loop detection algorithm is mainly based on a widely-used technique called A* heuristic search algorithm and minimum distance (or Djikstra's algorithm). Each transmission line is assumed to be a bidirectional edge, and the weight associated with each node is calculated using the number of edges connected to it. Each unidirectional edge has a weight of 0.5, hence at the beginning of the search all the weights will be integers. Weights serve as a measure of local connectivity of the respective nodes. The network information in the form of the admittance matrix (Y_{bus}) is a prerequisite. A suitable connectivity matrix is created using the Y_{bus} matrix. Degree of nodes and adjacency information can be easily extracted using the Y_{bus} of the network under analysis.

Preprocessing the network information is done in order to remove redundant information. For example, since a generation node (i.e. a node with degree equal to 1) cannot be a part of a power system loop, and can be ignored. Similarly, a node with a degree of 2 has to be either eliminated or collapsed only after analyzing its neighbor nodes. The preprocessing step greatly reduces the network and helps make the problem simpler. Storage of pertinent information is crucial as it may be needed in later stages. Network information has to be updated each time a network change is initiated.

With a reduced network, the actual loop investigation begins. A suitable starting point is chosen after a successive summation of weights of vertices for a fixed fraction of the total number of nodes in the network. A local minimally connected node is chosen to begin the process. Preference of forming a loop with minimum number of branches possible is chosen. A suitable network reduction routine is executed only after a decision over the quality of loop information is made. Quality implies that there is no repetition of loops or a loop detected in two different sequences and so on. Network information is revised to reflect the detection and the process continues. Target of setting up this framework is to detect loops irrespective of network size. Accordingly, very specific stopping criteria govern the convergence of the algorithm. Stopping criteria are primarily based on the weights of vertices remaining in the network. Numerous applications can be developed from this approach; one such application is estimation of loop flows in an interconnected bulk power system. Current status: testing of the coded algorithm on IEEE test systems. Primary concerns are memory management and computation efficiency especially for networks with large dimensioned Y_{bus}.

I. KEY FIGURE

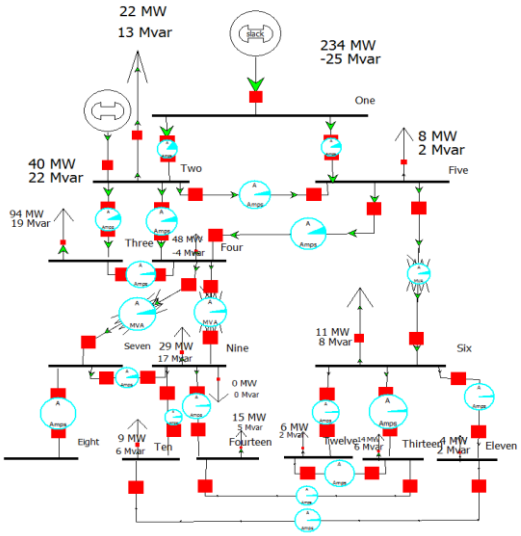

Figure 1: IEEE 14 Bus Test System to detect loops using proposed framework

II. RESULTS

Loops detected for the above test system:
[2 5 4 2], [13 6 11 10 9 14 13], [7 4 9 7], [5 4 7 9 10 11 6 5], [5 6 13 14 9 4 2 5], [2 1 5 2], [2 3 4 2], [6 12 13 6]

III. REFERENCES

[1] R. Diestel, *Graph Theory*, 2nd ed,. Springer-Verlag: New York, Inc. 2000, pp. 1-25.
[2] A. Tucker, *Applied Combinatorics*, 4th ed., Wiley and Sons, 2002, pp. 129-165.

Acknowledgement – "This work was funded by WECC as a subcontract from the United States Department of Energy under contract DOE-FOA0000068 for the project titled 'Regional Transmission Expansion Project (RTEP)"

Risk-oriented Preventive Control of Transmission Lines Overload

Yunfeng Wen[1], Yue Wang[1], Chuangxin Guo[1], Qinghua Wu[2]
1. Department of Electric Engineering, Zhejiang University, Hangzhou 310027, Zhejiang Province, China;
2. Department of Electrical Engineering & Electronics, the University of Liverpool, Liverpool, UK;
Email: zjuwyf@gmail.com; lionisxn@gmail.com; guochuangxin@zju.edu.cn; q.h.wu@liverpool.ac.uk

***Abstract*—Traditional preventive control strategies do not take into account the likelihood of each potential contingency, thus the dispatch results may often be conservative or radical. Aiming to achieve a reasonable tradeoff between economy and security, this paper develops a risk-oriented preventive control (ROPC) strategy. A three-state weather model is introduced to reflect the impact of weather conditions on the failure rate of transmission lines. Using the multi-objective optimization (MO) method, system security level associated with overload risk can be controlled in advance. A distance based multi-objective particle optimization (DSMOPSO) algorithm is adopted to solve the MO problem. Simulation results obtained on a six-bus system are analyzed in comparison with OPF and PSCOPF to show that the proposed ROPC could provide a useful decision-making tool to keep an optimal balance between system operational cost and overload risk under different weather conditions.**

I. KEY EQUATIONS

The three-state weather model is as follows:

$$\lambda^{\mathrm{n}} = \lambda_{avg}(1-F_{\mathrm{b}})/P_{\mathrm{n}} \tag{1}$$

$$\lambda^{\mathrm{a}} = \lambda_{avg}F_{\mathrm{b}}(1-F_{\mathrm{m}})/P_{\mathrm{a}} \tag{2}$$

$$\lambda^{\mathrm{m}} = \lambda_{avg}F_{\mathrm{b}}F_{\mathrm{m}}/P_{\mathrm{m}} \tag{3}$$

Transmission lines overload risk assessment:

$$p_i = 1-e^{-\lambda_i \Delta t} \tag{4}$$

$$P(\mathrm{E}_i) = P_i\prod_{j\in \mathrm{U}}(1-P_j) \tag{5}$$

$$Sev_j = \begin{cases} 0, & k \le 0.9 \\ 10k-9, & k > 0.9 \end{cases} \tag{6}$$

$$RISK = \sum_{i=1}^{\mathrm{n}} P(\mathrm{E}_i)\cdot Sev(\mathrm{E}_i) \tag{7}$$

The ROPC model is as follows:

$$\mathrm{Min} \quad \{COST, RISK\} \tag{8}$$

$$\text{s.t.} \quad P = B\theta \tag{9}$$

$$\left|F_{ij} = (\theta_i-\theta_j)/x_{ij}\right| \le F_{ij}^{\max} \tag{10}$$

$$P_{\mathrm{G}i}^{\min} \le P_{\mathrm{G}i} \le P_{\mathrm{G}i}^{\max} \tag{11}$$

II. KEY RESULTS

TABLE I
RESULTS OF OPF AND PSCOPF

	OPF	PSCOPF
PG1(MW)	127.5	67.554
PG2(MW)	37.5	97.446
PG3(MW)	45	45
COST($)	3467.5	3576.9
RISK1	0.0033	0.0001
RISK2	0.1212	0.0029
RISK3	0.7878	0.0197

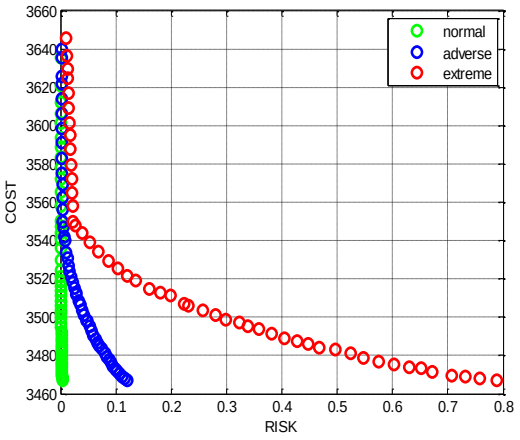

Figure 1. Comparision of ROPC in different weather conditions.

TABLE II
DECISION-MAKING OF ROPC IN DIFFERENT WEATHER CONDITIONS BASED ON THE VALUE OF N

	Acceptable	Tolerable	Intolerable
Normal weather	<= 1	2	> 2
Adverse weather	0	1	> 1
Extreme weather		0	> 0

TABLE III
SELECTION OF DIFFERENT OPERATING SCENARIOS WITHIN TOLERABLE RISK

Hour	PG1(MW)	PG2(MW)	PG3(MW)	COST	RISK	N
1	93.9	71.1	45	3516.2	0.0006	2
2	83.3	81.7	45	3538.2	0.0088	1
3	68.5	90.65	50.85	3583	0.0185	0

Optimal Incremental Placement of PMUs for Power System Observability

Fei Wang[1], Weiqi Zhang[2] and Puming Li[2]
[1]Department of Electrical and Electronic Engineering, The University of Hong Kong, Hong Kong
[2]Guangdong Power Dispatch Center, Guangdong Power Grid Co., Guangdong, China
Email: wangfei@eee.hku.hk

Abstract—**This paper presents a series of optimization models for Phasor Measurement Unit (PMU) placement with new considerations. Extended from the formulations based on integer linear programming, issues concerning uncertainty propagation are discussed and an improved model is proposed to alleviate the impact. Furthermore, as it is more valuable in practice with incrementally placing PMUs, a multistage installation framework based on dynamic programming is developed. With a novel index introduced, the presented framework is implemented with uncertainty propagation controlled in a certain level for each stage. Unlike other available approaches, when processing the immediate stage in this paper, current and future installations are simultaneously considered rather than just making decisions from fixed PMU locations. Minimum number of PMUs is guaranteed meanwhile with each installation. In addition, a postprocessing optimization for selection from multiple solutions in integer programming models is also presented. The proposed models are tested in IEEE 14-, 30-, 57- and 118-bus systems. With the results analyzed and discussed, it indicates the improved model can limit the uncertainty propagation in a fixed level, and the proposed multistage framework could be employed as a practical strategy for PMU placement planning.**

I. Key Equations

The proposed model with *M*-stage installations of PMUs for each stage *m* is formulated as

$$\min \quad C_m = \sum_{j \in I} x_j^{(m)} \tag{1}$$

Subject to

$$\sum_{j \in I} a_{ij}^{(M-t+1)} x_j^{(t)} \geq 1, \text{ for } t = m \text{ to } M \text{ and } i \in I \tag{2}$$

$$\sum_{j \in I} x_j^{(t)} = C_{t,\text{opt}}, \text{ for } t = m+1 \text{ to } M \tag{3}$$

where $a_{ij}^{(M-t+1)}$ is the element of matrix $\mathbf{A}^{M-t+1}$

When the effect of zero injections is considered, (4) is employed instead of (2).

$$\sum_{j \in I} a_{ij}^{(M-t+1)} x_j^{(t)} + \sum_{k \in I} a_{ik}^{(M-t)} \sum_{j \in ZI} a_{kj} w_{kj}^{(t)} \geq 1, \quad \text{for } t = m \text{ to } M \text{ and } i \in I \tag{4}$$

II. Key Figures

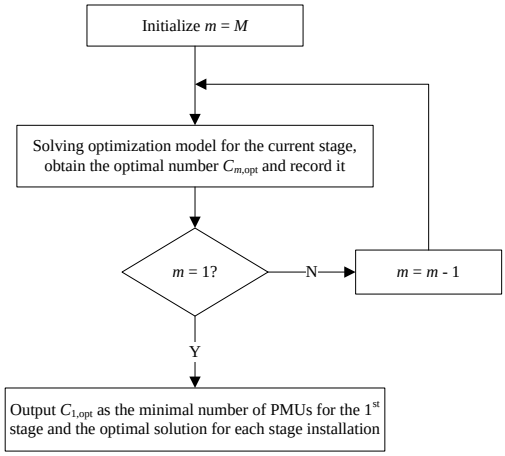

Fig. 1. Flow chart for incremental installation of PMUs.

III. Key Results

TABLE I
NUMBER OF PMUS REQUIRED FOR INCREMENTAL INSTALLATION CONSIDERING ZERO INJECTIONS

Test System	Stage 1	Stage 2	Stage 3	Total
IEEE 14	1	1	1	3
IEEE 30	3	2	2	7
IEEE 57	5	4	3	12
IEEE 118	9	4	16	29

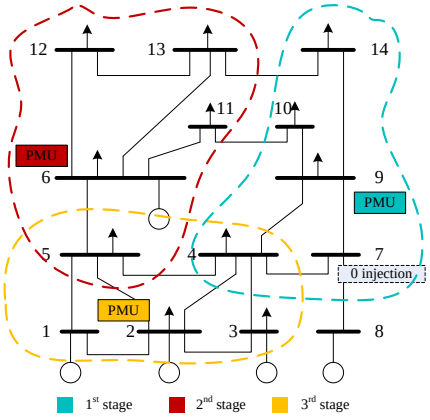

Fig. 2 Three-Stage Installation in IEEE 14-Bus System

Application of MIQCP Based SVC Allocation Method to a Complex Real-World Grid

Robert Wan-Fu Chang, *Student Member, IEEE*, Tapan Kumar Saha, *Senior Member, IEEE*
School of ITEE, The University of Queensland, Australia

Email: rwchang@itee.uq.edu.au and saha@itee.uq.edu.au

Abstract— **This paper demonstrates the applicability of a recently reported mixed integer quadratically constrained programming (MIQCP) placement algorithm on a large scale real-world power system, based on maximizing loadability. The MIQCP algorithm partially incorporates key quadratic constraints, which were absent in MILP placement methods reported in the past. A case study based on Powerlink Queensland's HV transmission network is presented, with the system containing 886 buses and 1087 branches. A comparison is presented between the MIQCP approach and the MILP approach, showing significant improvements in solution accuracy. Additionally, through verification by an exhaustive load flow search, MIQCP is shown to provide correct SVC placement in the 886 bus network. Finally, some observations are presented based on results involving multiple SVC placements in the network.**

Keywords- loadability, MIP, optimal location, SVC allocation

I. KEY EQUATIONS

Linear constraint equations for the optimization problem:

$$A \cdot p + A' \cdot l - GM \cdot P_G + \mu P_L = 0 \quad (1)$$

$$A \cdot q - H \cdot V^2 + A' \cdot m - GM \cdot Q_G + \mu Q_L - z = 0 \quad (2)$$

$$R \cdot p - X \cdot q + \tfrac{1}{2} CM \cdot V^2 + \tfrac{1}{2} k = 0 \quad (3)$$

$$X \cdot l - R \cdot m = 0 \quad (4)$$

$$R \cdot l + X \cdot m - k = 0 \quad (5)$$

Quadratic constraint equations:

$$(r_{ij}^2 + x_{ij}^2)(p_{ij}^2 + q_{ij}^2) - k_{ij} V_{j\max}^2 \le 0 \quad (6)$$

II. KEY TABLES

TABLE I
DEVIATIONS FROM NR LOAD FLOW SOLUTION

Variable	MIQCP Error		MILP Error	
	M	σ	M	σ
Bus voltage (pu)	0.0230	0.0296	0.0448	0.0582
Active branch flow (MW)	3.92	9.19	323	1320
Reactive branch flow (MW)	6.86	15.6	154	887
Active branch loss (MVAR)	0.226	0.571	0.834	4.71
Reactive branch loss (MVAR)	3.10	15.4	8.76	45.8

This work was supported by the Australian Research Council Linkage Project in conjunction with Powerlink Queensland.

TABLE II
OPTIMAL SVC PLACEMENT RESULTS

	MIQCP	MILP
Location (Bus)	629	-
Optimal Loadability	2.38	2.58
Compensation Rating (MVAR)	347	-
Solution Time (s)	55.50	0.33

TABLE III
KEY MIQCP OPTIMIZATION RESULTS FOR MULTIPLE SVCS

Number of SVCs	Loadability	Optimal Locations (buses)	Total Compensation (MVAR)	Solution Time (s)
1	2.3824	629	350	57.49
2	2.3911	629, 635	602	105.83
3	2.3936	313, 625, 629	924	114.41
4	2.3954	313, 621, 625, 629	1271	155.75
5	2.3965	302, 313, 379, 625, 629	1618	188.61

III. KEY FIGURES

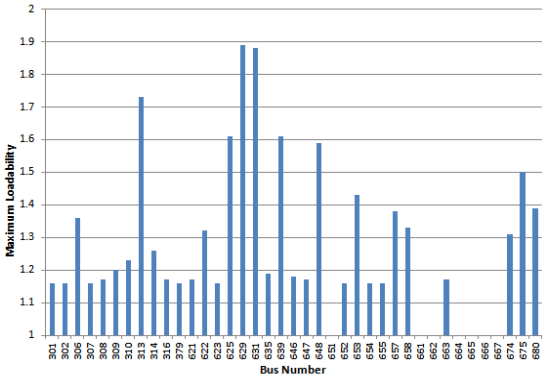

Figure 1. Plot of maximum loadability for each 275kV bus in the Queensland test network, confirming bus 629 as the optimal location.

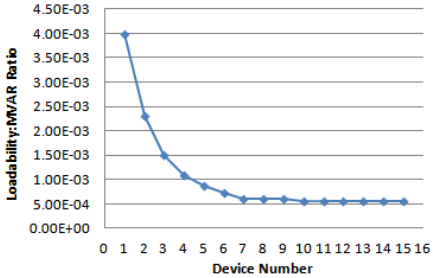

Figure 2. Loadability/MVAR ratio vs. total SVC number, showing reducing efficiency for loadability enhancement as more devices are used.

Daily Generation Scheduling for Reducing Unit Regulating Frequency Using Multi-Population Genetic Algorithm

Y. M. Li[1], W. Li[2], *Fellow, IEEE*, W. Yan[1], and X. F. Jia[3]
[1]Chongqing University, [2]BC Hydro, [3]Hebei Shijiazhuang Power Supply Company
Email: liyiming@cqu.edu.cn, wen.yuan.li@bchydro.com, cquyanwei@cqu.edu.cn and jiaxiaofeng3@163.com

***Abstract*-- The paper presents an optimization model of daily generation scheduling for reducing unit regulating frequency and an improved multi-population genetic algorithm (IMPGA) for solving the model based on load curve segmentation. Generating units are categorized into four classes and incorporated into the objective function or constraints in terms of regulating requirements. Load points on the load curve are aggregated to form equivalent multiple-level load curve representation. The global optimization is reached with coordination between the multiple-level load model and multi-population strategy of GA. The effectiveness of the presented model and algorithm is demonstrated using the IEEE 30-bus and IEEE 118-bus standard systems.**

I. Key Equations

For the units that do not have any hard limit on regulating times per day but their regulation frequency on the generation curve should be minimized, their regulating costs are considered in the objective function to reduce the regulating frequencies as possible.

$$\min F = \sum_{t=1}^{T}\sum_{i=1}^{N}\left[f_i\left(P_{i,t}\right)\Delta T + SC_i u_{i,t}\left(1-u_{i,t-1}\right)\right] + C\sum_{i\in\Theta} n_i \quad (1)$$

For the non-peaking units in the second class, a hard limit on regulations is enforced.

$$n_i \le N_{\max,i} \quad i \in \Psi \quad (2)$$

II. Key Figures

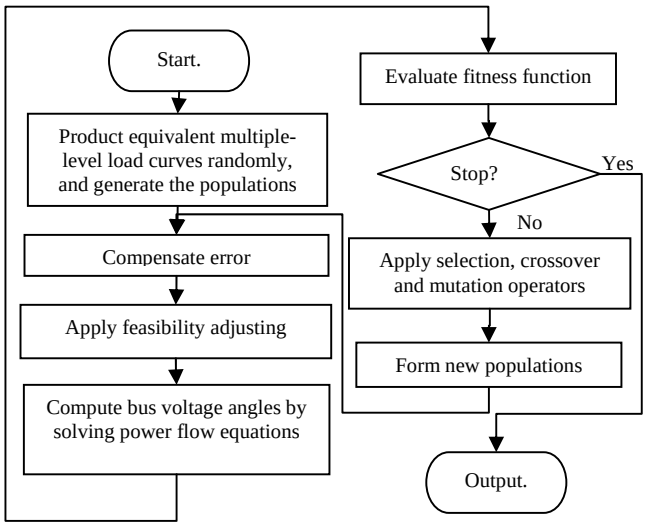

Fig.1 Flow chart of improved multi-population genetic algorithm.

III. Key Results

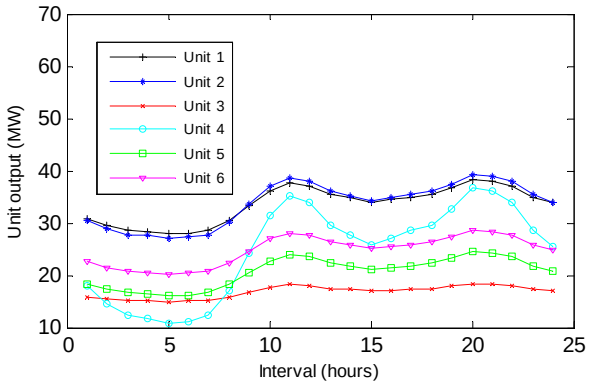

Fig.2 Generation scheduling of the 6 units in the IEEE 30-bus system by the conventional method

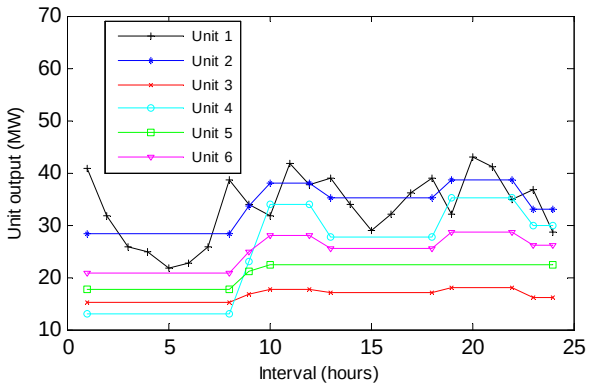

Fig.3 Generation scheduling of the 6 units in the IEEE 30-bus system by the proposed model.

TABLE I COMPARISON OF RESULTS FOR IEEE 30-BUS SYSTEM

Method	Generation cost ($)	Number of regulations in the day				CPU Time (s)
		Classes 2	Classes 3	Classes 4	Total	
Conventional Method	10825	92	23	23	138	24.61
Proposed Method	10835	20	2	23	45	19.79

TABLE II COMPARISON OF RESULTS FOR IEEE 118-BUS SYSTEM

Method	Generation cost (M$)	Number of regulations in the day				CPU Time (s)
		Classes 2	Classes 3	Classes 4	Total	
Conventional Method	3.619	1104	115	46	1265	34.61
Proposed Method	3.624	235	10	46	291	26.15

Synchrophasor State Estimation and Parameter Estimation on the New York Power System

Scott G. Ghiocel, Joe H. Chow
Dept. of Electrical, Computer, and Systems Engineering
Rensselaer Polytechnic Institute
Troy, NY 12180, USA

George Stefopoulos, Bruce Fardanesh,
Deepak Maragal, and Brent Blanchard
New York Power Authority
White Plains, NY 10601, USA

***Abstract*—In this paper, we examine state estimation using real synchrophasor data from the New York high-voltage transmission system. In the state estimation, we correct for systematic measurement error, such as phase angle biases and line parameter uncertainty. We also extend the formulation to estimate transformer tap ratios. The ability to correct errors and estimate parameter uncertainty depends on the configuration of measurements in the system and their redundancy. We analyze different configurations of PMU installations and the measurement redundancies provided by their synchrophasor measurements. We apply these state estimation techniques to real synchrophasor data and demonstrate the redundancy and parameter estimation concepts on a 14-bus observable subsystem in New York state. This observable subsystem includes some redundant measurements, which we use to estimate other parameters on the system. Using our algorithm, we successfully detect tap position changes in an autotransformer and correct for error and uncertainties. This provides a consistent state solution for use with other power system tools to improve reliability of power system operation and control.**

***Index Terms*—synchrophasor, state estimation, parameter estimation, redundancy, angle correction, transformer tap ratio**

I. Key Figures

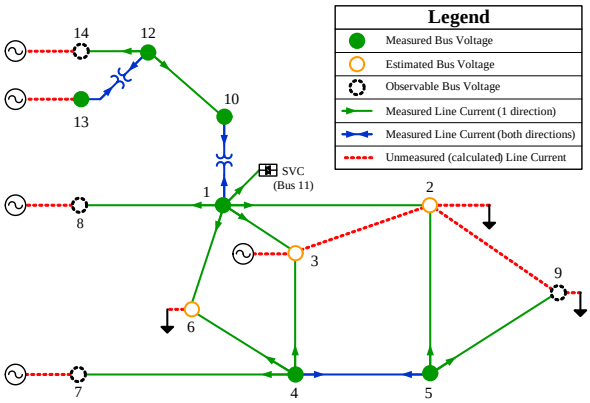

Figure 1: Observable Subsystem of the New York High-Voltage Transmission System

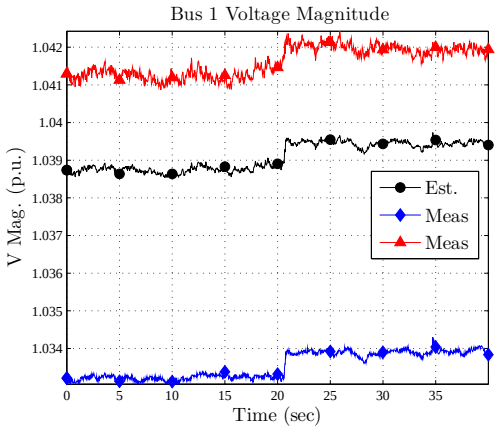

Figure 2: Voltage Magnitude at Bus 1

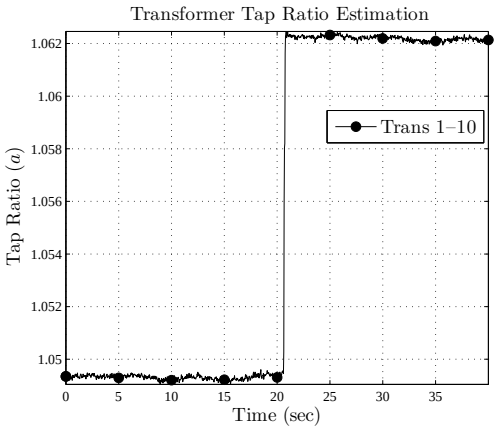

Figure 3: Transformer Tap Estimation

Measurement-Based Non-Iterative Direct State Calculation for Power Networks

Xinyu Tony Jiang and Joe H. Chow
Rensselaer Polytechnic Institute
Troy, NY, USA
jiangx4@rpi.edu, chowj@rpi.edu

Bruce Fardanesh, Deepak Maragal, and George Stefopoulos
New York Power Authority
White Plains, NY, USA
Bruce.Fardanesh@nypa.gov, Deepak.Maragal@nypa.gov, George.Stefopoulos@nypa.gov

***Abstract*— This poster describes a new method for solving for the state of a nonlinear AC power system in a non-iterative manner when given an adequate set of sufficiently accurate measurements from the system. This method is based on the Kipnis-Shamir relinearization technique. The Kipnis-Shamir technique was originally developed for cryptographic analysis, and the technique is used to solve over-defined sets of polynomial equations. This new state calculation method provides the same results as traditional iterative state estimation methods, and the method does not require an initial guess of system states.**

In our state calculation method, the measurement equations, which are the bus voltage magnitude equations and the active and reactive power flow equations between buses, are formulated in rectangular coordinates of the bus voltages. With this formulation, the nonlinear measurement equations become quadratic polynomial equations of the voltage variables. Because there are usually more measurements than what is necessary for observability of the system, the system is over-defined and the Kipnis-Shamir relinearization can be applied. The Kipnis-Shamir relinearization technique expands the quadratic variables to a higher variable space, and this allows the solution of the quadratic variables in a direct, non-iterative manner. The technique requires keeping track of the indices of bus voltages that make up each quadratic variable. After solving for the quadratic variables, the real and imaginary parts of the bus voltages can then be extracted using the indices.

The computation effort for the state calculation is dependent on the topology of the system to be solved. From examining the indices of the solution from the relinearization technique, we find that only certain combinations of bus connections contribute to the solution, and thus the computation effort can be reduced by analyzing the topology of the network. The computation effort can further be reduced by incorporating PMU measurements. PMU measurements can provide the real and imaginary components Keywords- Non-Iterative Solution; Measurement-Based Solution; State Solution, State Estimation, Power Flow

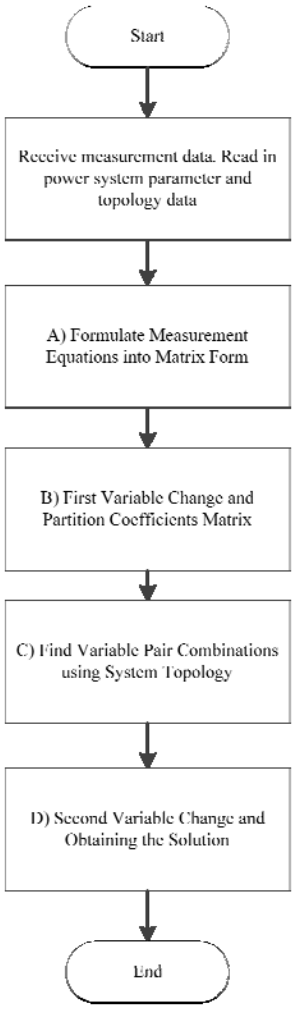

Figure 1. Flow chart for the measurement-based, direct, non-iterative power system state calculation algorithm.

Quantify Spinning Reserve in Systems With Significant Wind Power Penetration

Guodong Liu and Kevin Tomsovic
Department of Electrical Engineering and Computer Science
The University of Tennessee, Knoxville, TN 37996, USA
Email: *gliu5@utk.edu* and *tomsovic@utk.edu*

***Abstract*—The traditional unit commitment and economic dispatch approaches with deterministic spinning reserve requirements are inadequate given the intermittency and unpredictability of wind power generation. Alternative power system scheduling methods capable of aggregating the uncertainty of wind power, while maintaining reliable and economic performance, need to be investigated. In this paper, a new probabilistic model of security-constrained unit commitment is proposed to minimize the cost of energy, spinning reserve and possible loss of load. A new formulation of expected energy not served considering the probability distribution of forecast errors of wind and load, as well as outage replacement rates of various generators is presented. The proposed method is solved by mixed integer linear programming. Numerical simulations on the IEEE Reliability Test System show the effectiveness of the proposed method. The relationships of uncertainties and required spinning reserves are verified.**

***Index Terms*—Expected energy not served (EENS), security-constrained unit commitment (SCUC), wind power forecast error, spinning reserve, reliability, mixed integer linear programming (MILP)**

I. Key Equations

The net demand forecast error follows Gaussian distribution with expectation zero and standard deviation as

$$\sigma_t^d = \sqrt{\left(\sigma_t^l\right)^2 + \left(\sigma_t^w\right)^2} \tag{1}$$

The probability distribution of net demand forecast error is combined with the realization of uncertainties of generators in each scenario, then discretized into NL intervals. The *EENS* in scenario s during period t is formulated as

$$EENS_{s,t} = \sum_{l=1}^{NL} \left(\left(\frac{NL+1}{2} - l \right) \sigma_t^d - \mu_{s,t} \right) a_{s,t,l} b_{s,t,l} \tag{2}$$

with

$$\mu_{s,t} = \sum_{i \in A_{s,t}} R_{i,t} - \sum_{j \in U_{s,t}} P_{j,t} \tag{3}$$

In this paper, the spinning reserve requirements are determined by simultaneously optimizing the operating cost, start-up cost, reserve cost and expected cost of load shedding.

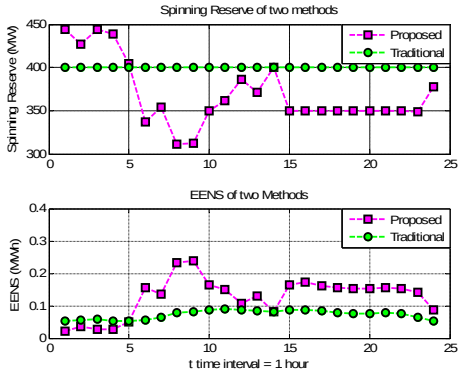

Fig. 1. Comparison of proposed and traditional methods

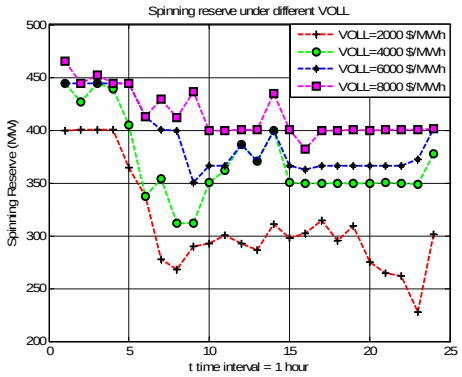

Fig. 2. Spinning reserve under different VOLL values

$$\min \sum_{t=1}^{NT} \{ \sum_{i=1}^{NI} [C_{i,t}\left(P_{i,t}, u_{i,t}\right) + S_{i,t}\left(u_{i,t}, u_{i,t-1}\right) + q_{i,t} R_{i,t}] + VOLL_t \cdot \sum_{s \in 1}^{NS} EENS_{s,t} p_{s,t} \} \tag{4}$$

II. Key results

The simulation results of proposed and tradition SCUC are shown in Fig. 1. The relationship between spinning reserve and VOLL is shown in Fig. 2.

Security-Constrained Unit Commitment with Wind Power Generation by Using Interval Linear Programming

B. R. Zhou, Q. Y. Jiang, *Member, IEEE*

***Index Terms*—security-constrained unit commitment, uncertainty, benders decomposition, interval liner programming.**

***Abstract*—Wind is considered as the most practicable renewable energy for large-scale application. Therefore, in recent years, there is a strong increase in the amount of wind power generation around the world. And then the volatility of wind power generation output has been a big challenge for the operation of power system such as unit commitment. This poster presents a security-constrained unit commitment model which takes into account the volatility of wind power generation. Using interval linear programming theory, this model can guarantee the security of the power system within the forecasting interval of wind power.**

I. Key Flow Chart

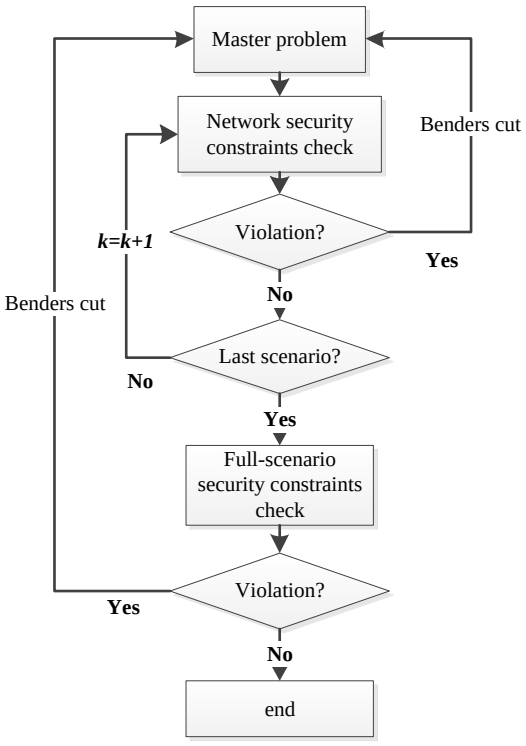

Fig.1. Overall flow chart of the proposed model

The master problem solves a unit commitment without network security constraints. One sub-problem (network security constraints check) checks whether the commitment and dispatch solution of master problem can satisfy the network security constraints. The other sub-problem (Full-scenario security constraints check), using interval linear programming theory, checks whether the worst-case security constraints can be satisfied with the schedule obtained in the master problem. The iterative process will continue until no violation occurs in both sub-problems.

II. Key Equations

These constraints are reformulated in interval formulation as follows:

$$\sum_{i=1}^{N_g} P_{i,t} u_{i,t} = \sum_{j=1}^{N_D} [P_{load}^{j,t,min}, P_{load}^{j,t,max}]$$

$$-FL_l \le \sum_{i=1}^{N_g} A_{i,l} P_{i,t} - \sum_{j=1}^{N_D} A_{j,l} [P_{load}^{j,t,min}, P_{load}^{j,t,max}] \le FL_l$$

$$\Delta V_b^{\min} \le \sum_{i=1}^{N_g} B_i Q_{i,t} - \sum_{j=1}^{N_D} B_j [Q_{load}^{j,t,min}, Q_{load}^{j,t,max}] \le \Delta V_b^{\max}$$

III. Key Results

TABLE Ⅰ
SYSTEM COST COMPARISON BETWEEN PERFECT FORECASTING SCENARIO (SSOF) AND MULTI-SCENARIO OBJECTIVE FUNCTION (MSOF)

	scenario 1	scenario 2	scenario 3	overall
SSOF	9068	9335	8714	8953
MSOF	9075	9361	8691	8950

TABLE Ⅱ
VIOLATION STATE OF BUS VOLTAGE CONSTRAINTS

fluctuation range	UC-NVC	UC-SVC	UC-FVC
0%	*N*	*Y*	*Y*
10%	*N*	*N*	*Y*
20%	*N*	*N*	*Y*

N means the bus voltage constraints cannot be satisfied and *Y* means the bus voltage constraints can be satisfied. UC with no voltage constraints (UC-NVC), UC with single-scenario voltage constraints (UC-SVC), UC with full-scenario voltage constraints (UC-FVC).

TABLE Ⅲ
THE SYSTEM COST

model	system cost	CPU time
UC-NVC	9068	2.607s
UC-SVC	9266	8.428s
UC-FVC	9400	19.848s

TABLE Ⅳ
THE COMPARISON OF SYSTEM COST

UC model	W-OL	W-E-0	W-E-30	W-E-60
system cost	9400	9343	9373	9400
wind generation excision	no	yes	yes	no

W-OL means wind generators must be online. W-E-x means that we can give some compensation to achieve the excision of wind generators, and x represents the compensation amount.

Robust and Flexible Power System Expansion Planning under Two Levels of Multiple Uncertainties

Diego Mejía-Giraldo
Department of Electrical and Computer Engineering
Iowa State University, Ames, IA
also with Universidad de Antioquia, Medellin, Colombia

James McCalley
Department of Electrical and Computer Engineering
Iowa State University
Ames, IA

***Abstract*—We present a methodology that obtains robust and flexible future capacity expansion plans under diverse types and sources of uncertainty. Uncertainties are classified as global and local. Scenarios are created using different realizations of global uncertainties; and we also consider another level of uncertainty within each scenario by modeling local uncertainties. Robustness is obtained by minimizing investment and operational costs using robust optimization; whereas flexibility is achieved by minimizing the maximum adaptation within different scenarios using robust optimization as well. Results obtained with our methodology in a 5-region US system under a 40-year planning horizon are presented.**

I. TWO-LEVELS OF UNCERTAINTIES

In order to carefully characterize the uncertainty treatment within the optimization, two types of uncertainties are used (see Fig. 1): *global*, those instances of situations that define a specific optimal investment direction; e.g. future environmental policies, shifts in demand, and trends of natural gas price, among others; and *local*, those parameters that can be parameterized by uncertainty sets around a central point defined by a global uncertainty.

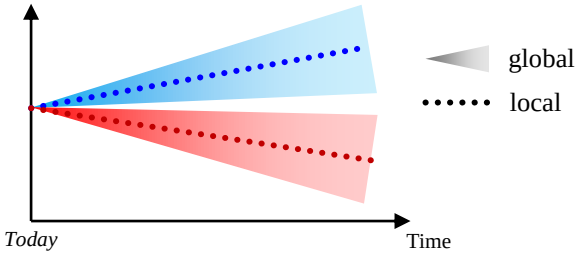

Figure 1. Global and local uncertainties

II. ROBUST OPTIMIZATION AND FLEXIBILITY

For each scenario, a robust optimal investment strategy is obtained through robust optimization modeling local uncertainties. Designing a system that is robust to global uncertainties is costly and unrealistic. It is more useful designing a flexible system, i.e. which can be efficiently adapted to different future scenarios. Flexibility is measured in terms of robust adaptation cost between different future scenarios *i* and *j* as follows:

$$AC(i,j)=\underset{y_t^{i\to j},z_t}{\text{minimize}}\left\{\sum_{t=\tau}^{T} IC_t^j \max\left(y_t^{i\to j}-x_t^{*i},0\right)+\sum_{t=\tau}^{T} OM_t^j z_t\right\}$$

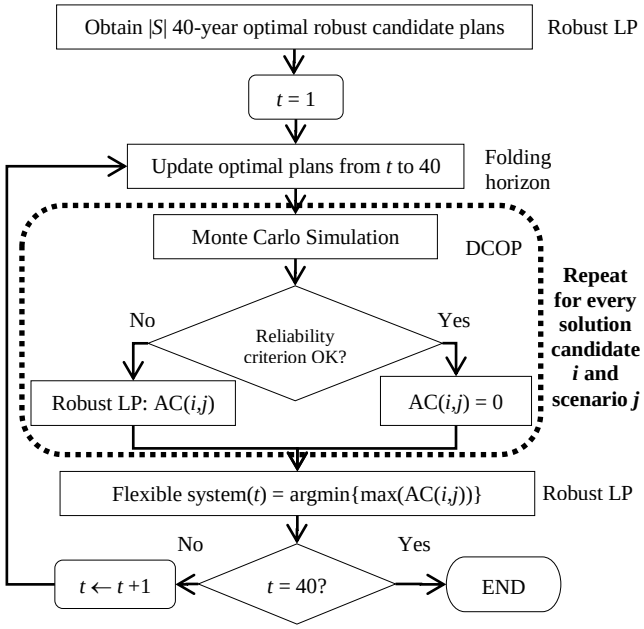

Figure 2. Multi-period planning

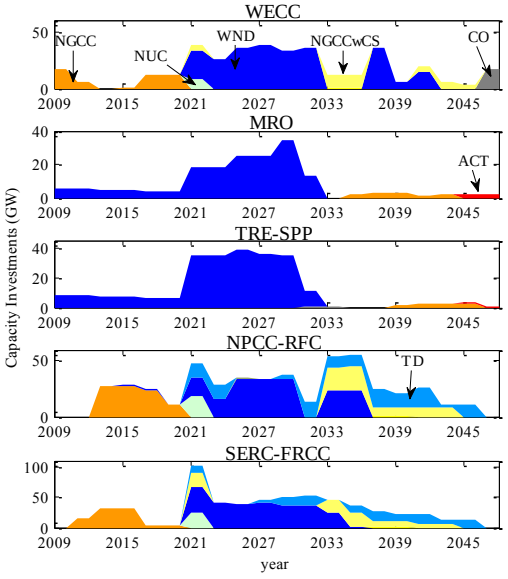

Figure 3. Robust and flexible portfolio

A Simultaneous Perturbation Approach of the Lagrange Relaxation Method for Solving Hydro-thermal Coordination Problems

Yu Xia and Joe H. Chow
Rensselaer Polytechnic Institute
Troy, NY, USA
xiay4@rpi.edu, chowj@rpi.edu

***Abstract*—** In this poster, we describe a new simultaneous perturbation technique for the Lagrange Relaxation method in solving a hydro-thermal scheduling and economic dispatch problems with inter-temporal constraints. Power system optimization problems are commonly posed as constrained optimization problems and formulated as linear or nonlinear programing problems using Lagrange multipliers in the objective functions. For constraints spanning multiple periods, the Lagrange Relaxation method relaxes the Lagrange multiplier for those constraints to decouple the optimization across time periods. Then the reformulated problem is solved iteratively until convergence, using some rather conservative stepsizes.

A simultaneous perturbation technique that achieves much better convergence properties has been proposed in [1]. In that paper, the discussion is on the coordination of one hydro generation with a composite steam unit. In this poster, we will expand the method to multiple steam units. An example of this application is shown in Figure 1 and Table 1. The solution of the problem is solved within 4 iterations. For case with no losses, the solution converges in one step, even though hydrothermal coordination is performed for 4 periods.

In the poster, we will also show results including optimal power flow using DC solution.

Key Words—Lagrange Relaxation, optimization, Hydro-thermal coordination, unit commitment

[1] J. H. Chow and S. G. Ghiocel, "A Lagrange Relaxation-Perturbation Approach for Solving Power System Dispatch Problems with Inter-Temporal Constraints," submitted to IEEE Transactions on Power Systems, 2012.

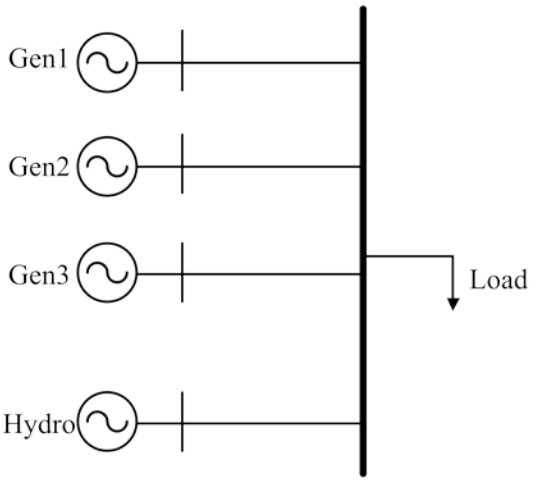

Figure 1. System topology with three thermal units and one hydro unit

Table 1 Example results, converge in 4 iterations

	T1	T2	T3	T4
Load(MW)	210	270	390	240
P_1 (MW)	33.3138	35.7251	41.2413	34.4931
P_2 (MW)	43.3274	47.5218	57.0821	45.3799
P_3 (MW)	114.1100	130.1678	165.8508	121.9993
P_h (MW)	24.3476	64.8302	146.2617	44.5604
λ ($/MWh)	26.5213	27.6694	30.3086	27.0824

Application of Non-linear Programming for Large-Scale AC-DC Power Flow Analysis

Zhijun Qin and Yunhe Hou
Department of Electrical and Electronic Engineering, The University of Hong Kong, Hong Kong
Email: zjqin@eee.hku.hk and yhhou@eee.hku.hk

***Abstract*—This paper proposes a robust, non-divergent model for large-scale AC-DC power flow analysis. By introducing relaxation variables into power flow equations, the conventional power flow model is turned into a non-linear programming model to minimize the L_2 norm of the relaxation variables subject to operation constraints and DC station control modes. The interior point method (IPM) is used to solve the model. Due to the special structure of the proposed model, the size of coefficient of correction equations in the IPM can be reduced to the same as Jacobian in the conventional Newton method. Further, the coefficient is symmetrical positive-definite with a diagonal perturbation, which leads to a better convergence than Newton direction. The model and algorithm proposed also have the following features: (1) no special initial value is needed; (2) strong robustness for power grids with plenty of small/negative impedance; (3) applicable for searching a desirable operation point by appropriate settings of inequality constraints; (4) striving for ultimate close to power flow solution avoiding to stop too early at a local minimizer. Numerical simulations on a 6527 buses power grid in China with 8 HVDC lines show that the proposed model has robust convergent property in the feasible region, around the boundary of the feasible region and even beyond the feasible region of power flow.**

I. KEY EQUATIONS

The AC-DC power flow analysis to solve $h(\boldsymbol{X}) = \boldsymbol{0}$ is converted into a non-linear programming model as:

$$\begin{aligned} &\min\ \boldsymbol{\varepsilon}^{\mathrm{T}}\boldsymbol{\varepsilon} \\ &\text{s.t.}\quad h(\boldsymbol{X}) - \boldsymbol{\varepsilon} = \boldsymbol{0} \\ &\qquad \overline{\boldsymbol{g}} \le g(\boldsymbol{X}) \le \underline{\boldsymbol{g}} \end{aligned} \tag{1}$$

By applying interior point method, the reduced KKT system can be solved by:

$$(\boldsymbol{M} - 2\mathrm{J}^{\mathrm{T}}(\boldsymbol{X})\mathrm{J}(\boldsymbol{X}))\Delta\boldsymbol{X} = -\boldsymbol{\psi} + 2\mathrm{J}^{\mathrm{T}}(\boldsymbol{X})\boldsymbol{L}_{y0} \tag{2}$$

where:

$$\boldsymbol{M} = \boldsymbol{F} + \nabla g(\boldsymbol{X})([\boldsymbol{u}]^{-1}[\boldsymbol{w}] - [\boldsymbol{l}]^{-1}[\boldsymbol{z}])\nabla^{\mathrm{T}} g(\boldsymbol{X}) \tag{3}$$

$$\mathrm{J}(\boldsymbol{X}) = \nabla^{\mathrm{T}} h(\boldsymbol{X}) \tag{4}$$

$$\boldsymbol{F} = \nabla^2 h(\boldsymbol{X})\boldsymbol{y} + \nabla^2 g(\boldsymbol{X})(\boldsymbol{z} + \boldsymbol{w}) \tag{5}$$

Other primal and dual variables are determined by:

$$\Delta\boldsymbol{y} = -2\boldsymbol{L}_{y0} - 2\mathrm{J}(\boldsymbol{X})\Delta\boldsymbol{X} \tag{6}$$

$$\begin{cases} \Delta\boldsymbol{l} = \nabla^{\mathrm{T}} g(\boldsymbol{X})\Delta\boldsymbol{X} + \boldsymbol{L}_{z0} \\ \Delta\boldsymbol{u} = -(\nabla^{\mathrm{T}} g(\boldsymbol{X})\Delta\boldsymbol{X} + \boldsymbol{L}_{w0}) \\ \Delta\boldsymbol{z} = -[\boldsymbol{l}]^{-1}[\boldsymbol{z}]\nabla^{\mathrm{T}} g(\boldsymbol{X})\Delta\boldsymbol{X} - [\boldsymbol{l}]^{-1}([\boldsymbol{z}]\boldsymbol{L}_{z0} + \boldsymbol{L}_{l0}^{\mu}) \\ \Delta\boldsymbol{w} = [\boldsymbol{u}]^{-1}[\boldsymbol{w}]\nabla^{\mathrm{T}} g(\boldsymbol{X})\Delta\boldsymbol{X} + [\boldsymbol{u}]^{-1}([\boldsymbol{w}]\boldsymbol{L}_{w0} - \boldsymbol{L}_{u0}^{\mu}) \end{cases} \tag{7}$$

II. KEY RESULTS

The test system is part of a power grid in China as shown in Table I. Two sets of data of test system are provided. Data (A) is the original data. Data (B) uses bus merging to eliminate part of small/negative impedance branches, as shown in Table II.

TABLE I
NUMBER OF COMPONENTS IN MARCH 2010

Power System resources	Number
AC buses	6527
AC lines	2688
transformers	5416
compensators	1816
synchronous machines	635
energy consumers	1137
converters	16
DC lines	8

TABLE II
NUMBER OF SMALL/NEGATIVE IMPEDANCE BRANCHES

Impedance Range	Data (A)	Data (B)
(1E-4～1E-3)	287	102
(1E-4～1E-5)	349	0
(0～1E-5)	143	0
(-1E-3～0)	1315	921
(-1E-3～-1E-4)	4	0

TABLE III
COMPARISON OF DIFFERENT ALGORITHMS ON DATA (A)

Algorithm	Convergent Property	Maximum Power Mismatch
Newton-Raphson with Flat Start	Diverge	N/A
Fast Decouple	Diverge	N/A
Newton-Raphson with Optimal Multiplier	Converge	4.361 pu
Proposed Algorithm	Converge	0.0669 pu

TABLE IV
COMPARISON OF DIFFERENT ALGORITHMS ON DATA (B)

Algorithm	Convergent Property in Feasible Region	Convergent Property beyond Feasible Region
Newton-Raphson with Flat Start	Diverge	Diverge
Fast Decouple Initiated Newton-Raphson	Converge	Diverge
Fast Decouple	Diverge	Diverge
Newton-Raphson with Optimal Multiplier	Converge	Diverge
Proposed Algorithm	Converge	Converge

Hierarchical two-level Voltage Controller for Large Power Systems (Central Coordinator Level Approach)

Javier Guerrero, *Member, IEEE*, Vaithianathan "Mani" Venkatasubramanian, Hong Chun, Farrokh Habibi-Ashrafi and Armando Salazar.

I. Introduction

Power Delivery substations typically include a number of transformers with variable taps, as well as reactive support capability in the form of switched capacitor and reactor banks. Voltage and reactive power (VAR) control is achieved the proper management of this devices as well as with adequate voltage scheduling of generation units. Because of the need for more efficient use of transmission infrastructure, access of non-utility generators to the power network and the increase in power electronics devices, voltage control has become an important aspect in modern power system operation [1]. On the other hand, the local character of the voltage control, the diversity of the control means and the interaction among them makes the task of coordinating reactive power resources particularly difficult. This document presents a two-level voltage controller for large power systems emphasizing the central coordinator level. The aim of the controller is to maintain the optimal voltage profile in the transmission network by coordinating the VAR control devices in the system. At the local level, the substation controllers maintain their respective substation bus voltages by using mostly local PMU measurements. The central coordinator provides the voltage set-points to the substations and also coordinates by enabling or disabling the local controllers as needed. The controller is being designed towards prototype implementation in Southern California Edison.

II. Supervisory Central Voltage Coordinator (SCVC) Formulation

The central coordinator SCVC (see Fig. 1) is responsible for overseeing smooth operation of substation voltage controllers while also ensuring an optimal voltage profile in transmission network. SCVC addresses the two objectives by two separate optimization tasks:

SCVC Task 1. Optimization of voltage reference values for various substations regulated by their own substation controllers: It is proposed that SCVC carries out optimal power-flow like calculations of state estimation power-flow models to compute optimal values of substation voltage profile aimed at minimizing MVAR losses while also keeping the changes in voltage profile reasonable. The voltage profile optimization may be carried out say a few times in a day when conditions change from say off-peak to peak and so on.

SCVC Task 2. Coordination of substation voltage controllers: Central coordinator SCVC needs to ensure that neighboring Substation Local Voltage Controllers (SLVC) do not interfere with each other while addressing their voltage alarms in their respective substations. It is proposed that the central coordinator carry out central optimization algorithm so that SCVC will decide which substation controllers should be enabled and which ones should be disabled to handle the voltage and VAR issues.

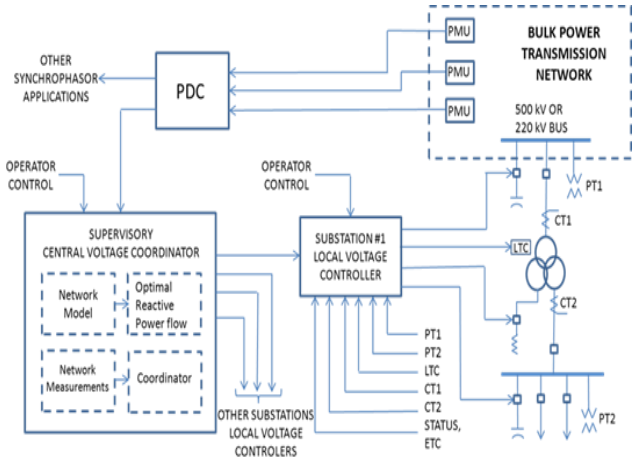

Fig.1 Conceptual design of the SCVC

III. References

[1] V. Venkatasubramanian, H. Chun, J. Guerrero, Farrokh Habibi-Ashrafi and Armando Salazar. "Hierarchical two-level voltage controller for Southern California Edison," *IEEE PES GM 2012*, to be published.

This work was supported in part by Southern California Edison Inc., Power System Engineering Research Center and US Department of Energy.

Mani V. Venkatasubramanian, Hong Chun and Javier Guerrero are with School of Electrical Engineering and Computer Science, Washington State University, Pullman, WA (email: mani@eecs.wsu.edu, hong.chun@email.su.edu, j.guerrerosedeno@email.wsu.edu).

Farrokh Habibi-Ashrafi and Armando Salazar are with Southern California Edison Inc., Los Angeles, CA.

Transmission Planning under Uncertainties of Wind and Load: Sequential Approximation Approach

Heejung Park
Electrical and Computer Engineering
The University of Texas at Austin
Austin, TX 78712–1710
Email: hjpark@mail.utexas.edu

Ross Baldick
Electrical and Computer Engineering
The University of Texas at Austin
Austin, TX 78712–1710
Email: baldick@ece.utexas.edu

I. Introduction

Wind power is one of the most promising renewable resources and it is expected to be used more in the future. One well-known concern with integrating wind power into the North American power system is the lack of transmission capacity due to the fact that most wind resources are generally located far from the load centers. Therefore, the power system needs to be upgraded, with new transmission corridors developed, and transmission system planning studies for wind integration are required.

Uncertainty of wind availability makes wind generators non-dispatchable because their generation capability changes in accordance with wind availability. Thus, wind generators have uncertain capability, even though they have rated capacities, and cannot be dispatched in the same way as conventional thermal generators. System load is also uncertain and affects dispatch of wind generators. Moreover, available wind and load are not independent. Generally speaking, inland wind tends to blow more during off-peak hours than on-peak hours in many areas in North America. We consider the dependency of wind and load, and hence we propose a transmission system planning model that represents two dependent random variables: wind power capability and load.

Probabilistic methods applied to transmission planning include [1], [2], [3]; however, [1], [2] only reflect the uncertainty on the load side and correlation of wind and load is not reflected in [3].

Our work contributes to implementing a stochastic optimization model in transmission system expansion planning in the realistic case that there are two correlated random variables, wind and load. Our results suggest that a relatively low computational effort can provide a solution to the stochastic optimization problem with a medium-scale test system.

II. Methodology

We examine the decision-making for upgrading transmission capacity of existing lines under uncertainties of both wind availability and load in order to utilize potential wind power, based on a 20% Renewable Portfolio Standard (RPS). A two-stage stochastic model is applied to the mathematical formulation [4]. At the first stage of the problem, the transmission investment decision is made under uncertainties of wind availability and load. A system operating problem is solved with the expanded system at the second stage when the uncertain parameters are known. We solve a sequence of optimization problems where continuous random parameters are replaced by approximations. The approximation is refined at each iteration of the sequence. Approximations of random variables are achieved by partitioning the sample space and taking expectation of samples in a cell of the partition [5]. Total cost at each iteration increases with refinement of the partition and is bounded above by the true cost, and so is convergent. We iterate until a pre-determined stopping criterion is satisfied. A wind energy integration goal is achieved by penalizing wind curtailment.

III. Case Study

As a case study, the Electric Reliability Council of Texas (ERCOT) data and a network model are applied. Base-case data for wind and load in Texas from March 2008 to February 2009 are used. For more realistic simulation, the base-case wind data is scaled up because annual wind energy of the base-case provides only 6% of the annual load energy. Several change-cases with proportional scale-up are considered to evaluate the sensitivity of the results to the level of wind development. Our network model as of 2007 has four geographical zones. For the purposes of simplification in network model, we adopt a detailed model of the high voltage system in the West zone that is assumed to contain all wind resources and candidate transmission lines but only represent the other zones by aggregated buses.

References

[1] M. Banzo and A. Ramos, "Stochastic optimization model for electric power system planning of offshore wind farms," *IEEE Trans. Power Systems*, vol. 26, no. 3, pp. 1338-1348, August 2011.

[2] B. G. Gorenstin, N. M. Campodonico, J. P. Costa, and M. V. Pereira, "Power system expansion planning under uncertainty," *IEEE Trans. Power Systems*, vol. 8, no. 1, pp. 129-136, February 1993.

[3] A. Martin and J. Salmerón, "Electric capacity expansion under undertain demand," *IEEE Trans. Power Systems*, vol. 13, no. 2, pp. 333-339, May 1998.

[4] A. Shapiro, D. Dentcheva, A. Ruszczynski, "Lectures on stochastic programming," MPS-SIAM Series on Optimization, 2009.

[5] Y. Ermoliev, R. J-B Wets, "Numerical techniques for stochastic optimization," Springer Series in Computational Mathematics, 1988.

Novel methodology for determining the location for the Battery Storage in a Microgrid

Luis F. Montoya, *Student member,IEEE.* D. Yu, A. Nasiri, *Senior Membes, IEEE.*
Department of Electrical & Computer Engineering
University of Wisconsin Milwaukee

***Abstract*— a new methodology to select the best location for storage in a Microgrid is proposed. The methodology is based on using the derivative terms coming from the Newton Raphson methodology for Power Flow. And, after obtaining the Jacobian when the nonlinear power flow equations system is solved, a method is proposed for the selection of the best point to inject both active and reactive power in the Microgrid. Therefore, (4) indexes were proposed; and tested for different load conditions, in order to prove their accuracy. The system used for this paper is the IEEE 14 bus system that is a system which is not exactly a distribution system, but it was used for simplification, and first solve the issue assuming a balanced power flow, which is not always the case in Microgrids that have unbalanced, and single phase lines throughout the ladder. Mat-power which is a Matlab tool has been used, as the way to analyze the steady state response of the system, and different scenarios for which renewable energy penetration is considered.**

Keywords-Distributed Generation (DG), Microgrid, slack bus ,PQ bus,

I. INTRODUCTION

In a much summarized way the concept that is being used nowadays, describes a Microgrid as a subsystem inside of a Power System, which normally operates at distribution level. Microgrid is characterized by the presence of renewable energy systems – with an unpredictable profiles – and most often has a battery storage system, which is used to backup the system; in terms of either injecting or absorbing active and reactive power, during the isolation & reconnection event. Renewable energy possible locations are defined principally based on the geographical advantages – insulation or wind speed. Herein, the assumption.

II. STORAGE LOCATION INDEXES

The Jacobian matrix is used to obtain a new value during the iterative power flow process. According to equation (1) if steady state is reached by the algorithm a small signal analysis can be done. P, Active power injected. Q, Reactive power injected. V, Voltage Phasor Magnitude, δ, Voltage Phasor Angle.

$$f(P,Q,V,\delta) = 0 \qquad (1)$$

After solving the Jacobian matrix following the Newton Raphson algorithm, the inverse of that matrix can be obtained as shown in (2) for the steady state, and considering that all buses are PQ buses, apart from the slack bus. A linearized model of the system is obtained using the Jacobian terms shown before.

$$\begin{bmatrix} \boldsymbol{U_1} & \boldsymbol{U_2} \\ \boldsymbol{U_3} & \boldsymbol{U_4} \end{bmatrix} \begin{bmatrix} \Delta P_2 \\ \Delta P_3 \\ \vdots \\ \Delta P_n \\ \Delta Q_2 \\ \Delta Q_3 \\ \vdots \\ \Delta Q_n \end{bmatrix} = \begin{bmatrix} \Delta \delta_2 \\ \Delta \delta_3 \\ \vdots \\ \Delta \delta_n \\ \Delta V_2 \\ \Delta V_3 \\ \vdots \\ \Delta V_n \end{bmatrix} \qquad (2)$$

The columns of the Jacobian inverse, represent the affection in angle and magnitude of Voltage in all the system when a small injection of active power or reactive power is done. The indexes are summarized as follows, subscript k denotes the node at which the variation in either active or reactive power is done :

$$\boldsymbol{i1} = \sum_{n=2}^{14} \frac{\partial \delta_n}{\partial P_k}, \boldsymbol{i2} = \sum_{n=2}^{14} \frac{\partial V_n}{\partial P_k}, \boldsymbol{i3} = \sum_{n=2}^{14} \frac{\partial \delta_n}{\partial Q_k},$$
$$\boldsymbol{i4} = \sum_{n=2}^{14} \frac{\partial V_n}{\partial Q_k} \qquad (3)$$

III. METHODOLOGY

The query for the selection proposed is summarized in the following table:

1st	• P and Q values are set for all the loads assuming renewable energy intermittency.
2nd	• Power Flow is solved using the Newton Raphson methodology.
3rd	• Indexces are obtained at steady state
4th	• **Stability eigen values based on the Jacobian Matrix are obtained based on the steady state solution. (Stability is also investigated)**
5th	• Different loading is set and go back to 2nd until all possible changes in PQ buses are done.

Table 1. Flow Chart of the query that is proposed for the selection

Multivariate Analysis for Correlations among Different Transformer Oil Parameters to Determine Transformer Health Index

Atefeh Dehghani Ashkezari, *Student Member, IEEE*, Hui Ma, *Member, IEEE*, Chandima Ekanayake, *Member, IEEE, and* Tapan K. Saha, *Senior Member, IEEE*

***Abstract*— The accurate assessment of the condition of transformer oil-paper insulation system is crucial for ensuring the reliable operation of power transformer. However, the information obtained from different chemical and electrical diagnostic tests performed on a transformer may have varying degree of significance for evaluating the overall insulation condition of the transformer. This paper investigates any correlations among different transformer oil characteristic tests and exploits the significance of individual oil characteristic test for the evaluation of transformer insulation conditions. Such investigation and exploitation will facilitate the proper weighting of various transformer oil tests in assessing transformer insulation condition. Numeric results obtained by applying multivariate analysis on a real oil test dataset are also provided in this paper.**

I. Key Results

TABLE I
THE DISTRIBUTION OF ASSIGNED HEALTH INDEX OF 170 OIL TESTS DATA

HI code	Definition	Number of Cases	Percentage
0	Excellent	54	32
1	Good	65	38
2	Fair	28	16
3	Poor	16	10
4	Unsatisfactory	7	4
Total		170	100

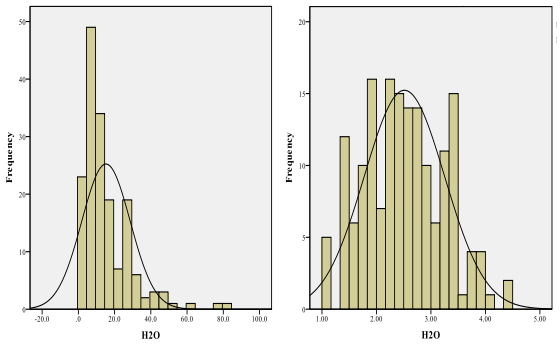

(a) (b)

Fig.1 Data normalization with logarithm transformation (using moisture content H_2O as example) (a) original data (b) normalized data

Atefeh Dehghani Ashkezari (atefeh@uq.edu.au), Hui Ma (huima@itee.uq.edu.au), Chandima Ekanayake (chandima@itee.uq.edu.au) and Tapan Saha (saha@itee.uq.edu.au) are with the School of ITEE, The University of Queensland, Brisbane, Queensland, Australia.

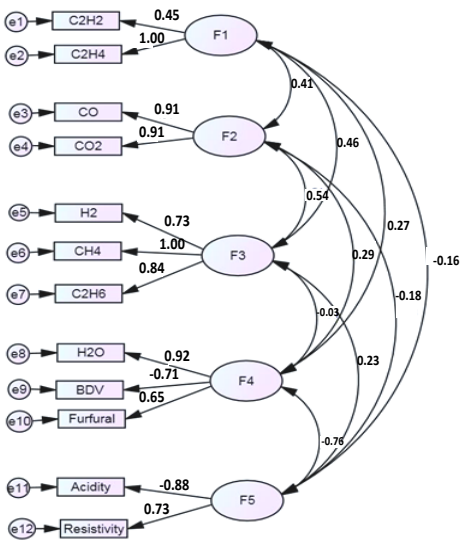

Fig. 2 Common factor analysis of oil test data

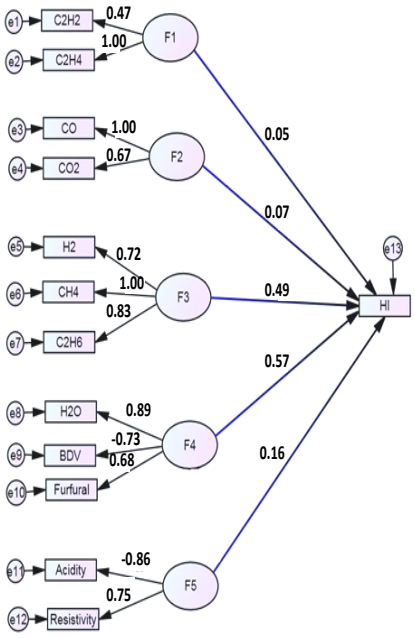

Fig. 3 The effects of common factors on health index

A Study on Suitability of Different Transformer Winding Models for Frequency Response Analysis

M. F. M. Yousof, *St. Member, IEEE*, Chandima Ekanayake, *Member, IEEE*, Tapan K. Saha, *Senior Member, IEEE*, and Hui Ma, *Member, IEEE*

***Abstract*--This paper discusses on the applicability of three methods namely *n*-ladder network, multi-conductor transmission line (MTL) and hybrid MTL to model the transformer winding frequency response. These methods have been used to model an actual transformer winding with end-to-end short circuit configuration. The corresponding model parameters are calculated based on winding construction and geometrical information. The frequency response curves obtained from different models are compared with the measured frequency response. Based on the obtained results, the suitability of considered techniques for modelling the end-to-end short circuit winding configuration is discussed.**

I. Key Figure

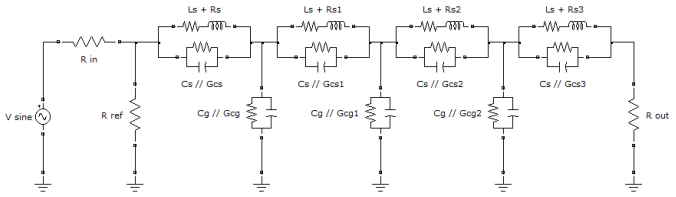

Fig. 1. *n*-stage ladder network model used in MATLAB

II. Key Equations

Key equations in MTL model are

$$d\boldsymbol{V}(x)/dx = -\boldsymbol{Z}\boldsymbol{I}(x) \quad (1)$$

$$d\boldsymbol{I}(x)/dx = -\boldsymbol{Y}\boldsymbol{V}(x) \quad (2)$$

$$\begin{bmatrix} \boldsymbol{I_S} \\ \boldsymbol{I_R} \end{bmatrix} = \begin{bmatrix} \boldsymbol{Y_C}\coth(\sqrt{\boldsymbol{ZY}}\,l) & -\boldsymbol{Y_C}\,csch(\sqrt{\boldsymbol{ZY}}\,l) \\ -\boldsymbol{Y_C}\,csch(\sqrt{\boldsymbol{ZY}}\,l) & \boldsymbol{Y_C}\coth(\sqrt{\boldsymbol{ZY}}\,l) \end{bmatrix} \begin{bmatrix} \boldsymbol{V_S} \\ \boldsymbol{V_R} \end{bmatrix} \quad (3)$$

$$\frac{V_{out}}{V_{in}} = \frac{V_R(n)}{V_S(1)} = \frac{\hat{\Phi}_{n+1,1} \cdot 50}{\hat{\Phi}_{1,1} \cdot 50 + \hat{\Phi}_{1,1} \cdot \hat{\Phi}_{n+1,n+1} + \hat{\Phi}_{n+1,1} \cdot \hat{\Phi}_{1,n+1}} \quad (4)$$

Hybrid MTL model introduces two new equations which are (5) and (6).

$$\boldsymbol{Y} = -\boldsymbol{Q}\left(\boldsymbol{I_n} + \boldsymbol{Y_s}\boldsymbol{Z}\right)^{-1} \quad (5)$$

$$\boldsymbol{Y_s} = diag(I_t^2 Y_{s1}, I_t^2 Y_{s2}, \ldots, I_t^2 Y_{sn}) \quad (6)$$

Mohd Fairouz Mohd Yousof (m.mohdyousof@uq.edu.au), Chandima Ekanayake (chandima@itee.uq.edu.au), Tapan Kumar Saha (saha@itee.uq.edu.au), and Hui Ma (huima@itee.uq.edu.au) are with the School of ITEE, The University of Queensland, St Lucia, Brisbane, QLD-4072, Australia.

III. Key Results

TABLE I
PARAMETER OF THE TRANSFORMER WINDING

Number of disc	40
Number of turns per disc	14
Conductor width (mm)	1.18
Conductor height (mm)	5.69
Conductor insulation thickness (mm)	0.20
Pressboard thickness between discs (mm)	2.05
Winding outer circumference (m)	0.562
Winding inner circumference (m)	0.396
Insulation thickness between HV and LV winding (mm)	3.28

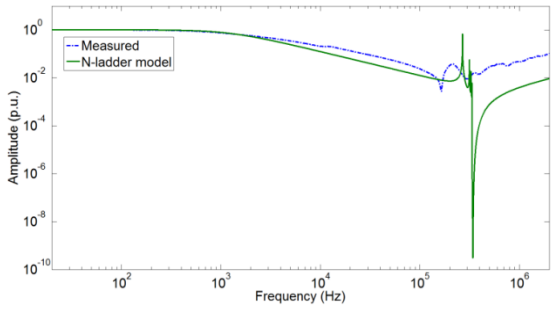

Fig. 2. Comparison between *n*-ladder network model and measurement

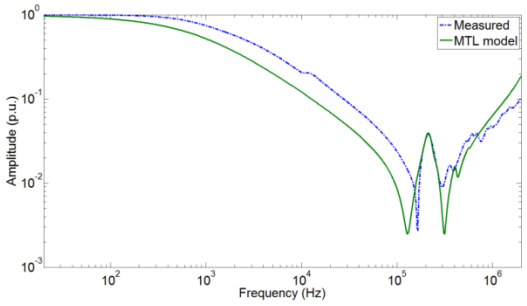

Fig. 3. Comparison between MTL model and actual measurement with small flux penetration

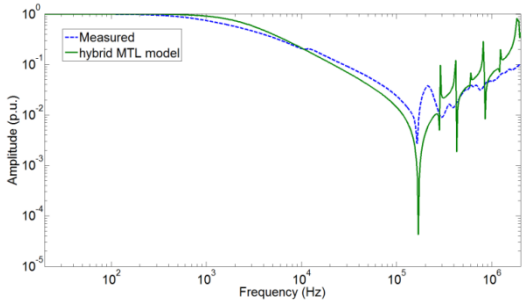

Fig. 4. Comparison between hybrid MTL model and actual measurement (α = 0.6)

Optimal Maintenance Strategy for Wind Turbines with Markov Decision Processes

Salman Kahrobaee, *Student Member, IEEE*, and Sohrab Asgarpoor, *Senior Member, IEEE*
Department of Electrical Engineering,
University of Nebraska-Lincoln, Lincoln, NE 68588, USA,
Email: *skahrobaee@huskers.unl.edu*, and *sasgarpoor1@unl.edu*

***Abstract*-- As wind power generation is growing, there are some concerns raised with regard to efficiency, and availability of wind turbines. Wind turbines consist of many moving and rotating subassemblies installed at high elevation. In addition, they are exposed to the weather changes including variable wind speed and temperature which not only affects the wind power generation, but also increases the chance of failure due to imposing stress on wind turbines' parts. Therefore, it is critical to develop an effective maintenance strategy to preserve the health, and improve the reliability of wind turbines. Inspection, corrective maintenance, preventive maintenance, and replacement are some of the options currently being practiced by maintenance supervisors for reliable, safe, and efficient operation of wind turbines. Using the estimated cost of selected maintenance strategies as well as penalties and rewards for having unhealthy or healthy equipment, the cost/benefits can be determined. We propose to develop an analytical technique for wind turbines, and quantify the equipment maintenance rate by maximizing the benefit or the availability of the equipment. We model the wind turbine operation using Markov Processes, and provide the results for the optimum inspection, and maintenance strategies based on the condition of wind turbine and the site.**

I. Key Figures

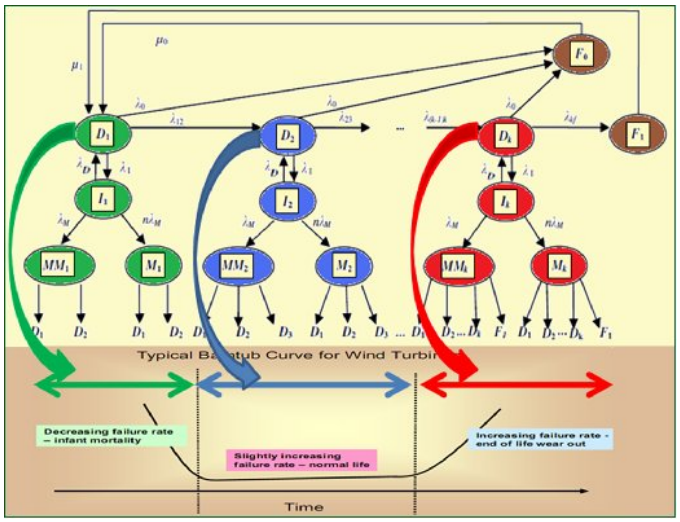

Fig. 1. The Markov Model proposed considering different operation durations of a wind turbine modeled by a bathtub curve

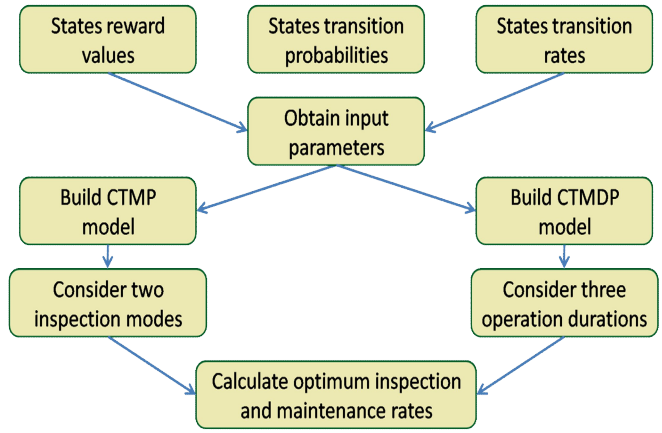

Fig. 2. Method of study based on Markov Process to determine the optimum maintenance rates.

II. Key Results

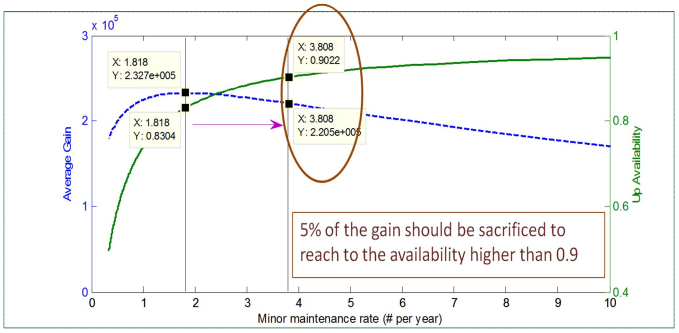

Fig.3. Average gain and turbine availability as a function of maintenance rate.

Inspection rate	First operation duration (first 3 years)	Middle operation duration (year 3 to 12)	Last operation duration (year 12 to 20)	Availability
4.4 times a day	do nothing	do nothing	do nothing	0.8304
Every 47 days	minor maintenance	do nothing	major maintenance	0.9787

Fig. 4. Optimum decisions based on continuous-time Markov Decision Process

Expanding the Global Reach of IEEE PES

What the organization has done and where it should go next

Laurie Stewart [#]*,Dr. Sarah Riforgiate[#], Dr. Noel N. Schulz*
Department of Communication Studies[#]
Department of Electrical & Computer Engineering*
Kansas State University
Manhattan, KS
lmstewar@ksu.edu

Abstract— IEEE and the IEEE Power & Energy Society (PES) are international organizations with members, chapters, conferences and activities worldwide. While both of these organizations were started in the United States, recent growth in membership has been strong outside North America. PES is reviewing its reach and impact outside of North America. PES is working to expand its impact on power and energy professionals globally. With this expansion there are many boundaries that must be explored. Currently, communication research for PES has found that personal interactions are the number one influencer for increasing PES member numbers and participation. It is important to see if this translates well into other countries. This poster will highlight the efforts and programs of PES to expand its global reach. It will also describe some of the cultural boundaries that PES must work with as it expands globally.
Keywords-global reach, communication

Cyber-Physical Security in a Substation

Junho Hong, *Student Member*, *IEEE*,
Chen-Ching Liu, *Fellow*, *IEEE*,
Washington State University

Email: jhong@eecs.wsu.edu, liu@eecs.wsu.edu

***Abstract*— Cyber-Physical security for a substation has been proposed. Cyber intrusion can be evaluated by temporal anomaly detection, which is based on attacker's generated foot print. IEEE 39-bus system has been used for testing. Its Supervisory Control And Data Acquisition (SCADA) system has been enabled to communicate with a control center. Intrusion scenarios have been conducted using the cyber-physical security testbed. The cyber attack consists of compromising the substation gateway and generating fake status & analog data. Synergy between cyber and power mitigation strategies has been tested.**

I. Temporal Anomaly Detection

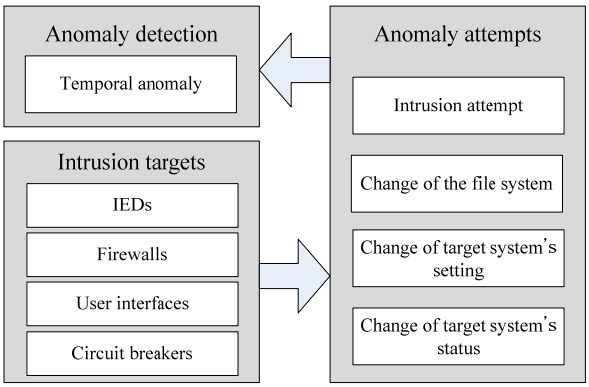

Fig. 1. Intrusion Detection in a Substation

II. Cyber-Physical security Testbed

Cyber intrusion scenarios have been conducted on the substation's IT network using a SCADA testbed at University College Dublin (UCD). The impact on power grid's operation condition was evaluated and a mitigation strategy implemented. The testbed consists of a simulated power grid and SCADA system. It comprises two control centers and two substations. A tool for power system simulation is modeling the electric grid. IEEE 39-bus system and its control center have been implemented. Control commands can be initiated from the substation and/or control center's user interface. The grid response is reported.

III. Intrusion Simulation and Mitigation

The first intrusion scenario involves compromising the substation gateway (T5). Attacker can monitor, modify and generate all measured analog and status values using the compromised gateway. A false signal is generated and a trigger open (T6) command is sent to substation Circuit Breaker (CB).

The second scenario is to generate forged CB status at the gateway. As a result, control center operators will observe fake data for the CB status. However, the actual status has not changed.

Mitigation actions are needed on substation IT and power grid. For IT mitigation, an Intrusion Detection System (IDS) has been used. An Optimal Power Flow (OPF) algorithm, with an objective function that minimizes the grid's load shedding costs, is used for power system mitigation.

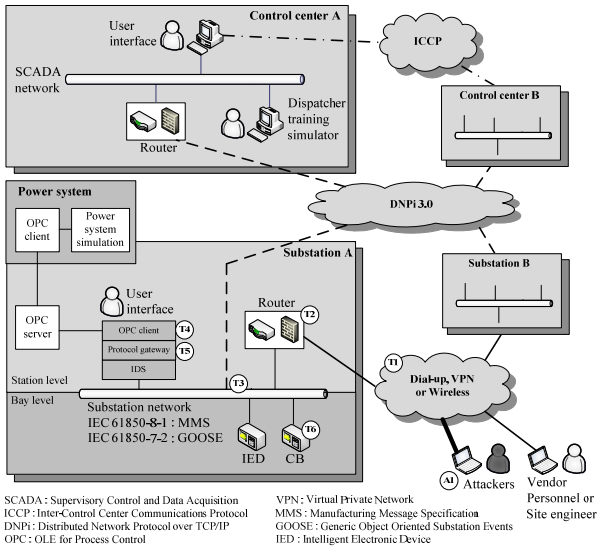

Fig. 2. Testbed for Cyber-Physical Security

IV. Conclusion

Cyber intrusions in the substation IT network have been tested and vulnerability assessment has been performed using the cyber-physical testbed. The proposed temporal anomaly detection algorithm, which is based on intruder's foot print, is able to detect cyber intrusions. The anomaly detection algorithm can be extended to perform a simultaneous substation attacks evaluation using the correlation coefficient between generated substations intrusion logs. Further efforts are required in order to implement the algorithm. Power system's mitigation strategy has been performed using OPF, which minimizes the load shedding costs.

A New Reliability Model of Direct Cyber-Power Interdependencies

Bamdad Falahati and Yong Fu
Department of Electrical and Computer Engineering, Mississippi State University, Mississippi State, 39762, USA
Email: *bf229@msstate.edu*, *fu@ece.msstate.edu*

Abstract— Smart grid initiatives are becoming more and more achievable through the use of information infrastructures that feature peer-to-peer communication, monitoring, protection and automated control. The analysis of smart grid operation requires considering the reliability of the cyber network as it is neither invulnerable nor failure free. In this Poster, four types of interdependencies are defined and a new concept of state mapping is proposed to map the failures in the cyber network to the failures of the power network. Furthermore, in order to evaluate the impact of direct cyber-power interdependencies on the reliability indices, two optimization models are introduced to maximize the data connection in the cyber network and minimize the load shedding in the power network. The effectiveness of proposed reliability evaluation method is shown by a smart microgrid application. The methodology presented in this poster is a start point to optimize the future power grid which has increasingly interdependencies between cyber and power networks.

I. Key Equations

Reliability Evaluation formulation:

$$\beta_w = \begin{cases} 1 & if \sum_{b=1}^{N_B} R_{rb} < N_b \\ 0 & if \sum_{b=1}^{N_B} R_{rb} = N_b \end{cases}$$

Optimization problem for the cyber-Power network:

$$Min \quad LC_i^T = \sum_{d=1}^{N_D} LC_d$$

S.t.

$$\sum_{l=1}^{N_L} \kappa_{ml} \cdot PL_l = \sum_{g=1}^{N_G} \mu_{mg} \cdot PG_g - \sum_{d=1}^{N_D} \lambda_{md} \cdot PD_d + \sum_{d=1}^{N_D} \lambda_{md} \cdot LC_d \qquad \forall m$$

$$PL_l = \frac{\theta_m - \theta_n}{x_{mn}} \qquad \forall l \in (m,n)$$

$$PG_g^{\min} \le PG_g \le PG_g^{\max} \qquad \forall g$$

$$0 \le LC_d \le PD_d \qquad \forall d$$

$$-PL_l^{\max} \le PL_l \le PL_l^{\max} \qquad \forall l$$

$$\theta_{ref} = 0$$

II. Key Flowchart

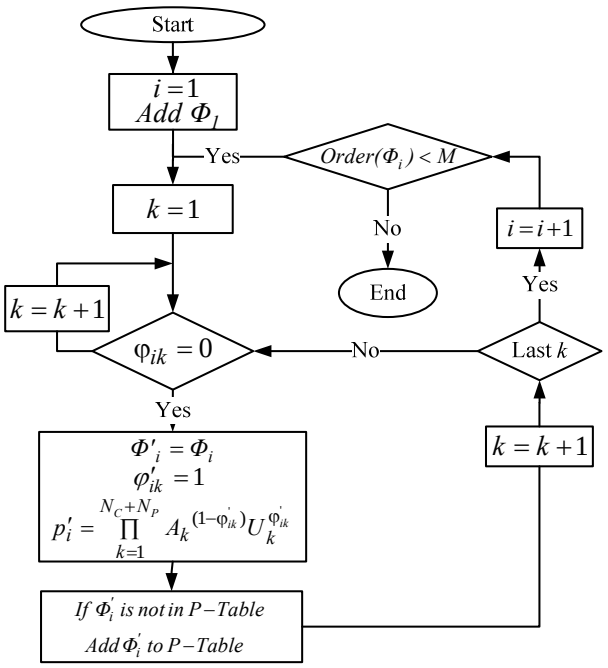

Fig. 1. Reliability assessment procedure

III. Key Results

TABLE I
LOLP and EENS of Four Different Topologies

Topology	# of Switches	LOLP	EENS (p.u)
Bus Topology	4	0.035844	0.083678
Ring -1	5	**0.021643**	**0.01924**
Redundant Star	6	0.021659	0.019132

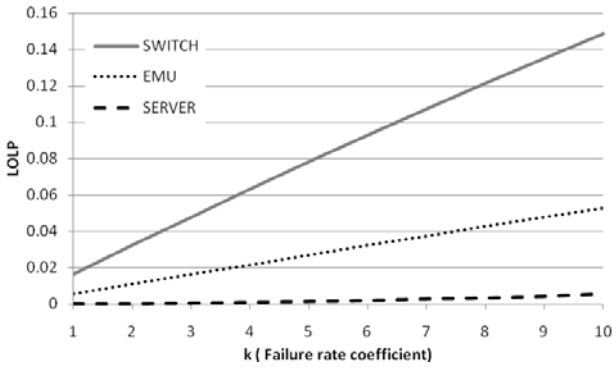

Fig. 2. LOLP of the cyber-power system vs failure rates

Defend-Attack-Defend in Power Grid: Global Optimality with transmission line switching

Wei Yuan, Long Zhao, and Dr. Bo Zeng

Department of Industrial and Management Systems Engineering
University of South Florida, Tampa, Florida 33620
Email: {weiyuan,longzhao}@mail.usf.edu, bzeng@usf.edu

***Abstract*—Power grid vulnerability is a major concern for our society. Defend-Attack-Defend (DAD) Models are widely used in power grid contingencies and security studies. Line switching, which is one of the most effective operations to mitigate deliberate outages or attacks, is introduced to alleviate transmission violation and reducing operating cost.**

In this paper, we introduce transmission line switching operations represented by binary decision variables in the third level, the Optimal Power Flow model (OPF), to the Defend-Attack-Defend (DAD) model. This formulation enables that the power grid operators can switch off transmission lines once an attack is realized on the power grid to mitigate the damage. Then the model is regarded as a two stage robust optimization with mixed integer recourse problem.

A novel algorithm, nested column and constraint generation (NCCG) algorithm, is presented as an efficient algorithm to solve the problem to global optimality. This algorithm is a finitely convergent and derives an exact solution.

Numerical results are computed and provided based on IEEE 24 bus reliability test system. We will also study the Defend-Attack-Defend (DAD) Models without transmission line switching and compare the results of Defend-Attack-Defend (DAD) Models with transmission line switching to evaluate the benefits of transmission line switching.

I. Key Equation

The mixed integer nonlinear programming (MINLP) formulation of the Defend-Attack-Defend model with transmission line switching is shown below,

$$\min_{\mathbf{w}\in\mathbb{W}} \max_{\mathbf{v}\in\mathbb{V}} \min_{\{\mathbf{z},\mathbf{p_l},\mathbf{g_j},\mathbf{d_n},\delta_\mathbf{n}\}} \sum_{n\in\mathcal{N}} d_n \tag{1}$$

$$st.\ \ p_l x_l = z_l(w_l + v_l - w_l v_l)[\delta_{O(l)} - \delta_{D(l)}],\ \ \forall l \tag{2}$$

$$\sum_{j\in\mathbf{Jn}} g_j - \sum_{l|O(l)=n} p_l + \sum_{l|D(l)=n} p_l + d_n = D_n, \forall n \tag{3}$$

$$-p_l^{max} \le p_l \le p_l^{max},\ \ \forall l \tag{4}$$

$$-\delta^{max} \le \delta_n \le \delta^{max},\ \ \forall n \tag{5}$$

$$0 \le g_j \le g_j^{max},\ \ \forall j \tag{6}$$

$$0 \le d_n \le D_n,\ \ \forall n \tag{7}$$

$$z_l \in \{0,1\},\ \ \forall l \tag{8}$$

Where,

$\mathbb{W} = \{w_l \in \{0,1\}, \sum_l w_l \le R\}$ defender's hardening decision set.

$\mathbb{V} = \{v_l \in \{0,1\}, \sum_l (1-v_l) \le S\}$ attacker's attack decision set

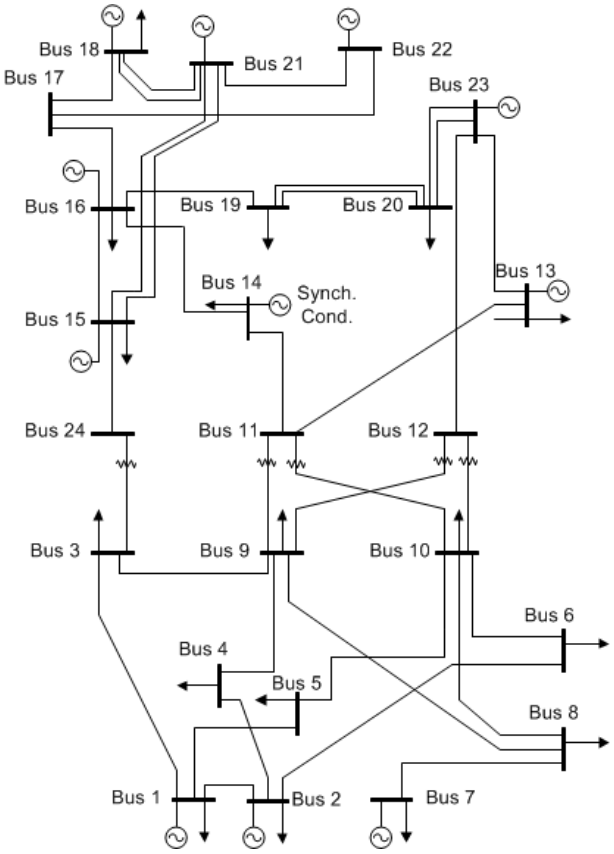

Fig. 1. IEEE 24 bus reliability test system

z_l is the binary line switching decisions variables.

p_l, g_j,d_n,δ_n are decision variables for transmission line power flow, generating level of generators,load shed, and phase angles of buses separately.

A linearized formulation of the above model is given in solving this model. A cutting plane based nested column and constraint generation (NCCG) algorithm will be presented and implemented in the poster.

II. Key figures

An case study based on IEEE 24 bus reliability test system is conducted to test the algorithm.

Power Systems Operations Planning with Coordinated Cyber Attacks

Siddharth Sridhar and G. Manimaran
Department of Electrical and Computer Engineering
Iowa State University
Ames, Iowa 50010
Email: sridhar, gmani@iastate.edu

***Abstract*—Existing power system operations planning techniques make provision for $(N-1)$ contingencies within its scope. This approach was acceptable for cases where component failures occurred naturally and were not induced. With extensive use of computer systems for monitoring and control of physical processes in the power system, the attack surface has increased tremendously, thus exposing the system to coordinated cyber attacks. The operations planning processes should now accommodate cases of $(N-k)$ contingencies, where $k > 1$. However, operating the system at an operating point that is $(N-k)$ secure at all times is not economically viable. Given that these events are low-frequency events, it is important to develop a mitigation strategy that constrains system operation only when a coordinated cyber attack is imminent. This poster presents our proposed approach to mitigating coordinated cyber attacks directed at power systems, given this constraint.**

I. Existing Operations Planning Approaches

The shortcomings of existing approaches are as follows - i) Only $(N-1)$ contingencies are accounted for, ii) cyber threats are not included within the scope, and iii) threat scenarios considered are "static", that is, the probability of component failure does not change dynamically as in the case of cyber attack probability. To overcome these, the following operations planning framework is proposed.

II. Proposed Approach

Fig. 1 presents the proposed framework that includes coordinated cyber attacks within the scope of power systems operations planning. The framework consists of four sequential steps. Of these, steps 1 and 2 are performed offline and steps 3 and 4 are done online.

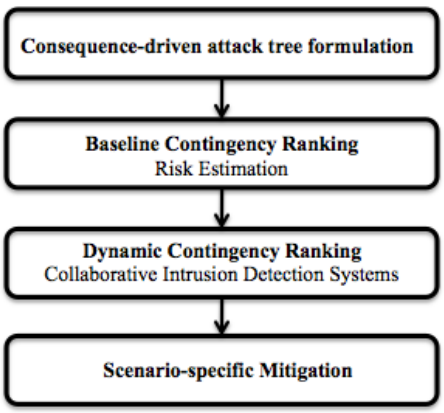

Fig. 1. Framework for Operations Planning

1. Consequence-driven Attack Tree Formulation: The possible number of coordinated attack vectors (CAV) that can be obtained from combinations of physical and cyber components in a system is enormous. It is infeasible to address impact from each and every CAV. Instead, a consequence-driven approach (advocated by NERC Cyber Attack Task Force), in which the different CAV that lead to a particular scenario/consequence of interest are identified will be adopted. The idea is to develop algorithms that smartly enumerate impactful CAV for a given system without following a brute force enumeration approach. This step will provide a set of different CAV for a particular scenario to step 2.

2. Baseline Contingency Ranking: The risk metric is a combination of *credibility* of a contingency - the likelihood that it will happen, and its *severity* - the consequence if it is successful. We define risk as the product of the probability of a given successful coordinated cyber attack $(P(Z))$ and the impact it causes on the physical system security or adequacy (γ). This risk metric provides a baseline ranking for CAVs, which is provided to step 3.

3. Dynamic Contingency Ranking: Power system operators face a security vs. economy decision during operations planning. Operating the system at an $(N-k)$ secure state at all times is not economically viable. The need is to make the system $(N-k)$ secure only when an attack is imminent. To this end, we propose a collaborative intrusion detection system that provides the control center with information on imminent CAVs. This solution will alter the baseline ranking depending on the current state of the cyber system, thus assisting the system operator in decision making. This refreshed ranking will be provided to the operator to make operational decisions in step 4.

4. Scenario-specific Mitigation: The mitigation depends on the coordinated attack vector indicated by the ranking. For example, contingencies that involve tripping multiple transmission lines may require modifying pre-attack operating points to constrain transmission flow. Mitigation requires the identification of a safe operating region by defining security boundaries. The final step in this framework will include modification of system operating points such that the system is secure even if the attack is successful.

A Secure and Privacy-Preserving Communication Scheme for AMI Network

Pan Deng and Liuqing Yang
Department of Electrical and Computer Engineering
Colorado State University
Fort Collins, CO 80523
wsdp@lamar.colostate.edu, lqyang@engr.colostate.edu

***Abstract*—As a core component of the future smart grid, Advanced Metering Infrastructure (AMI) integrates a two-way communications network which enables utilities and customers to actively monitor and manage their energy use. While the deployment of AMI brings enormous industrial and social benefits, security and privacy issues in this huge network need to be properly addressed. In this poster, we propose a data communication scheme for the AMI network with particular considerations on these issues. In our approach, we require strict device authentication when a smart meter joins or leaves the network. Data confidentiality as well as customer privacy associated with sensitive metering data are protected by taking advantage of in-network aggregation with homomorphic encryption. Each in-network message is digitally signed for data integrity. Security analysis shows the resistance of our proposed scheme to typical cyber-attacks. Performance evaluation based on simulations also confirms that our scheme is feasible in terms of total aggregation time.**

I. Key Equations

These equations illustrate the data aggregation process for a simplified aggregation tree as shown in Fig. 3.

$$C_2 = E(D_2), S_2 = S(C_2||TS)$$
$$C_3 = E(D_3), S_3 = S(C_3||TS)$$

$$M_2 \rightarrow M_1 : \{C_2, S_2\}$$
$$M_3 \rightarrow M_1 : \{C_3, S_3\}$$

$$I_1 = C_1 * C_2 * C_3 \bmod n^2$$
$$S_1 = S(I_1||TS)$$
$$M_1 \rightarrow \text{Collector} : \{I_1, S_1\}$$

$$D_{final} = D(I_1 * I_4 \bmod n^2)$$
$$= \sum_{i=1}^{5} D_i \bmod n = \sum_{i=1}^{5} D_i$$

II. Key Figures

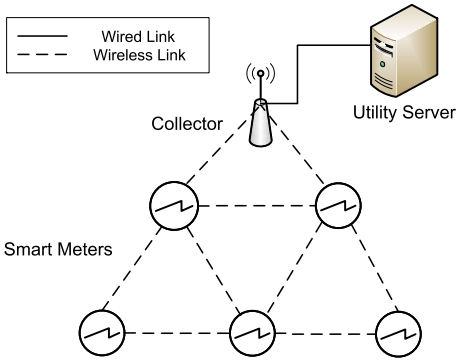

Fig. 1. AMI network architecture

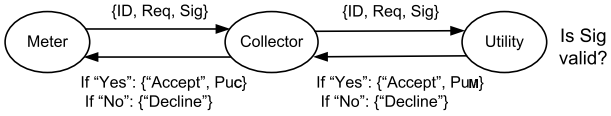

Fig. 2. Device Registration Process

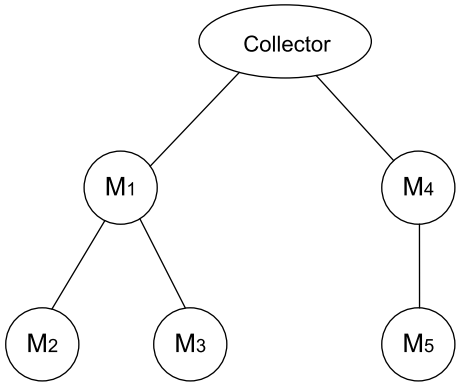

Fig. 3. A simplified aggregation tree

Risk Assessment Based on Information Entropy of Cascading Failure in Power Systems

Youwei Jia, *IEEE Student Member*, Zhao Xu, *Member, IEEE*

***Abstract*—Along with the high pace of power network interconnection development in recent years, power system operational uncertainty is increasing rapidly and system dynamic behavior is becoming more and more complicated, which makes the risk assessment of cascading failures and catastrophic events in power systems more challenging. Therefore advanced methods of high reliability to assess risks of cascading failures under various power systems operation conditions need to be developed. In this paper, a risk assessment framework for cascading failures based on the information entropy principle has been developed. The developed method aims at identifying the worst case cascading development among all other possibilities to support system operators in preparing countermeasures accordingly beforehand. A case study of cascading failure analysis for IEEE 30-bus system is carried out in details. *N-1* contingencies are selected as the initiating events of cascading failures. The weighting factors of all types of severity (i.e. transmission line overload, bus voltage violation, real/reactive power violation of generators) are determined by entropy principle, as compared with conventional methods which use fixed values according to expertise information with different focus. Finally, the feasibility and effectiveness of this proposed approach are demonstrated through MATLAB. The results show a high potential of this proposed method for further research and application.**

I. KEY EQUATIONS

- Entropy weight

The entropy of an index is defined as:

$$H_i = -k\sum_{j=1}^{n} f_{ij} \ln f_{ij} \qquad i = 1, 2, \cdots, m \tag{1}$$

The entropy weight of the i^{th} index is defined as:

$$\omega_i = \frac{1 - H_i}{m - \sum_{i=1}^{m} H_i} \tag{4}$$

- Severity of violation

i) Transmission line overload

$$Sev(L) = \begin{cases} \sum_i \left(\frac{F_{ki} - F^s_{k\,i}}{F^s_{k\,i}}\right)^{2m} & F_{ki} > 1.4F^s_{k\,i} \\ 0 & F_{ki} < 1.4F^s_{k\,i} \end{cases} \tag{5}$$

ii) High-limit/low-limit bus voltage violation

$$Sev(V_H) = \begin{cases} \sum_i \left(\frac{\Delta V_i}{V_{i-upper}}\right)^2 & V_i > V_{upper} \\ 0 & V_i < V_{upper} \end{cases} \tag{6}$$

$$Sev(V_L) = \begin{cases} \sum_i \left(\frac{\Delta V_i}{V_{i-lower}}\right)^2 & V_i < V_{lower} \\ 0 & V_i > V_{lower} \end{cases} \tag{7}$$

iii) Active/reactive power violation of generators

$$Sev(P) = \begin{cases} \sum_i \left(\frac{\Delta P_i}{P_{i-margin}}\right)^2 & P_i < P_{\min} or P_i > P_i > P_{\max} \\ 0 & P_{\min} \le P_i \le P_{\max} \end{cases} \tag{8}$$

$$Sev(Q) = \begin{cases} \sum_i \left(\frac{\Delta Q_i}{Q_{i-margin}}\right)^2 & Q_i < Q_{\min} or Q_i > Q_i > Q_{\max} \\ 0 & Q_{\min} \le Q_i \le Q_{\max} \end{cases} \tag{9}$$

- Risk assessment based on entropy weight

$$Sev = w_L Sev(L) + w_{V_H} Sev(V_H) + w_{V_L} Sev(V_L) + w_P Sev(P) + w_Q Sev(Q) \tag{10}$$

$$R(X) = P(X) \cdot Sev(X) \tag{11}$$

II. KEY FIGURE

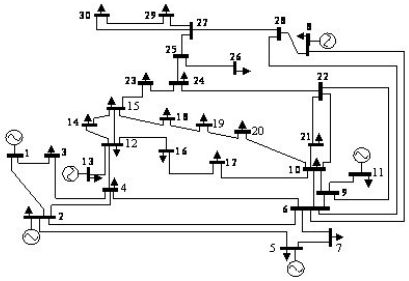

Fig. 1. Schematics of IEEE 30-bus system

III. KEY RESULTS

TABLE I. RISK RANKING OF CASCADING CHAINS

Ranking	Outage chains	Total risk	Load shedding
1	6,7,5,15,19,21	0.9397	251.45MW
2	6,7,18,15,19,21	0.2484	82.34MW
3	6,7,1,15,19,21	0.1953	32.12MW
4	6,3,2	0.1762	0
5	6,3,4	0.1718	0

The total load loss was taken as the severity criterion, the resulted risk based ranking matched the load loss based in Table I, which demonstrates the effectiveness of the proposed risk assessment approach.

Hybrid Multi-terminal LCC HVDC with a VSC converter: A case study of Simplified South East Australian System

Mai H. Nguyen[1,2], Tapan K. Saha[1,2] and Mehdi Eghbal[1]
[1] Queensland Geothermal Energy Centre of Excellence
[2] School of Information Technology and Electrical Engineering
The University of Queensland, Brisbane, Australia

***Abstract*— The hybrid multi-terminal HVDC (MTDC) with a combination of LCC (Line Commutated Converter) and VSC (Voltage Source Converter) eliminates all the disadvantages of these two HVDC technologies. Complex control schemes are required to operate this system under different operating conditions. This paper presents control schemes for a hybrid MTDC to guarantee a safe operation under different loading conditions and when faults occur. The developed control scheme is implemented on the Simplified South East Australian 14 generator system in DIgSILENT PowerFactory environment. The simulation results demonstrate the effectiveness of the proposed control scheme in reducing the grid active power losses and significantly improving the system transient stability.**

Keywords- Multi-terminal HVDC, LCC HVDC, VSC HVDC, transient stability

I. INTRODUCTION

The proposed hybrid MTDC configuration:

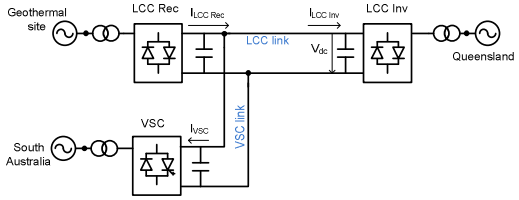

TABLE I ACTIVE POWER LOSS OF GRID WITH AND WITHOUT THE VSC STATION

Case	Heavy loading		Medium heavy loading	
	Without VSC	With VSC	Without VSC	With VSC
P_{loss} (MW)	950	748	604	593

II. SIMULATION RESULTS

A. Heavy loading condition

1) LCC Inverter

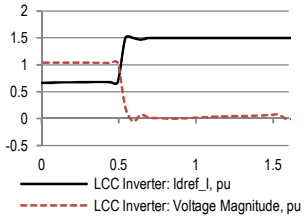

Extinction Angle control

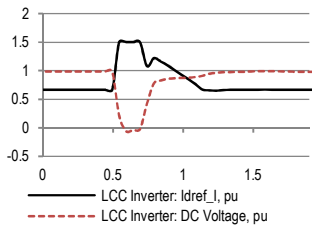

DC Voltage control with VDCOL

2) LCC Rectifier

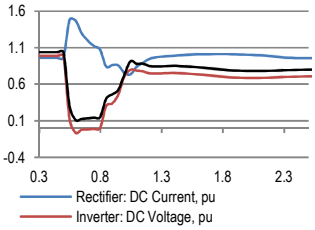

DC current control without VDCOL

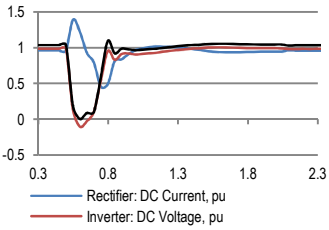

DC current control with VDCOL

3) VSC Station

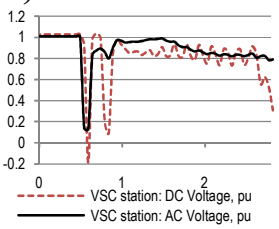

DC voltage control

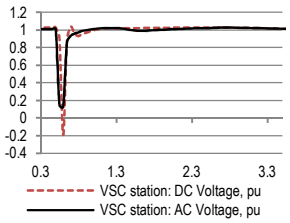

Active power control

B. Medium heavy loading condition

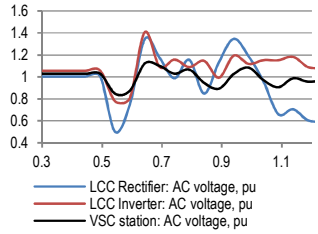

With original VDCOL

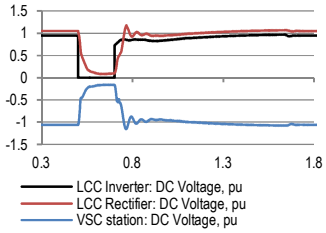

With tuned VDCOL

III. CONCLUSION

• LCC inverter station could not be operated in constant extinction angle control mode.

• At LCC rectifier, current control is more robust compared to the active power one.

• VSC station should not be operated in DC voltage control mode

• VDCOL function should be installed in both LCC rectifier and inverter. However, the parameters of VDCOL need to be properly tuned for each operating condition

Design of Robust Power Oscillation Damping Controller for Large-scale PV Plant

Rakibuzzaman Shah, *Student Member, IEEE*, N. Mithulananthan, *Senior Member, IEEE*, and Kwang.Y.Lee, *Fellow, IEEE*

***Abstract*— Large-scale photovoltaic (PV) plants are becoming a reality in many countries. Studies suggest that the large-scale PV plants can have either a positive or negative influence on power system oscillation, which depends on many factors, including their location and sizes. Given the fact that these plants cannot be located in their ideal location for placement in power system, it is important to consider designing controllers for flawless integration. In this paper, a minimax Linear Quadratic Gaussian (LQG) based power oscillation damper (POD) for large-scale PV plant is proposed for oscillation damping. As a benchmark system for oscillatory stability analysis, the two-area test system is used to demonstrate the system performance with the designed controller. The robustness of the designed controller is verified under different operating conditions by eigenvalue analysis and non-linear power system simulation. Simulation results demonstrate that the proposed controller for PV plant improves the damping of inter-area mode for a wide range of operating conditions.**

I. Key Equations

State-space representation of linearized power system with uncertainty can be expressed as

$$\Delta\dot{x}(t) = A\Delta x(t) + B_1\Delta u(t) + B_2\xi(t) + B_2 w(t) \quad (1)$$

$$y(t) = C_2\Delta x(t) + D_2\xi(t) + D_2 w(t) \quad (2)$$

$$\zeta(t) = C_1\Delta x(t) \quad (3)$$

The uncertainty input ξ can be expressed by equation (4)

$$\xi = \tilde{\phi}\,\tilde{C}_1\,\Delta x \quad (4)$$

The state and output equations of minimax LQG optimal controller can be expressed as

$$\dot{x}_c = (A - B_1 G_\tau^{-1}\gamma_\tau^T)x_c - ((B_1 G_\tau^{-1} B_1^T - \frac{1}{\tau}B_2 B_2^T)X_\infty)x_c$$
$$+ (I - \frac{1}{\tau}Y_\infty X_\infty)^{-1}(Y_\infty C_2^T + B_2 D_2^T) \quad (5)$$
$$\times (D_2 D_2^T)^{-1}(y - (C_2 + \frac{1}{\tau}D_2 B_2^T X_\infty)x_c)$$

$$u = -G_\tau^{-1}(B_1^T X_\infty + \gamma_\tau^T)x_c \quad (6)$$

R. Shah and N. Mithulananthan are with the School of Information Technology and Electrical Engineering, The University of Queensland, Australia (e-mail: md.shah@uq.edu.au; mithulan@itee.uq.edu.au)

K. Y. Lee is with Department of Electrical and Computer Engineering, Baylor University, Waco, TX 76798-7356, USA (e-mail: Kwang_Y_Lee@baylor.edu).

II. Key Results

TABLE I
EM Modes of Closed-Loop System with Full-Order Minimax LQG POD

EM Mode Index	Mode Type	Eigenvalues of closed-loop system (Full order controller)	Freq.(Hz)	% damping of closed-loop system (Full order controller)
1	Inter-area	-0.167±j3.24	0.51	5.15
2	Local	-0.479±j6.05	0.96	7.89
3	Local	-0.4818±j6.25	0.97	7.73

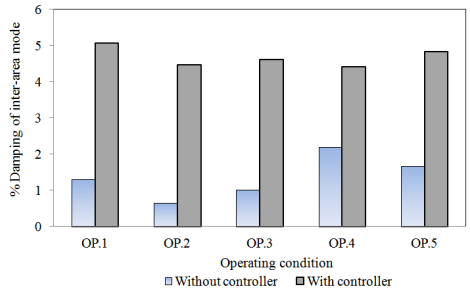

Fig. 1 Percentage of damping for operating conditions

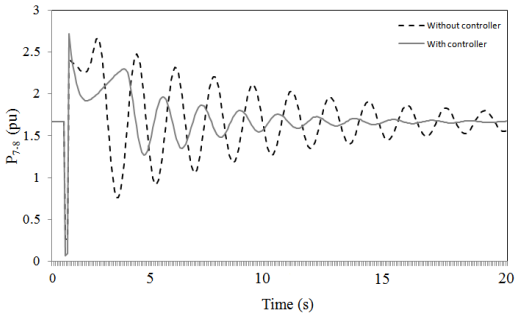

Fig. 2 Oscillation of active power

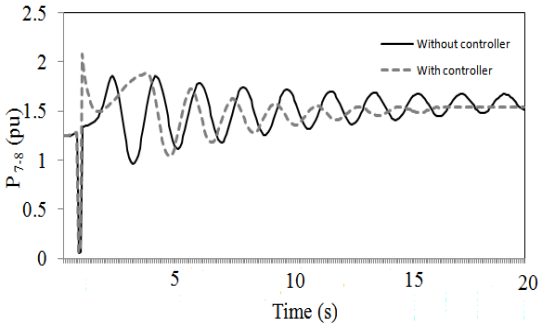

Fig. 3 Oscillation of active power in tie-line for OP.5

Design Considerations in Development of Active Mobile Substations

Nima Yousefpoor, Babak Parkhideh and Subhashish Bhattacharya
Future Renewable Electric Energy Delivery and Management (FREEDM) System Center
Department of Electrical and Computer Engineering
North Carolina State University
Raleigh, NC 27695
{nyousef, bparkhi, sbhattacharya}@ncsu.edu

***Abstract*— This paper proposes *transmission*-level active mobile substations that provide back-up in case of power transformer failure or forced reduced operation scenarios in addition to power flow control for seasonal renewable energy transmission. These functions altogether have been aggregated not only because of the technical merits but also to address the economic concerns regarding the cost of the power electronics for transmission applications. The proposed technology is called Convertible Static Transmission Controller (CSTC) which is transportable and connected across the substation power transformer and can be reconfigured to the required modes of operation. The power electronic building block for CSTC is the standard three phase 10-20 MVA drive converter which its high availability and reliability can reduce the overall cost of the power electronics for utility applications. In order to obtain high efficiency and low generated harmonic distortions, a group of converters are operated with line frequency (60Hz) and staggered with medium voltage Harmonic Neutralizing (HN) circuits through the proposed advanced angle control structure vs. PWM methods. From the supervisory control point of view, while the CSTC can operate similarly to BTB HVDC or UPFC applications, it can also operate as the substation voltage/phase angle regulator. The latter enables the CSTC to operate locally without changing the substation power flow and consequently the meshed power system. This mode of operation can be deployed to extend the life time of the existing power transformers without complicating the power system operation and be used as an asset management tool for utilities and system operators.**

Keywords-Active Mobile Substation; Recovery Transformer; Transformer life extender; Disaster Management

I. KEY FIGURES

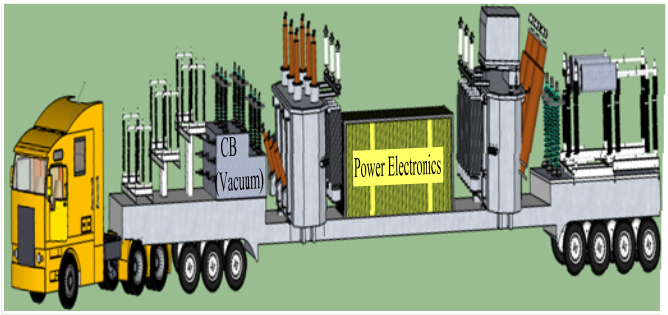

Figure 1. Conceptual illustration of the proposed active mobile substation

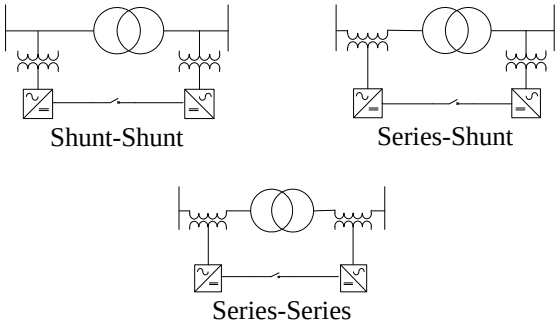

Figure 2. Different connecting configurations of the CSTC at the substation.

II. KEY RESULTS

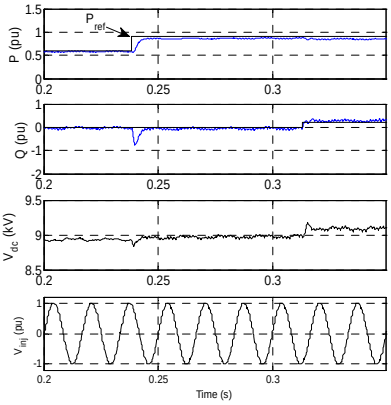

Figure 3. PSCAD simulation results for 20MVA active mobile substation operation in BTB HVDC mode; angle-controlled

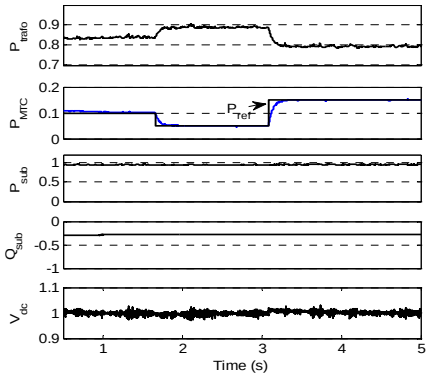

Figure 4. PSCAD simulation results in per unit for AMS operation for transformer partial bypass

ATP Modeling of Internal Transformer Faults for Relay Performance Testing

Elizaveta O. Egorova, *Student Member, IEEE*
Department of Electrical and Computer Engineering
Michigan Technological University, Houghton, MI
Email: eoegorov@mtu.edu

Abstract—**Transformers are very important elements of any power system. Unfortunately, they are subjected to through-faults and abnormal operating conditions which can affect not only the transformer itself but also other equipment connected to the transformer. Thus, it is essential to provide sufficient protection for transformers as well as the best possible selectivity and sensitivity of the protection. Nowadays microprocessor-based relays are widely used to protect power equipment. Current differential and voltage protection strategies are used in transformer protection applications and provide fast and sensitive multi-level protection and monitoring.**

The elements responsible for detecting turn-to-turn and turn-to-ground faults are the negative-sequence percentage differential element and restricted earth-fault (REF) element, respectively. During severe internal faults current transformers can saturate and slow down the speed of relay operation which affects the degree of equipment damage.

The scope of this work is to develop a modeling methodology to perform simulations and laboratory tests for internal faults such as turn-to-turn and turn-to-ground for two step-down power transformers with capacity ratings of 11.2 MVA and 290 MVA. The simulated current waveforms are injected to a microprocessor relay to check its sensitivity for these internal faults. Saturation of current transformers is also studied in this work.

All simulations are performed with the Alternative Transients Program (ATP) utilizing the internal fault model for three-phase two-winding transformers. The tested microprocessor relay is the SEL-487E current differential and voltage protection relay.

I. KEY EQUATIONS

The key equations are given for the negative-sequence percentage restraint differential element and for the restricted earth-fault element of the SEL-487E relay.

$$IOP87Q = |\sum 3I2kC| \quad (1)$$

$$RST87Q = \max(|3I2kC|) \quad (2)$$

$$3I2 = |1\ a^2\ a| \times \begin{vmatrix} IAkCFC \\ IBkCFC \\ ICkCFC \end{vmatrix} \quad (3)$$

$$3I_0 = I_A + I_B + I_C \quad (4)$$

$$I_N = I_A + I_B + I_C \quad (5)$$

II. KEY FIGURES

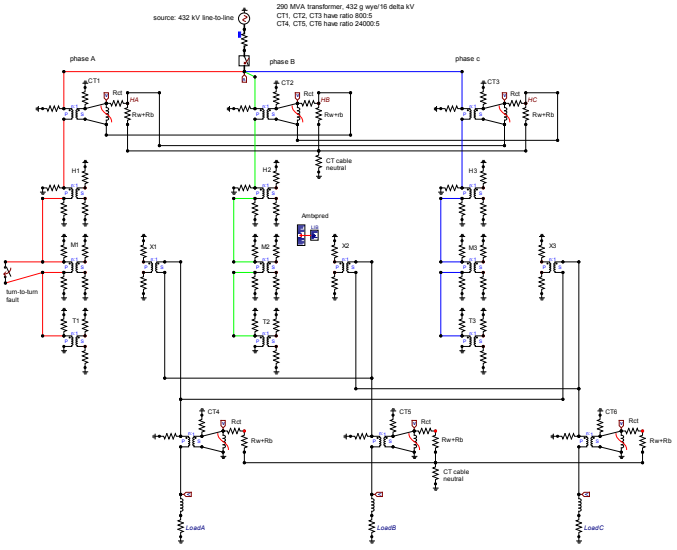

Figure 1. ATP configuration of the 290-MVA transformer for turn-to-ground faults.

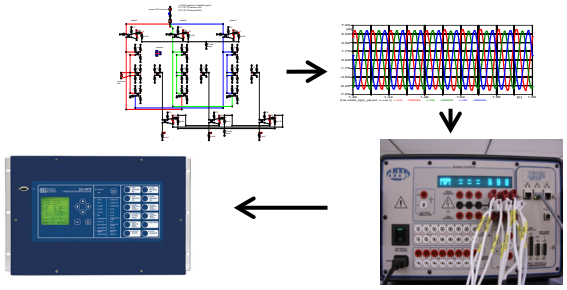

Figure 2. Modeling methodology: ATP model-pl4 file-Doble Test Set-SEL-487E relay.

III. KEY RESULTS

The results showed that the ATP internal fault model can be used for testing microprocessor relays for any percentage of turns involved in an internal fault. An interesting observation from the experiments was that the SEL-487E relay is more sensitive to turn-to-turn faults than advertized for the transformers studied. The sensitivity of the restricted earth-fault element was confirmed. CT saturation cases showed that low accuracy CTs can be saturated with a high percentage of turn-to-turn faults, where the CT burden will affect the extent of saturation.

Calculation of Available Transfer Capability under Transient Stability Constraints for Tie-lines Considering N - 1 Contingencies

Masashi Hitosugi, Yuta Ohsaki, Shinichi Iwamoto
Power Systems Laboratory, Department of Electrical Engineering and Bioscience, Waseda University, 169-8555, Tokyo Japan
Hideo Hosogoe, Mitsuhiro Matsumoto
Tohoku Electric Power Company, Sendai, 980-8550, Miyagi, Japan
Email: hitosugi.masashi.pwrs@gmail.com

***Abstract*—Fast and accurate evaluation of the available transfer capability (ATC) of tie-lines has become an increasingly important problem in the deregulation process from the viewpoint of the effective network utilization. Therefore, we propose an efficient calculation method of ATC under transient stability constraints in this paper. First, we considerably reduce the calculation time by focusing on ATC characteristics. Second, we propose (1) a new index that rapidly determines critical cases by using a transient energy function, and (2) an ATC calculation method that uses the relation between an increment of generator output and critical clearing time, which is determined by trial and error. Finally, we compare ATC for the tie-line fault case with the ATC estimated by the proposed method. We validate the method by running simulations using an Institute of Energy Economics Japan EAST 10-machine 47-bus power system.**

Ⅰ. KEY EQUATIONS

$$ATC_{estimate} = \frac{\Delta Ptie \times (0.1 - CCT_{present})}{CCT_{future} - CCT_{present}}$$

$$\begin{aligned} V_i &= \int_0^t (M_i \frac{d\omega_i}{dt} - P_{mi} + P_{ei}(Y^P, \theta) + R_i P_{COA}) \cdot \omega_i dt \\ &= \int_0^{\omega_i} (M_i \omega_i) d\omega_i + \int_{\theta_i^s}^{\theta_i} (-P_{mi} + P_{ei}(Y^P, \theta) + R_i P_{COA}) d\theta_i \\ &= \frac{1}{2} M_i \omega_i^2 + \int_{\theta_i^s}^{\theta_i} (-Pm_i + Pe_i(Y^P, \theta) + R_i P_{COA}) d\theta_i \\ &= V_{ki} + V_{pi} \end{aligned}$$

$$\text{Proposed\_index} = \left(V_{iup}^{1pu}(T_{cl}) - V_{iup}^{base}(T_{cl})\right) \times \theta_{iup}^{1pu}(T_{cl})$$

Ⅱ. KEY FIGURES

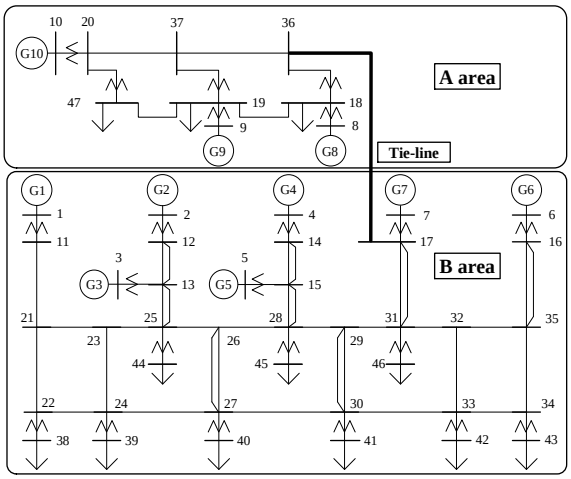

Figure 1 EAST 10-machine 47-bus power system

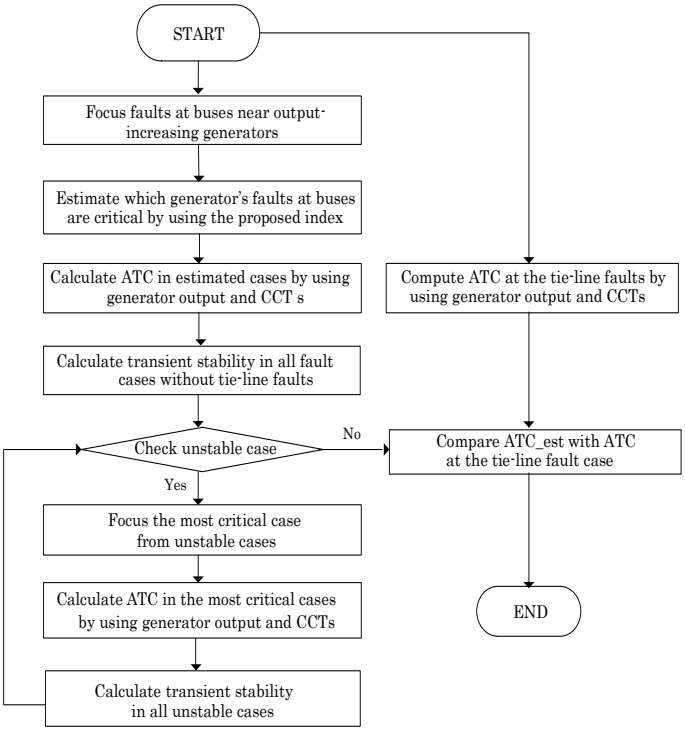

Figure 2 The flowchart of the proposed method

Ⅲ. KEY RESULTS

Table 1 Accuracy of the proposed method

case	ATC (TrueValue)	ATC (Proposed Method)
G10_up-Gall_down fault20-other37	0.76	0.77
G10_up-Gall_down fault36-other17	0.90	0.89

Table 2 Accuracy of unstable-case screening method

case	stepping-out time[s]	rank	True_ATC[pu]	rank
G10/fault20-other37	1.14	**1**	0.90	**1**
G10/fault37-other36	1.19	**2**	0.93	**2**
G9/fault37-other36	1.34	**3**	1.00	**3**
G10/fault36-other37	1.96	4	1.20	5
G10/fault37-other20	2.15	5	1.14	4
G9/fault36-other37	2.70	6	1.27	7
G9/fault19-other18	3.85	7	1.22	6

Electromechanical Mode Estimation Using Instrumental Variable Method

Yong Jia[1,2], *Student Member*, *IEEE*, Zhengyou He[1], *Member*, *IEEE*, Yilu Liu[2], *Fellow*, *IEEE*
1. Department of Electrical Engineering, Southwest Jiaotong University, Chengdu, Sichuan 610031, China
2. Department of Electrical Engineering and Computer Science, Univeristy of Tennessee, Knoxville, TN 37909, USA
Email: yongjgy@hotmail.com, hezy@swjtu.cn, *and* liu@utk.edu.

***Abstract*— Measured ambient data in power systems are known to contain the characteristics of electromechanical modes that give considerable insight into dynamic stability. This paper discusses the use of the Instrumental Variable (IV) method to estimate power system electromechanical modes. An auto-regressive moving-average (ARMA) model is used to describe a block of random ambient data, and the Least Squares (LS) and IV methods are used to estimate the auto-regressive (AR) parameters. Accuracy of the frequency and damping ratio of oscillations are used to measure the performance of these methods. Based on the two-area test model and actual ambient power system data, comparison of the two methods demonstrates that the IV method has better accuracy.**

I. KEY EQUATIONS

The guiding equations of the immune based controller are:

$$y(k) = -\sum_{i=1}^{na} a_i y(k-i) + \sum_{i=0}^{nc} c_i e(k-i) \tag{1}$$

$$\begin{aligned} &\varphi(k) = [-y(k-1), -y(k-2), \cdots, -y(k-na)]^{\mathrm{T}} \\ &\theta = [a_1, a_1, \cdots, a_{na}] \\ &v(k) = C(q^{-1})e(k) \end{aligned} \tag{2}$$

$$\begin{aligned} &\hat{\theta} = \arg\min V_N(\theta) \\ &V_N(\theta) = \frac{1}{N}\sum_{k=1}^{N} \frac{1}{2}\varepsilon^2(k \mid \theta) \\ &\varepsilon(k \mid \theta) = y(k) - \hat{y}(k \mid \theta) \end{aligned} \tag{3}$$

$$\begin{aligned} \hat{\theta}^{\mathrm{LS}} &= \arg\min V_N(\theta) \\ &= \left[\frac{1}{N}\sum_{k=1}^{N} \psi(k)\psi^{\mathrm{T}}(k)\right]^{-1} \frac{1}{N}\sum_{k=1}^{N} \psi(k)y(k) \end{aligned} \tag{4}$$

$$\hat{\theta}^{\mathrm{IV}} = \left[\frac{1}{N}\sum_{k=1}^{N} \xi(k)\psi^{\mathrm{T}}(k)\right]^{-1} \frac{1}{N}\sum_{k=1}^{N} \xi(k)y(k) \tag{5}$$

II. KEY RESULTS

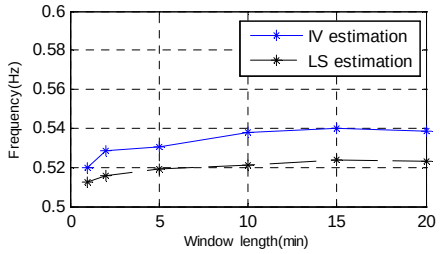

Fig 1. Frequency of inter-area mode versus window length.

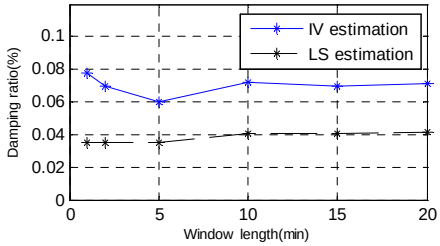

Fig 2. Damping ratio of inter-area mode versus window length.

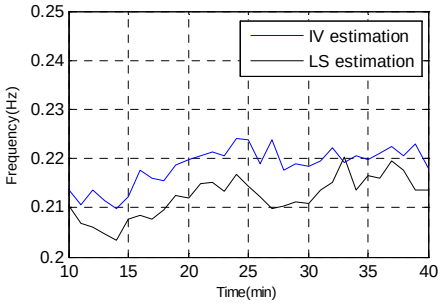

Fig. 3. Frequency estimation of 0.22 Hz mode.

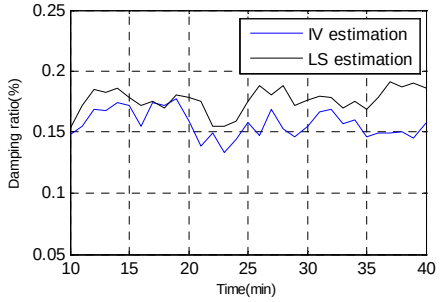

Fig. 4. Damping ratio estimation of 0.22 Hz mode.

Improvement of Available Transfer Capability under Transient Stability Constraints by Secondary Battery System Installation on Generator Bus

Masaya Takiguchi, Yasunori Tomita, and Shinichi Iwamoto
Power Systems Laboratory, Department of Electrical Engineering and Bioscience,
Waseda University, Tokyo, 169-8555, JAPAN
Email: takiguchi.masaya.pwrs@gmail.com

***Abstract*— The introduction of renewable energy sources has increased the size and complexity of the electric power system. Transient stability has emerged as a considerable problem under such an environment. In addition, the concept of available transfer capability (ATC)—which is a measure of the transfer capability remaining in the physical transmission line—has been receiving increased attention. Therefore, we focus on ATC under transient stability constraints (transient stability ATC) and use it as an index of the improvement in transient stability. Enhanced transient stability ATC brings not only the economical advantage of tie-lines between utilities but also an increase in the number of renewable energy sources that can be introduced. In this paper, we propose the use of a secondary battery system on a generator bus for improving transient stability and determine the output of the secondary battery system by using control theory associated with a linear-quadratic regulator. Finally, we verify the effects of the proposed method by using the Institute of Energy Economics Japan EAST 10-machine 47-bus power system model.**

I. KEY EQUATIONS

$$\dot{\delta}_{(i)} = \omega_0(\omega_{(i)} - 1) \quad (1)$$

$$M_{(i)}\dot{\delta}_{(i)} = P_{m(i)} - P_{e(i)} - D_{(i)}(\omega_{(i)} - 1) \quad (2)$$

$$P_{e,new(i)} = P_{e(i)} + P_{bs} \quad (3)$$

II. KEY FIGURES

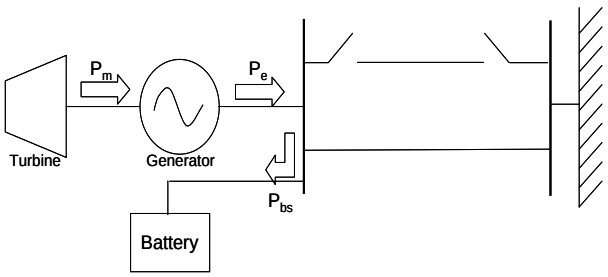

Figure 1. Image of the proposed method

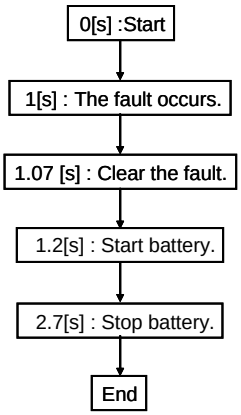

Figure 2. Flowchart of the proposed method

III. KEY RESULTS

Table 1. The results of transient stability ATC

	tie-line PF [pu]	ATC [pu]	Improvement [pu]
initial condition	3.596	-	-
without battery	4.170	0.574	-
proposed method	4.494	0.898	0.324

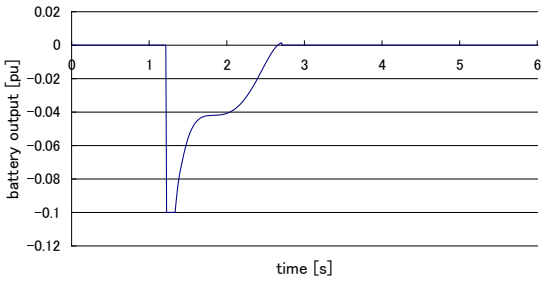

Figure 3. The output of the battery system

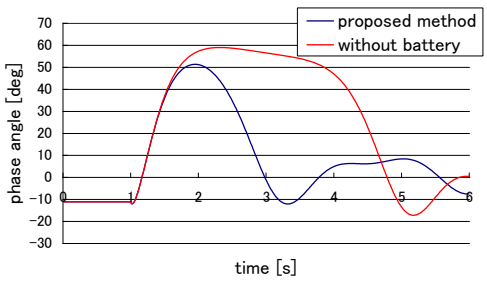

Figure 4. Phase Angle $\delta_{(1)}$

Phasor State Estimation from PMU Measurements with Bad Data

Dongliang Duan[1], Liuqing Yang[1] and Louis L. Scharf[2]
Department of Electrical and Computer Engineering, Colorado State University, Fort Collins, CO 80523, USA.
Department of Mathematics, Colorado State University, Fort Collins, CO 80525
Email: Dongliang.Duan@colostate.edu, lqyang@engr.colostate.edu, scharf@engr.colostate.edu

***Abstract*—With synchronization from Global Positioning System (GPS) satellite signals, direct accurate and synchronized measurements of the voltage and current phasors in the power system become available via phasor measurement units (PMU). With these synchrophasor measurements, the performance of the state estimate (SE) in the supervisory control and data acquisition (SCADA) system for power grid can be greatly improved. However, due to communication errors, equipment failures, spiky noise or malicious data attack, some detrimental data can occur among the measurements. The largest residual removal (LRR) algorithm is commonly used for phasor state estimation with bad data. Here, we show that this method cannot guarantee correctness unless data redundancy is very abundant. We then establish the equivalence between the approaches of bad data removal and bad data estimation and subtraction. In addition, we propose two new algorithms by exploiting the sparsity of the bad data, including sparsity regularized minimization (SRM) and projection and minimization (PM). All algorithms are tested by simulations on standard IEEE 14-bus test system and our projection and minimization (PM) algorithm provides the best performance.**

I. Key Equations

The system model is an over-determined linear system as:

$$\boldsymbol{m} = \boldsymbol{H}\boldsymbol{s} + \boldsymbol{b} + \boldsymbol{\eta}$$

The bad-data processing algorithms are

$$\text{LRR: } \hat{i}_b = \arg\max_i \|(\boldsymbol{m} - \boldsymbol{H}(\boldsymbol{H}^{\mathcal{H}}\boldsymbol{H})^{-1}\boldsymbol{H}^{\mathcal{H}}\boldsymbol{m})_i\|_2^2$$

$$\text{SRM: } (\hat{\boldsymbol{s}}, \hat{\boldsymbol{b}}) = \arg\min_{(\boldsymbol{s},\boldsymbol{b})} \left(\|\boldsymbol{m} - \boldsymbol{b} - \boldsymbol{H}\boldsymbol{s}\|_2^2 + \lambda \cdot \text{spar}(\boldsymbol{b})\right)$$

$$\text{PM: } (\hat{b}, \hat{i}_b) = \arg\min_{(b,i)} \|b\boldsymbol{H}_\perp \boldsymbol{I}(:,i) - \boldsymbol{H}_\perp \boldsymbol{m}\|_2^2$$

II. Key Figures

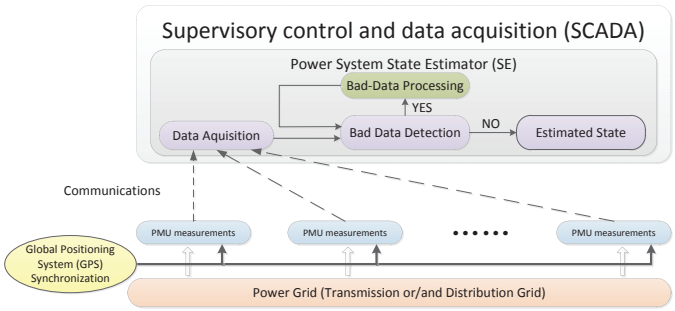

Fig. 1. State estimate from PMU measurement with bad data.

III. Key Results

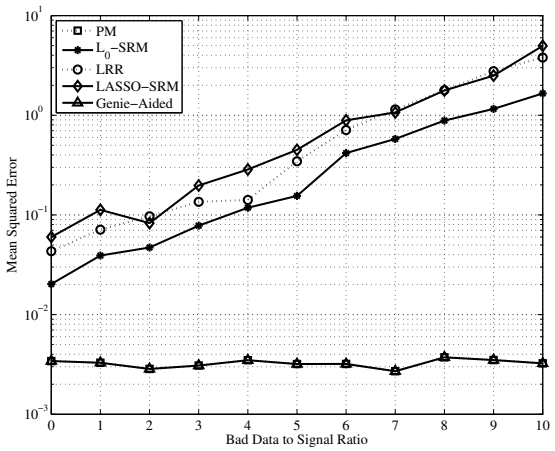

Fig. 2. The state estimation performance for partial measurement with 1 bad data.

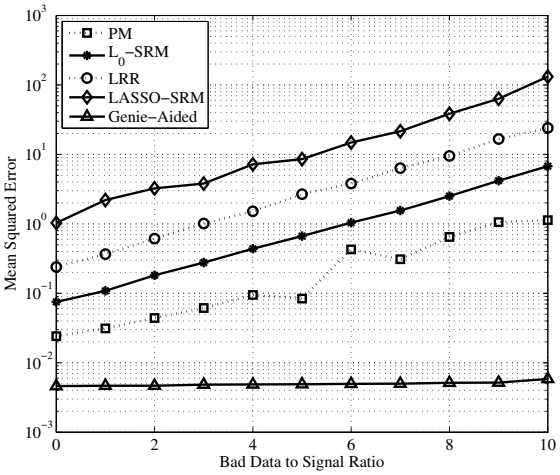

Fig. 3. The state estimation performance for partial measurement with 3 bad data.

A Model Predictive based Emergency Control Scheme using TCSC to Improve Power System Transient Stability

Xiaochen Du[1],Damien Ernst[2],and Peter Crossley[1]
[1]University of Manchester, Manchester, United Kingdom (xiaochen.du@postgard.manchester.ac.uk, peter.crossley@manchester.ac.uk)
[2]University of Liege, Liege, Belgium (dernst@ulg.ac.be)

Abstract— **A model predictive based emergency control scheme aiming to improve power system transient stability is described in the poster. The control action utilizes a thyristor controlled series compensation (TCSC) technique. The model predictive control (MPC) technique was first studied during the 1960s and is now widely used in power systems. At this stage, the existing work is based on the assumption that the system dynamics are fully observable using step by step integration. However, such estimation is difficult in real time when the fault conditions, such as fault location, type and duration, are unknown. In this emergency control scheme, supervised learning (SL) approaches are utilized to predict power system dynamics by assuming each control action has been taken. Furthermore, a feature selection technique, that chooses the most relevant features, is used to improve the performance of the SL prediction. The model predictive control (MPC) technique is performed every discrete time interval, so the optimal control action is always selected. The proposed control scheme has been verified using a two machine four-bus system, and simulation results show it can effectively maintain system synchronism following a large disturbance.**

I. KEY EQUATIONS

Model predictive control optimizes the control decisions by selecting control actions that result in a minimum value for the cost functions. The cost function is calculated according to the prediction of system dynamics assuming every control action has been taken. The system dynamics are represented by

$$f : X \times U \times \{0, 1 \ldots N\text{-}1\} \quad (1)$$

in which X is the space of system states, U the set of H possible control actions, and N the control horizons; where x[n] ∈X and u[n] ∈U are the system state and control actions taken at time step n. Thus

$$x\,[n+1] = f\,(x[n], u[n], n) \quad (2)$$

II. KEY FIGURES

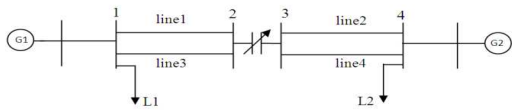

Figure 1. Network of the test system

III. KEY RESULTS

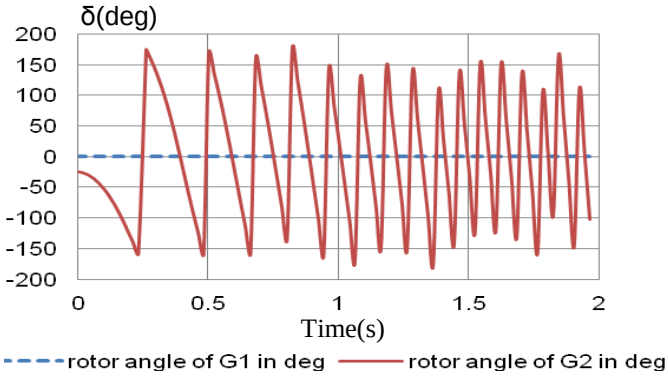

Figure 2. Evolution of rotor angles during emergency conditions

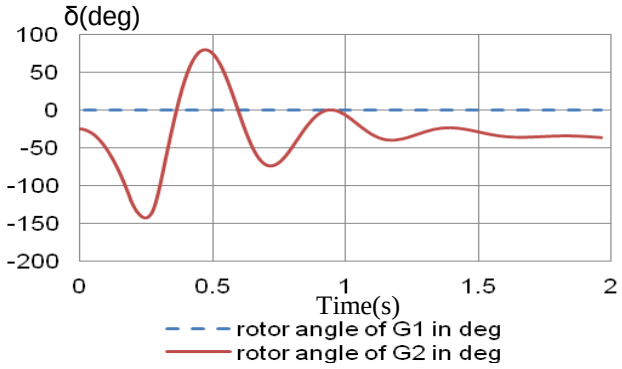

Figure 3. Evolution of rotor angles when the MPC scheme is activated

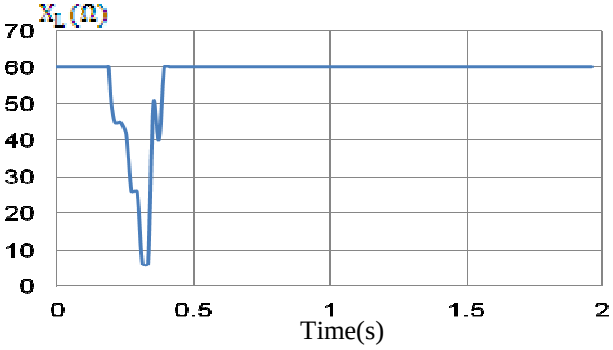

Figure 4. Compensation level in the post fault period

Subsynchronous Oscillation Analysis in Conventinal Power Plants and Wind Farms

Hamed Khalilinia and Mani Venkatasubramanian
School of Electrical Engineering and Computer Science
Washington State University
Pullman, WA 99163, USA
hkhalili@eecs.wsu.edu, mani@eecs.wsu.edu

***Abstract*— SSR is an electric power system condition where the electric network exchanges energy with a turbine generator at one or more of the natural frequencies below the synchronous frequency of the system. The subsynchronous oscillations in conventional thermal power plant is well-understood and documented in the literature. Also recently some records show the occurrences of this phenomenon in a system related to wind farms. In the previous NASPI meeting we discussed wind farm related subsynchronous oscillations in an industrial case [1]. Wind farms are typically located in remote areas due to favorable wind conditions and are therefore connected to the power system via weak transmission lines. Therefore, it is quite possible for an HVDC line to be used to transmit large amount of electrical power from the wind farm, or it is quite likely that the transmission lines be series-compensated. In addition most of the typical wind generators connect to the network using some power electronic converters. All of these can cause the excitation of Subsynchronous oscillation in the wind farms. These kind of oscillations can grow and may result in the failure of the turbine shaft. Even if the Subsynchronous Oscillations be stable, in most of the cases a low magnitude oscillation remains on the shaft for a long time and damps very slowly. Therefore, disturbances like switching, and fault can cause fatigue of the turbine shaft. To avoid failure of the turbine shaft, SSR must damp rapidly and completely. For designing appropriate controller, analysis and detection of sub-synchronous oscillation is significant issue. For the purpose of subsynchronous oscillation analysis some offline methods like as modal analysis and nonlinear simulations have been used. At the end because of some limitations of offline modal analysis, such as inaccurate model, some measurement-based methods have been developed for the purpose of SSR monitoring.**

I. KEY FIGURE

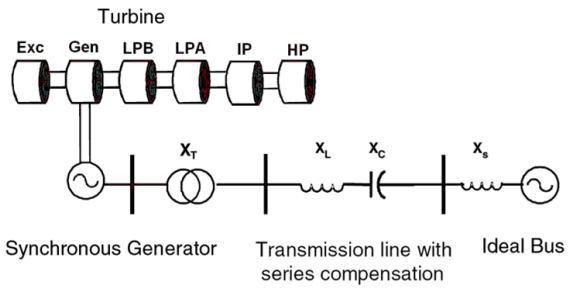

Fig. 1. IEEE First Benchmark Model

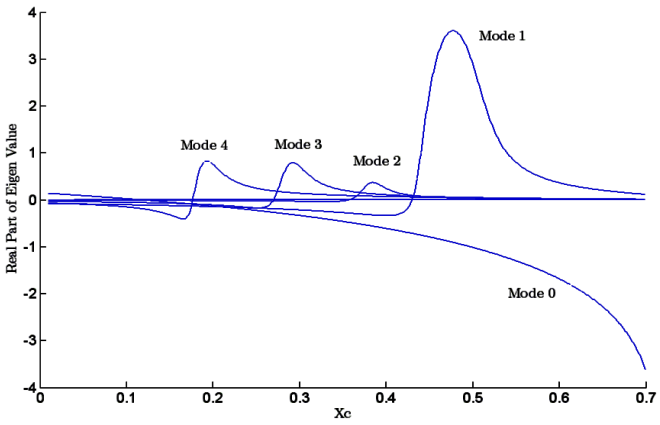

Fig. 2. SSR Modes of First Benchmark Model in 0.9 p.u active power and different level of series compensation

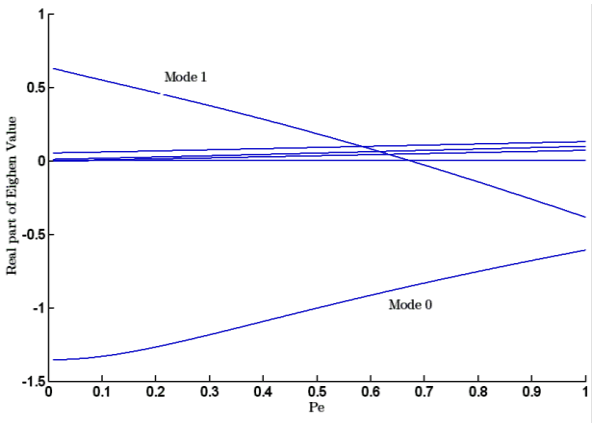

Fig. 3. SSR Mode of First Benchmark Model in 60% series compensation and different amount of active power

II. KEY REFERENCE

[1]https://www.naspi.org/site/Module/Meeting/Reports/SubReports/workgroup.aspx

Improving Power System Dynamic Stability via Operating Condition Adjustment Using PMU Data

Goodarz Ghanavati & Paul Hines
College of Engineering and Mathematics
University of Vermont
Burlington, USA
gghanava@uvm.edu

***Abstract*—This paper presents a method to enhance power system dynamic stability using principal component analysis on PMU data without a network model. The method identifies the best set of remedial actions, and improves system stability by re-dispatching generators based on their relative contributions to the fluctuations in PMU data.**

Keywords-Power system stability; principal component analysis; phasor measurement unit

I. INTRODUCTION

Several large blackouts have happened worldwide in past few years [1]. One of the goals of smart grid in transmission systems is to reduce the risk of blackouts by developing advanced monitoring and assessment tools. Phasor measurement units (PMU) have provided an opportunity for monitoring the power system in a more precise manner. In [2], signs of proximity of a dynamical system to instability are illustrated. Some of these signs are increase in variance and autocorrelation of measured signals. This method is applied to power systems in [1]. Reference [3] presents another index of system stress, which is the largest singular value of time window of data. In [4], modal sensitivity is used to adjust operating conditions to improve damping.

The purpose of this paper is to provide a tool for improving system stability based on PMU data using principal component analysis.

II. METHOD AND RESULTS

We used principal component analysis (PCA) to reveal hidden information in PMU data. PCA transforms a set of correlated variable to a set of uncorrelated variables called principal components. The first principal component has the largest variance, which is equal to the largest singular value of time window of data. Therefore, it can be used as an indicator of system stress level.

Component loadings are the correlation of principal components and measured variables. The value of loading of variables on the first principal component show that how these variables contribute to the system dynamics.

We did the analysis on IEEE 39 bus system. We added a random term to the load at each bus to account for variability of demand. This term is equal to 1% of load at each bus. We simulated the system using PSAT dynamic simulator, and used procedure in [1] to prepare data for analysis. We applied PCA to voltage magnitude of system buses. The loading coefficients of voltage magnitude of generator buses on first principal component were sorted. Order of these loading coefficients shows how generators in different locations contribute to the system stress level.

Fig. 1. shows how system stress level varies with generation dispatch method. System load was gradually increased in the simulation. In the low stress case, generators for which their terminal bus voltage has a low loading on the first principal component, generate more power. In this figure, the variance of the first principal component is used as a measure of system stress. In conclusion, smart re-dispatching of generators can reduce system stress level.

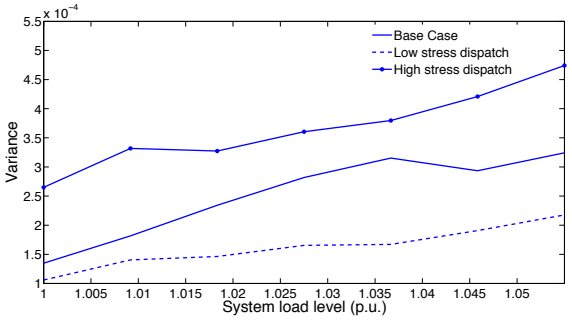

Figure. 1. Variance of 1st principal component for different generation dispatch cases

REFERENCES

[1] P. D. H. Hines, E. C. Sanchez, B. O'Hara, and C. Danforth, "Estimating Dynamic Instability Risk by Measuring Critical Slowing Down," IEEE Power and Energy Society General Meeting, pp. 1-5, July 2011.

[2] M. Scheffer, J. Bascompte, W. A. Brock, V. Brovkin, S. R. Carpenter, etc., "Early-warning signals for critical transitions," in Nature, vol. 461, Sep. 2009, pp. 53-59.

[3] T. Overbye, P. Sauer, C. DeMarco, B. Lesieutre, M. Venkatasubramanian, "Using PMU Data to Increase Situational Awareness," PSERC Final Project Report 10-16, , Sep. 2010.

[4] Z. Huang, N. Zhou, F. Tuffner, D. Trudnowski, "Use of Modal Sensitivity to Operating Conditions for Damping Control in Power Systems," 44th Hawaii International Conference on System Sciences (HICSS), pp. 1-9, Jan 2011.

Modal Analysis of grid connected Photovoltaic

Yashodhan Agalgaonkar, Bikash C Pal, Sara Nachian
Control & Power Research Group, Department of Electrical & Electronics Engineering,
Imperial College London
London, United Kingdom
b.pal@imperial.ac.uk

Abstract— **Many governments across the world are now offering conducive policies to promote Solar photovoltaic (PV). Hence PV systems are becoming cost effective. Its share amongst the power system generation sources is steadily growing. During past few years solar plant ratings have increased. Both, traditional kilo watt (kW) rated roof top PV plants and medium voltage (MV) megawatt (MW) capacity PV plants are now operational in many systems. Many kW & MW rated PV plants are in planning stage. However, PV integration with the existing power system gives rise to many research challenges. Traditional power system mainly consists of synchronous generators. Hence traditionally electromechanical interactions between these synchronous machines had an impact on oscillatory behavior of a Power system. As power injection from stochastically varying PV sources is growing it is important to analyze its impact on the system stability. The analysis of the impact of PV on the small signal stability of a power system is studied in this work.**

Typical PV system consists of a PV panel, a power converter and a grid interface. In the model of a PV, module variables are algebraic that is, they change instantaneously and the modeled dynamics are those of the power converter controller. Power converter control structure consists of a Maximum power point tracking (MPPT), an active & reactive power control and a phase locked loop (PLL). The analysis provides explanation of the impact of this closed-loop control on the power system stability. Two systems are modeled in this study; namely Single Solar Infinite Bus (SSIB) system and solar connected multi-machine system. Both the systems are modeled using Matlab/Simulink.

In the case of SSIB system impact on Eigen values and mode shapes is studied for different weather conditions. Also impact of variation in solar cell parameters and variation in power converter control parameters on Eigen values is studied. Further sensitivity to different power system conditions such as voltage variation, power factor variation and variation in grid strength is studied. In multi-machine case dynamic models of synchronous generators and solar are integrated. Different possible power system operating scenarios with solar are studied. Observation and conclusion obtained from Eigen value and participation factor analysis is presented.

I. KEY FIGURES

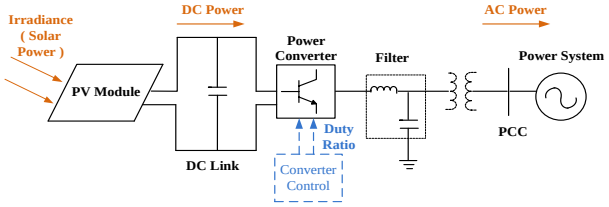

Studied System 1 : Single Solar Infinite Bus (SSIB) System.

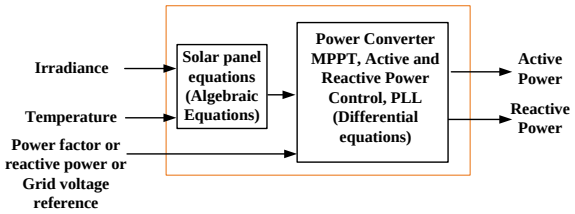

Studied System 1 : SSIB system model for stability study .

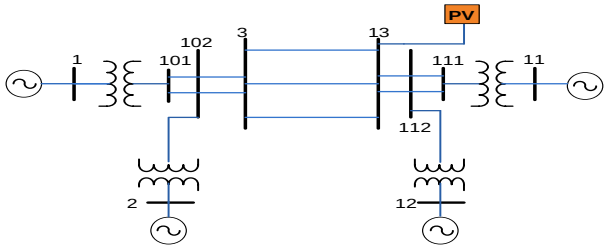

Studied System 2: Four machine two area systems with Solar.

II. KEY RESULTS AND TABLES

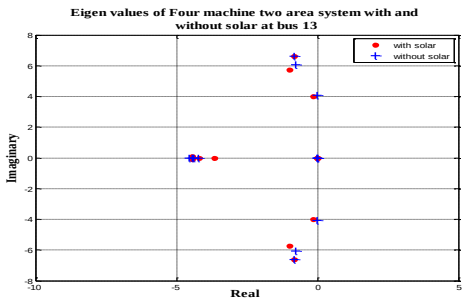

Figure 1: Eigen values for multi machine system with and without solar.

Other results such as sensitivity of SSIB system to solar parameters, power converter control parameters and grid strength will be included in the final draft of the poster.

Multi-Agent Based Controller for Multi-Terminal VSC HVDC Transmission System

Mohammad Nazari and Mehrdad Ghandhari
Electric Power Systems, Department of Electrical Engineering, KTH Royal Institute of Technology, Stockholm, Sweden
Email: nazarim@kth.se and mehrdad.ghandhari@ee.kth.se

***Abstract*— Multi-terminal HVDC transmission system is finding its way to the power system. One of the main issues in these systems is controlling DC voltage in the DC grid. This paper presents the application of multi-agent controller to control the DC voltage and active power in multi-terminal HVDC system. Multi-agent system uses autonomous decision making entities to perform its job which makes it possible for the controller to learn, and therefore control the DC voltage even without communication. A new control strategy and decision making algorithm is proposed. The control system consists of a supervisor agent, middle agents for each terminal and physical layer agents. The control system uses multi-agent system to implement voltage margin control on the HVDC system using cost functions which are defined for each terminal. To evaluate the performance of the multi-terminal HVDC system and the multi-agent controller, a multi-terminal system is developed in the MATLAB/SIMULINK environment. The effectiveness of the multi-Agent controller is examined for different scenarios.**

I. KEY EQUATIONS

The guiding equations of the multi-agent controller are:

$$Cost_{i-UP} = \begin{cases} (V - V_2)^2 & if \;\; P = P_{cont} \\ (P - P_{\min})^2 & if \;\; P < P_{cont} \\ (P - P_{cont})^2 & if \;\; P > P_{cont} \end{cases} \quad (1)$$

$$Cost_{i-DOWN} = \begin{cases} (V - V_1)^2 & if \;\; P = P_{cont} \\ (P - P_{cont})^2 & if \;\; P < P_{cont} \\ (P - P_{\max})^2 & if \;\; P > P_{cont} \end{cases} \quad (2)$$

II. KEY FIGURES

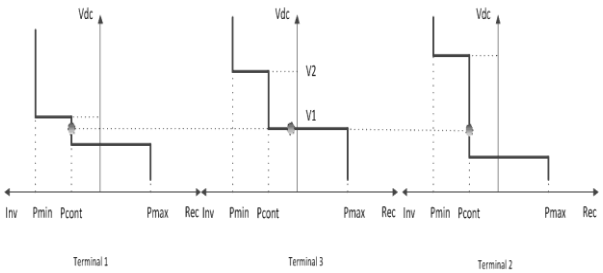

Figure 1. Characteristic of voltage margin for controllers

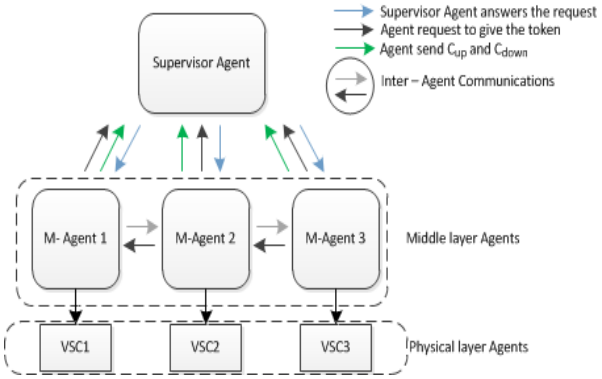

Figure 2. Agent based controller communication

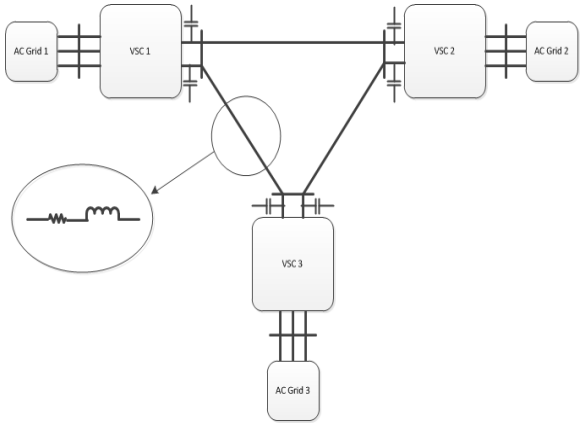

Figure 3. Configuration of the test grid

III. KEY RESULTS

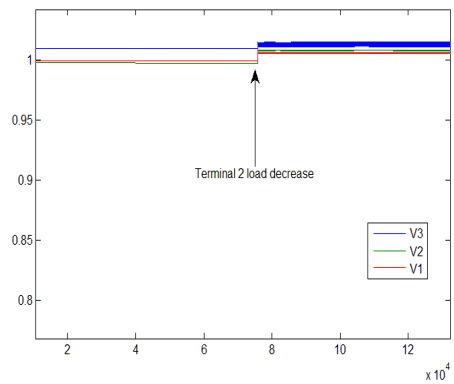

Figure 3. DC voltage change during a 90% load decrease in terminal 2 the voltage control token took by terminal 1 from terminal 3

Electric Vechile Smart Charging to Mitigate Distribution System Overloads

Pooya Rezaei and Paul Hines
College of Engineering and Mathematics
University of Vermont
Burlington, VT
pooya.rezaei@uvm.edu and paul.hines@uvm.edu

***Abstract*—This study provides a comparison among several smart charging methods that have been proposed to mitigate the impacts of Electric Vehicle Charging on distribution infrastructure. We use US National Household Travel Survey data to model travel behavior, which show that travel behavior is much more varied than what has been modeled in previous studies. We calculated the factor of equivalent transformer aging, to see the charging effects on a distribution transformer and also the percentage of successful charges, to find the impacts on the drivers.**

Keywords- Plug-in electric vehicles, smart charging, transformer aging.

I. INTRODUCTION

Plug-in Electric Vehicles (PEVs) will result in increased loading on the distribution system, occurring at random times during the day. With high penetrations of PEVs, uncontrolled charging may have harmful effects on the distribution system infrastructure. Some studies have investigated these effects and proposed various mitigation methods, which are usually called "Smart Charging" strategies. In this study, we compare several smart charging methods in the literature. Our criteria include transformer aging and percentage of successful charges. The authors are using the same model in [1] to calculate transformer aging based on the ambient temperature in two locations including Burlington, VT and Phoenix, AZ. The percentage of successful charges is calculated whenever the PEVs have been plugged in long enough to get full charge. To that end, if the battery State of Charge (SOC) is 95% when the PEV is leaving, the number of successful charges is increased by 1. Otherwise, this incident will be counted as an unsuccessful charge.

II. SIMULATION AND RESULTS

We used the NHTS data as is in [1] to model realistic travel demand patterns and thereby PEV load. The NHTS data show that travel behavior is more erratic than is usually modeled in many previous studies, which typically assume that everyone leaves in the morning and arrives in the evening. We have used Monte Carlo Simulation to simulate random travel behavior for 6 PEVs charging from a 25 kVA transformer.

Table 1 summarizes the simulation results, which are the average over 500 iterations. This table shows how the location and charging method can significantly affect the Factor of Equivalent Aging (F_{EQA}) and percentage of successful charges. Also, the results show that if one uses a smart charging method that decides on charge management based on transformers temperatures not only does smart charging reduce transformer aging, but also increases the percentage of successful charges compared to other charging methods.

Table I Comparison of different charging methods

CHARGING TYPE	LOC	CHARGE RATE	F_{EQA}	% SUCCESSFUL
NO PEVS	VT	N/A	0.13	N/A
NO PEVS	AZ	N/A	0.81	N/A
UNCONTROLLED	VT	1.4 KW	0.34	100
UNCONTROLLED	VT	7 KW	1.06	100
UNCONTROLLED	AZ	1.4 KW	1.93	100
UNCONTROLLED	AZ	7 KW	5.11	100
AFTER MIDNIGHT	VT	1.4 KW	0.15	60.5
AFTER MIDNIGHT	VT	7 KW	5.21	79.5
AFTER MIDNIGHT	AZ	1.4 KW	0.9	60.5
AFTER MIDNIGHT	AZ	7 KW	18.67	79.5
LOAD CUTTING	VT	1.4 KW	0.18	95.1
LOAD CUTTING	VT	7 KW	0.15	64.6
LOAD CUTTING	AZ	1.4 KW	1.07	95.1
LOAD CUTTING	AZ	7 KW	0.91	64.6
[3]*	VT	1.4 KW	0.20	84.7
[3]*	VT	7 KW	0.28	78.7
[3]*	AZ	1.4 KW	1.20	84.7
[3]*	AZ	7 KW	1.58	78.7
TEMP-BASED	VT	1.4 KW	0.30	99.6
TEMP-BASED	VT	7 KW	0.50	98.3
TEMP-BASED	AZ	1.4 KW	1.25	98.8
TEMP-BASED	AZ	7 KW	1.61	96.9

* Randomized charging strategy (15 minute intervals) proposed in [3]

REFERENCES

[1] A. Hilshey, P. Rezaei, P. Hines, and J. Frolik, "Electric Vehicle Charging: Transformer Impacts and Smart, Decentralized Solutions," *IEEE PES General Meeting*, 2012.

[2] Oak Ridge National Laboratories. 2009 nhts user notes. Oak ridge national laboratories. [Online]. Available: http://nhts.ornl.gov/2009/pub/usernotes.pdf

[3] Q. Gong, S. Midlam-Mohler, V. Marano, and G. Rizzoni, "Study of pev charging on residential distribution transformer life," *IEEE Trans. Smart Grid*, vol. 3, no. 1, pp. 404 –412, March 2012.

A DFT-Based Frequency Estimator for Three-Phase Power Systems

Luoyang Fang, Dongliang Duan, and Liuqing Yang
Department of Electrical and Computer Engineering,
Colorado State University, Fort Collins, CO 80523, USA

***Abstract*—Control and protection of power systems require the estimation of system frequency in real-time. Deviations in system frequency from its nominal value indicate the need of control actions. As a result, frequency estimation is very important for power systems. In this work, we propose a DFT-based frequency estimation algorithm for three-phase power systems by analyzing the positive sequence component. Our proposed frequency estimation algorithm can be divided into two steps: (1) a coarse frequency estimate by locating the DFT sample with the maximum magnitude and (2) estimate the fractional frequency deviation by interpolating the two nearest neighbors of the maximum obtained in the first step. Simulations show that our proposed algorithm has the best performance when compared with existing alternatives.**

I. Key Equations

$$U_+[n]=\frac{1}{3}\left(U_a[n]+\mathrm{e}^{j\frac{2}{3}\pi}U_b[n]+\mathrm{e}^{-j\frac{2}{3}\pi}U_c[n]\right)$$

$$V^{2N}_{+\mathrm{FFT}}=\mathrm{FFT}\{U^{2N}_+\}$$

$$k_m=\mathrm{argmax}_k|V^{2N}_{+\mathrm{FFT}}[k]|$$

$$\hat{\delta}=\frac{\tan(\pi/2N)}{\pi/2N}\frac{|V^{2N}_{+\mathrm{FFT}}[k_m+1]|-|V^{2N}_{+\mathrm{FFT}}[k_m-1]|}{|V^{2N}_{+\mathrm{FFT}}[k_m+1]|+|V^{2N}_{+\mathrm{FFT}}[k_m-1]|},$$

$$\hat{f}=(k_m+\hat{\delta})\frac{f_s}{2N}$$

II. Key Figures

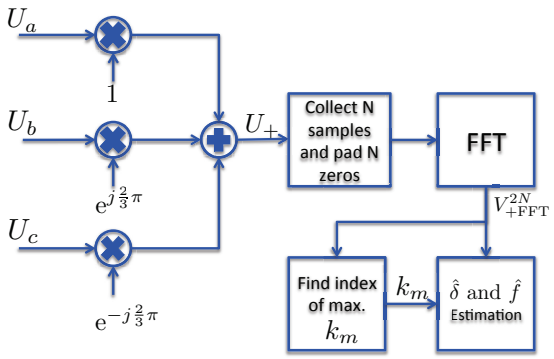

Fig. 1. Procedure of proposed algorithm

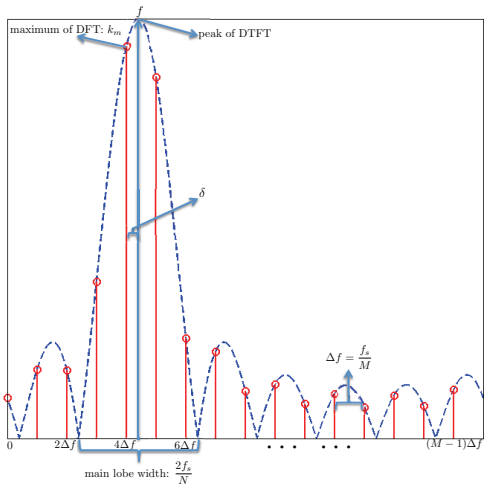

Fig. 2. DTFT (dashed line) and DFT samples

III. Key Results

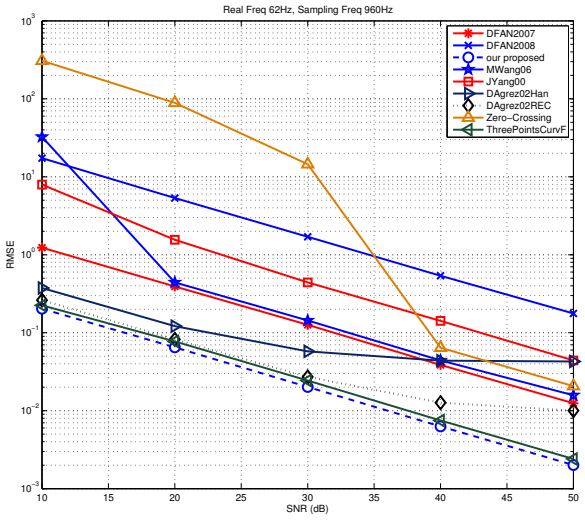

Fig. 3. RMSE Comparison with $f = 62$ Hz, $f_s = 960$ Hz and $N = 16$.

A New Control Strategy for Electromechanical Disturbances In Power Networks

Meimanat Mahmoudi
Department of Electrical Engineering and Computer Science
University of Tennessee
Knoxville, USA

Kevin Tomsovic
Department of Electrical Engineering and Computer Science
University of Tennessee
Knoxville, USA

***Abstract*—This paper addresses the problem of mitigating electromechanical disturbances in power systems. A control strategy using the control objective suggested by zero-reflection controllers to maintain the power and frequency deviation in a constant proportion is proposed. To achieve this goal, a conventional PSS is modified with a supplementary damping torque based on wide-area measurements. Simulation results on irregular grids of dissimilar generators show improvements in the power system dynamics.**

Keywords- Electromechanical wave propagation; power system stabilizer; impedance matching ;

I. INTRODUCTION

Power systems oscillations usually result from electromechanical disturbances induced by local imbalance between the mechanical power received by generators and their respective power injection into the grid. If the protection and control systems do not function correctly in response to these oscillations, the disturbance can propagate over the network, which might eventually lead to cascading failures. Preventive control approaches can schedule generation or determine control settings to conservatively operate the system away from limits. With today's uncertain pattern of flows, this is not only an expensive approach but essentially futile given the wide variety of possible disturbances. A corrective control that could respond to major disturbances in real-time would be far more attractive in fully utilizing system capacity. However, corrective control is difficult not only due to the extremely short time that may be available for response but also the scale of the controls that may need to be deployed.

A key challenge in the power network analysis is how to model the propagation of perturbations, which determines the power network stability and helps to design the control mechanism. Historically, power system dynamics have been mainly studied using time domain simulations, which yield results that convey limited insight, especially of the spatial characteristics of dynamic behavior. The traveling wave perspective brings new understanding of large system dynamics, because it directly relates spatial and temporal information. In this presentation, we use the electromechanical wave point of view afforded by the continuum model [1] to explore the possibility of control actions to mitigate disturbance propagations.

II. PROBLEM FORMULATION

A number of new controllers have been designed based on the electromechanical wave propagation phenomenon. In [2], a zero-reflection controller has been proposed. As simulations on a uniform continuum system demonstrate, this controller appears to work well in elimination of electromechanical wave reflections through control of generators at the edges of the grid. Another approach based on improving power system stabilizers (PSS) by utilizing wide-area measurements is presented in [3]. More specifically, the time delay for disturbance propagation from the fault location to the controlled PSS is exploited to inject additional damping torque. Simulation results on a small uniform system shows improved damping after applying modifications to conventional PSS.

We propose a new control strategy using the control objective suggested in zero-reflection controller to keep the power and frequency deviation in a constant proportion. To achieve this goal, we modify conventional PSS with a supplementary input signal. We verify through simulation on irregular grids of dissimilar generators that the traveling waves, which occur in response to disturbances, are dampened using this controller.

III. CONCULSION AND FUTURE WORK

This paper shows that the application of the new control strategy on PSS leads to improved power system dynamics. However, those results must be verified with realistic simulation cases. In addition, since using remote signals represents additional complexity, the real benefit of such control should be investigated in comparison with distributed control, which only uses measurements from neighboring generators.

SELECTED REFERENCES

[1] J.S. Thorp, C.E. Seyler, C.E., and A.G. Phadke, "Electromechanical wave propagation in large electric power systems," *IEEE Transactions on Circuits and Systems I: Fundamental Theory and Applications*, vol.45, no.6, pp.614-622, Jun 1998.

[2] B. C. Lesieutre and E. G. Verghese, "A Zero-Reflection Controller for Electromechanical Disturbances in Power Networks," *Power Systems Computation Conference (PSCC)*, Sevilla, June 2002.

[3] M. Ali, J. Buisson and Y. Phulpin, "Improved control strategy to mitigate electromechanical wave propagation using PSS," *MELECON 2010 - 2010 15th IEEE Mediterranean Electrotechnical Conference* , vol., no., pp.35-40, April 2010.

Non Linear Harmonic Domain Analysis of an Induction Machine in DQ Reference

Pablo Rodríguez and José Manuel Cañedo

Center for Research and Advanced Studies (CINVESTAV), Guadalajara, JAL 45019, México

Email: prodrigue@gdl.cinvestav.mx and josec@gdl.cinvestav.mx

***Abstract*— The induction machine is used in a wide variety of applications as a means of converting electric power to mechanical work, this leads the machine to work in the nonlinear region or saturation region, which causes the generation of harmonics. The harmonics may create some resonance, stability problems and power losses in the power system. The analysis of the harmonics in time domain to obtain the steady state of the system may be slower in computational time; therefore is convenient to use the dynamic harmonic domain method. With this method the harmonic content of the variables of study is obtained in a rapid and effective way. This poster presents a non linear induction machine model, under balanced conditions, in the dynamic harmonic domain in DQ reference; shows the influence caused by the saturation in the currents, flux linkages and electromagnetic torque.**

I. Key Equations

The saturation curve polynomial adjustment can be represented as:

$$\lambda_m = a_1 i_m + a_2 i_m^2 + a_3 i_m^3 \tag{1.1}$$

where:

$$i_m = i_s + i_r \tag{1.2}$$

The equations representing the system in the dynamic harmonic domain are:

$$\dot{\mathbf{i}}_\mathbf{h} = \mathbf{B}_\mathbf{h}^{-1}\mathbf{V}_\mathbf{h} + (\mathbf{B}_\mathbf{h}^{-1}\mathbf{A}_\mathbf{h} - \mathbf{D}_\mathbf{h})\mathbf{i}_\mathbf{h} \tag{1.3}$$

$$\dot{\boldsymbol{\omega}}_\mathbf{r} = c_1 c_2 \left(\boldsymbol{\lambda}_\mathbf{ds}\mathbf{i}_\mathbf{qs} - \boldsymbol{\lambda}_\mathbf{qs}\mathbf{i}_\mathbf{ds}\right) \tag{1.4}$$

where:

$$A_h = \begin{bmatrix} -rs_h & 0_h & 0_h & 0_h \\ 0_h & -rs_h & 0_h & 0_h \\ 0_h & \omega_r\lambda_{md} & -rr_h & \omega_r\left(L_{lrh}+\lambda_{md}\right) \\ -\omega_r\lambda_{mq} & 0_h & -\omega_r\left(L_{lrh}+\lambda_{mq}\right) & -rr_h \end{bmatrix} \tag{1.5}$$

$$B_h = \begin{bmatrix} L_{lsh}+\dot{\lambda}_{mq} & 0_h & \dot{\lambda}_{mq} & 0_h \\ 0_h & L_{lsh}+\dot{\lambda}_{md} & 0_h & \dot{\lambda}_{md} \\ \dot{\lambda}_{mq} & 0_h & L_{lrh}+\dot{\lambda}_{mq} & 0_h \\ 0_h & \dot{\lambda}_{md} & 0_h & L_{lrh}+\dot{\lambda}_{md} \end{bmatrix} \tag{1.6}$$

II. Key Results

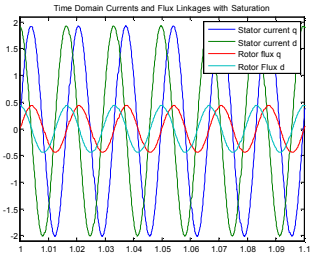

Figure 1. Steady state stator currents and rotor flux linkages with saturation in time domain

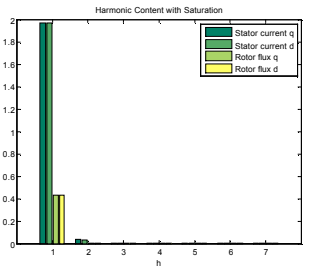

Figure 2. Harmonic content in stator currents and rotor flux linkages with saturation

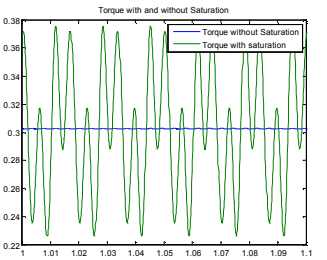

Figure 3. Steady state torque in time domain with and without saturation

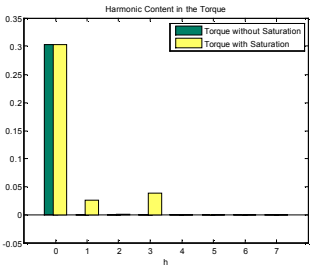

Figure 4. Harmonic content in the torque with and without saturation

Appropriate Placement of Series Compensators to Improve Transient and Small Signal Stability

Amin Nasri, Mehrdad Ghandhari, Robert Eriksson
Electric Power System Department, KTH Royal Institute of Technology, Stockholm SE 100-44, Sweden,
Email: amin.nasri@ee.kth.se, mehrdad.ghandhari@ee.kth.se and robert.eriksson@ee.kth.se

***Abstract*—Series Flexible AC Transmission Systems (FACTS devices) can provide significant improvement in power system transient and small signal stability by controlling power flows in the transmission lines. Since the transmitted active power is inversely proportional to the impedances of the lines, FACTS devices can control the power flows by changing the total impedance of each transmission line. It should be considered that the effectiveness and performance of these devices depend highly on their locations in the power system. This paper introduces a novel method based on trajectory sensitivity analysis (TSA) for the optimal placement of series FACTS devices to improve both transient and small signal stability. The proposed method considers impedances of transmission line as power system parameters which can be changed and calculates the trajectory sensitivity of power system state variables (e.g. rotor angles and speed of generators) and algebraic variables (e.g. bus voltages) to these parameters in the presence of most probable critical faults. In this calculation, power system differential algebraic equations and linearized trajectory sensitivity equations are solved simultaneously with the specified initial conditions. When there is no fault in the system (before fault occurrence), oscillations in the trajectory sensitivities show how effective the transmission lines are for improving small signal stability and power oscillation damping. After power system being subjected to severe faults, the variation in trajectory sensitivities determine the most effective places for installing series FACTS devices to improve transient stability of power system. Two stability improvement index are defined based on the trajectory sensitivities to show the appropriate places to install series FACTS devices and the transmission line with the highest positive index will be the most suitable location. This method is implemented in MATLAB®10b using the IEEE 3-machine 9-bus test system and Thyristor Controlled Series Capacitors (TCSC). Simulation with industrial software verifies the obtained results.**

I. Key Equations

$$\dot{\underline{x}} = \underline{f}(\underline{x}, y), \quad 0 = \begin{cases} g^-(\underline{x}, y) & s(\underline{x}, y) < 0 \\ g^+(\underline{x}, y) & s(\underline{x}, y) > 0 \end{cases} \tag{1}$$

$$\underline{x} = \begin{bmatrix} x & \lambda \end{bmatrix}^T \qquad \underline{f} = \begin{bmatrix} f & 0 \end{bmatrix}^T \tag{2}$$

$$x(t_0) = x_0, \; y(t_0) = y_0 \tag{3}$$

$$\dot{\underline{x}}_{\underline{x}_0} = \underline{f}_{\underline{x}}(t)\underline{x}_{\underline{x}_0} + \underline{f}_y(t) y_{\underline{x}_0}, \quad 0 = g_{\underline{x}}(t)\underline{x}_{\underline{x}_0} + g_y(t) y_{\underline{x}_0} \tag{4}$$

$$\underline{x}_{\underline{x}_0}(t_0) = I, \; y_{\underline{x}_0}(t_0) = -(g_y(t_0))^{-1} g_{\underline{x}_0}(t_0) \tag{5}$$

where x are the dynamic states, y are the algebraic states and λ are the parameters of the system. $\underline{f}_{\underline{x}}$, $\underline{f}_y$, $g_{\underline{x}}$ and g_y are time varying functions which are calculated along the system trajectories. Events in the system occurs when $s(\underline{x}, y) = 0$.

II. Key Figures and Results

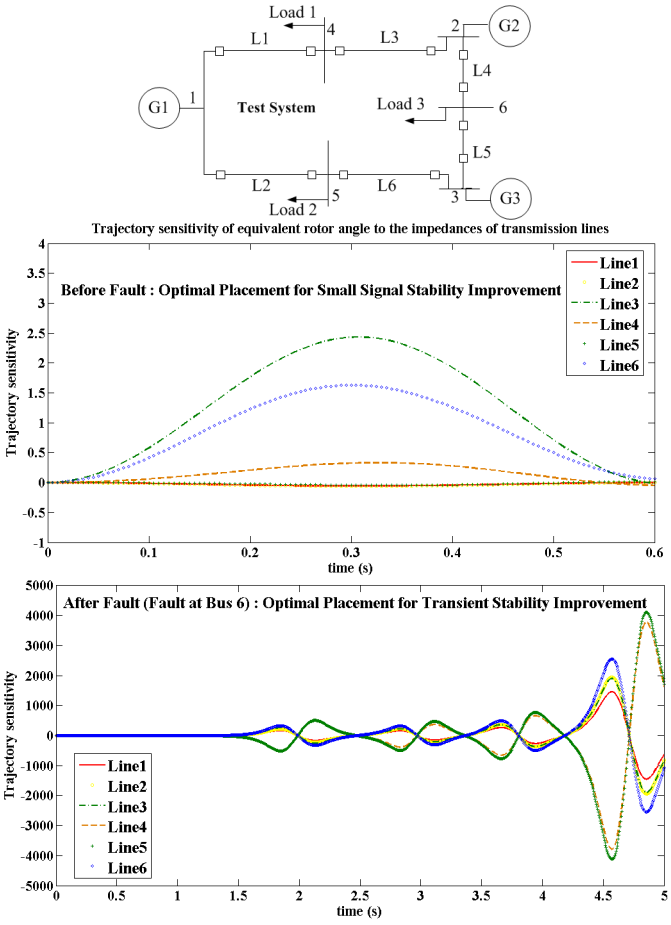

Fig. 1. Test system and trajectory sensitivities of $_{eq}$ to impedances of transmission lines (before and after fault at t = 1s).

Table I shows line 3 and line 6 are the most suitable places to install TCSC for improving transient and small signal stability of this test system.

TABLE I
Transient and small stability improvement index for each transmission line

	Line 1	Line 2	Line 3	Line 4	Line 5	Line 6
Small Signal	6.7060	4.0214	**96.6942**	11.4140	0.0157	**69.7316**
Transient	8.3764	10.8795	**25.6545**	-3.2701	-3.9108	**25.4792**

System Identification based VSC-HVDC DC Voltage Controller Design

Ling Xu, *Student Member, IEEE,* Lingling Fan, *Senior Member, IEEE,* and Zhixin Miao, *Senior Member, IEEE*

***Abstract*—VSC-HVDC system is adopted more and more for its flexible control capability. DC voltage control can affect fault ride through capability. System identification based DC voltage control will be designed in this paper. Simplified linear model of the open-loop system will first be extracted using Matlab System Identification Toolbox. Based on such model, controller specifications of the DC voltage control can be met by proper design. The contribution of this paper is to develop an experiment approach to obtain input/output dynamic responses for the open loop system, where the d-axis current reference is the input and the dc-link voltage is the output. To avoid system instability due to power mismatch, the d-axis current reference is computed from the power transmitted divided by the ac voltage magnitude. Simulation demonstrates the accuracy of the estimated model and the effectiveness of the control.**

I. Key Equations

The DC link model extracted based on System Identification Toolbox is:

$$G(s) = \frac{v_{dc}(s)}{i_d(s)} = \frac{4.848s^5 - 8.438e6s^4 - 2.659e10s^3}{s^5 + 6.342e5s^4 + 6.445e9s^3} \frac{-6.69e15s^2 + 2.843e18s + 1.02e18}{+8.727e14s^2 + 4.292e16s + 3.781e16} \quad (1)$$

The DC link voltage controller is:

$$C(s) = \frac{K_p s + K_i}{s} \quad (2)$$

II. Key Figures

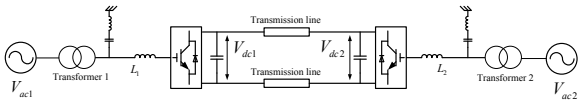

Fig. 1. Topology of a two terminal VSC-HVDC system.

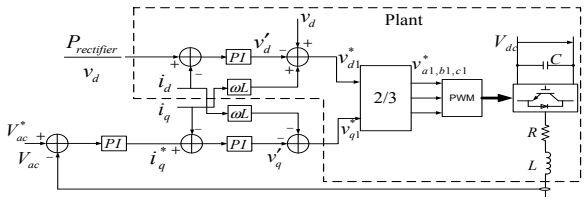

Fig. 2. Detailed controller of the inverter station.

III. Key Results

L. Xu, L. Fan and Z. Miao are with Department of Electrical Engineering at University of South Florida, Tampa FL (Emails: lxu@mail.usf.edu; linglingfan@usf.edu; and zmiao@usf.edu).

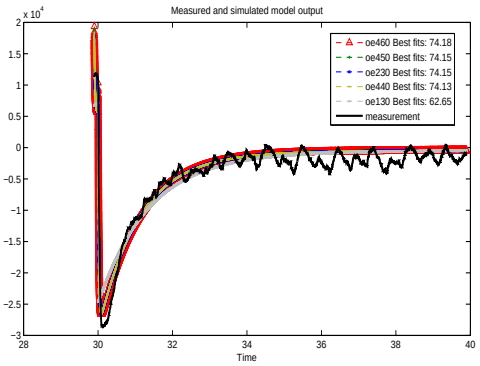

Fig. 3. Identified DC-link models with various orders.

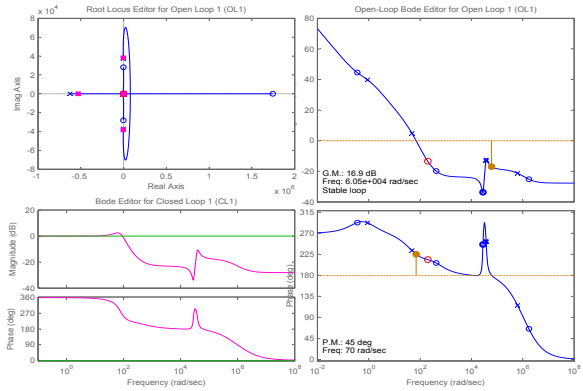

Fig. 4. Controller characteristics plot of identified model.

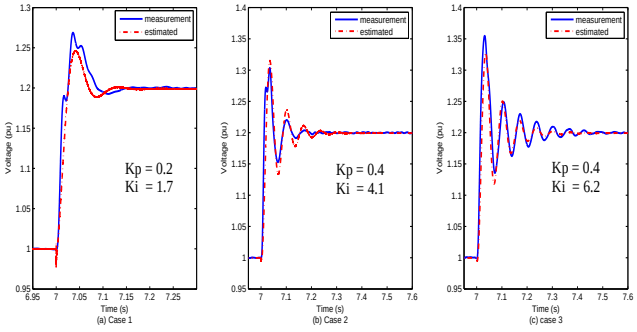

Fig. 5. Validations of identified model with its controller under different combinations of parameters.

Novel approach for Transmission Line Loss Minimization Using Power Flow Controllers

Gopiram Maddela*,Rama Gokaraju* and Kalyan K.Sen**
*Department of Electrical and Computer Engineering, University of Saskatchewan, Saskatoon, SK. Canada
**Westinghouse Electro-Mechanical Division Technology center, Mount Pleasant, PA 15666 USA
Email: *grm464@mail.usask.ca, rama.krishna@usask.ca , senkk@ieee.org*

Abstract— **Present utility networks are more complex and vulnerable to more disturbances compared to the past. The resulting power flow in these networks causes overloading or under loading in some transmission lines that could limit power flow between two areas and cause additional losses. Using FACTS devices, the ability to transfer power through desired paths has become more convenient and secure. Traditionally compensating devices are placed in the longest transmission lines. This paper implements a new approach of FACTS placement in the shortest lines to re-configure the power flow to reduce overall losses and achieve improved voltage stability. The performance of this approach is tested by implementing it in the IEEE 12 bus system. PSAT (DSA Tools software) and PSS/E software are used to develop and test the case system. Also the effectiveness of this technique was examined with different FACTS devices.**

I. Key Equations

The guiding equations of power flow controllers are:

$$P = \frac{VsVr}{X_l}\sin(\delta s - \delta r)$$

$$Q = \frac{VsVr}{X_l}\{\cos(\delta s - \delta r) - \frac{Vr}{Vs}\}$$

II. Key Figures

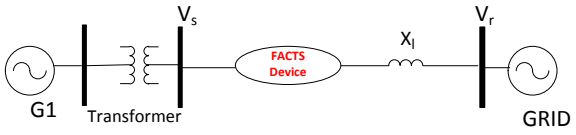

Figure 1. Placement of FACTS device

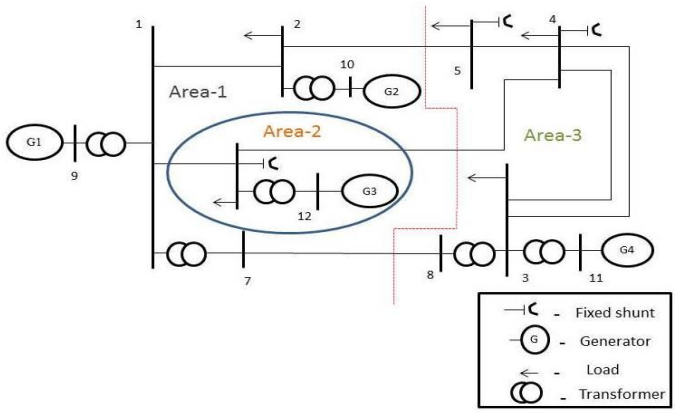

Figure 2. IEEE 12 –bus system

III. Key Results

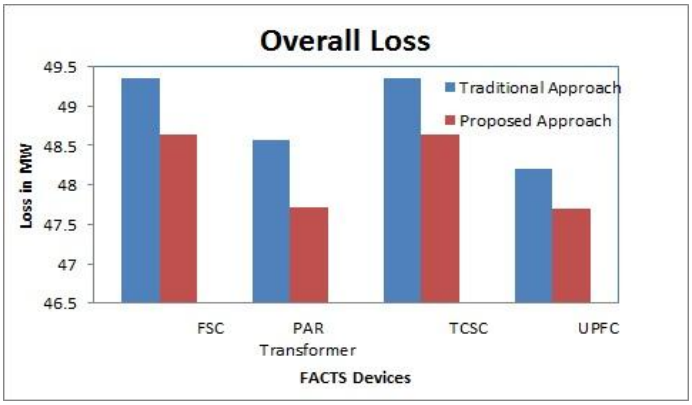

Figure 3.Performance Comparison for Different FACTS devices

	Loss in MW/Year			
	FSC	PAR Transformer	TCSC	UPFC*
No FACTS Device	436248	436248	436248	436248
Traditional Approach	432306	425385.6	432306	422232
Savings	3942	10862.4	3942	14016
Proposed Approach	426086	417939.6	426086	417852
savings	10161.6	18308.4	10161.6	18396

Table 1.Performance Comparison between Traditional and proposed approaches

Sustainable Energy and Distributed Generation Scenario in the Brazilian Electricity Sector

Tiago R. Ricciardi, Diogo Salles, Ricardo Torquato, and Walmir Freitas
Department of Electrical Energy Systems
University of Campinas, Campinas, SP, 13083-852, Brazil
Email: {ricciardi, dsalles, torquato, walmir}@ieee.org

***Abstract*—Brazil holds a lead position in renewable energy production and distributed generation. The economic growth of the country in the recent years is pulling up the electricity consumption and accelerating the installed generation capacity in the electric power system. This paper discusses the current scenario of distributed and renewable generation in Brazilian electricity sector as well as the potential for increasing sustainable sources in the future.**

I. Key Table

TABLE I
AGGREGATED BRAZILIAN POWER GENERATION INSTALLED CAPACITY

Type	Present (Nov/2011)			Near Future[2]			Growth Rate
	#	MW	%	#	MW	%	%
Large Hydro	180	78,141	67.3	205	103,619	62.0	33
Renewable[1]	**1,266**	**13,866**	**11.9**	**1,772**	**25,002**	**15.0**	**80**
Fossil	1,061	22,120	19.1	1,183	35,110	21.0	59
Nuclear	2	2,007	1.7	3	3,357	2.0	67
Total	**2,509**	**116,134**	**100.0**	**3,163**	**167,088**	**100.0**	**44**

[1]Includes biomass, small-hydro, wind and PV generation. [2]Currently in construction or granted by the regulatory authority.

II. Key Figures

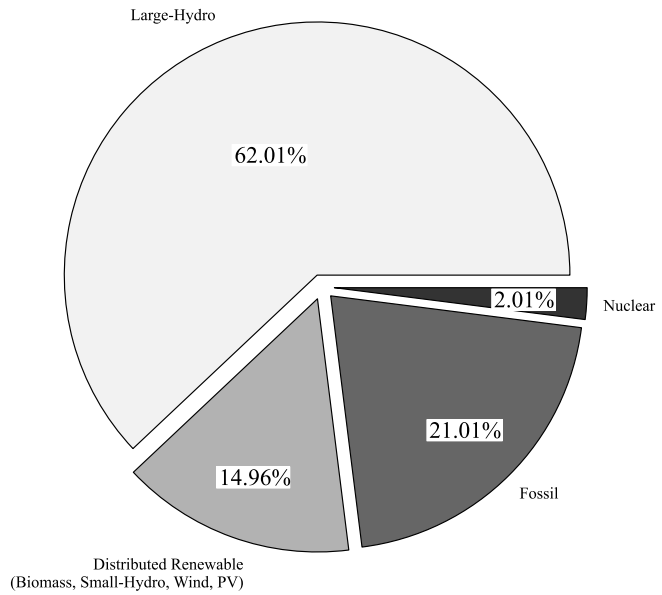

Fig. 1. Expected Brazilian electricity generation installed capacity by source for the near future (Source: [1]).

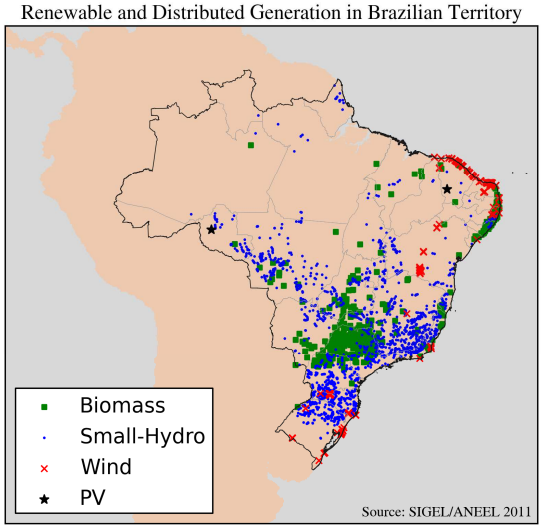

Fig. 2. Renewable and distributed generation in Brazilian territory (Source: [2]).

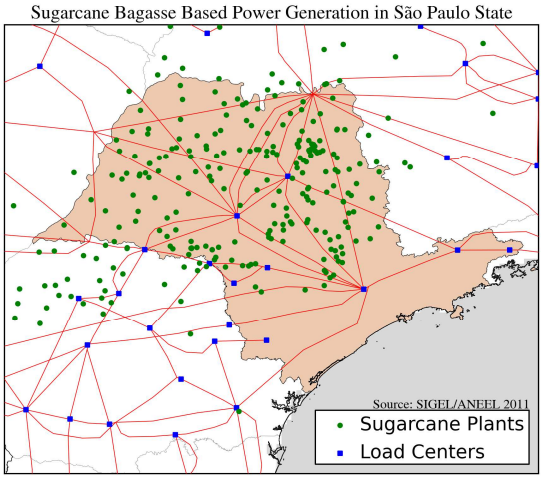

Fig. 3 Penetration of sugarcane bagasse based power generation in São Paulo state (Source: [2]).

References

[1] Banco de Informações da Geração – BIG. (2011). Agência Nacional de Energia Elétrica – ANEEL. [Online]. Available: http://www.aneel.gov.br/area.cfm?id_area=15

[2] Sistema de Informações Georreferenciadas do Setor Elétrico – SIGEL. (2011). Agência Nacional de Energia Elétrica – ANEEL. [Online]. Available: http://sigel.aneel.gov.br/

Review of International Guides for the Interconnection of Distributed Generation into Low Voltage Distribution Networks

Ricardo Torquato, Tiago R. Ricciardi, Diogo Salles, and Tiago Barbosa
Department of Electrical Energy Systems
University of Campinas, Campinas, SP, 13083-852, Brazil
Email: {torquato, ricciardi, dsalles}@ieee.org and barbosat@dsee.fee.unicamp.br

Henrique F. F. Costa
Companhia Energética de Minas Gerais
Belo Horizonte, MG, 30190-131, Brazil
Email: hffcosta@cemig.com.br

***Abstract*—This paper presents a review of the requirements adopted by distribution companies worldwide to facilitate the connection of SSDG units while maintaining the integrity of the public low voltage distribution network, both in terms of safety and supply quality. Issues like disconnect switch, protection, power quality and incentive policies are examined.**

I. KEY TABLE

TABLE I
SUMMARY OF THE REQUIREMENTS FOR INTERCONNECTING DGS AT LV NETWORKS ACCORDING TO DIFFERENT UTILITIES/COUNTRIES

Requirement	Utility Company/Country			
	New York State Public Service Commission	**COPEL**	**BC Hydro**	**Saskatoon**
Disconnect Switch	- Visible, accessible, manual - Interlocking - Tripolar, gang-operated and load break switch - Located within 10 feet of the utility's external meter - Must be lockable in the open position with a utility padlock	- Visible and accessible - Allow manual operation - Interlocking - Tripolar switch - Located close to metering panel	- Visible and accessible - Allow manual operation - Tripolar, gang-operated and load break switch - Located close to metering panel - Must be lockable in the open position	- Visible, accessible - Allow manual operation - Interlocking - Tripolar, gang-operated and load break switch - Located close to metering panel - Must be lockable in the open position
Protection functions	- Under/Over frequency, Under/Over voltage, anti-islanding (< 2 sec)	- Under/Over frequency, Under/Over voltage, overcurrent (50/51 and 50/51N), anti-islanding	- Under/Over frequency, Under/Over voltage, overcurrent (50/51), anti-islanding (< 2 sec)	- Under/Over frequency, Under/Over voltage, overcurrent (50/51), anti-islanding (< 2 sec)
Power Quality Indices	- PF correction measures are necessary if PF < 0.9 - IHD < 3% and THD < 5% at PCC	- PF < 0.92 (reactive compensation required for synchronous DG) - Voltage unbalance < 1.5%	- PF from 0.9 leading to 0.9 lagging - THD < 5% - Voltage unbalance < 3% - DC injection < 0.5% of the DG nominal current	- PF from 0.95 leading to 0.9 lagging - Voltage unbalance < 3% - DC injection < 0.5% of the DG nominal current
Incentives Policy	Net-metering	Not implemented in Brazil	Feed-in tariff/Net-metering	Net-metering
Requirement	**Utility Company/Country**			
	Hydro One	**UK**	**Germany**	**Australia**
Disconnect Switch	- Visible and accessible - Allow manual operation - Interlocking - Tripolar, gang-operated and load break switch - Located close to metering panel - Must be lockable in the open position	- Visible and accessible - It must be lockable in the open position - Phase and neutral wiring are isolated - Located close to metering panel	- Visible and accessible - Load break and tripolar switch with galvanic isolation - In case of unavailability of an accessible isolation switch, an automatic disconnection unit based on 3ϕ voltage monitoring can be used.	- Visible and accessible - Located close to metering panel - Must be lockable in the open position
Protection functions	- Under/Over frequency, Under/Over voltage, overcurrent (50/51), anti-islanding (< 2 sec)	- Under/Over frequency, Under/Over voltage, overcurrent (50/51) - Tripping of the DG must be within 0.5 seconds for a change in load at the generator terminals in excess of ± 25%	- Under/Over frequency, Under/Over voltage, anti-islanding (< 5 sec)	- Under/Over frequency, Under/Over voltage, anti-islanding (< 2 sec)
Power Quality Indices	- PF from 0.9 leading to 0.9 lagging - Voltage fluctuation must be lower than 4% - Voltage unbalance < 2% - DC injection < 0.5% of the DG nominal current	- PF from 0.95 leading to 0.95 lagging - Voltage unbalance < 2% - DC injection < 20 mA	- PF from 0.9 leading to 0.8 lagging - The capacitors must not be connected to the grid before the generator and have to be disconnected with it - To limit unbalance, DGs larger than 4.6 kVA (PV > 5 kWp) shall be 3ϕ - DC injection < 1A	- PF from 0.8 leading to 0.95 lagging - DC injection < 5 mA
Incentives Policy	Feed-in tariff/Net-metering	Feed-in tariff	Feed-in tariff	Feed-in tariff

Enhancement of Distribution Systems Stability by Proper Placement of Renewable Energy Sources (RES)

N. K. Roy and H. R. Pota
School of EIT, The University of New South Wales @ ADFA, Canberra ACT 2600, Australia
Email: *n.roy@student.adfa.edu.au, h.pota@adfa.edu.au*

***Abstract*— This paper proposes a distributed generator (DG) placement methodology based on newly defined term reactive power loadability (Q loadability). The effectiveness of the proposed planning is carried out over a distribution test system representative of the Kumamoto area in Japan. Firstly, the ranking of the buses of the system are determined using Q-V analysis without DG. Then DG is placed at different buses and it is seen that the system static voltage stability is sensitive to the location of RES. Finally, a number of suitable locations are identified for two principal types DG, *i. e.*, wind and solar, separately to enhance the stability margin of the system. Q loadability is defined as the rate of change of reactive power margin of the load bus with DG compared to without DG. Higher value of Q loadability signifies that the system is less vulnerable to voltage collapse. Negative value of Q loadability signifies that the system does not have adequate reactive power support. It is found that strong buses are a good choice for wind generator installation and weak buses are a good choice for solar installation to increase Q loadability. As the location of DG depends on environmental constraints and availability of primary resources, five best locations (priority list) for wind and solar type DG are given in Table I. Depending on operational requirements, distribution network service provider will decide proper site for DG installation among these buses.**

I. KEY EQUATIONS

In this paper, a squirrel cage induction type wind generator is employed which consumes reactive power from the system. A solar generator is used which has an inverter operating range of +/- 0.99 power factor. The reactive power capability of equivalent machine is determined by the combined MVA rating of the inverters and actual power level of the PV plant such that

$$Q_{\max} = \sqrt{M_{Base}^2 - P_{Gen}^2} = -Q_{\min} \tag{1}$$

All the loads are modeled as constant power load ($\alpha=\beta=0$) to carry out the analysis.

$$P(V) = P_0\left(\frac{V}{V_0}\right)^{\alpha} \tag{2}$$

$$Q(V) = Q_0\left(\frac{V}{V_0}\right)^{\beta} \tag{3}$$

II. KEY FIGURES & RESULTS

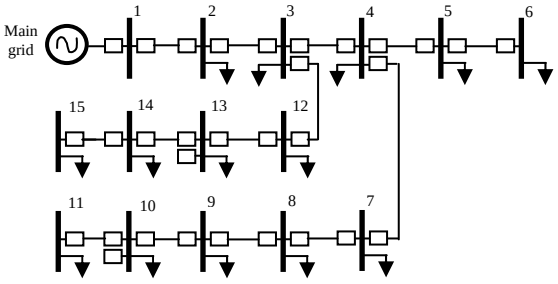

Fig. 1. Kumamoto 15 bus test system.

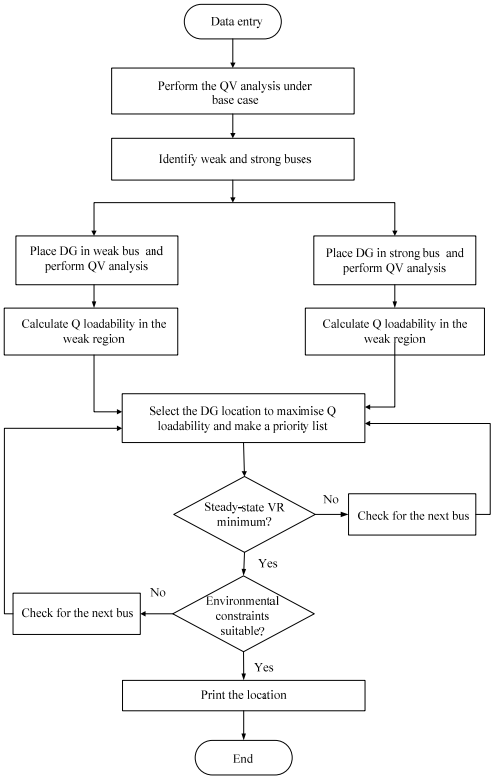

Fig. 2. Flow-chart of the proposed DG placement methodology.

TABLE I
SUITABLE LOCATION FOR WIND AND SOLAR DG

DG Type	Suitable location
Wind	Bus 4, 7, 5, 3, 2, respectively
Solar	Bus 10, 11, 13, 14, 15, respectively

Revisiting Damping Performance of the Queensland Network under Wind Power Penetration

Nilesh Modi , Tapan Kumar Saha
School of ITEE, The University of Queensland
Brisbane, Australia
Email: nilesh.modi@uqconnect.edu.au and saha@itee.uq.edu.au

Abstract— **To meet Australian renewable energy target of generating 20% of renewable energy by 2020, large scale wind farms are being planned to be connected to the Queensland network. Considering this large scale wind power integration, it is of prime importance to investigate its influence on power system stability. In this paper, small-signal stability of the Queensland network has been re-visited considering near future wind power penetration. The expected wind power is integrated to the nearest available high voltage bus of the grid via step up transformer and transmission line with appropriate capacity. Aggregated doubly fed induction generator model is used to simulate wind farms. This paper investigates the impact of wind power integration on the damping of electromechanical modes of the Queensland grid. Wind power is accommodated by considering load growth and generator displacement individually for getting useful insight into its impact on damping of the grid. PSS/E and Mudpack software is used to carry out simulations.**

Keywords- doubly fed induction generator, small-signal stability, wind farm, wind power generation

I. KEY TABLES

TABLE I
PROJECTS UNDER DEVELOPMENT AND CONSIDERATION

Under Development		Under Consideration	
Project	**Nameplate Capacity (MW)**	**Project**	**Power Generation (MW)**
Bowen	120-240	High Road	40
Crediton	40-90	Mount Emerald (Arriga)	220
Forsayth	70	Windy Hill II	24
High Road	35	Archer Point, Cooktown	120-240
Windy Hill II	24	Kennedy Wind Farm	700

TABLE II
WIND GENERATION SCENARIO IN NORTH QUEENSLAND

Wind Farm	**Scenario (in MW)**				
	A	**B**	**C**	**D**	**E**
Cooktown	80	80	80	80	80
Bowen	90	90	90	90	90
Arriga	-	220	220	220	220
High Road	-	-	100	100	100
Kennedy	-	-	-	350	450
Forsyth	-	-	-	70	70
Crediton	-	-	-	-	90
Total (MW)	170	390	490	910	1100

This work was supported by Powerlink, Queensland through an Australian Research Council Linkage Project.

II. KEY RESULTS

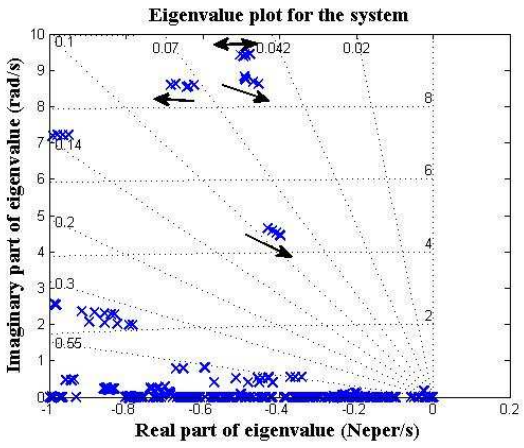

Figure 1. Eigenvalue results showing movement of modes under different wind generation scenario. The arrow indicates the movement of modes from base case to different wind power case.

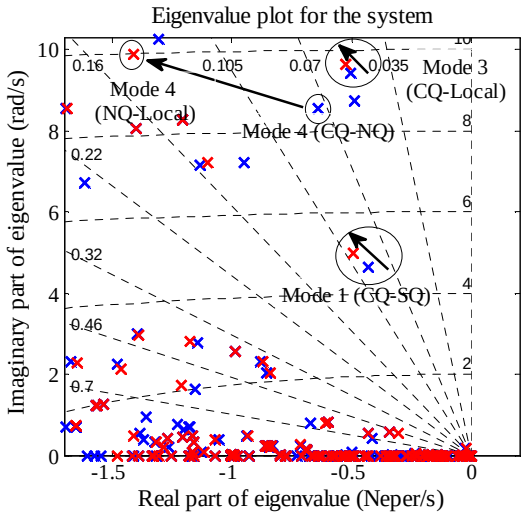

Figure 2. Comparison between eigenvalue plot of the Queensland network considering generation displacement: 'x'(blue) indicates eigenvalue before generation displacement (base case), 'x'(red) indicates eigenvalue after generation displacement (Scenario E).

Inertial response capability of DFIG wind turbine

Stefanie Kuenzel
Control and Power Research Group, Department of Electrical and Electronic Engineering
Imperial College London, UK
Email: stefanie.kuenzel06@imperial.ac.uk

***Abstract*—Wind turbines under normal operation are usually set to produce at maximum power output since they do not require costly fuels. This means that they are limited in the inertial response they can physically supply. In the rated regime they can supply power by releasing some kinetic energy by slowing down. In the rated regime they can decrease the pitch angle temporarily to increase the wind power extraction. At the onset of the rated regime the wind turbine control will first reduce the pitch angle. Since for small pitch angles this is not sufficient, the control will then also slow the turbine down. This paper analyzes the inertial response that can be provided by a 700 MW group of wind farms. Simulink simulations consider the different wind regions and assume optimal power point tracking before the disturbance.**

I. Introduction

A. Key Equations

Equations of wind power extraction and kinetic power release can be used to model the power release/absorbtion of a 2.3 MW wind turbine during a change in rotational speed analytically.

$$J = P_r^{2.1346} \times 1.7459 \times 10^{-7} \tag{1}$$

$$\Delta P_{mech} = \frac{0.5J(w_{old}^2 - w_{new}^2)}{\Delta time} \tag{2}$$

$$\Delta P_t = 0.5\rho\pi R^2 (C_p(\lambda, \beta) - C_{pmax}) v_w^3 \tag{3}$$

$$\lambda = \frac{\omega_t R}{v_w} \tag{4}$$

B. Key Figures

Figure 2 shows that a turbine in subrated condition can only supply temporary additional power by releasing kinetic energy while the turbine is slowed down. A turbine in rated condition can decrease the pitch angle for increased power output. If this is insufficient the turbine will slow down thereafter.

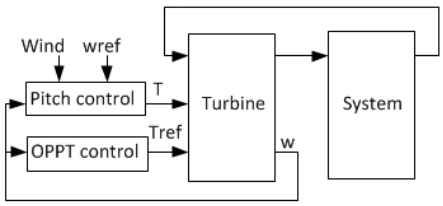

Fig. 1. Simulink setup of simulation

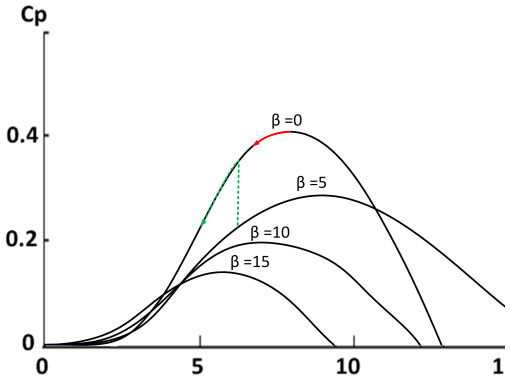

Fig. 2. Frequency response options for turbine working on OPPT curve; solid arrow for subrated regime, dashed arrow for rated regime

C. Key Results

From Figure 3 an extra torque command of 15% was send to the turbine at 5 seconds. It can be seen that in the subrated regime (12.4 m/s) the turbine can only produce extra power for a limited amount of time by releasing kinetic energy. Just at the onset of the rated regime the turbine behavior is very similar, since the pitch angle is very small and the largest part of the response is still supplied by the kinetic energy stored in the turbine. At 13m/s most of the response can be sustained as long as the turbine components can carry the additional stress, since the response can come mainly from the pitch angle.

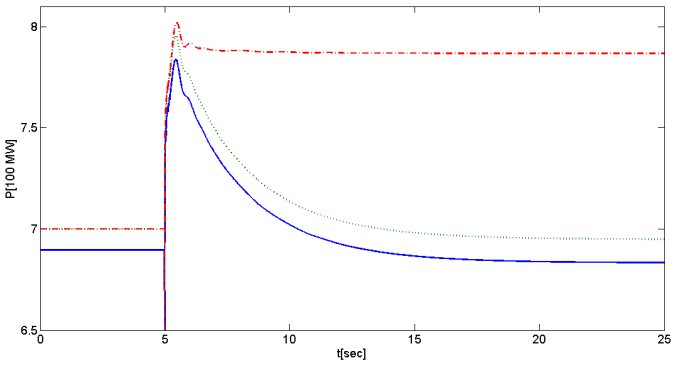

Fig. 3. Frequency response capability of 700 MW group of wind farms at wind speeds of $12{:}4\,m{=}s$ (solid line), 12.47 m/s (dotted) and 13 m/s (dotted and dashed)

Analysis and Mitigation of Transient Overvoltage with Integration of Small Scale Power-Electronic Interfaced DG

T. Aziz, T. K. Saha and N. Mithulananthan
School of ITEE, The University of Queensland, Australia.
Email: taziz@itee.uq.edu.au

***Abstract*— As the amount of non-scheduled small scale distributed generation (DG) units are increasing, lack of fault ride through (FRT) capability of these generators may have an adverse affect on the overall power system. This study focuses on the basics of transient overvoltage issue arising under faulty condition with integration of power-electronic (PE) interface based DG units in a system. Reasons behind this overvoltage issue and its impact on DG integration with present grid standard have been investigated. A methodology has been utilized to overcome this overvoltage issue in a system, which has conventional generator as well as wide penetration of full-converter based solar and wind generation. An IEEE industrial test system with varieties of motor loads has been used to carry out the analysis and to verify the methodology.**

I. KEY EQUATIONS

Dynamics of voltage at DC link capacitor of PE-interfaced DG can be expressed through following equations:

$$\frac{C}{2}\frac{dV_{dc}^2}{dt} = P_{ext} - \left(P_{sf} + \frac{L}{3\hat{V}_s^2}\frac{dP_s^2}{dt}\right) \quad (1)$$

$$\frac{dV_{dc}^2}{dt} = \frac{dy_0}{dt} + \left[-\frac{1}{C}bP_s e^{j(2\theta_0+\psi)}.e^{j2\omega_0 t} - \frac{1}{C}bP_s e^{-j(2\theta_0+\psi)}.e^{-j2\omega_0 t}\right] \quad (2)$$

II. KEY FIGURES

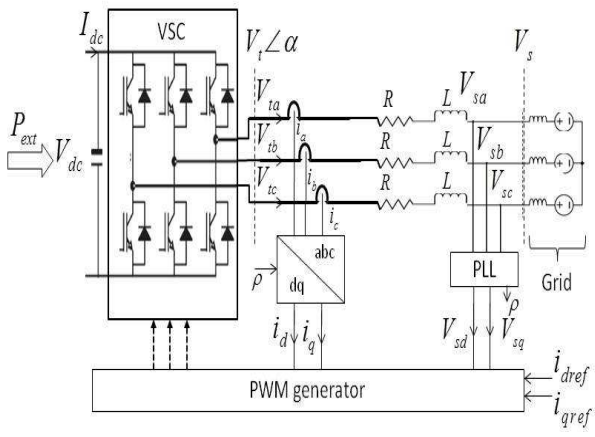

Figure 1. Schematic diagram of PE-interface for DG integration to grid.

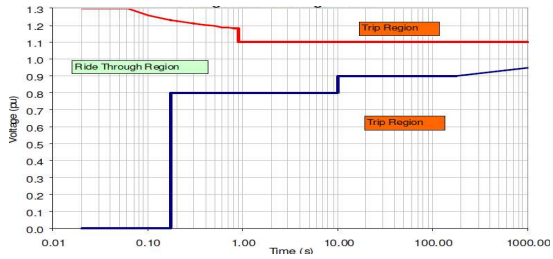

Figure 2. Voltage ride through requirements set by Australian Energy Market Operator (AEMO).

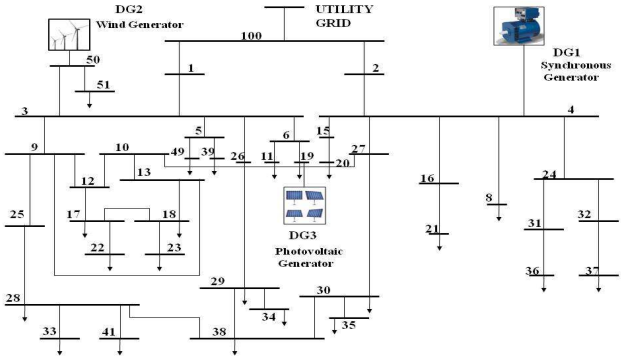

Fig. 3. Test distribution system with disitributed generation units.

III. KEY RESULTS

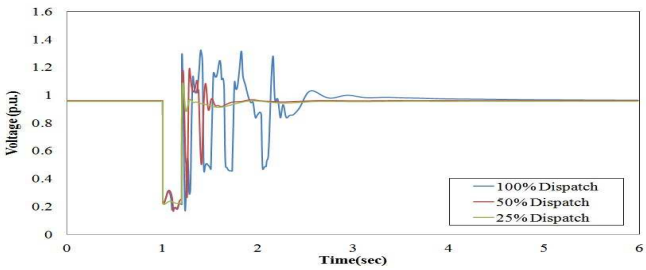

Fig. 4. Voltage excursions at point of common coupling (PCC) of wind generator (bus 50) with various dispatch.

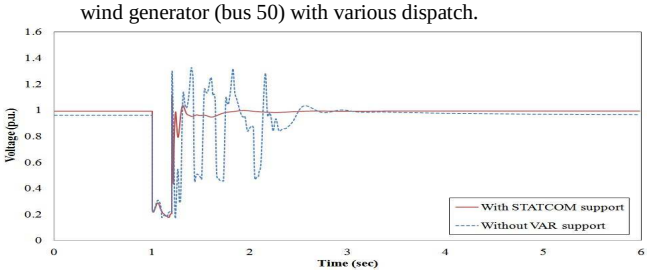

Fig. 5. Voltage recovery at bus 50 with balanced three phase fault at generator vicinity.

Probabilistic Power Flow for Transmission Systems with Photovoltaic Generation Considering Power Dispatching Operation

Miao Fan, *Student Member, IEEE*, Vijay Vittal, *Fellow, IEEE*, Gerald T. Heydt, *Fellow, IEEE* and Raja Ayyanar, *Senior Member, IEEE*

School of Electrical, Computer, and Energy Engineering, Arizona State University, Tempe, AZ 85287, USA, Email: miao.fan@asu.edu, vijay.vittal@asu.edu, heydt@asu.edu and rayyanar@asu.edu

***Abstract*— This paper proposes a novel probabilistic power flow (PPF) algorithm considering the conventional generation behaviors to balance the uncertainties of photovoltaic (PV) generations. PV generation may have a significant impact on transmission systems because its production is easily influenced by ever-changing environmental conditions. However, the generation dispatching law is taken as the means to compensate for PV generation power and to enhance the power systems stability. Therefore, it is more realistic to consider the generation dispatching behavior into the PPF algorithm. The proposed PPF algorithm is based on cumulant method to avoid convolution calculations. Gram-Charlier expansion is applied to approximate the cumulative distribution function (CDF). A 2497-bus representation of the Arizona area of the Western Electricity Coordinating Council (WECC) system is used as a test system to evaluate the performance of the proposed algorithm compared with Monte Carlo simulation (MCS).**

I. KEY EQUATIONS

The guiding equations of the PPF algorithm are:

$$\begin{cases} y = g(x) \\ z = h(x) \end{cases} \tag{1}$$

$$\Delta P_{gen} = T\Delta P_{PV} \tag{2}$$

$$\begin{cases} \Delta x = \begin{pmatrix} \Delta\delta \\ \Delta|V| \end{pmatrix} = \underbrace{\left[S_{P_L}, \left(S_{P_{PV}} + S_{P_{gen}} T \right), S_Q \right]}_{S_{amend}} \begin{pmatrix} \Delta P_L \\ \Delta P_{PV} \\ \Delta Q \end{pmatrix} \\ \Delta z = G\Delta x = GS_{amend}\Delta y = L_{amend}\Delta y \end{cases} \tag{3}$$

$$f_{\Delta x_i}(\Delta x_i) = \frac{1}{|a_{i1}|} f_{\Delta y_1}\left(\frac{\Delta y_1}{a_{i1}}\right) * \frac{1}{|a_{i2}|} f_{\Delta y_2}\left(\frac{\Delta y_2}{a_{i2}}\right) * \cdots * \frac{1}{|a_{in}|} f_{\Delta y_n}\left(\frac{\Delta y_n}{a_{in}}\right)$$

$$f_{\Delta z_j}(\Delta z_j) = \frac{1}{|b_{j1}|} f_{\Delta y_1}\left(\frac{\Delta y_1}{b_{j1}}\right) * \frac{1}{|b_{j2}|} f_{\Delta y_2}\left(\frac{\Delta y_2}{b_{j2}}\right) * \cdots * \frac{1}{|b_{jn}|} f_{\Delta y_n}\left(\frac{\Delta y_n}{a_{jn}}\right) \tag{4}$$

$$f_P(P) = \int_{-\infty}^{\infty} \frac{\Gamma(a+b)}{\Gamma(a)\Gamma(b)} \left(\frac{R}{R_{\max}} \right)^{a-1} \left(1 - \frac{R}{R_{\max}} \right)^{b-1} 1/\sqrt{2\pi} k\sigma_{\Delta T} \exp\left[-\left(P/R - 1 \right)^2 / 2k^2 \sigma_{\Delta T}^2 \right] |R|^{-1} dR \tag{5}$$

II. KEY FIGURES

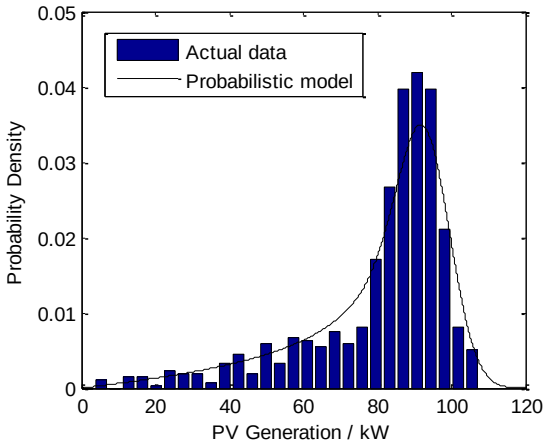

Figure 1. PDF curve of PV generation

III. KEY RESULTS

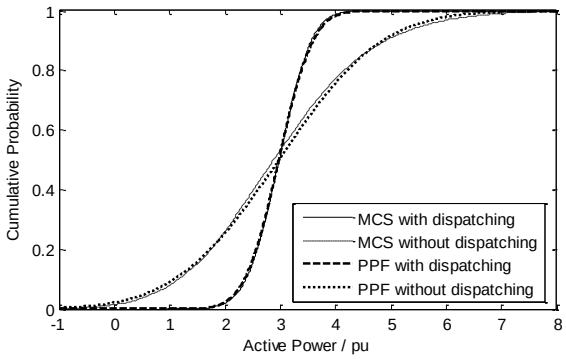

Figure 2. CDF curves of the line flow active power through line 86291-14006 considering generation dispatching operation

TABLE I
COMPARISON OF THE RESULTS FOR THE LINE FLOW ACTIVE POWER THROUGH LINE 86291-14006

	With gen model		Without gen model	
Index	MCS	PPF	MCS	PPF
ARMS / %	0	0.0035%	0	0.0095%
mean / pu	2.97683	2.97500	2.97683	2.97500
std / pu	0.46272	0.48561	1.48475	1.47075
10% CL / pu	2.37775	2.35294	1.17150	1.09162
90% CL / pu	3.55900	3.59756	4.91375	4.86092

Transient Stability Assessment of the Systems with High Penetration of Photovoltaic Generation

Sara Eftekharnejad, Gerald T. Heydt, Vijay Vittal
School of Electrical, Computer and Energy Engineering
Arizona State University
Tempe, AZ 85287, USA
Email: seftekha@asu.edu

***Abstract*—With the rapid movement towards achieving systems with high penetration of renewable energy resources, which is a direct result of the new Renewable Portfolio Standards (RPS), power systems are facing unprecedented structural and market based changes. As most of these changes are expected to occur in a near future, the impact of these resources on the power grids needs to be studied. Among the renewable energy resources, photovoltaic (PV) systems have been given a significant attention in the recent years. As more PV systems are installed in the power grids, more conventional generators, such as the aged fossil based units, are displaced with utility scale as well as rooftop PVs. Due to the distinct characteristics of the PV systems, with high penetration of these resources, a change in static as well as transient behavior of the power systems is expected. However, the exact effect of these changes is yet to be studied and preventive measures should be taken to mitigate the potential adverse effects of these systems. Although the PV systems are installed closer to the loads, with high penetration of these resources their impact will no longer be limited to the distribution systems but rather observed at the transmission systems. This work investigates the impacts of high penetration of photovoltaic systems on transmission system transient stability. Simulation studies are conducted on a large power system to identify the beneficial or detrimental impacts of large scale integration of PV systems into the existing power systems. Various PV penetration levels are studied for comparison purposes to observe the behavior of the system as PV generation levels increase. Case studies simulated in this work range from a generator outage, double line outages to a three phase fault on the transmission system. Effects of cloud cover are also examined on the studied system to observe the behavior of the weather fluctuations on the transmission level bus voltages.**

I. KEY TABLES

TABLE I
SUMMARY OF PV PENETRATION LEVELS

PV generation (MW)	2158	4316	6475	8633	10792
PV level by name plate (%)	10	20	30	40	50
PV level (%) (by energy)	2.5	5	7.5	10	12.5

TABLE II
SUMMARY OF THE STUDIED AREA

Total Load	MW	13276.82
	MVAr	2187.90
Total Generation	MW	21571.03
	MVAr	2238.72
Total Export	MW	7650.83
	MVAr	63.4
Total Losses	MW	607.82

II. KEY RESULTS

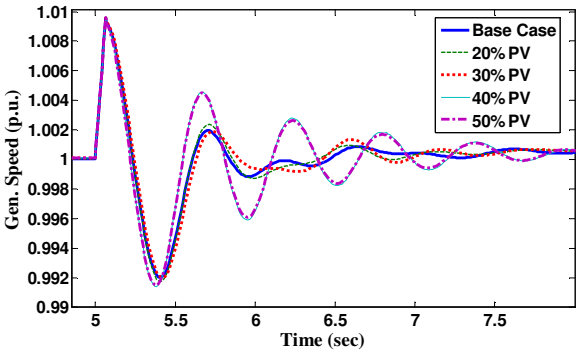

Figure 1. An example of the detrimental impact of high PV penetration following a three phase fault at the transmission system.

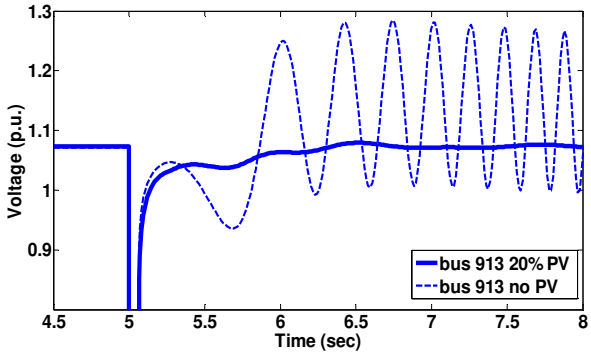

Figure 2. An example of the beneficial impact of high PV penetration following a double line outage at the transmission system.

Cascading Tripping out of Numerous Wind Turbines in China: Fault Evolution Analysis and Simulation Study

Xi Ye, Ying Qiao, Zongxiang Lu, *Member, IEEE*

***Abstract*-- Cascading tripping out of numerous wind turbines will threaten the security of power grid with high wind power penetration. This paper focuses on those failures that happened successively in Northwest and North China 2011. Firstly, analyzes the typical failure evolution process over spatial and temporal scales, and then studies how important factors impact those failures which sweep over the total wind farm clusters because of unusual voltage fluctuation from three aspects: the weak network, the wind power integration style and the operating condition. In addition, this paper also discusses the internal mechanism of those cascading tripping out failures by simulation verification based on a region power grid in China.**

I. KEY EQUATIONS

U-P sensitivity derivation of a simple system integrated with Bulk Wind Power:

$$\begin{bmatrix} \overset{n\times 1}{\Delta P} \\ \overset{(n-r)\times 1}{\Delta Q} \end{bmatrix} = -\begin{bmatrix} \overset{n\times n}{H} & \overset{n\times(n-r)}{N} \\ \overset{r\times n}{M} & \overset{(n-r)\times(n-r)}{L} \end{bmatrix} \times \begin{bmatrix} \overset{n\times 1}{\Delta\theta} \\ \overset{(n-r)\times(n-r)}{U^{-1}} \quad \overset{(n-r)\times 1}{\times \Delta U} \end{bmatrix} \tag{1}$$

$$U^{-1}\Delta U = (-MH^{-1}N + L)^{-1} \times MH^{-1}\Delta P = S_{\text{up}}\Delta P \tag{2}$$

$$\frac{\Delta U}{U} = -\frac{P_1}{\left(V_1^2 B_c - \frac{V_1^2}{X}\right)^2 - \left(P_1^2 + Q_1^2\right)}\Delta P = S_{up}\Delta P \tag{3}$$

II. KEY FIGURES

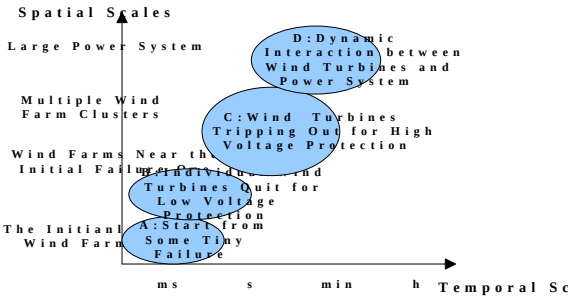

Fig. 1 Typical Procedures in Corresponding Spatial-Temporal Scales

III. KEY RESULTS

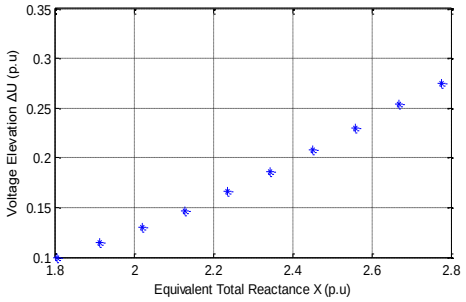

Fig. 3 Relationship between the Terminal Voltage Elevation ΔU and Equivalent Total Reactance X

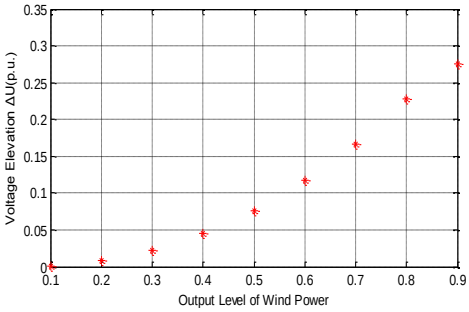

Fig. 4Relationship between the Terminal Voltage Elevation ΔU and Wind Power Output Level

Tab. 1 *U-Q* Sensitivity

Wind Farm	0.85 Output	0.9 Output	0.3 Output	0.4 Output
Wind Farm 1	0.0100	0.0145	0.0019	0.0020
Wind Farm 2	0.0100	0.0146	0.0020	0.0020
Wind Farm 3	0.0131	0.0196	0.0020	0.0021
Wind Farm 4	0.0407	0.0601	0.0022	0.0023
Wind Farm 5	0.0417	0.0613	0.0025	0.0025
Wind Farm 6	0.0414	0.0611	0.0024	0.0025
Wind Farm 7	0.0449	0.0663	0.0027	0.0027
Wind Farm 8	0.0451	0.0665	0.0027	0.0028
Wind Farm 9	0.0962	0.1362	0.0028	0.0030
Wind Farm 10	0.0967	0.1368	0.0029	0.0030
Wind Farm 11	0.1061	0.1489	0.0028	0.0030
Wind Farm 12	0.1243	0.1719	0.0029	0.0030

IV. KEY CONCLUSIONS

The cascading tripping out failures usually experience four typical development procedures. The weak network, the integration style of centralized integration and the operation condition of high wind output level contribute together to the dominant factors in the cascading failure evolution process. The research results based on the real region power grid indicate the poor voltage stability under heavy loaded condition is one of the internal mechanisms that those failures frequently occur there. What's more, the unity power factor control mode is another reason that those failures will evolute very rapidly.

Reliability Quantification and Visualization for Optimal Asset Dispatch in Electric Microgrids

Mayank Panwar, *Student Member IEEE*,
Advanced Power Engineering Laboratory, Department of Electrical and Computer Engineering,
Colorado State University, Fort Collins, CO 80523, USA,
Email: *mayank@rams.colostate.edu*

Abstract **- Microgrids are a heterogeneous combination of distributed generation, renewable energy sources and demand response assets located at distribution levels (lower voltage levels, typically < 69kV). Microgrids are designed to serve local loads in a small geographical area typically spanning a city and are capable of performing islanded operation when required, hence increasing reliability of electric power system as a whole. Black start up capability when bulk power grid goes down and blackout occurs, peak shaving capability to reduce feeder load by up to 20-30 percent of total feeder load and frequency control are some of the characteristics. Microgrids assist in enhanced penetration of renewable resources and increase distributed generation participation. There is a single point of control for a cluster of assets at different locations. Controllable generation assets such as diesel, natural gas and mixed fuel generators, fuel cells, uncontrollable assets such as solar photovoltaic, combined heat and power (CHP), load shedding and storage resources such as HVAC, Plug-in Hybrid Vehicles (PHEVs) form a microgrid.**

Reliability calculations are presented here for an operational microgrid in city of Fort Collins - FortZED RDSI, a US Department of Energy funded project [1]. The project was aimed at feeder peak load reduction by 20%. The results achieved were in range of 6.6-18.5% for final period of test runs from August 15 to September 1, 2011. The test run data obtained from data acquisition system was processed in MATLAB to remove inconsistencies, excursions and measurement errors.

The original data obtained from the tests was time-stamped and reduced only for changes in the asset output. This time scale irregularity was to be dealt with to do any further analysis on the data. So, the data was processed using a Simulink sampling model to obtain uniformly time-stamped data with a time resolution of one second. The test runs spanned over a period of three periods with a total of about 40 days. The data was further reduced to extract just the test run time period data for further analysis.

Some performance metrics such as starting reliability, average run time, service factor, net capacity factor, net output factor, availability factor and weighted service factor were calculated using the NERC criterion for performance [2]. Most of the assets showed performance comparable to the present bulk power system that is a significant criterion for any microgrid system to be integrated to main grid and perform satisfactorily within strict operation criterion. A metric used to quantify the performance was the *peak reserve ratio (PRR)*.

$$\text{PRR} = \frac{\text{RDSI Capacity} - \text{RDSI Output}}{\text{Net Feeder Load} + \text{RDSI Output}}$$

Next step is to conceive a visualization tool for these performance metrics. Visualization is an important aspect to present data in a comprehensive form which could assist better performance of a microgrid. This would assist the operator at the control center to make informed decisions on asset dispatch based on the past performance of individual assets or combination of assets which is reflected in reliability metrics of the assets and the system.

I. RESULTS

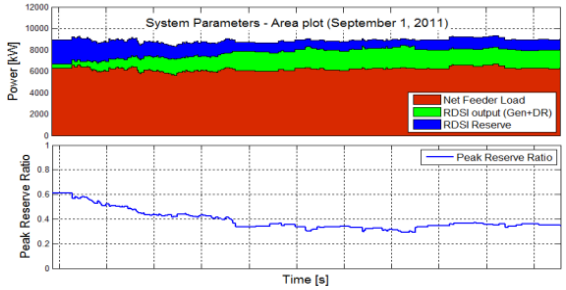

Figure 1: RDSI system performance quantified using the peak reserve ratio metric.

II. REFERENCES

[1] Fort Collins FortZED RDSI project website [Online] Available: http://www.fortzed.com/ Accessed: 4/20/2012

[2] NERC 2007 Generating Unit Statistical Brochure - Units Reporting Events (Revised 04/09) [Online] Available: http://www.nerc.com/page.php?cid=4|43|47

Acknowledgement - This material is based upon work supported by the US-Department of Energy through FortZED RDSI and Power Systems Engineering Research Center (PSERC).

Targeted Conversion of AC lines to DC lines for Improved Power System Dispatch

Omar A. Urquidez*, Le Xie*
*Department of Electrical and Computer Engineering, Texas A&M University, College Station, TX USA
Email:dantes92@tamu.edu, Lxie@ece.tamu.edu

***Abstract*— In this paper the concept of targeted conversion of AC lines to DC lines is proposed for improved security-constrained economic dispatch by incorporating the converted line into the formulation to improve flow pattern control and relieve flow constraints on both the converted line and the remaining AC system. The proposed model treats the flow on the converted line as an independent control variable for the operator to utilize. It is shown that the introduction of this additional control variable significantly decreases the dispatch cost through congestion relief. Wind curtailment due to transmission congestion, is also shown to be significantly relieved. The technical feasibility of the implementation, combined with the economic benefits, suggests that targeted conversion of AC lines to DC lines is a promising approach to best utilize the transmission grid for maximized social welfare. Numerical examples on a 24-bus system modeling ERCOT demonstrate the technical feasibility and economic benefits for renewable energy resources by use of the proposed conversion.**

Our method contrasts with two current paradigms: 1) building new AC lines to relieve interzonal congestion is the best path forward; 2) DC lines are used for ultra long distance transmission or system synchronization. The proposed line conversion is readily implementable with much lower time and capital costs. A metric deemed percent of total relief (PTR) is used to compare results from different line conversions normalized by the dispatch savings shown in a total relief scenario. Numerical experiments show that the carefully placed conversion can reach PTR values near 100. The experiments also show that PTR levels of higher than 90 even a significantly more stress grid system that has double the wind capacity and 50 percent more demand.

I. Key Equations

The economic dispatch formulation of the mixed AC-DC system is formulated as follows:

$$\min_{P_{INJ,p},P_{EXT,q},P_{Gi}} \sum C_{Gi} \cdot P_{Gi} + \left(P_{INJ} + P_{EXT}\right) \cdot 0$$

s.t.

$$P_{Gi}^{\min} \le P_{Gi} \le P_{Gi}^{MAX}, i \in G \quad (1)$$

$$P_{INJ,p} = -P_{EXT,q} \le F_{DC}^{MAX} = F_i \quad (2)$$

$$\left|F_{AC}\right| \le F_{AC}^{MAX} \quad (3)$$

$$\sum_{i \in G} P_{Gi} = \sum_{i \in L} P_{Li} \quad (4)$$

$$B_{R-AC} = A_{AC} \cdot diag(b_{AC}) \cdot A_{AC}^{T} \quad (5)$$

$$H_{AC} = diag(b_{AC}) \cdot A_{AC}^{T} \cdot B_{R-AC}^{-1} \quad (6)$$

$$F_{AC} = H_{AC} \cdot P_{AC} \quad (7)$$

II. Key Figures

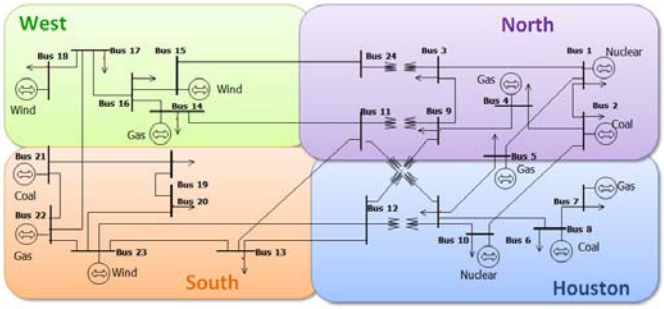

Figure 1. ERCOT Model System modified from IEEE RTS 24.

III. Key Results

TABLE I
DISPATCH COST AT CURRENT WIND AND LOAD LEVELS

	Line	Dispatch Cost (k$/day)	Dispatch Cost Decrease (k$/day)	% of Total Relief
Base Case	-	30,512.45	-	-
Total Relief	-	30,481.19	31.26	100.00
Trial 1	2-6	30,483.28	29.17	93.31
Trial 2	5-10	30,483.17	29.27	93.64
Trial 3	11-13	30,481.19	31.26	100.00
Trial 4	11-14	30,481.19	31.26	100.00
Trial 5	15-24	30,507.28	5.17	16.54

TABLE II
DISPATCH COST AT INCREASED WIND AND LOAD LEVELS

	Line	Dispatch Cost (k$/day)	Dispatch Cost Decrease (k$/d)	% of Total Relief
Base Case	-	40,518	-	-
Total Relief	-	35,950	4,568	100.00
Trial 1	2-6	40,257	263	5.77
Trial 2	5-10	40,214	304	6.66
Trial 3	11-13	36,364	4,154	90.93
Trial 4	11-14	39,670	849	18.57
Trial 5	15-24	40,062	456	9.98

Optimal Incentive Design to Facilitate Solar PV Investments

Indrajit Das, *Student Member, IEEE,* Kankar Bhattacharya, *Senior Member, IEEE,*
and Claudio Cañizares, *Fellow, IEEE,*
Department of Electrical and Computer Engineering, University of Waterloo, Waterloo, Canada.

***Abstract*—Solar photovoltaic (PV) generation has become an economically feasible and clean energy supply option for large scale grid connected operations. From a power generation planning perspective, the design of a feasible incentive that lures investors to participate in the solar PV generation market is required. In this context, the province of Ontario, Canada, has a Feed-in-Tariff (FIT) program to encourage investment in large scale solar PV projects [1]. Thus, an optimization model is presented to determine an optimal incentive rate that will facilitate investments in grid-connected solar PV projects. The model determines a range of feasible FIT values that will provide investors with a guaranteed internal rate of return (IRR). It also identifies the most preferred zones in the province for new PV installations, from a system planning perspective. The model is applied to the case of Ontario, to determine the optimal FIT.**

I. Introduction

The objectives of this work are as follows:

- Develop an optimization model to determine optimal incentives for large-scale solar PV projects.
- Incorporate transmission line flow limits, bus angle limits, and dc load flow to represent system security issues.
- The optimal FIT should guarantee a minimum Internal Rate of Return (IRR) to the investor.

II. Modeling

The model is a non-linear programming (NLP) problem with an objective function that minimizes the net present value of the payment that investors in solar PV projects will receive from the planning authority.

The various planning constraints are the following:

- Supply demand balance
- Conventional energy generation limit
- Solar PV energy generation limit
- Transmission line flow limits
- Bus angle limits
- Dynamic constraint on solar PV capacity addition
- Initial year investment constraint
- Terminal year investment constraint
- Solar PV lifetime constraint
- IRR constraints

III. Case Studies

The Ontario transmission system model is shown in Fig. 1 [2]. For a 10% reduction in conventional generation capacity and 17% IRR, the optimal plan solution is a FIT rate of 24.61 cents/kWh, and the size, site and timing of solar PV installation is 2771 MW capacity in the Ottawa zone (Fig. 1), in the ninth year. Figure 2 shows the variation in FIT with reduction in conventional generation capacity for various IRR values.

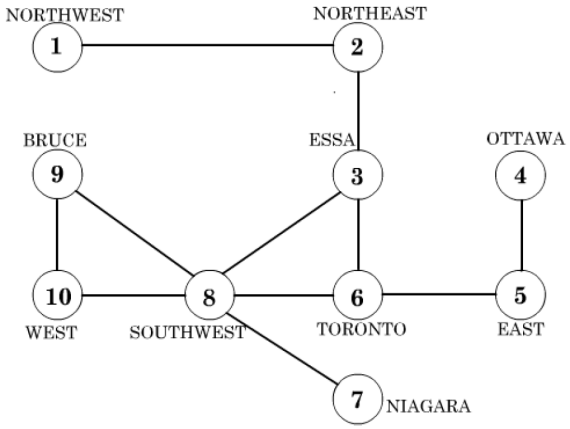

Fig. 1. Ten-zone simplified transmission model of Ontario

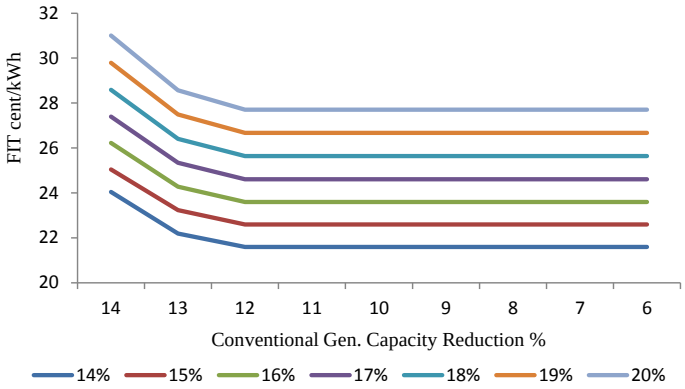

Fig. 2. Variation of FIT with conv. gen. for various IRR (Legend: IRR %)

References

[1] *FIT Program*, 2010, Ontario Power Authority. [Online]. Available: http://fit.powerauthority.on.ca/fit-program

[2] *Ontario Transmission System*, 2009, Independent Electricity System Operator (IESO). [Online]. Available: www.ieso.ca/imoweb/pubs/marketReports/OntTxSystem_2009aug.pdf

Evaluation of Islanding Detection Techniques for Inverter-Based Distributed Generation

Omar N. Faqhruldin E.F. El-Saadany, and H. H. Zeineldin
Power and Energy Systems Group, Department of Electrical and Computer Engineering, University of Waterloo, Waterloo, Ontario, Canada,
Email: *ofaqhrul@uwaterloo.ca*

***Abstract*— In this paper; four islanding detection techniques for inverter-based distributed generator (DG) are presented. The techniques are: decision tree (DT), support vector machine (SVM), radial basis function network (RBF), and probabilistic neural network (PNN). In literature, these techniques were proposed as islanding detection methods. However, the proposed techniques face various limitations such as the size and type of the used distribution network and the limitation of the extracted features. This paper overcomes these limitations and gives a very accurate comparison between these techniques by extracting seven features from damped-sinusoid model of the voltage and frequency waveforms using the MATLAB/SIMULINK and also using the IEEE 34-bus distribution system. The results show that out of the four tested techniques, PNN technique can accurately detects islanding for inverter based DG.**

I. KEY FIGURES

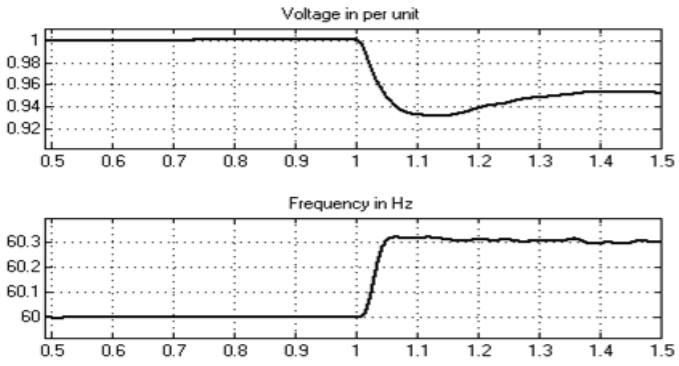

Fig. 1. Plots of PCC voltage and system frequency due to an islanding event at t=1 s for +10% active power and +1% reactive power mismatch for an RLC load.

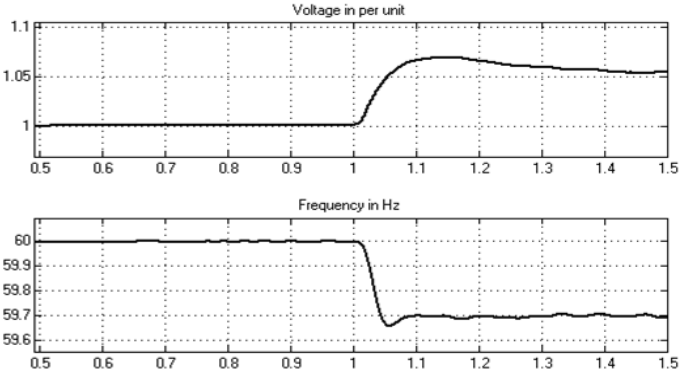

Fig. 2. Plots of PCC voltage and system frequency due to an islanding event at t=1 s for -10% active power and -1% reactive power mismatch for an RLC load.

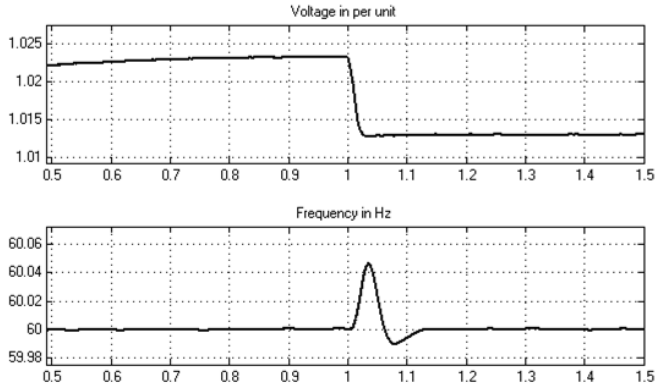

Fig. 3. Plots of PCC voltage and system frequency due to 100-kW load switching at bus 838 (non-islanding event) at t=1 s.

II. KEY RESULTS

Table 1: Overall Performance of the Four Techniques

	Classification accuracy (%)		
	Islanding	Non-islanding	Overall
SVM	88.89	81.82	85
DT	88.49	91.67	90
RBFNN	95.83	92.31	94
PNN	97.96	96.08	97

An Enhanced Fault-Ride-Through Capability of Doubly-Fed Induction Generators during Grid Faults

Maher Abdelkhalek Azzouz
University of Waterloo
Electrical & Computer Engineering
Waterloo, Canada
mazzouz@uwaterloo.ca

Ehab El-Saadany
University of Waterloo
Electrical & Computer Engineering
Waterloo, Canada
ehab@uwaterloo.ca

***Abstract*—This paper discusses a new improved fault ride through technique of wind turbines equipped with doubly-fed induction generators (DFIG). The proposed technique replaces the conventional crowbar with a rotor current limiter (RCL) which is inserted to the rotor circuit upon grid faults detection. In additional to inserting a RCL, demagnetizing rotor currents are injected in order to reduce the induced high voltage appears on the rotor side converter. The proposed method allows the rotor side converter to stay connected to the system such that the DFIG can continue its normal operation immediately after the fault clearance. The simulation results show that the proposed technique limits the rotor inrush currents, DC voltage fluctuations, electromagnetic torque pulsations, and reactive power absorption during the fault and after the fault clearance.**

I. EQUATIONS

The following three equations, generally, describe the rotor voltage and stator flux of DFIG:

$$\vec{v}_r = \vec{v}_{ro} + \left(R_r + \left(\frac{L_m}{L_s} \right)^2 R_s + \sigma L_r \left(\frac{d}{dt} - j\omega_r \right) \right) . \vec{i}_r \tag{1}$$

$$\vec{v}_{ro} = \frac{L_m}{L_s} \left(\vec{v}_s - \left(\frac{R_s}{L_s} + j\omega_r \right) \vec{\psi}_s \right) \tag{2}$$

$$\vec{\psi}_s = \frac{V_s}{j\omega_s} e^{j\omega_s t} = \Psi_{sf} e^{j\omega_s t} \tag{3}$$

The induced rotor voltage under normal operation can be calculated as

$$\begin{aligned} \vec{v}_{ro} &= \frac{L_m}{L_s} V_s \left(1 - \frac{\omega_r}{\omega_s} \right) e^{j\omega_s t} \\ &= \frac{L_m}{L_s} s V_s e^{j\omega_s t} \\ &\approx s V_s e^{j\omega_s t} \end{aligned} \tag{4}$$

The induced rotor voltage under full voltage dip can be calculated as

$$\vec{v}_{ro} = -\frac{L_m}{L_s} \left(\frac{1}{\tau_s} + j\omega_r \right) \vec{\Psi}_0 e^{-t/\tau_s} \tag{5}$$

$$\begin{aligned} \vec{v}_{ro}(t_o) &= -\frac{L_m}{L_s} \frac{\omega_r}{\omega_s} V_s \\ &\approx (1-s) V_s \end{aligned} \tag{6}$$

II. KEY FIGURE

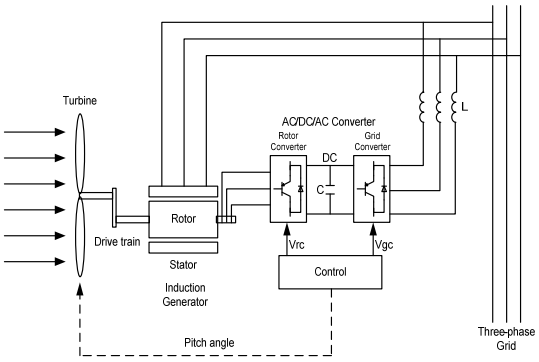

Fig. 1 Wind Turbine with DFIG

III. KEY RESULTS

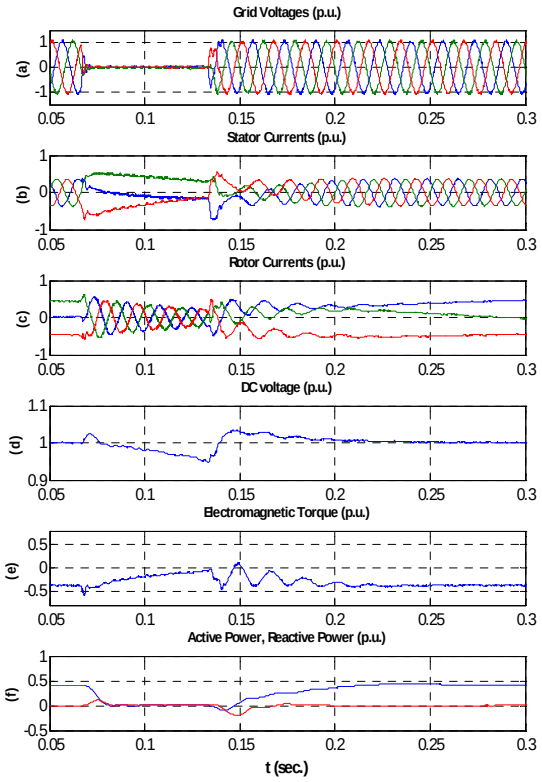

Fig. 2 WECS response during the grid fault using the proposed protection

Increasing Renewable Energy Utilization through Nonlinear Load Frequency Control Model

Toshiki Takayama, Yuya Maruno and Shinichi Iwamoto
Power Systems Laboratory, Department of Electrical Engineering and Bioscience,
Waseda University, Tokyo, 169-8555, JAPAN
Email: *takayama.toshiki.pwrs@gmail.com*

Abstract— **Environmental problems have prompted the spread of renewable energies such as wind and solar power. In addition, the Fukushima Daiichi nuclear disaster resulting from the Great East Japan Earthquake has raised safety concerns about nuclear power plants in Japan, and has also increased the adoption of renewable energies. However, this wide-scale introduction of renewable energies may adversely affect load frequency control (LFC), which maintains deviations of frequency and tie-line power flow within certain tolerances. In this paper, we focus on frequency deviations caused by changes in generator output. Moreover, we propose a method to optimally allocate renewable energy and secondary battery systems in order to increase the amount of energy from renewable power sources in the power grid under pre-specified frequency constraints. Instead of the conventional linear LFC model, the proposed method employs a nonlinear LFC model that performs a detailed analysis by solving the swing equations of individual generators to calculate state variables in the system. Finally, to validate the proposed method, we perform numerical simulations using a 9-machine 20-bus power system.**

Ⅰ. KEY EQUATIONS

$$\begin{cases} \dfrac{d\delta_i}{dt} = \omega_i - 2\pi f_0 \\ \dfrac{d\omega_i}{dt} = \dfrac{\pi f}{H_i}\left(P_{mi} - P_{ei}\right) \end{cases} \quad (1)$$

$$\begin{cases} AR_1 = -\beta\Delta f_1 - \Delta P_{tie} \\ AR_2 = -\Delta f_4 \end{cases} \quad (2)$$

Ⅱ. KEY FIGURES

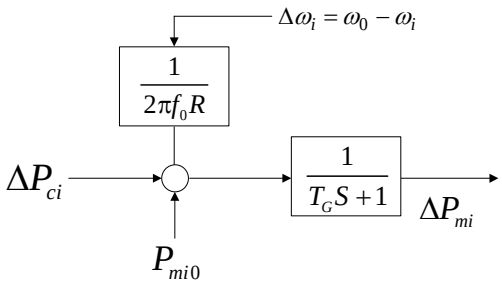

Fig. 1. Block diagram of the governor

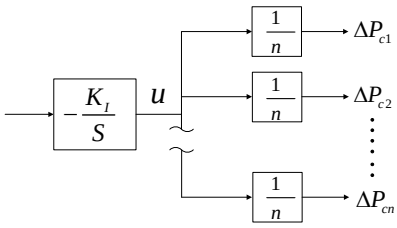

$$\Delta P_c = \Delta P_{c1} + \Delta P_{c2} + \cdots + \Delta P_{cn}$$

Fig. 2. Concept of the ΔP_c calculation

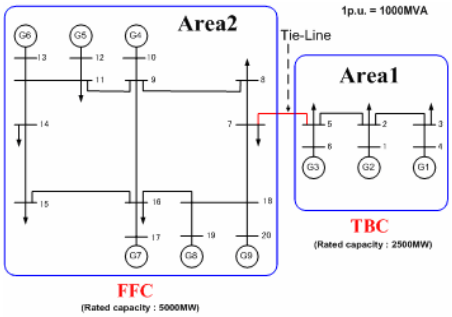

Fig. 3. 9-machine 20-bus system

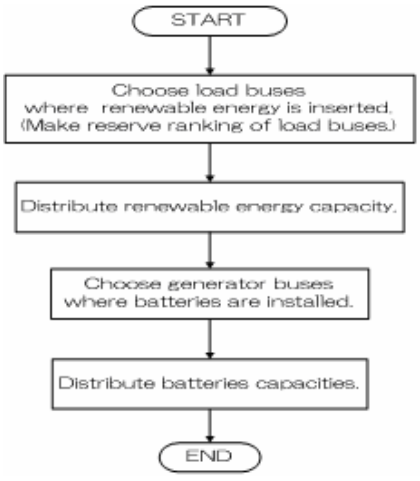

Fig. 4. Flowchart of the proposed method

Ⅲ. KEY RESULTS

TABLE 1. Simulation Results

	Installed capacity [pu]	Improvement [pu]	Percentage [%]
Conventional	0.367	—	—
Without battery	0.386	0.019	5.18
With battery	0.462	0.095	25.9

PQ and PV control of photovolatic generator in three-phase distribution system

Sarina Adhikari, Student member, IEEE, Fangxing Li, Senior member, IEEE
Dept. of Electrical Engineering and Computer Science
University of Tennessee at Knoxville (UTK)
Knoxville, TN 37996, USA
sadhikar@utk.edu;fli6@utk.edu

***Abstract*—Due to the increasing environmental concerns, there is a growing interest towards the renewable energy based Distributed Energy Resources (DERs) like photovoltaic (PhV) generators. With the maximum power point tracking (MPPT) controls, the efficiency of the PhV systems can be optimized. A method of MPPT control on the basis of power balance between the DC and AC side in a two stage PhV configuration is developed. With proper controls of the PhV inverters, these generators are capable of producing necessary amount of reactive power so as to provide required voltage support. Similarly, the amount of real (P) and reactive (Q) power can be controlled to match the load profile. The MPPT control is integrated with voltage and PQ controls separately as PV and PQ control objectives and system impacts studies are performed. The control algorithms have been tested in IEEE 13-bus distribution feeder. The simulation results proves the capability of PV systems in controlling voltage of the weak buses of the distribution system as well as in providing desired amount of real and reactive power while operating PhV at MPP. The effectiveness of the control algorithms is clearly visible from the results presented.**

Keywords- photovoltaic generators; voltage control; real and reactive power control; Maximum power point tracking(MPPT)

I. KEY FIGURES

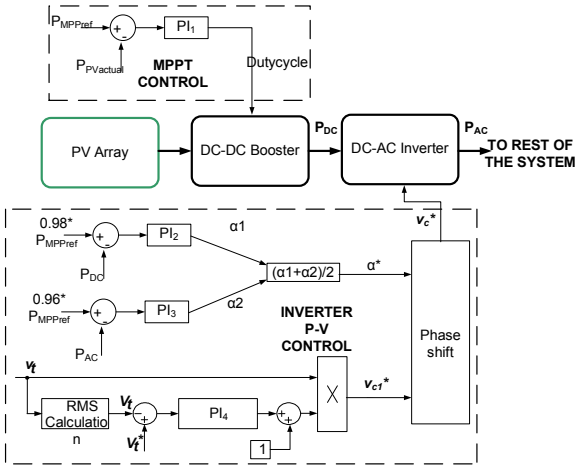

Fig. 1. MPPT Control Diagram and configuration.

II. KEY EQUATIONS

The equations related to voltage control, PQ control and modeling of Solar PV are as follows:

$$v_c^*(t) = v_t(t)\left[1 + K_P\left(V_t^*(t) - V_t(t)\right) + K_I \int_0^t \left(\left(V_t^*(t) - V_t(t)\right)dt\right)\right] \quad (1)$$

$$v_{c1}^* = \left[1 + K_{P1}(Q^* - Q_{act}) + K_{I1}\int_0^t (Q^* - Q_{act})dt\right]v_t(t) \quad (2)$$

$$\alpha^* = K_{P2}(P^* - P_{act}) + K_{I2}\int_0^t (P^* - P_{act})dt \quad (3)$$

$$I = I_{PV} - I_o\left[\exp\left(\frac{V + R_S I}{V_{therm} a}\right) - 1\right] - \frac{V + R_S I}{R_{sh}} \quad (4)$$

III. KEY RESULTS

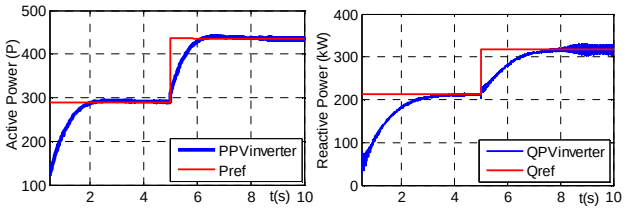

b) Active power a) Reactive power

Fig. 2. Active and reactive power control results.

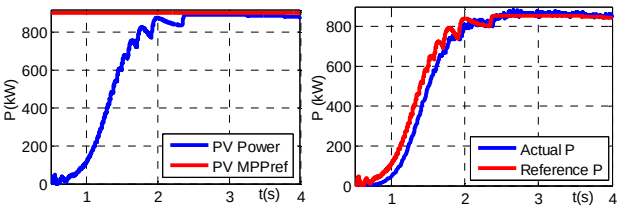

b) PV Array power a) PV inverter power output

Fig. 3. MPPT control results.

Solar Panel DC-DC Converter Configuration for Optimizing Output Power

Carl B. Westerby, *Student Member IEEE*

***Abstract*—Renewable energy is continuing to grow around the world to meet the constantly increasing demand for power. Photovoltaic (PV) solar is a key component in the spectrum of renewable energy. An important control topology for PV panels is maximum power point tracking (MPPT), which varies the voltage in order to achieve the maximum amount of power. One of the main ways that this type of control can be realized is by perturbing (increasing or decreasing) the output voltage and observing the change in power. This proposal compares the performance of a single DC-DC converter, operating on two solar panels in parallel, to the performance of two DC-DC converters, operating on individual panels. The advantage of having multiple converters is that each converter optimizes the power of the individual panel connected to it. As the irradiance of one panel drops, the MPPT voltage (V_{MPPT}) of an individual controller varies more, making it is easier to achieve MPPT.**

I. SIMULATION SETUP

The power output can be simulated by inputting a voltage ramp to the PV panel(s) and measuring the output current. Shading and drops in irradiance can be modeled as variations in the short-circuit current of a panel. The two configurations are shown below.

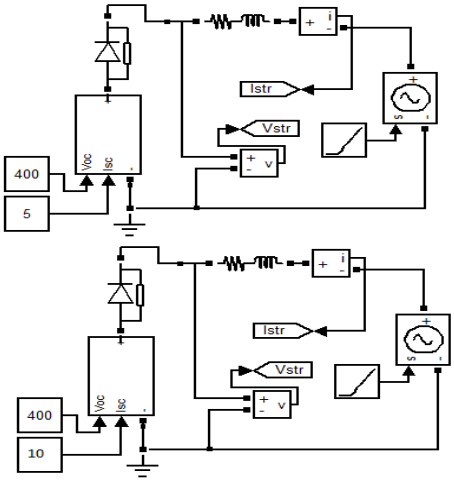

Figure 1: Two (2) converters, one for each panel

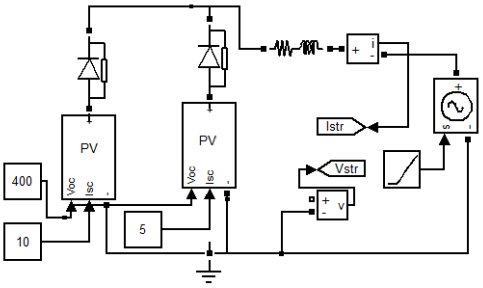

Figure 2: One (1) converters, two panels in parallel

II. KEY RESULTS

The following figure plots the power difference ($P_{1converter}$-$P_{2converters}$) between two converters in parallel and one converter with two PV panels in parallel. The short circuit current of one panel is held at 10A, and the other is varied from 10A to 1A.

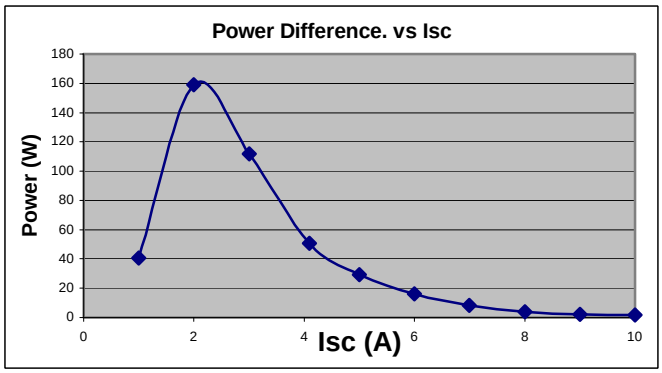

Figure 3: Power difference between two (2) converters and one (1) converter vs. panel short-circuit current

The positive power indicates that the multiple converter configuration's output is greater. As the short-circuit current decreases, the power difference increases until the second panel begins to turn off.

Another issue is the voltage required to achieve MPPT. Since resolution of a perturb and observe (PO) control method is limited by the DC-DC converters ability to adjust voltage, the voltage at MPPT is important. The following figure plots the V_{MPPT} against the panel short-circuit current.

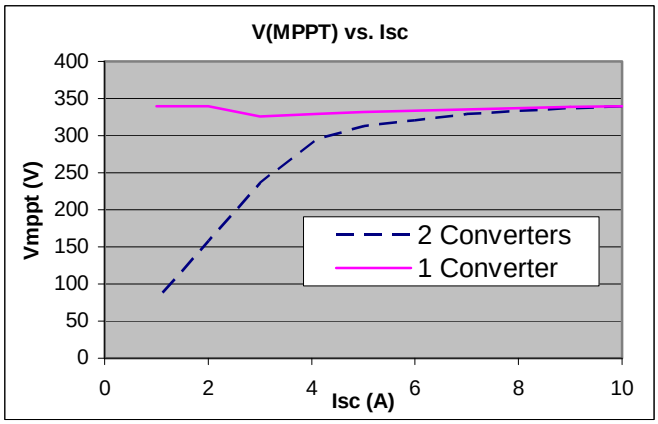

Figure 4: V_{MPPT} vs. panel short circuit current

The individual converter V_{MPPT} voltage varies more as the short-circuit current drops. This means that less precision is needed to achieve MPPT. This makes MPPT controller design easier since less converter resolution is needed.

MW Resource Assessment Model for a Hybrid Energy Conversion System With Wind and Solar Resources †

Subhadarshi Sarkar, *Student Member, IEEE* and Venkataramana Ajjarapu, *Fellow, IEEE*
Department of Electrical and Computer Engineering, Iowa State University, Ames, IA 50011 USA
Email: ssarkar@iastate.edu and vajjarap@iastate.edu

***Abstract*—The combined utilization of renewables such as wind and solar energy is becoming increasingly attractive. This work aims to develop a procedural tool that will facilitate the development and deployment of a utility scale wind-solar hybrid energy conversion system (HECS). It will result in a methodology for identifying suitable hybrid plant locations and calculating an optimized plant sizing and energy storage control strategy which will allow for reliable power injection that is capable of meeting the demands of a variable load. Proper methods need to be employed that consider the inherent variability of these two technologies while determining the performance of a wind-solar HECS. A HECS Identification tool has been developed which creates a pairing of different wind and solar locations to form individual hybrid sites based on resource complementarity and the geographical layout. A stochastic approach has been utilized to develop the MW Resource Assessment Model (MWRAM) of a wind and solar HECS at any given site. The parameters required to define the probabilistic models have been computed from site-specific data using the maximum likelihood estimation method. Different applications of the model to assess resource benefits including capacity factors and reserve requirements from effective utilization of both wind and solar energy have been explored at different levels of varying wind and solar proportions.**

I. MW Resource Assessment Model (MWRAM) Flowchart

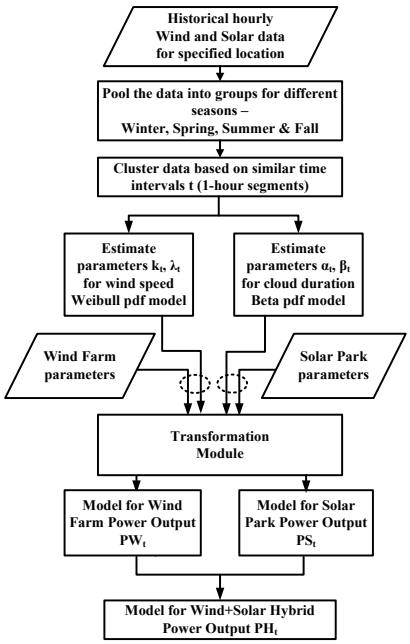

II. Key Equations

Transformation Theorem: Let x be a random variable following a probability density function $f_x(x)$ and cumulative distribution function $F_x(x)$ such that $f_x(x) = \frac{dF_x(x)}{dx}$. We have another variable y such that $y = g(x)$. Suppose we need to determine the density $f_y(y)$ in terms of the density $f_x(x)$ of x. We assume that x is continuous and $g(x)$ is continuous. To find $f_y(y)$ for a given y, we solve the equation $y = g(x)$ for x in terms of y. Let x_i be all the real roots of $y_i = g(x_i)$, then $f_y(y) = \sum_i \frac{f_x(x_i)}{|g'(x_i)|}$, where $g'(x) = \frac{dg(x)}{dx}$.

III. Key Figures and Results

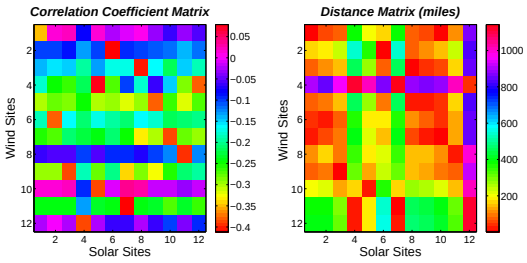

Fig. 1. HECS ID Tool: Correlation Coefficient Matrix and Distance Matrix

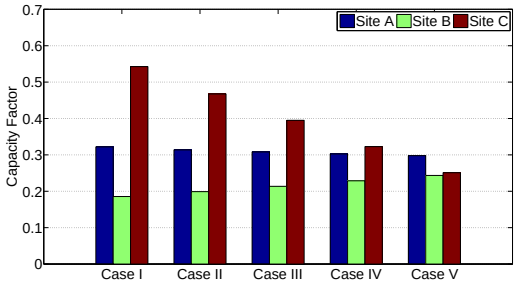

Fig. 2. Annual Average Capacity Factors for Sites A, B, C

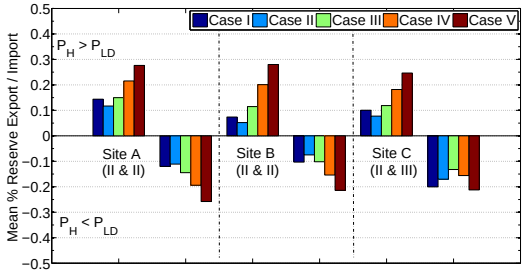

Fig. 3. Mean Percentage Reserve Requirements for Sites A, B, C

† Sarkar, S.; Ajjarapu, V.; , "MW Resource Assessment Model for a Hybrid Energy Conversion System With Wind and Solar Resources," *Sustainable Energy, IEEE Transactions on* , vol.2, no.4, pp.383-391, Oct. 2011

Multi-objective Stochastic Distribution Feeder Reconfiguration in Systems with Wind Power Generators and Fuel Cells Using Point Estimate Method

Ahmad Reza Malekpour
Department of Electrical and Computer Engineering
Kansas State University
Manhattan, KS, USA
e-mail: malekpour@k-state.edu

Anil Pahwa
Department of Electrical and Computer Engineering
Kansas State University
Manhattan, KS, USA
e-mail: pahwa@k-state.edu

***Abstract*— This paper presents a multi-objective algorithm to solve stochastic distribution feeder reconfiguration (SDFR) problem for systems with distributed wind power generation (WPG) and Fuel Cell (FC). The four objective functions investigated are 1) the total electrical energy losses, 2) the cost of electrical energy generated, 3) the total emissions produced, and 4) the bus voltage deviation. A probabilistic load flow based on point estimate method (PEM) is employed to include the uncertainty in WPG and load demand, concurrently. Different wind penetration strategies are examined to capture all economical, operational and environmental aspects of the problem. An interactive fuzzy satisfying optimization algorithm based on Adaptive Particle Swarm Optimization (APSO) is employed to determine the optimal plan for each strategy. The proposed method is applied to Tai-Power system and the results are validated in terms of efficiency and accuracy.**

I. KEY EQUATIONS

The stochastic distribution feeder reconfiguration (SDFR) problem includes minimization of four objective functions as:

1) Energy losses

$$\tilde{f}_1(X) = \sum_{i=1}^{Nbr} R_i \times |I_i^t|^2 \quad (1)$$

2) Cost of electricity generation

$$\tilde{f}_2(X) = price_{grid} \times \tilde{P}_{grid} + \sum_{j=1}^{N_{WPG}} price_{WPG,j} \times \tilde{P}_{WPG,j} + \sum_{k=1}^{N_{FC}} price_{FC,k} \times \tilde{P}_{FC,k} \quad (2)$$

3) Emission produced

$$\tilde{f}_3(X) = \sum \left(\tilde{E}_{FC} + \tilde{E}_{WPG} + \tilde{E}_{grid}\right)$$

$$\tilde{E}_{FC} = CO_2^{FC} + NO_X^{FC} + SO_2^{FC} = EF_{FC}.\sum_{k=1}^{N_{FC}} \tilde{P}_{FC,k}$$

$$\tilde{E}_{grid} = CO_2^{grid} + NO_X^{grid} + SO_2^{grid} = EF_{grid}.\tilde{P}_{grid}$$

$$\tilde{E}_{WPG} = 0 \quad (3)$$

4) Voltage deviation

$$\tilde{f}_4(X) = \max[|1 - V_{min}|, |1 - V_{max}|] \quad (4)$$

II. KEY FIGURE

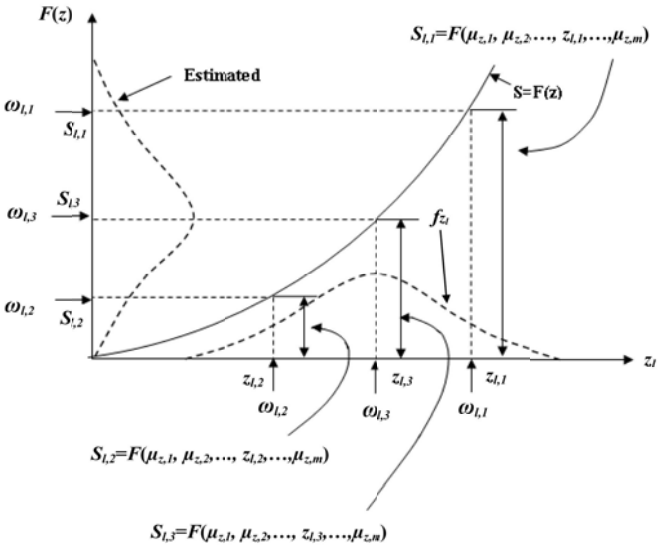

Fig. 1. The concept of the 2m+1 PEM scheme

III. KEY RESULT

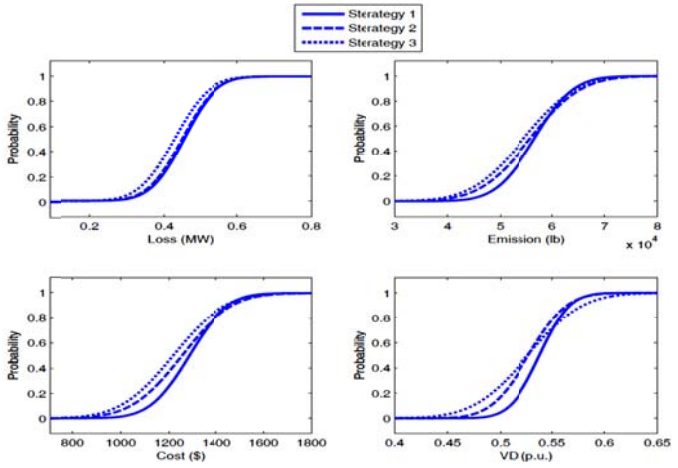

Fig. 4. Cumulative probability distributions of the four objective functions for different wind power penetration strategies

Probabilistic Optimal Sizing of Stand-Alone PV Systems with Modeling of Variable Solar Radiation and Load Demand

Simon K. K. Ng, *Student Member, IEEE*, J. Zhong, *Senior Member, IEEE* and John W. M. Cheng, *Member, IEEE*
Centre for Electrical Energy Systems, Department of Electrical and Electronic Engineering, The University of Hong Kong, Hong Kong, China,
Email: *kkng@eee.hku.hk, jzhong@eee.hku.hk, john.cheng@clp.com.hk*

***Abstract*— This paper presents a comprehensive sizing methodology which could contain all key elements necessary to obtain a practical sizing result for a stand-alone photovoltaic (PV) system. First, a stochastic solar radiation model based on limited/incomplete local weather data is formulated to synthesis various chronological solar radiation patterns. This enables us to evaluate a long-term system performance and characterize any extreme weather conditions. Second, a stochastic load simulator is developed to simulate realistic load patterns. Third, two reliability indices, Expected-Energy-Not-Supplied (EENS) and Expected-Excessive-Energy-Supplied (EEES), are incorporated with an Annualized Cost of System (ACS) to form a new objective function called an Annualized Reliability and Cost of System (ARCS) for optimization. We then apply a particle swarm optimization (PSO) algorithm to obtain the optimum system configuration for a given acceptable risk level. An actual case study is conducted to demonstrate the feasibility and applicability of the proposed methodology.**

I. Key Figures

Fig. 1 Optimal Sizing Platform

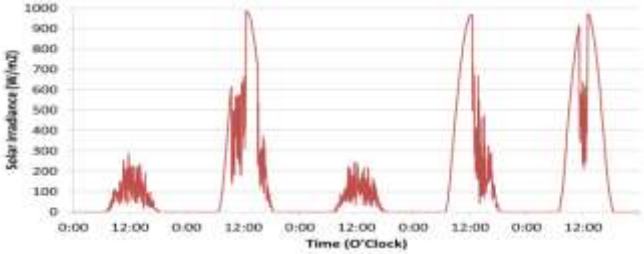

Fig. 2 Simulated chronological solar radiation

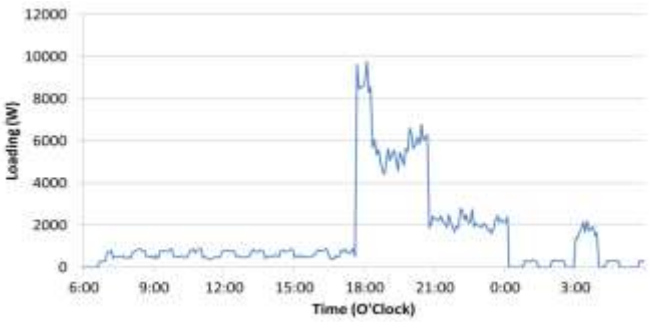

Fig. 3 Simulated result of load simulator

II. Key Equations

A. Optimization sizing objective

$$\min_{N_{PV},N_{bat}} \; ARCS = \{VoLL \cdot EENS_a + VOEE \cdot EEES_a + (C_{acap}^{PV} + C_{amain}^{PV}) P_{PV}^{peak} N_{PV} + (C_{acap}^{bat} + C_{arep}^{bat} + C_{amain}^{bat}) N_{bat} E_{bat}\} \quad (1)$$

B. Constraints

$$LOLP \le \overline{LOLP} \quad (2)$$

$$N_{PV} = 0,1,2 \ldots \quad (3)$$

$$N_{bat} = 0,1,2 \ldots \quad (4)$$

III. Key Results

TABLE I
Optimal Sizing Results of Different Risk Levels Using PSO Algorithm

Acceptable LOLP	N_{PV}^*	N_{bat}^*	ACS(US$)
1%	125	26	65,441
2%	120	23	60,324
5%	112	18	51,883

TABLE II
Sensitivity Analysis of Varying Number of PV Modules

	Number of PV modules				
	100	110	**120**	130	140
EENS/year (kWh)	2,557	1,142	**493**	235	122
EEES/year (kWh)	62	635	**1,992**	3,753	5667
ACS (US$)	55,157	57,741	**60,324**	62,908	65,491
ARCS(US$)	137,725	101,905	**100,004**	115,464	137,399

Battery Switch Station Modeling and its Economic Evaluation in Microgrid

Miao Yiqun, Jiang Quanyuan, Cao Yijia
College of Electrical Engineering, Zhejiang University, Hangzhou 310027, China
Email: *zjumiaoyiqun@gmail.com, jqy@zju.edu.cn, yjcao@hnu.edu.cn*

***Abstract*—Featured by its flexible and reliable operation microgrid has a great prospect for utilizing renewable resources. Battery switch station (BSS) is an important solution to supply energy for electric vehicles. In this paper a new business model of microgrid-based BSS is proposed. According to battery and charger constraints, a new optimal dispatching strategy of microgrid containing BSS or energy storage station (ESS), wind generator, photovoltaic system, fuel cell, micro turbine and diesel generator is given. The optimization is solved by mixed integer linear programming (MILP). Test cases are carried out to illustrate that additional benefits can be realized by utilizing the BSS as the storage device of the microgrid instead of traditional ESS.**

I. KEY EQUATIONS

$$\min F = f_{g+} + f_{r,BSS} + f_{r,\mu G} - f_{g-} - f_s \tag{1}$$

$$s.t. \quad E_i^t - E_i^{t-1} + (P_{i-}^{t-1} - P_{i+}^{t-1})\Delta t = 0 \tag{2}$$

$$\begin{cases} U_{i+}^t - U_{i+}^{t-1} \le U_{i+*}^t \\ U_{i-}^t - U_{i-}^{t-1} \le U_{i-*}^t \end{cases} \tag{3}$$

$$\begin{cases} U_{i+\#}^t \le \dfrac{E_{\text{on},i}^t}{e_0} \\ U_{i-\#}^t \le 1 - \dfrac{E_{\text{on},i}^t}{e_0} \\ 0 \le E_{\text{on},i}^t \le e_0 \end{cases} \tag{4}$$

$$\begin{cases} U_{i+\#}^t \ge U_{i-*}^t \\ U_{i-\#}^t \ge U_{i+*}^t \end{cases} \tag{5}$$

II. KEY FIGURES

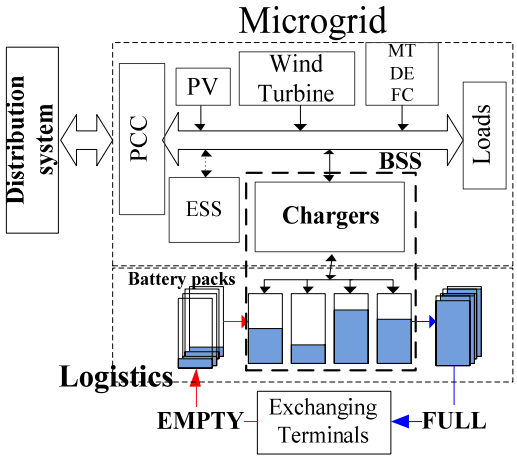

Fig. 1. The business model of microgrid based battery switch station.

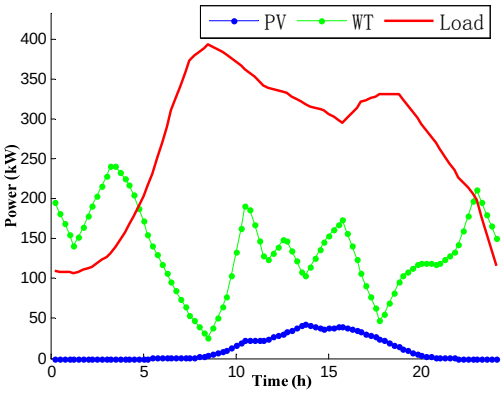

Fig. 2. Load, PV and wind generation curves.

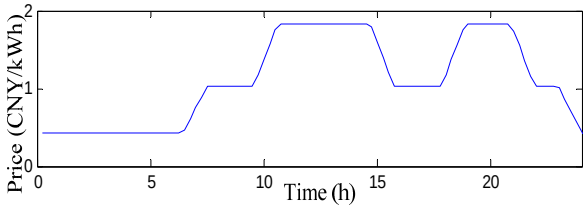

Fig. 3. The power price curve.

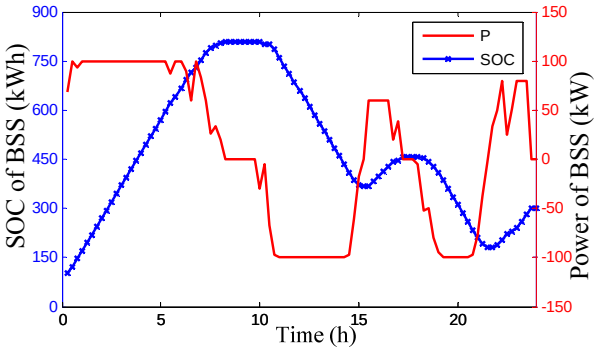

Fig. 4. Energy stored in BSS and its power.

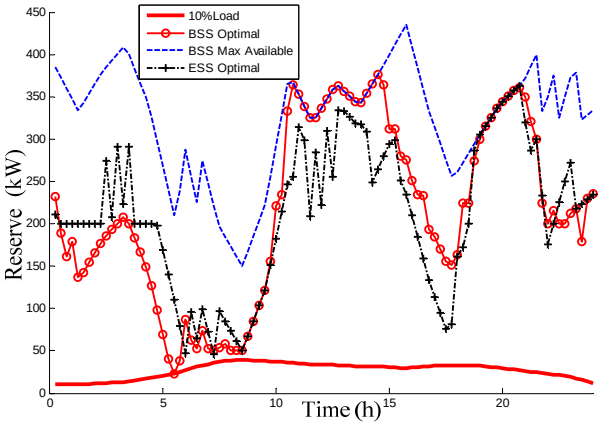

Fig. 5. Reserve comparison of ESS case and BSS case.

Flatness-Based Automatic Generation Control with Wind Units

Maryam H Variani and Kevin Tomsovic
Dept. of Electrical Engineering and Computer Science
University of Tennessee, Knoxville, TN 37996, USA,
Email: mhassani@utk.edu and tomsovic@utk.edu

***Abstract*— To allow for high penetration of distributed generation and alternative energy units, it is critical to minimize the complexity of generator controls and the need for close coordination. We propose that existing controls should be replaced by a two-tier structure of local control operating within a global context of situational awareness. In local control, individual components and individual loads operate in a manner to follow some desired trajectory based on local observations. The global control, on the other hand, refers to the desired trajectory which is determined by the context of the overall system needs for reliability, speed, and robustness. Flatness as an extension of controllability for non-linear systems is a key to enable planning and optimization at various levels of the grid in this structure. In this study, implementation of flatness-based control on Automatic Generation Control (AGC) of a multi-machine system with high penetration of wind energy is investigated. The approach is implemented on a 3-machine, 9-bus system for two different scenarios: imposing load perturbation, and adding wind generation unit to the system. The proposed strategy demonstrates promising performance in mitigating the frequency deviations and overall structure that could facilitate other non-traditional generators.**

I. KEY EQUATIONS

The guiding equations of the flatness based controller are:

$$\dot{\delta}_{(i)} = \omega_{(i)} - \omega_0$$

$$\ddot{\delta}_{(i)} = \frac{1}{2H}\left(P_{m(i)} - \sum_{\substack{j=1 \\ i\neq j}}^{n} \frac{\delta_{(i)} - \delta_{(j)}}{X_{ij}} - P_L - D\left(\omega_{(i)} - \omega_0\right) \right)$$

$$\delta_{(i)}^{(3)} = \frac{1}{2H}\left(\frac{1}{\tau_T} P_{gv(i)} - \frac{1}{\tau_T} P_{m(i)} - \sum_{\substack{j=1 \\ i\neq j}}^{n} \frac{\dot{\delta}_{(i)} - \dot{\delta}_{(j)}}{X_{ij}} - D\ddot{\delta}_{(i)} \right)$$

$$\delta_{(i)}^{(4)} = \frac{1}{2H}\left(\begin{array}{l} \frac{1}{\tau_T \tau_g} u - \frac{1}{\tau_T \tau_g} \frac{\omega_{(i)} - \omega_0}{R} - \left(\frac{1}{\tau_T \tau_g} + \frac{1}{{\tau_T}^2} \right) P_{gv} \\ + \frac{1}{{\tau_T}^2} P_m - \sum_{\substack{j=1 \\ i\neq j}}^{n} \frac{\ddot{\delta}_{(i)} - \ddot{\delta}_{(j)}}{X_{ij}} - D\dddot{\delta}_{(i)} \end{array} \right)$$

II. KEY FIGURES

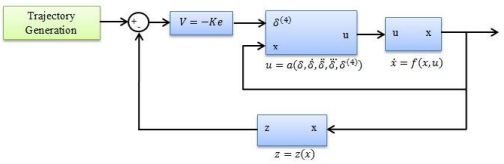

Figure 1. Flatness-Based control block diagram.

III. KEY RESULTS

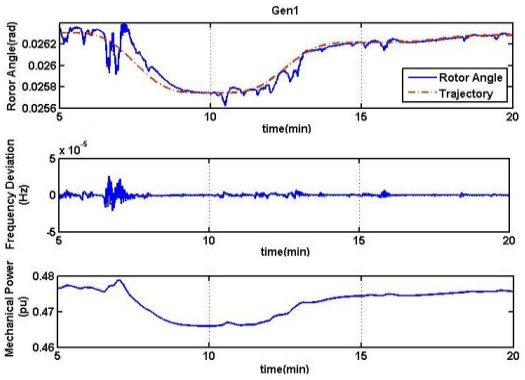

Figure 2. Rotor Angle, Frequency Deviation and Mechanical Power in Generator 1.

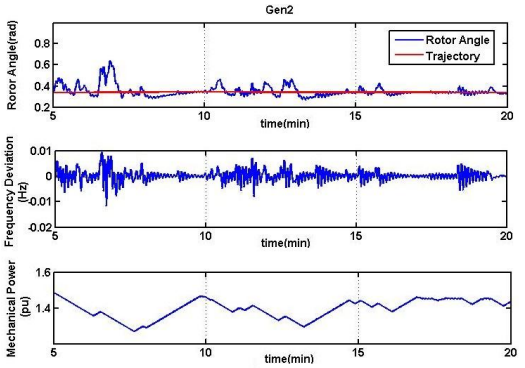

Figure 3. Rotor Angle, Frequency Deviation and Mechanical Power in Generator2.

Dynamic Models of Wind Turbines for Stability Studies

Felipe Wilches and Joe H. Chow
Department of Electrical, Computer, and Systems Engineering
Rensselaer Polytechnic Institute
Troy, NY

***Abstract*— Wind power is becoming a major energy resource. In fact, the installed wind power capacity has increased considerably during the last fifteen years and is projected to increase much more in the years to come. Despite this fact, currently there are no standard generic dynamic models for wind turbine generators and most existing models are property of WTG manufacturers subject to property rights. This situation hinders the WTG investigation by researchers and university investigators. This need nonetheless is currently being addressed by the Wind Generation Modeling Group (WGMG) of the Western Electricity Coordinating Council (WECC) and steps towards a generic model have been made.**

The purpose of this investigation is to implement the dynamic generic models advanced by the WECC for Type 3 (doubly-fed asynchronous generator) and Type-4 (full converter generator) wind turbines for stability studies, provided in [1]. These two types of WTGs were chosen because they represent more than half of the current WTG installed and their share is expected to increase even more. The models will be implemented in the Power System Toolbox (PST), a MATLAB-based software package available for university research [2], and follow the modular approach of the model used by the WECC. These models have as input the wind velocity, the desired active and reactive power and sense the voltage at their point of interconnection to grid. Since these models relate wind variations to dynamics of real and reactive power, researchers can then study the impact of high penetration of wind energy on the frequency and voltage stability of a large power grid.

Keywords- Wind Turbine Generator, dynamic modeling, wind power, voltage stability, frequency stability

[1] K. Clark, N. W. Miller, and J. Sanchez-Gasca, Modeling of GE Wind Turbine-Generators for Grid Studies, General Electric Internatinal, Inc., version 4.4, 2009.

[2] J. H Chow and K. W. Cheung, " PST reference. "A Toolbox for Power System Dynamics and Control Engineering Education," IEEE Transactions on Power Systems Engineering, vol. 7, no. 4, pp. 1559-1564, 1992.

Power System Transient Stability Enhancement Using Direct Drive Wind Generators

Hasmina Tari Mokui, Mohammad A.S. Masoum, Mansour Mohseni, and Moayed Moghbel
Department of Electrical and Computer Engineering
Curtin University, Perth, WA 6845, Australia
Email: *h.mokui@postgrad.curtin.edu.au, m.masoum@curtin.edu.au, mansour.mohseni@curtin.edu.au*
and *moayed. moghbel@postgrad.curtin.edu.au*

***Abstract*—Recent grid codes requires the wind farms not only to ride through the fault disturbances but also support the stability of nearby grid during severe network disturbances. This paper presents the impact of direct drive wind generators to the improvement of fault ride through (FRT) capability of fixed speed wind turbine. Three operational strategies have been investigated, i.e. without reactive power support, considering reactive power support complying with the Danish grid codes (with and without considering overloading of the converter currents). The proposed control strategies enable the direct drive wind generators to inject the required reactive power in order to help stabilizing the nearby fixed speed wind generators during faults. Simulation studies are carried out by using MATLAB/SIMULINK**

I. KEY EQUATIONS

$$P_w = \frac{1}{2}\pi\rho R^2 v_w{}^3 C_p(\lambda,\beta) \quad (1)$$

$$\lambda = \frac{\omega_r R}{v_w} \quad (2)$$

$$|I| = \sqrt{I_d^2 + I_q^2} = \sqrt{\left(\frac{P}{|V_s|}\right)^2 + \left(\frac{Q}{|V_s|}\right)^2} \quad (3)$$

II. KEY FIGURES

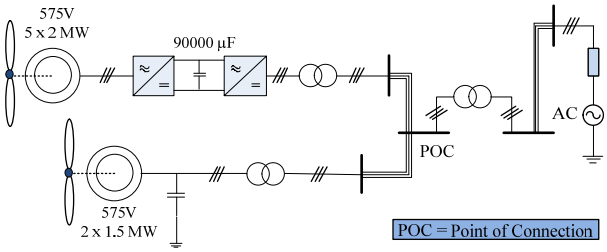

Figure 1. Schematic diagram of the simulated system

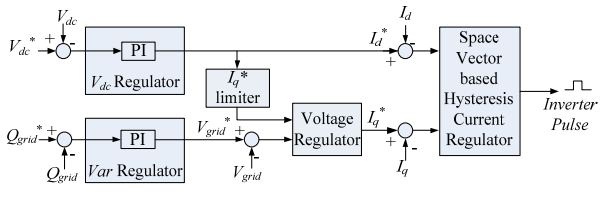

Figure 2. Control block diagram of the simulated grid side converter (at direct drive wind generators)

III. KEY RESULTS

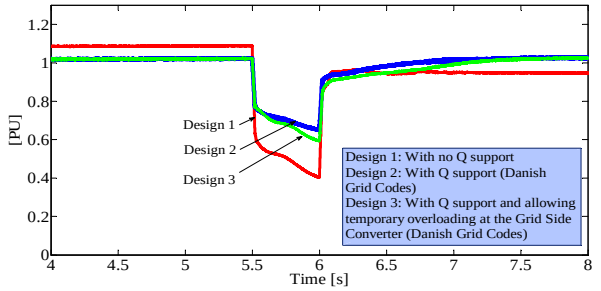

Figure 3. Voltage profiles at Point of Connection (Bus 25) under a 50% voltage sag, sustained for 500 ms

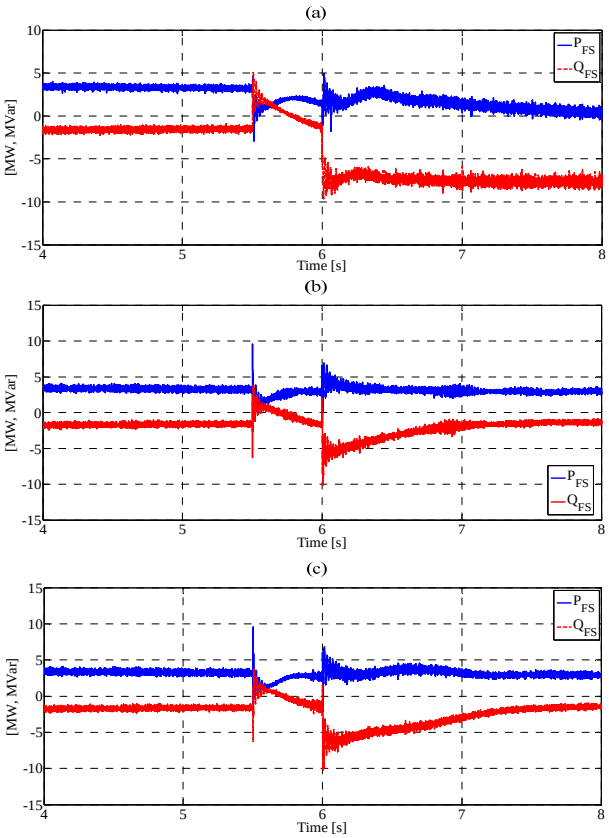

Figure 4. P-Q response for fixed speed wind generators under a 50% voltage sag, sustained for 500 ms: (a) Design 1; (b) Design 2; (c) Design 3

Impact Study of Multiple Source Harmonic Interactions with Distributed Energy Resources

R. Arghandeh, R. P. Broadwater

Keywords—Harmonics, Energy Resources, Efficiency, Impact Study

I. Summary

SMART Grid realization involves a steady increase in Distributed Energy Resource (DER) adoption and Plug-in Electric Vehicle adoption into the distribution network. Many of the DER devices create harmonics. Harmonic interactions due to many DERs are a source of concern for utilities. Harmonic flows cause thermal damage and overloading on transformers and conductors. Moreover, harmonic currents may disturb the operation of protection systems.

Harmonics are sinusoidal components with higher frequencies that are an integral multiple of the fundamental frequency. They freely move back and forth between the harmonic source and loads. Harmonics waste the grid capacity, creating thermal losses. In some cases the thermal losses can be so great as to damage and/or destroy equipment. Fig.1 depicts the power flow for the fundamental frequency and a 13th harmonic component.

In this research the interaction harmonics produced from multiple, different sources such as solar, wind and energy storage systems are analyzed. The aim is predict harmonic interactions that could lead to equipment damage in distribution networks. For quantifying harmonic effects, Total Harmonic Distortion (THD) and Total Demand Distortion (TDD) are applied.

The test circuit simulation results are presented in Fig. 2. It shows the effect of capacitor bank size on Total Harmonic Current Distoration, THD_I. Moreover, higher voltage levels in harmonic sources cause higher THD_I on the load side.

II. Key Equations

Equations for harmonic analysis include fundamental rms voltage and current total harmonic distortion and total harmonic demand distortion, as given by, respectively:

$$THD_V = \frac{\sqrt{\sum_{h=2}^{\infty} V_h{}^2}}{V_1} \quad (1)$$

$$THD_I = \frac{\sqrt{\sum_{h=2}^{\infty} I_h{}^2}}{I_1} \quad (2)$$

$$TDD = \frac{\sqrt{\sum_{h=2}^{\infty} I_h{}^2}}{I_L} \quad (3)$$

III. Selected Simulation Results

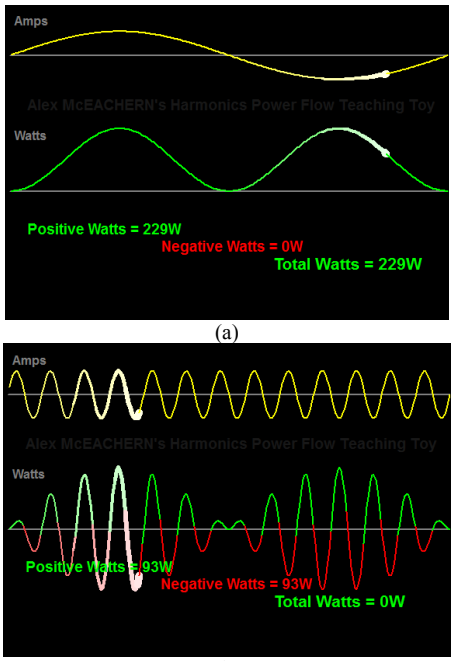

Fig. 1. Harmonics power flow, (a) Fundamental frequency power, (b) the 13th harmonic component power.

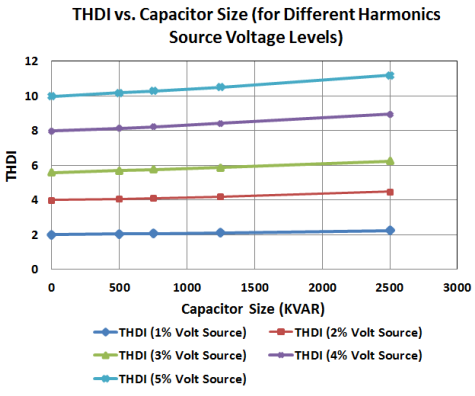

Fig. 2. THDI in a sample circuit with capacitor bank and different levels of voltage in the harmonics source.

Reza. Arghandeh is with with Virginia Tech – ECE Department, Blacksburg, VA 24061, USA. (e-mail: reza6@vt.edu).

Robert Broadwater is Professor of Virginia Tech – ECE Department, Blacksburg, VA 24061, USA. (e-mail: dew@vt.edu).

Methodology for Monitoring, Control and Operation of Power Systems with Wind Farms

Evangelos Farantatos, *Student Member IEEE*, Renke Huang, *Student Member IEEE*, Yongnam Cho, *Student Member IEEE*, Evangelos Polymeneas, *Student Member IEEE*, Zhenyu Tan, *Student Member IEEE*, George J. Cokkinides, *Senior Member, IEEE, and* A. P. Meliopoulos, *Fellow, IEEE*

***Abstract*— This paper presents an infrastructure and a monitoring and control approach for systems with wind farms that enables coordination of the operation of wind farms with the bulk power system and maximizes the utilization of the available wind energy at the wind farm locations. A hierarchical optimization scheme is proposed in this work. In particular, a system level optimization defines the optimal operating point for the wind farms, the thermal generating units and other controllable devices in the system. At each wind farm, a lower level optimization procedure is performed which defines the operating condition of each wind turbine at the wind farm. The proposed infrastructure is enabled by a distributed state estimation procedure that evaluates the real time model of the system and the wind farms, used by the hierarchical optimization scheme, continuously with speeds of 60 times per second.**

I. PROPOSED WIND FARM MONITORING AND CONTROL SCHEME

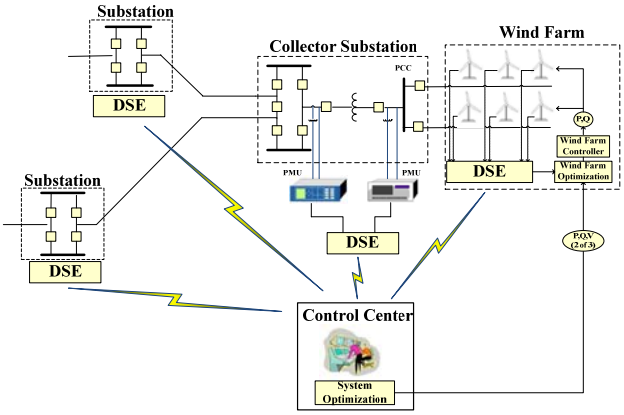

Fig. 1. Illustration of the Overall approach

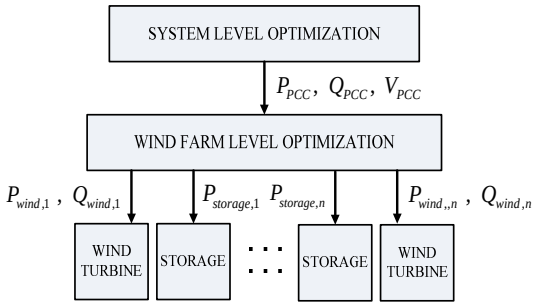

Fig. 2. Hierarchical Optimization

Substation and Wind Farm Distributed State Estimation

- Executed at all the substations and the wind farms of the system utilizing PMU measurements, providing the real time model of the system

System Optimization

- Defines the optimal operating condition at the PCC of each wind farm given the aggregate model of the substations and the wind farms

Wind Farm Optimization

- Defines the operating condition for each wind turbine subject to the directives for the wind farm set by the system optimization

II. KEY RESULTS

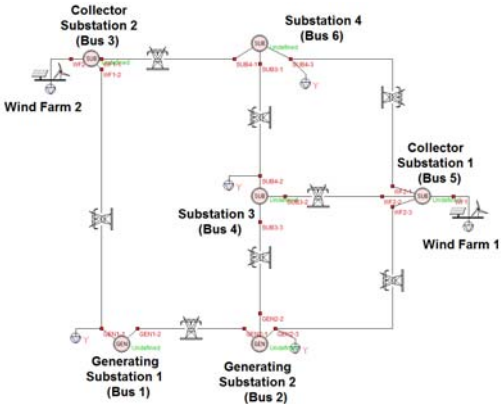

Figure 3: Single Line Diagram of Test System

TABLE 1: SYSTEM VOLTAGE PROFILE

Bus Number	Voltage Magnitude before optimization (KV)	Voltage Magnitude after optimization (KV)
1	79.60	79.81
2	79.63	79.76
3	77.50	79.40
4	75.72	78.01
5	76.96	77.59
6	74.92	77.67

TABLE 2: SYSTEM LEVEL OPTIMIZATION OBJECTIVE VALUE

	Before optimization	After optimization
Objective Value $\left(\sum_{i=1}^{M}(V_i - V_{i,rated})^2\right)$	50.3434	11.2329

TABLE 3: WIND FARM LEVEL OPTIMIZATION OBJECTIVE VALUE

	Before optimization	After optimization
Objective Value $\left(\sum_{i=1}^{M}(V_i - V_{i,rated})^2\right)$	0.1208	0.0789

Solar Irradiance Estimations for Solar Panels of Varying Tilt and Azimuth Angles Using Global and Diffuse Horizontal Radiation Measurements

Yazmin Najera and W. Mack Grady
Department of Electrical and Computer Engineering.
The University of Texas at Austin, Austin, Texas, USA
Email: yazminnajera@gmail.com and grady@mail.utexas.edu

***Abstract*— This document describes preliminary results of a program that predicts the solar irradiance available to solar photovoltaic (PV) systems by using only Global Horizontal (GH) and Diffuse Horizontal (DH) measurements. To gather GH and DH values, our group uses various measuring tools provided by Austin Energy and the State Energy Conservation Office (SECO). One of these tools consists of pyranometers that rotate a shadow band across a PV sensor every minute. This sensor records a GH value when there is no shadow and the DH value when the sensor detects a shadow. Three DH measurements are taken and the lowest value is used in our models. These measurements are then aggregated to a file that is later used by a Solar Data Analyzer (SDA). The SDA then uses various solar equations to determine the solar irradiance that would be available to solar panels depending on their tilt and azimuth angles. Estimations are then compared to the irradiance values measured by a Li-Cor sensor. Results showed a small percent error between estimated and measured values for the month of January, 2012. The expected insolation values for solar panels at varying tilt/azimuth angles will be available to solar PV owners to help them determine the functionality of their systems. This data can also be used by utilities and the public for solar project-planning around the Austin area. Furthermore, the SDA has the potential to estimate solar irradiance estimations in other parts of the country given that GH and DH values are known.**

I. Key Equations

Estimation of the Direct Normal (DN) or beam irradiance:

$$DN = GH - DH \quad (1)$$

Equations 2 and 3 are used for the estimated maximum solar irradiance ($P_{incident}$) available. θ_{sun}^{Zenith} is the position of the sun in the sky from the vertical and $\beta_{incident}$ is the angle between the rays of the sun and a vector perpendicular to a solar panel's surface.

For $\theta_{sun}^{Zenith} \leq 85°$

$$P_{incident} = DH + \frac{(GH - DH)}{\cos(\theta_{sun}^{Zenith})} * \cos(\beta_{incident}) \ \frac{W}{m^2} \quad (2)$$

To avoid overcorrection, for $\theta_{sun}^{Zenith} > 85°$

$$P_{incident} = DH + (GH - DH) * \cos(\beta_{incident}) \ \frac{W}{m^2} \quad (3)$$

II. Key Figures

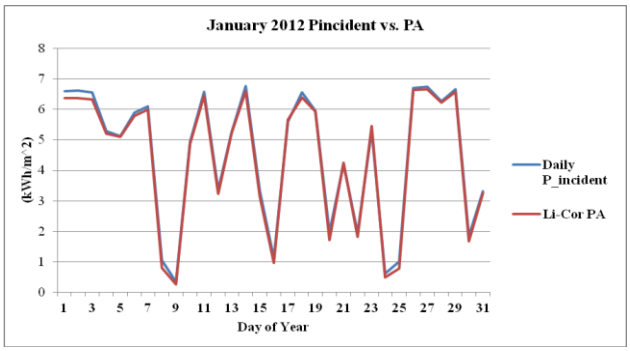

Figure 1. Jan. 2012 estimated ($P_{incident}$) vs. measured (Li-Cor PA) values.

III. Key Results

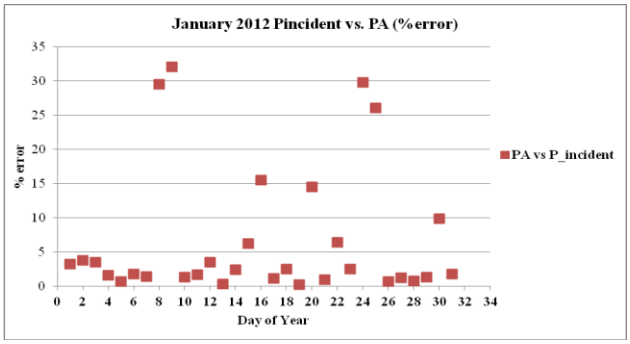

Figure 2. Jan. 2012 $P_{incident}$ vs. Li-Cor sensor PA percent errors. Less than 10% error is experienced during days with insolation values exceeding 2 kWh/m^2. However, during very rainy/cloudy days, the error is significant reaching up to 32%.

Novel Control Strategies for DFIG Wind Turbines During Grid Disturbances that Comply With Strictly Grid Codes

Santos Kihwele
Department of Electrical and Electronics Engineering, Yonsei University, Seoul, South Korea
Email: kihwele2002@yahoo.com

***Abstract*—This poster presents a detailed model of novel control strategies for a DFIG system during grid disturbances. It focuses on the operation of DFIG wind turbines during a transient state, and analyzes how the peak rotor transient current can be controlled using a crowbar protection circuit. Furthermore, the influence of crowbar action on the reactive power dynamic control using both RSC and GSC to support the PCC-voltage during grid disturbances is presented. Reactive power control (unity power factor) and voltage control modes are the two necessary and interchangeable control modes, which the DFIG wind turbine can operate between steady state and transient state operations. When the crowbar is engaged at the time of fault initiation and clearance, the GSC can be operated in STATCOM mode to support the PCC voltage, while the RSC is blocked by the crowbar. Due to the RSC intermediate connection to the rotor windings between the fault initiation and clearance time, the dynamic reactive power using both converters is changed to the PCC voltage control mode by redefining the current reference values for reactive power control. With this proposed novel control strategy, DFIG wind turbines contribute to improve LVRT capability during the network disturbance, thereby complying with strict known grid codes.**

Keywords-Crowbar, DFIG, LVRT, Wind Turbine.

I. KEY FIGURE

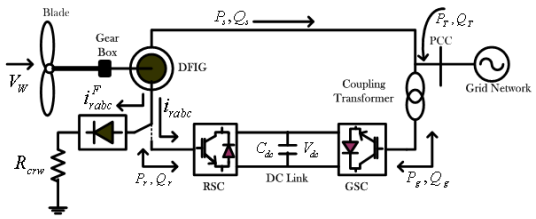

Figure 1. Basic configuration of DFIG wind turbines

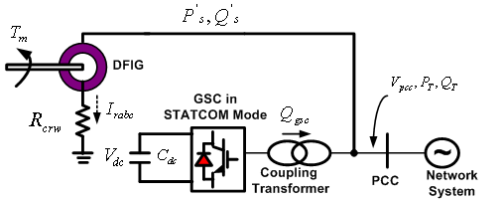

Figure 2. DFIG with activated crowbar and GSC as the STATCOM

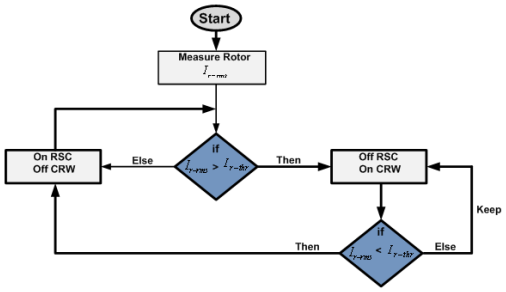

Figure 3. Crowbar and rotor switching algorithm

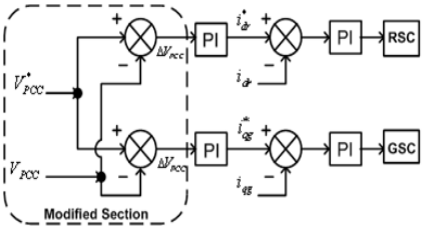

Figure 4. A modified control loop for the RSC and GSC during $T_{dp\text{-}c}$

II. KEY RESULTS

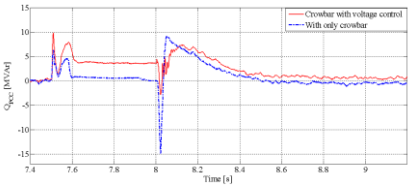

Figure 5. Reactive power response with Novel control strategies

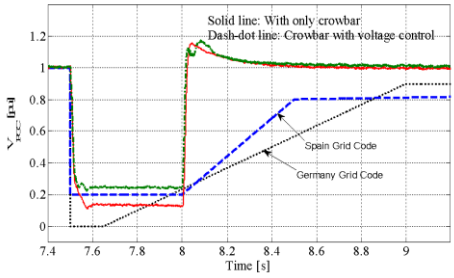

Figure 6. PCC voltage responses complying with the grid codes during 500 ms grid fault with Novel control strategies

Optimal Penetration of Three Types of Wind Turbine Generators

Baohua Dong and Sohrab Asgarpoor, Department of Electrical Engineering,
University of Nebraska–Lincoln; sasgarpoor1@unl.edu

Abstract—The quickly increasing widespread use of wind generation extensively decrease carbon emissions, reduce the effect on global warming, and cut down the dependence on fossil fuels. However, the variability, intermittency and non-dispatched characteristics of wind generation trigger some serious stability and reliability challenges in the electric power industry. Moreover, the penetration of wind generation in U.S. may be significantly increased from 2% now to 20% in 2030. How to optimize the penetration of wind generation is becoming an important issue.

The project will focus on optimizing the penetration of three major types of wind turbine generators (Fixed speed induction generator (FSIG), doubly fed induction generator (DFIG), direct drive synchronous generator (Permanent magnet synchronous generator (PMSG) is major.) to improve the system stability based on small signal stability analysis. The stability research in the comparisons between FSIG or DFIG and the conventional synchronous generator, between FSIG and DFIG is already good enough. Generally, the following conclusions can be drawn from all those studies:

1) FSIG, DFIG, and PMSG are respectively the old-popular, now-popular, and future-popular wind turbine generator technologies.

2) FSIG can improve power systems transient stability, but in comparison with DFIG, it is poor. DFIG has a good ability to ride through faults and it can work as a power reactive compensator during faults. Therefore, majority of wind farms is equipped with DFIG.

3) The comparison of the different impacts in stability of DFIG and PMSG is not sufficiently enough and there is no generally accepted conclusion so far.

4) Power system transient stability is noticeably degraded at high penetration level due to the high reactive power demand of wind generation under some disturbances.

Therefore, high penetration of wind generation not only stop improving power system stability in comparison with low penetration level, but also can decrease power systems stability in comparison with the case without wind generation under some disturbances. Therefore, calculating the optimal penetration is significantly important to system planning and system operations.

The project will firstly analyze and compare the different impacts of DFIG and PMSG in stability analysis; Secondly, the optimal penetration of FSIG, DFIG and PMSG will be got by particle swarm optimization (PSO) based on small signal stability analysis; next, the much simulation will be done via PSCAD software to verify if the analysis in optimization theory is correct. The indicators of Critical Clearing Angle (CCA) and Critical Clearing Time (CCT) will be replaced by maximum rotor speed deviation and the oscillation duration to judge the transient performances because they are more efficient in terms of computation time. Last, the rules and results about optimal penetration of wind generation will be identified well.

Modeling of Tidal Energy Conversion Systems for Primary Response Testing

Maren Kuschke, Susanne Pertzsch, Kai Strunz

***Abstract*—The power generation changes from conventional to renewable generators resulting in new challenges for the grid operators. One important aspect is reserve power. Due to fluctuating resources as wind and photovoltaics, the need for reserve power even increases. In this paper, it is studied, how tidal energy conversion systems can be controlled providing primary response. Thereby, the rotor speed is an important control parameter varying the power output for a given tidal current velocity as desired. A network model is proposed containing a synchronous motor load for testing the tidal turbine influence on the grid. Simulation is carried out in Matlab/Simulink. The results validate the proposed control for primary response.**

***Index Terms*—Tidal energy conversion system, modeling, primary reserve, simulation, power systems.**

I. Motivation and Contributions

Today, mainly conventional power plants provide system services. Due to the fluctuating power generation of wind and photovoltaics, more reserve will be required. Tidal energy conversion systems (TECS) can make a contribution to reserve power. Their power output can be determined far in advance which makes tidal energy a reliable resource in the renewable energy portfolio. Due to its fast reaction on grid frequency changes, it can be a good alternative, especially for primary reserve.

This is the motivation for the work presented in this poster that is distinguished through three contributions.

- First, a detailed model of the TECS itself with converter control is given.
- Second, the control of a TECS with fixed pitch for primary response is proposed as presented in Fig. 1. For realizing a lookup-table, power coefficient and complementary rotor speed are necessary which can be calculated by the given equations. Thereby, the set-point for the power coefficient is defined by the use of a droop.
- Third, the model is implemented in simulation software validating the described control strategies.

II. Simulation Results

The testing system contains a synchronous motor load representing the power grid. Since there is no other power generation unit, the effect of the tidal turbine primary response on the grid frequency can be studied best. The simulation results in Fig. 2 show that the proposed control works well and can be an important contribution to the grid integration of TECS.

M. Kuschke, S. Pertzsch and Professor K. Strunz are with SENSE Laboratory, Department of Electrical Engineering and Computer Sciences, Technische Universität Berlin, Germany (e-mail: maren.kuschke@ieee.org).

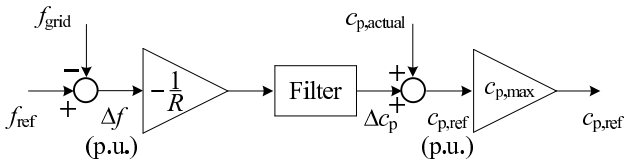

Fig. 1. Control of power coefficient

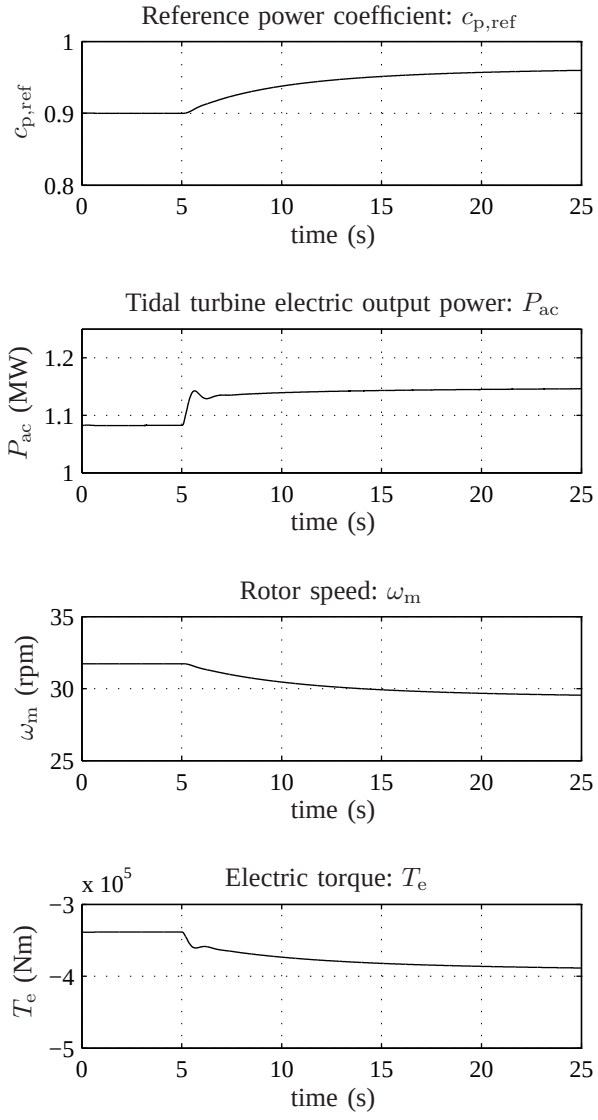

Fig. 2. Simulation results for the tidal generator side

Quantifying Variability in Power Systems: Comparison of Four Metrics

M. Lwin, *Student Member*, IEEE, S. Santoso, *Senior Member*, IEEE

***Abstract*—One of the primary challenges with integrating a high percentage of renewable energy resources, such as wind, into a power system is the variability of the output. Traditional generators have a level of controllability that allows them to be dispatched when required. In contrast, the power output of a wind power plant varies with the resource. High variability can impact system operations and affect reliability of the system. Photovoltaic (PV) generation can also present similar challenges at high penetration levels. It is therefore important to quantify the characteristics of the variability for both measured and forecasted data.**

The goal of this poster is to compare four different metrics that characterize the variability in wind power output. The four metrics that will be compared are: standard deviation of step-changes, coefficient of variation, Ultra-Diurnal Variation Metric, and Conditional Range Metric. Specifically, comparing the metrics for each data set will demonstrate how each metric quantifies particular aspects of wind power variability.

The approach will be to apply each metric to different time-series data with increasing levels of variability. Initially, the metrics will be compared using synthetic time-series data, such as a sinusoidal function. Further analysis will be made with more complex functions, ultimately ending with real-world power output data.

I. Key Equations

Standard deviation of step-changes:

$$y_{i,k} = \frac{1}{k}\sum_{m=1}^{k} x_{ki+m} - \frac{1}{k}\sum_{m=1}^{k} x_{k(i-1)+m}$$

$$s_{y_{i,k}} = \sqrt{\frac{1}{q-2}\sum_{i=1}^{q-1}\left(y_{i,k} - \frac{1}{q-1}\sum_{i=1}^{q-1} y_{i,k}\right)^2}$$

Coefficient of variation:

$$CV = \frac{\sigma_x}{\mu_x}$$

$$\hat{\mu}_x = \left(\frac{1}{n}\right)\sum_{k=1}^{n} x_k$$

$$\hat{\sigma}_x^2 = \left(\frac{1}{n-1}\right)\sum_{k=1}^{n}(x_k - \hat{\mu}_x)^2$$

Ultra-Diurnal Variation Metric:

$$P_{\tilde{x}}(e^{j\omega}) = \sum_{k=-\infty}^{\infty} r_{\tilde{x}}(k)\cdot e^{-jk\omega}$$

$$\alpha = \sqrt{\frac{\int_{\omega_o}^{\pi} \hat{P}_{\tilde{x}}(e^{j\omega})\, d\omega}{\int_{0}^{\pi} \hat{P}_{\tilde{x}}(e^{j\omega})\, d\omega}}$$

$$UDVM = \frac{\sigma}{\mu}\cdot\alpha$$

Conditional Range Metric:

$$M_k = M_{up_k} - M_{low_k}$$

$$CRM_{i,k,l_j} = \left[M_{low_{i,k,l_j}}, M_{up_{i,k,l_j}}\right]$$

II. Key Figures

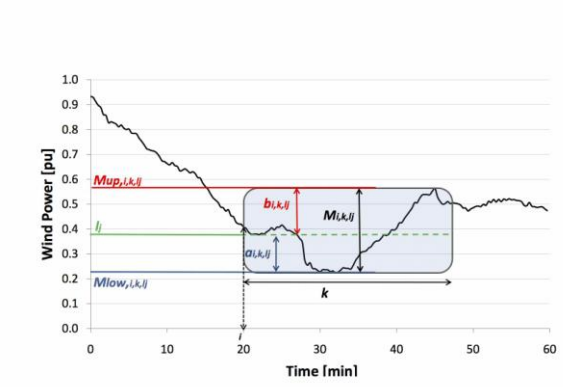

Fig. 1. Uniquely defined conditional range M_{i,k,l_j} for each initial time i, time interval length k, and wind power interval average production level l_j.

References

[1] T. Boutsika and S. Santoso, "Quantifying Short-Term Wind Power Variability Using the Conditional Range Metric," *IEEE Transactions on Sustainable Energy*, vol.99, pp.1, 2012.

[2] P. Doody and S. Santoso, "A Comparative Metric to Quantify the Variability of Wind Power," *Power & Energy Society General Meeting, 2009. PES '09. IEEE*, pp.1-6, July 2009.

Hardware and Software Testing Platform for Battery Management Systems in the Presence of Renewables

Jesse Hill, Chika Nwankpa
Department of Electrical and Computer Engineering
Drexel University
Philadelphia, PA 19104
jrh62@drexel.edu nwankpa@ece.drexel.edu

Abstract – With continued demand for "smart" technologies, implementation of hardware such as batteries and renewable energy sources (i.e. solar panels) has become a huge economic undertaking. In order to better utilize these resources and thus maximize the lifetime of the elements, control schemes looking to both maximize the economic/financial gains while also preventing over usage have become even more important. The work presented examines both software and hardware configurations. The software portion looks to determine an optimal dispatch that while preventing wasteful resource allocation still provides a maximum saving to the consumer. The flexibility of being able to change constraints or variables instantaneously allows for repeated and constant testing without the need for proper hardware conditions. The hardware portion, on the other hand, provides a platform to validate as well as introduce more variability to the problem. Some of the more complex complications within a hardware environment such as intermittency of solar input or other uncertainties give the opportunity for increased understanding of the unknowns to further bolster the software portion. The combination of these two testing platforms provides a flexible environment for understanding various issues associated with renewable energy management. Resources for hardware testing are housed within the Drexel Center for Electric Power Engineering (CEPE). This project is part of Drexel's Green Initiative.

I. KEY EQUATIONS

$$\min C_{LMP} * P_{UTILITY}$$
$$s.t.\ P_{SOLAR} + P_{BATTERY} + P_{UTILITY} = P_{LOAD} \quad (1)$$

$$B_o + \sum_{i=1}^{present} \sum_{j=1}^{present} b_{ij} \leq B_{min} \quad (2)$$

$$B_o + \sum_{i=1}^{present} \sum_{j=1}^{present} b_{ij} \geq B_{max} \quad (3)$$

$$B_o + \sum_{i=1}^{End} \sum_{j=1}^{24} b_{ij} \geq b_o \quad (4)$$

$$\sum_{i=1}^{24} sw_i \leq sw_{max} \quad (5)$$

II. KEY RESULTS

Base Case Simulation Results		
Metric	Do-Nothing	Default Settings
Objective Function	0.9743	0.6138
Switching Operations	N/A	10
Cycles	N/A	5
Savings	N/A	36.96%
Cycles/Savings Ratio	N/A	0.135

Table 1 – Base Case Results

Comparison of Start/End Charge		
Metric	100% Results	40% Results
Objective Function Value	0.6139	0.5850
Number of Cycles	5	4
Percent Savings	36.99%	39.96%
Cycles/Savings	0.135	0.100

Table 2 – Altered Start/End Charge Results

III. KEY FIGURES

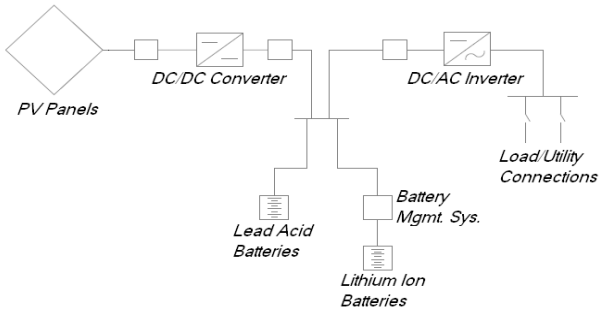

Figure 1 – Sample Battery System Setup

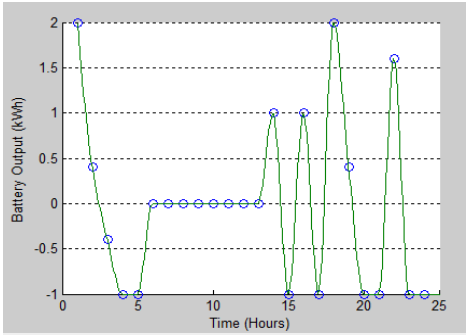

Figure 2 – Sample Battery Dispatch Schedule

Protection Coordination Between HVDC Offshore Wind System and AC Grid

Lina He (Advisor: Prof. Chen-Ching Liu)
University College Dublin, Belfield, Dublin 4, Ireland,
Email: Lina.He@ucdconnect.ie

***Abstract*— An off-shore wind farm based on induction generators is connected to the ac grid through a bipolar VSC-HVDC link. The wind farm side VSC (WFVSC) controls the magnitude and frequency of the offshore ac side voltage to enable the collection of all offshore wind power. The grid side VSC (GSVSC) is assigned to control the dc grid voltage and provide reactive power for the ac grid. It results in electric variables of ac and dc sides being coupled with each other, such as active power, voltages and currents. When the ac grid close to the PCC undergoes a three-phase short circuit fault, the dc grid suffers a severe overvoltage. This might damage the insulation of dc devices and reduce the reliability of costly HVDC system. To avoid these unnecessary damages, the dc overvoltage protection setting is required to be coordinated with the insulation capability of devices. For a single-phase short circuit fault case in the ac grid, it is found that the dc grid does not suffer a serious overvoltage. However, the unbalanced condition of the ac grid during the fault in turn results in second order harmonics in the dc side due to the pulse width modulation (PWM) control. They can be used as the indicators of ac grid unbalanced faults, such as 100 Hz protection. In some hybrid ac/dc networks, 100 Hz protection is coordinated with ac grid protection, functioning as a backup protection of the unbalance faults in the ac grid.**

I. KEY FIGURES

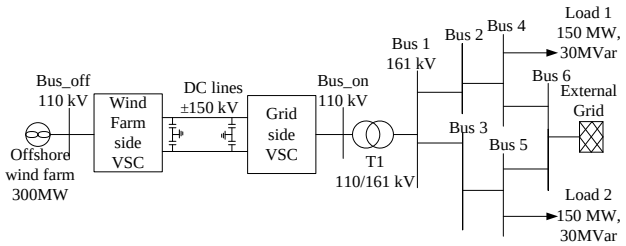

Figure 1. Test System

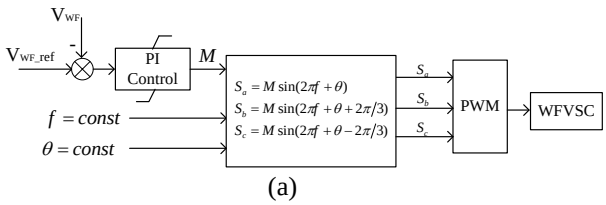

(a)

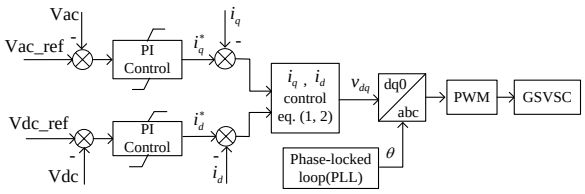

(b)

Figure 2. Controller Configurations: (a) WFVSC, (b) GSVSC

II. KEY FIGURES

The decoupling controller equations are:

$$v_d = -(K_{ip} + \frac{K_{iI}}{s})(i_q^* - i_q) + \omega L i_q + v_{sd} \quad (1)$$

$$v_q = -(K_{ip} + \frac{K_{iI}}{s})(i_d^* - i_d) - \omega L i_d + v_{sq} \quad (2)$$

III. KEY RESULTS

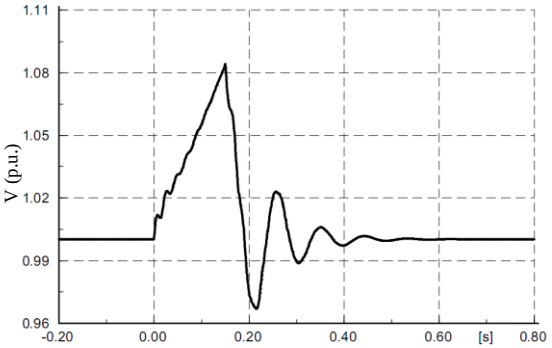

Figure 3. Positive Pole DC Voltage of Test System Under Three-Phase Short-Circuit Fault at Line 1-2

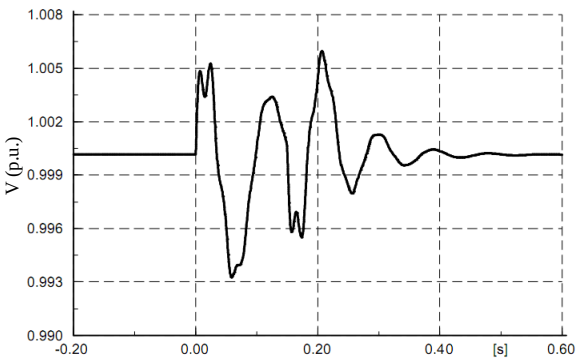

Figure 4. Positive Pole DC Voltage of Test System Under Single-Phase Short-Circuit Fault at Line 1-2

Transient Stability Assessment with Large Scale Wind penetration

Prem K Naik

Department of Electrical and Computer Engineering
University of Auckalnd, Auckland, NewZealand

Email: prem.k@ieee.org

Abstract **- Larger penetration of wind generation has required assessment of various stability analyses. Integration of increasing wind generation while maintaining the integrity of the New Zealand power system, the Electricity Commission (now Electricity Authority) initiated Wind Generation Investigation Project (WGIP) to assess the likely impacts. "Effect of wind generation on management of frequency excursions" and "Effect of wind generation on transient stability" are two issues explicitly identified.**

It is assessed that displacement of generation providing frequency support during under frequency excursions by minimal technical capability wind units will change system inertia and impact network performance during under frequency excursions. Investigation for critical fault clearance analysis indicates that increased wind generation output by displacing other generation, will result in reduced power system transient stability.

Traditional synchronous machines possessing Inertia has governor control action for smaller disturbance. Significant investigation has also been done for very large disturbances. With high wind energy penetration the effect on transient stability for light load period is attracting attention especially with reduced effective mass system inertia.

This poster will review the investigation and modeling approach for reduced inertia and propose equivalent and effective inertia of the wind farms. Capture effective inertia in modeling and a review of standard based wind farm integration approachhese instructions give you the basic guidelines for preparing papers for IEEE conference proceedings.

I. Key Equations

Energy function–Lyapunov function

The accelerating power is expressed as the negative gradient of a potential energy function V

$$M\frac{d^2\delta}{dt^2} = -\frac{\partial V(\delta)}{\partial \delta}$$

$$V_{PE} = -P_m\delta - P_e^{max}cos\delta$$

The energy function V(δ,ω) of the system, for classical model of Single machine infinite bus (SMIB) power system, Vtotal=VKE+VPE

$$V(\delta,\omega) = \frac{1}{2}M\omega^2 + [-P_m(\delta-\delta_s) - P_e^{max}(cos\delta - cos\delta_s)]$$

II. Key Figures

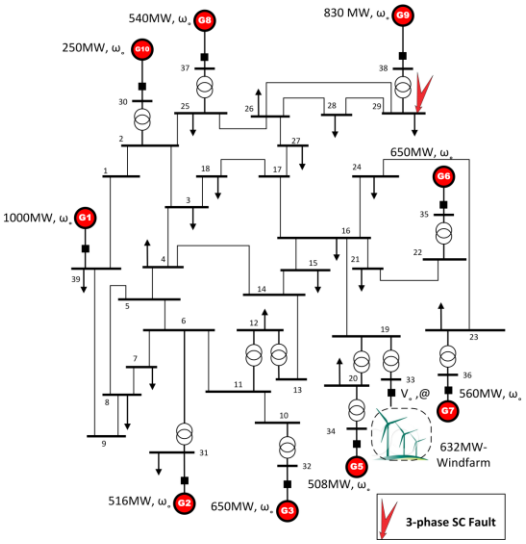

Fig. 1 IEEE 39 BUS test system, 10 Generators, Windfarm at BUS 33

III. Results

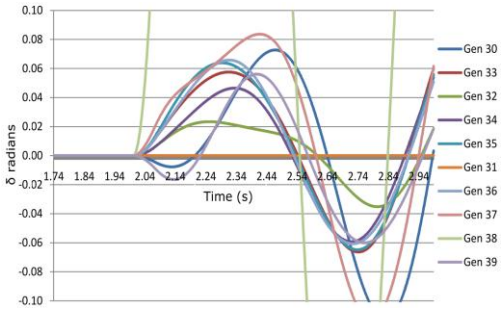

Fig. 2 Swing curves for fault on Bus 29, CCT-80ms, line 29-26 removed

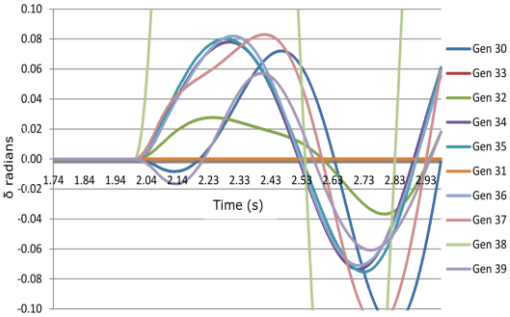

Fig. 3 Swing curves for fault on Bus 29, windfarm at Bus 33

Distributed Online Monitoring of Quasi-Static Voltage Collapse in Multi-area Power Systems

Le Xie, and Yang Chen
Department of Electrical and Computer Engineering
Texas A&M University, College Station, Texas 77843
Email: Lxie@ece.tamu.edu

Huaiwei Liao
Louis Dreyfus Highbridge Energy
Stamford, CT
Email: hwliao@ieee.org

***Abstract*—With an increasing penetration of variable resources into power grids, an effective scheme of online voltage instability monitoring becomes more significant. However, centralized schemes may be unreliable due to the possible divergence of global state estimator near voltage collapse or the difficulty to obtain reliable transfer limits.**

Our research focuses on a novel distributed framework for monitoring potential quasi-static voltage collapse in interconnected multi-area power systems. A novel performance index is presented based on the sensitivity of the smallest singular value of the power flow Jacobian matrix with respect to the regional load vector. The performance index applies *overlapping decomposition* in order to monitor the entire interconnected system with minimal area-level information exchange. Theoretical justification and practical implementation of distributed voltage stability monitoring are presented. By comparing the value of the performance index with a numerically robust threshold at each administrative control area, each area will be able to monitor quasi-static voltage instability at the entire interconnection level.

Numerical simulations in the IEEE 300-bus system illustrate the effectiveness of the proposed performance index and the threshold.

I. Key Equations

The key equations for distributed monitoring of quasi-static voltage collapse in multi-area power systems are presented as follows.

Large scale power systems can be formulated by a coupled set of nonlinear differential and algebraic equations (DAEs),

$$\dot{x} = f(x,u,y,p), \tag{1}$$
$$0 = g(x,u,y,p). \tag{2}$$

Define distributed performance index for area k

$$PI_{dk} = \left\| \frac{\partial (1/\sigma_{mdk})}{\partial S_{dk}} \right\|_{\infty}, \tag{3}$$

and corresponding distributed ratio

$$\tau_k(j) = \frac{PI_{dk}(j)}{PI_{dk}^{Normal}}. \tag{4}$$

Proposition 1: Consider the power system in DAEs (1) and (2). System-wide voltage collapse is about to happen when there exists at least one control area k whose PI_{dk} satisfies

$$PI_{dk}^{Collapse} \geq \gamma, \tag{5}$$

where γ is the threshold for monitoring voltage collapse.

Proposition 2: Consider the power system in DAEs (1) and (2). System-wide voltage collapse is about to happen when there exists at least one control area k whose τ_k satisfies

$$\tau_k \geq \bar{\gamma}, \tag{6}$$

where $\bar{\gamma} = 10$ is a robust threshold for all control areas.

II. Key Results

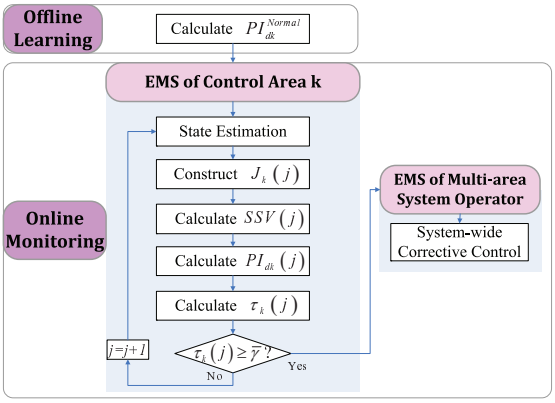

Fig. 1. Implementation of distributed monitoring algorithm for area k.

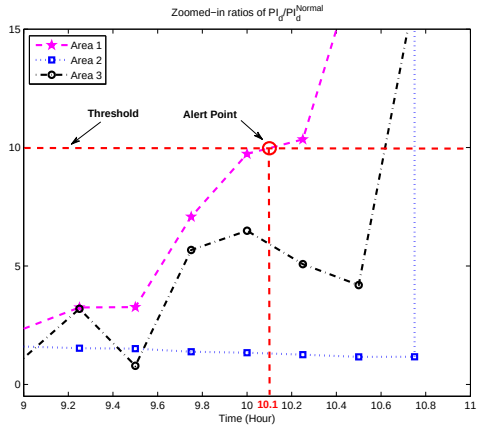

Fig. 2. Zoomed-in distributed monitoring for IEEE 300-bus system.

External Data Exchange Issues for State Estimation in Power Systems

Kai Yin Kenny Poon and Anjan Bose

Washington State University, Pullman, Washington

Email: kpoon@eecs.wsu.edu and bose@wsu.edu

***Abstract*— Nowadays, large interconnections comprise several reliability coordinators and many balancing authorities. Each reliability coordinator and balancing authority has its own control center with its own state estimator for monitoring the area under its control. The portion of the network which is outside a utility's control area is known as the external network and the modeling of the external system is required for a state estimator monitoring an internal system. In reality, each of these reliability coordinators has a unique external model which causes the largest errors in the real time models for maintaining situation awareness.**

In recent years, there has been a renewed interest in the situation awareness for the entire interconnection as a result of recent cascading blackouts which affected an area not covered by any one control center. The feasibility of performing state estimation on multi-area or interconnected systems has already been studied from an algorithmic viewpoint. Most of these studies have been in the investigation of state estimation schemes involving independent state estimators for each control area and a central coordinator, and it has been illustrated that such state estimators can be solved.

The actual implementation of a state estimator, however, depends on various factors, such as the time skew of data, the accuracy of the network database, the availability of raw data versus state-estimated data, and sensitive issues regarding the proprietary nature of the data. These issues are studied in this dissertation to determine the data exchange requirements for minimizing the errors in state estimation

Specifically, the effects of various levels of data exchange between the external model and the state estimator on state estimation accuracy are studied. This includes investigating the retention of more detailed external models than the present day practice of only retaining equivalents at the boundary buses. The differences between exchanging SCADA data versus state estimated data are also investigated, where time skew is considered in the exchange of state estimated data between the internal system and the external model. The importance of correct topology knowledge during state estimation is investigated, and finally, the effects of various types and levels of data exchange during state estimation on ensuing contingency analysis accuracy are also studied. All the studies are performed on two test bed systems. The first one is the IEEE-118 bus system and the second one is the 1648 bus system.

I. KEY FIGURES

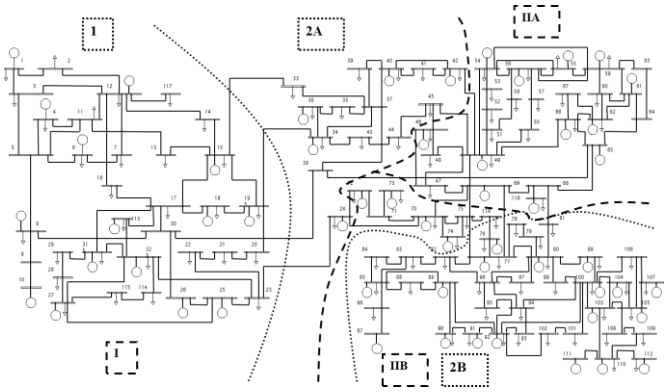

Figure 1. IEEE-118 bus test system configurations

II. KEY EQUATIONS

A. *State Estimation Accuracy Metric*

$$J = \frac{1}{n}\sum_{i=1}^{n}\left[\left(\vec{V}_i - \vec{V}_i^{PF}\right)\left(\vec{V}_i - \vec{V}_i^{PF}\right)^*\right] \quad (1)$$

where $\vec{V}_i$ is the estimated complex voltage at bus i

$\vec{V}_i^{PF}$ is the complex voltage at bus i from the power flow solution

n is the total number of internal system buses

B. *Contingency Analysis Accuracy Metric*

$$J_{cont} = \frac{1}{n}\sum_{i=1}^{n}\sqrt{\left[\left(\vec{V}_i - \vec{V}_i^{PF}\right)\left(\vec{V}_i - \vec{V}_i^{PF}\right)^*\right]} \quad (2)$$

where $\vec{V}_i$ is the estimated complex voltage at bus i

$\vec{V}_i^{PF}$ is the complex voltage at bus i from the power flow solution

n is the total number of internal system buses

Measurement-based Coherency Identification Technique via Independent Component Analysis

M. A. M. Ariff, and B. C. Pal
Department of Electrical and Electronics Engineering
Imperial College London, SW7 2AZ London, UK
Email: mam310@imperial.ac.uk, b.pal@imperial.ac.uk

***Abstract*—An approach to identify the coherent area in the interconnected power system using independent component analysis (ICA) is proposed. The ICA is applied to the generator speed and bus angle data, with the assistant of Hilbert-Transform Empirical Mode Decomposition (HT-EMD) to identify the coherent areas of the 16-machine 68-bus system model. The results show that the proposed method is capable to identify the coherent group of generator and buses following a disturbance in the system. The accuracy of the coherent group obtained using ICA method is compared with the results obtained using model-based direction cosine method. The proposed method provides an analytical tool to assist the special protection system (SPS) in minimizing the frequency and impact of wide-area blackout.**

***Index Terms*—Coherency identification, measurement-based, independent component analysis, power system.**

I. Key Figures

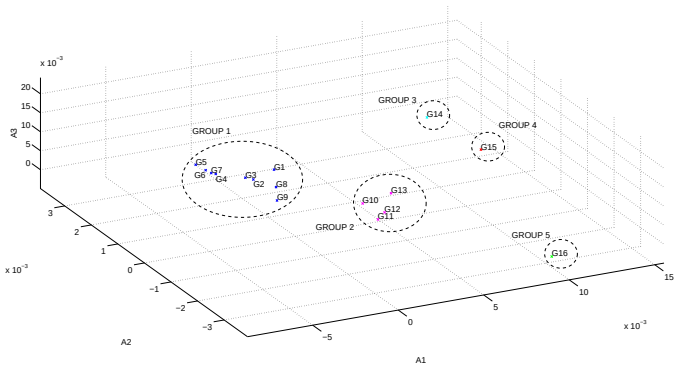

(a) Generators coherent groups

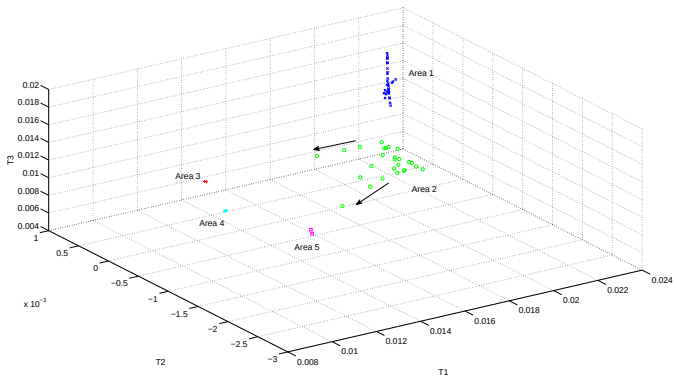

(b) Network buses coherent groups

Fig. 1. Coherency plot of 16-machine 68-bus system model

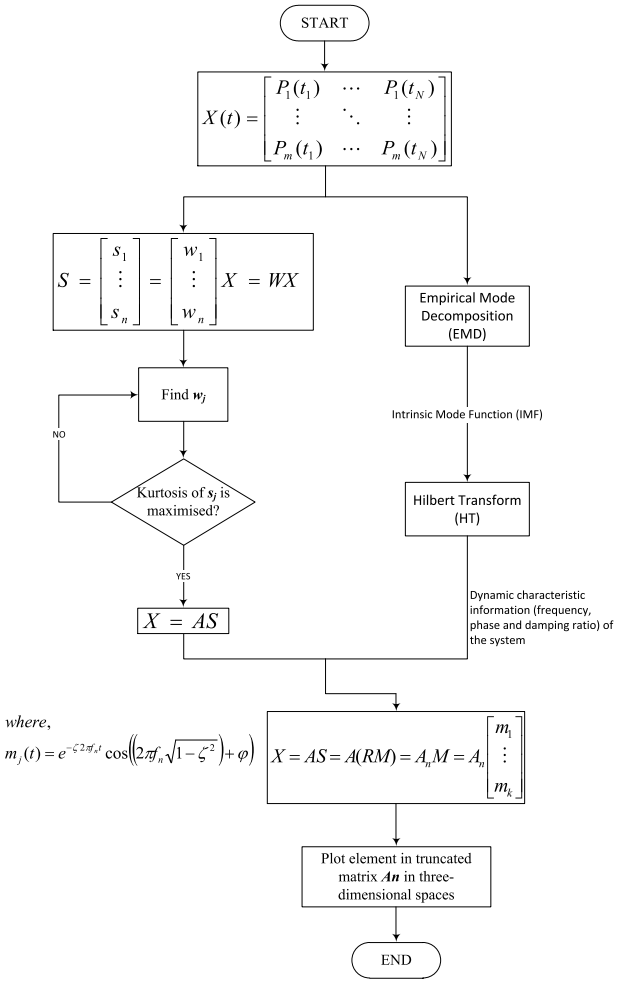

Fig. 2. Flowchart of the proposed methodology

Reliability Modeling of Dynamic Thermal Rating

Hamid Shaker-Ardakani
Department of Electrical and Computer Engineering
University of Calgary
Alberta, Canada
Email: hshakera@ucalgary.ca

Hamidreza Zareipour
Department of Electrical and Computer Engineering
University of Calgary
Alberta, Canada
Email: h.zareipour@ucalgary.ca

Mahmud Fotuhi-Firuzabad
Department of Electrical Engineering
Sharif University of Technology
Tehran, Iran
Email: fotuhi@sharif.edu

***Abstract*—transmission expansion in developed countries has become a challenging task mainly because of the regulatory regimes and right-of-way issues. Thus, it is becoming more and more important to efficiently utilize the existing transmission infrastructure.**

For shorter transmission lines, thermal limit is normally the main constraint in loading the line. To determine the secure loading limit of a line, thermal line rating is normally calculated considering conservative weather conditions, such as low wind speeds and high ambient temperatures. This type of thermal rating, known as static thermal rating (STR), usually underestimates the true thermal limit of the line [1]. Dynamic Thermal Rating (DTR) of transmission lines is an alternative approach which utilizes real-time meteorological information to estimate the thermal rating of a transmission line. In this method, regarding the characteristics of the transmission line, some measurement stations are installed along the line to measure the real-time weather conditions of the desired line. Compared to STR, DTR has been shown to provide a higher line rating without sacrificing system security [2]. Normally, DTR provides the system operator with greater transmission line capacity, which in turn results in lower overall short-term system operation costs.

In addition to the short-term operational benefits and system security enhancements achieved by using DTR, it may potentially improve long-term system reliability. Composite system reliability assessment studies [3] have been widely presented in the literature. However, to the best of authors' knowledge, neither a reliability model of transmission lines equipped with DTR nor a composite reliability assessment of systems with DTR are available in the literature.

In view of this, in this research work, a reliability analysis procedure is proposed for a transmission line equipped with a Dynamic Thermal Rating (DTR) system by proposing Markov models of the DTR system and the line equipped with it. Moreover, to model the annual variations of line DTR and take into account the uncertainty of meteorological data, the proposed Markov model is extended to a fuzzy-based reliability model. The proposed model was employed in composite reliability assessment of power systems. Because of the fuzzy annual DTR, the load curtailment optimization model necessary for reliability assessment contained fuzzy constraints. To do this, an Interactive Method Resolution (IMR) technique [4] for solving fuzzy optimization problems was developed to handle the fuzzy constraints associated to the lines equipped with the DTR system. In the IMR technique, fuzzy constraints are transformed to some crisp constraints by assigning a satisfaction degree to each of them. Solution of the optimization problem is found using these satisfaction degrees and also a feasibility degree for the objective function to satisfy all constraints with the maximum satisfaction degree while minimizing the objective function.

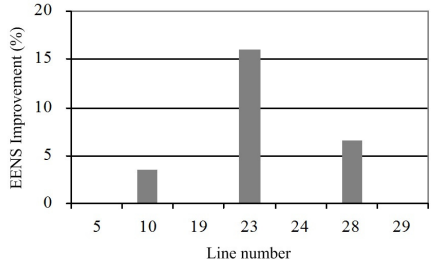

Fig. 1. Percentage improvement in system EENS using DTR compared to the system EENS using STR for the IEEE-RTS.

The main contributions of this paper can be summarized as follows:

1) **A Markov model is proposed for reliability assessment of transmission lines equipped with DTR system.**
2) **Annual DTR calculation using fuzzy methods is proposed.**
3) **Composite reliability of power systems in presence of lines with DTR is analyzed.**

The numerical results were presented, which demonstrated that the proposed Markov model properly represented the reliability of the DTR system. It was shown that using more measurement stations or less reliable components decreased the availability of the DTR system. On the other hand, having spare components for the DTR system increased its reliability. Furthermore, four different cases were used to estimate the composite reliability of the IEEE-RTS. As expected, it was also observed that properly selecting lines for adding a DTR system was important. Fig. 1 shows that using DTR in some lines, like line 25, will greatly improve the system reliability, while for some other lines it would not improve the reliability of the system.

REFERENCES

[1] M. W. Davis, "A new thermal rating approach: The real time thermal rating system for strategic overhead conductor transmission lines – part i: General description and justification of the real time thermal rating system," *IEEE Trans. Power App. Syst.*, vol. 96, no. 3, pp. 803 – 809, May. 1977.

[2] K. Hur, M. Boddeti, N. D. R. Sarma, J. Dumas, J. Adams, and S. K. Chai, "High-wire act," *IEEE Power Energy Mag.*, vol. 8, no. 1, pp. 37 – 45, Jan./Feb. 2010.

[3] R. Billinton and R. N. Allan, *Reliability evaluation of power systems*, 2nd ed. Plenum publishing co., 1996.

[4] M. Jimenez, M. Arenas, A. Bilbao, and M. V. Rodriguez, "Linear programming with fuzzy parameters: An interactive method resolution," *European Journal of Operational Research*, vol. 177, no. 3, pp. 1599 – 1609, Mar. 2007.

An Online Intelligent Alarm-Processing System Based on Abductive Reasoning Network

Jianan Mu, Wenchuan Wu, Hongbin Sun, Qinglai Guo, Yang Zhang, Boming Zhang
Department of Electrical Engineering, Tsinghua University, Beijing, 100084, China
Email: mjn06@mails.tsinghua.edu.cn and shb@tsinghua.edu.cn

***Abstract*—Large amounts of alarms coming into control center when faults occur have harassed operators for a long time, especially when there are false alarms, missing alarms or multiple faults. An online intelligent alarm-processing system based on abductive reasoning network (ARN) is developed to deal with the alarms automatically. Models and real-time data of the power system are collected from both supervisory control and data acquisition system / energy management system (SCADA/EMS) and fault information system, including primary and secondary models. First, when alarms arrive, rules reflecting cause-effect relationship between faults and alarms and between alarms themselves are established automatically, and the whole abductive reasoning network is constructed. Then, all the coming alarms are located on the network and traced back to the roots. Third, possible diagnoses are sifted and picked out according to their false alarm rate and missing alarm rate. At last, the diagnosis results are presented to the operators in several friendly manners. The system has been applied to the district control center of Jiaxing, China and is functioning well.**

I. Key Equations

$$MissingRate(\Delta)=\frac{\left|Expect(\Delta)-H\cap Expect(\Delta)\right|}{\left|Expect(\Delta)\right|}\times 100\% \quad (1)$$

$$FalseRate(\Delta)=\frac{\left|H-H\cap Expect(\Delta)\right|}{\left|H\right|}\times 100\% \quad (2)$$

II. Key Figures

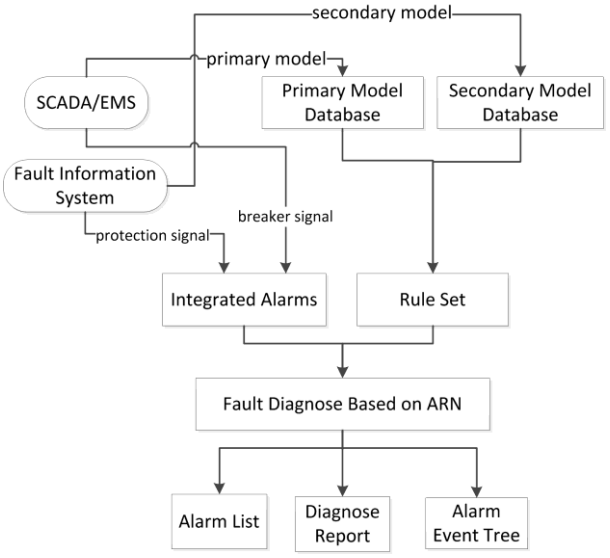

Fig. 1. Architecture of the proposed system.

III. Key Results

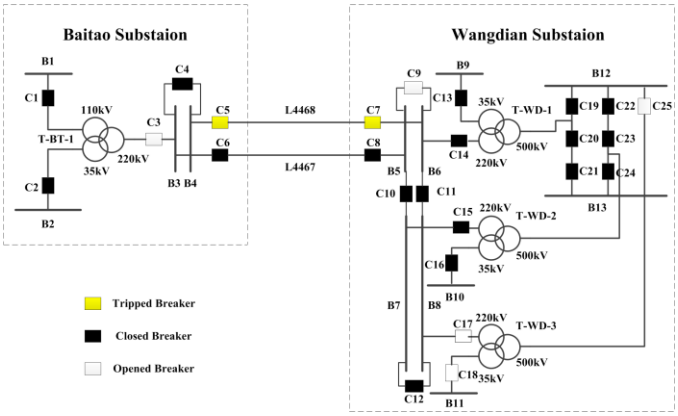

Fig. 2. Part of the power system in Jiaxing, China

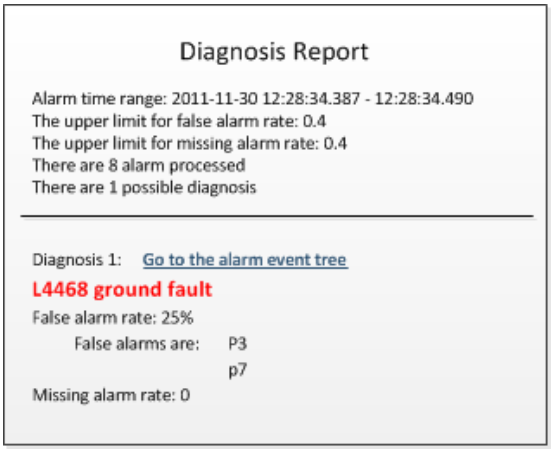

Fig. 3. Diagnosis report, including the fault device and fault type, false alarm rate and missing alarm rate, and false alarms and missing alarms.

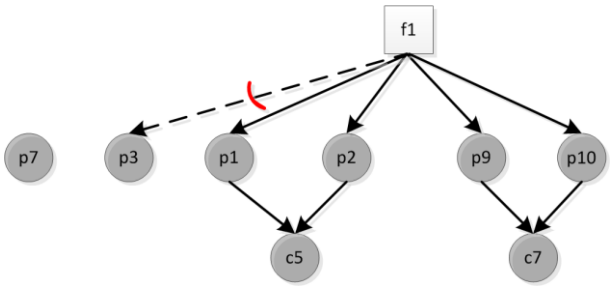

Fig. 4. Alarm event tree of the diagnosis result, the rule "***f1→p3***" is block because ***C5*** has been trip by ***p1*** in advance

The Effect of Parameter and Measurement Uncertainties on Hybrid State Estimation

Markos Asprou and Elias Kyriakides
Department of Electrical and Computer Engineering
KIOS Research Center for Intelligent Systems and Networks, University of Cyprus
Nicosia, Cyprus
asprou.markos@ucy.ac.cy, elias@ucy.ac.cy

Mihaela Albu
Department of Electrical and Computer Engineering
"Politehnica" University of Bucharest
Bucharest, Romania
albu@ieee.org

***Abstract*—The tool of state estimator constitutes the cornerstone of the Supervisory Control and Data Acquisition (SCADA) system since many monitoring and control applications rely on it. Therefore, state estimator should provide accurate and reliable estimations of the power system states. In this work, two major sources of uncertainties that deteriorate the performance of state estimator will be examined. Specifically, the measurement uncertainty and the uncertainty arising from the limited knowledge of the transmission line parameters are considered. Further, the effect of the use of synchronized measurements along with the conventional measurements for compensating the two sources of uncertainty will be also examined.**

Keywords- Hybrid state estimator, conventional measurements, measurement uncertainty, parameter uncertainty, synchronized phasor measurements.

I. INTRODUCTION

The synchronized measurements are distinguished by their high fidelity and their ability to provide both magnitude and angle information with specified measurement uncertainty. It is very interesting though to investigate the effect of measurement uncertainty of both conventional and synchronized measurements in the overall state estimation performance. Further, another source of uncertainty that deteriorates the performance of the state estimator is the approximation of the values of the transmission line parameters. The deviation of the considered line parameters values from their real ones introduce uncertainty to the power system state estimator and deteriorate its performance considerably. In this work, a comparison of the performance of the hybrid state estimator taking into account both sources of uncertainty will be performed.

II. CASE STUDIES

A. Hybrid state estimator accuracy taking into consideration measurement uncertainties

Three case studies were performed for examining the effect of measurement uncertainty on the state estimator accuracy. In the first case study both conventional and PMU measurements are assumed to be perfectly accurate (without associated measurement uncertainties). In the second case study the conventional measurements are considered together with the associated standard uncertainties, while the PMU measurements are assumed to be perfectly accurate. In the last case study both conventional and PMU measurements are considered with the associated standard uncertainties. In Fig. 1, the voltage magnitude and voltage angle residuals respectively are illustrated for the three case studies, when the hybrid state estimator is applied to the IEEE 14 bus system.

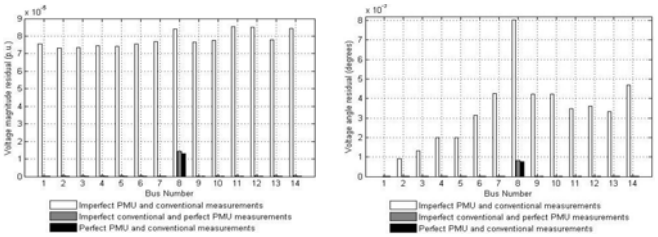

Fig. 1. Voltage magnitude and angle residuals for the IEEE 14 bus system

B. Hybrid state estimator accuracy taking into consideration line parameters uncertainties

The uncertainties associated with the transmission line parameters are considered in this Section. The line parameters are assumed to follow a uniform distribution spanning from (nominal value -30%) to (nominal value + 30%). In Fig. 2, the voltage magnitude and angle residuals are shown in the cases where measurement uncertainties and line parameters are considered.

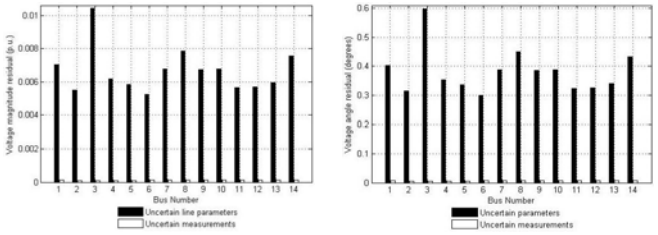

Fig. 2. Voltage magnitude and angle residuals for the IEEE 14 bus system

III. CONCLUSIONS

The results for this system show that the limited knowledge of the line parameters affects significantly more the performance of the hybrid state estimator. This indicates the immense need for perfect knowledge of the line parameter

This work was co-funded by the European Regional Development Fund and the Republic of Cyprus through the Research Promotion Foundation (Project KY-POY/0609/16) and by the Romanian National Research Council through the Grant IDEI 1402 TAMPERE (Advanced measurement solutions and parameter estimation techniques for active distribution networks).

Power Quality Monitoring for Microgrids

Patricio Mendoza-Araya
Wisconsin Electric Machines and Power Electronics Consortium
University of Wisconsin-Madison
Madison, Wisconsin 53706
mendozaaraya@wisc.edu

***Abstract*—Microgrids are becoming the de facto solution for distributed generation aggregation not only in the grid-tied case, but also in the islanded case. There are some issues that need to be addressed in both cases, being one of the most important ones the power quality within the microgrid. Even though there are solutions to power quality problems for traditional electric power systems, microgrids present a set of particular characteristics that enable novel solutions to be developed. This work presents a monitoring system that gathers the power quality information, potentially from several points within the microgrid. The monitoring system has two components: a data logger, which listens to any power quality event that may happen, and records the event's information in a database; and a human-machine interface, which displays the information stored in the database and enables the interpretation and analysis of the event's information through phasor diagrams and waveform plots, among others. This power quality information is extremely valuable when studying the power quality issues in a microgrid, and, furthermore, allows a better power quality control to be performed in a microgrid.**

I. Key Figures and Results

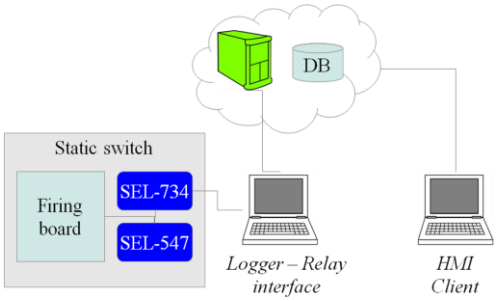

Figure 1. Monitoring unit block diagram

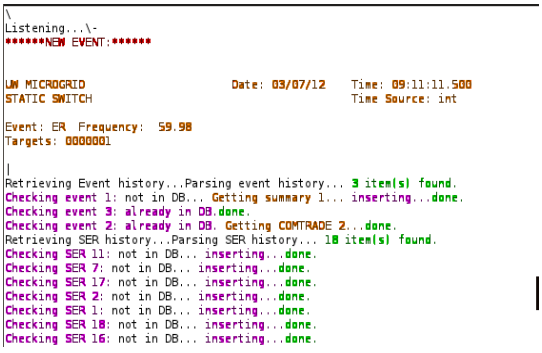

Figure 2. Logger screen output

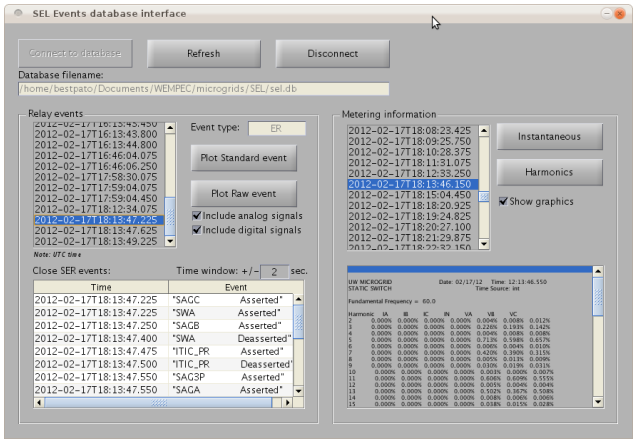

Figure 3. Human-Machine interface main screen

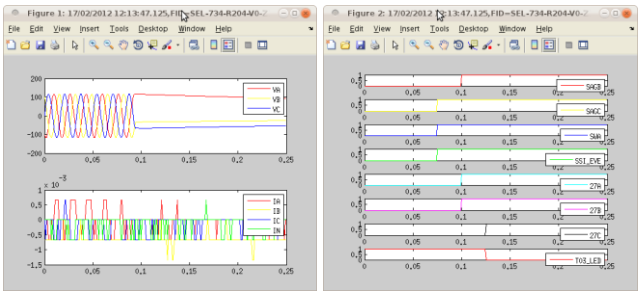

Figure 4. Analog and digital waveform displays

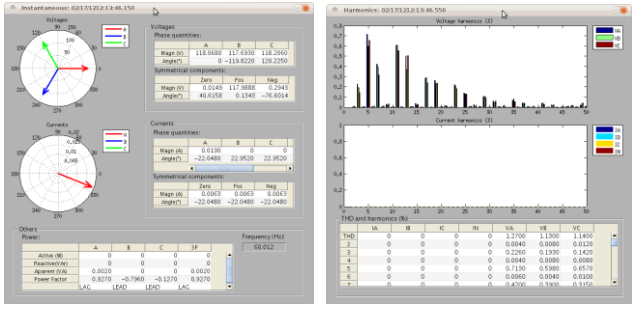

Figure 5. Instantaneous and harmonic displays

STATISTICAL AND PREDICTIVE MODELING OF AUTOMATED METER READING SYSTEM OUTAGES

Prasad Shinde, *Student Member IEEE* and Dr. Mariesa Crow, *Fellow IEEE*
Department of Electrical and Computer Engineering,
Missouri University of Science and Technology, Rolla, MO 65409, USA
Email: prasad.shinde@mst.edu, crow@ieee.org

Abstract - An automated meter reading (AMR) system is a metering technology that enables power utility companies to receive customers' energy usage data centrally over a communication network. The installed automated meters also provide a daily log of outage events for each customer. A utility company can greatly benefit by using this information for outage management. However, outage data is frequently corrupted and the outage flags registered by these automated meters do not reflect true outages. In this study, historic outage data was analyzed and validated by comparing with known occurrences of outage events. A histogram analysis was performed to study the distribution of multiple outages. A novel probabilistic model is introduced using fuzzy logic based algorithm to analyze outage flags and to determine a degree of accuracy for each outage indication. A generalized model is developed to gather essential network information, pertinent to outage indications. This information is combined along with outage data from outage analysis system (OAS) and is passed on to the fuzzy logic system that yields a crisp value for confidence index in AMR outage flags. The proposed model is developed for analysis of AMR system outages at Ameren Missouri.

I. KEY FIGURES

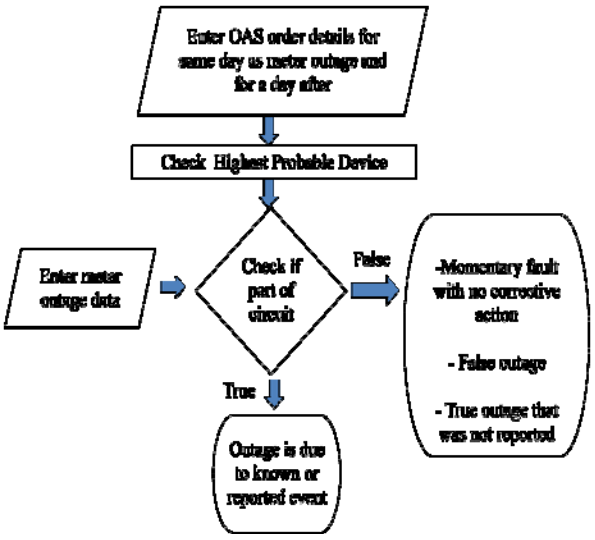

Figure 1 Outage validation algorithm

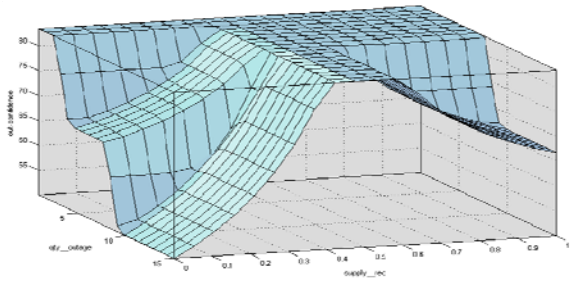

Figure 2 Surface for mapping input outage information to output confidence index

II. KEY RESULTS

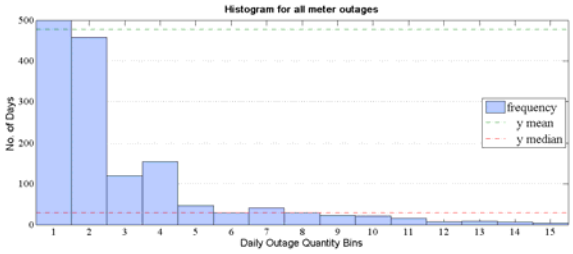

Figure 3 Histogram analysis plot for all meters (with median and mean)

Table 1 Sample result of Outage Validation

Meter ID	Total No. of days flags received	Total no. of flags received	No. of days meter data confirmed	No. of flags validated	Meter success rate per day basis (%)	Meter success rate overall (%)
52699412	70	119	4	6	5.71	5.04
52705149	13	15	4	5	30.77	33.33
52699387	7	9	4	4	57.14	44.44
52717365	1	1	1	1	100	100
52717614	171	886	17	58	9.94	6.55
94131734	3	6	4	7	75	85.71
94117013	3	6	5	8	60	75

Table 2 Sample result of predictive fuzzy model indicating confidence index in meter outage indication

Meter number	Outage Reliability Index (%)
46533803	29.4
17564393	75.8
52699530	75.9
52717614	27.9

Event Analysis Engine for Oscillation Monitoring using Synchrophasors

Zaid Tashman and Vaithianathan "Mani" Venkatasubramanian
School of Electrical Engineering and Computer Science
Washington State University, Pullman WA 99164, USA
Email: ztashman@wsu.edu, mani@eecs.wsu.edu

***Abstract*— Oscillation monitoring system (OMS) is being developed as a real-time tool, integrated within OpenPDC for monitoring the frequency, damping ratio as well as the mode shape of poorly damped electromechanical oscillations in power systems using synchrophasor data. OMS takes synchrophasor data in C37.118 format as input, and stores modal analysis results in SQL database in real-time, which can also be used for offline analysis as well. OMS consists of two engines as seen in Fig.1. The Damping Monitor engine continuously running and estimating the damping, frequency as well as mode shape of poorly damped oscillatory modes from ambient synchrophasor data. On the other hand, the Event Analysis engine only works whenever an event occurs in the system. It carries out automatic expert system-like rule based Prony type analysis of system responses during the occurrence of disturbances in the system. It uses three different algorithms, namely Prony, Matrix Pencil and Hankel Total Least Square, to estimate the system modes and these estimates from the three algorithms will then go through a set of predefined consistency rules to trigger an alarm whenever there is a consistent estimate of a poorly damped mode across three engines. This paper summarizes the theory of OMS and highlights the implementation features at several industry members and the results obtained from these implementations.**

I. Introduction

The Event Analysis engine receives voltage and current signals from multiple PMUs. All signals from each PMU will be grouped together for local oscillation analysis. At the same time, the event analysis engine automatically choses specific signals and performs inter-area oscillation analysis in parallel using multi-threading techniques. After analyzing all these PMU data using the three algorithms, the results will be crosschecked to find consistent dominant local and inter-area modes. If a predefined number of consistent estimates, say four consecutive consistent estimates was detected, then an alarm will be triggered. Fig.2 and Fig.3 shows the frequency and the damping ratio results from the event in Fig.1 calculated Event Analysis engine in OMS.

OMS has been implemented in several utilities, and it is successfully providing early warning on poorly damped inter-area as well as local modes in real-time [1]. OMS has also been able to detect sustained zero damped subsynchronous oscillations using synchrophasor data in real-time caused by a nearby wind farms [2].

II. Key Results

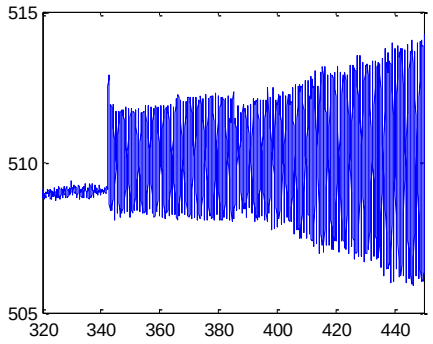

Figure 1: An Event Showing Oscillations in Voltage Magnitude Signal

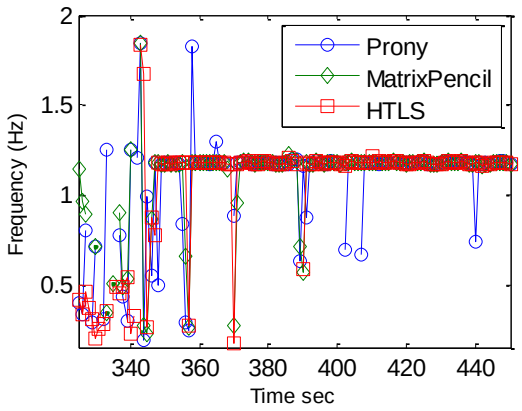

Figure 2: OMS Frequency Estimates

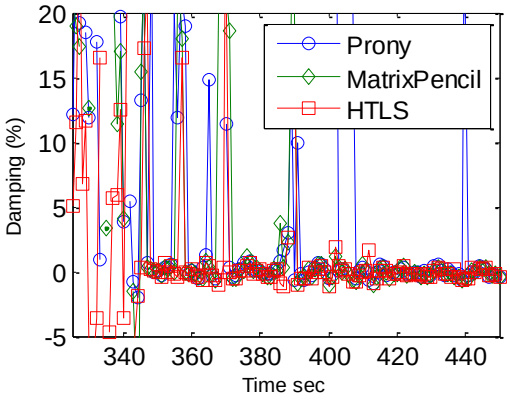

Figure 3: OMS Damping Ratio Estimates

Coupon Incentive-based Demand Response (CIDR) in Smart Grid

Haiwang Zhong
Department of Electrical and Computer Engineering
Texas A&M University
College Station, TX 77840
Email: zhonghw04@tamu.edu

Le Xie
Department of Electrical and Computer Engineering
Texas A&M University
College Station, TX 77840
Email: lxie@ece.tamu.edu

Qing Xia
Department of Electrical Engineering
Tsinghua University
Beijing, China 100084
Email:qingxia@tsinghua.edu.cn

***Abstract*—A new type of demand response (DR) program referred to as coupon incentive-based demand response (CIDR) is presented as an alternative to residential consumer demand response programs. Enabled by pervasive mobile communication capabilities and smart grid technologies, load serving entities (LSEs) could offer residential consumers coupon incentives to reduce power consumption in a given period of time, offsetting potential losses due to wholesale electricity price spikes. In contrast with real-time pricing or peak load pricing, CIDR program maintains simple flat retail rate structure on consumer side while providing effective voluntary-based incentives for DR. An iterative procedure is designed to realize the real-time interaction between the independent system operator, the LSEs and consumers. CIDR can increase the profit of the LSEs and achieve almost the same social welfare as under the real-time pricing scheme. CIDR is compatible with current flat retail rate pricing scheme so the implementation is straightforward. A numerical experiment demonstrates the potential benefits of CIDR programs.**

I. Key Euqations

The mathematic formulation of the proposed model is presented as follows:

1) The Consumer's Model

$$\rho_c = k\Delta P_{di}, \quad i = 1, 2, \ldots, N \tag{1}$$

$$0 \le \Delta P_{di} \le \Delta P_{di}^{max}, \quad i = 1, 2, \ldots, N \tag{2}$$

2) The LSE's Model

$$\max \rho_{RR}(P_d - \Delta P_d) - \rho_{RTP}(P_d - \Delta P_d) - \rho_c \Delta P_d \tag{3}$$

$$s.t. \qquad \rho_c = k\Delta P_{di}, \quad i = 1, 2, \ldots, N \tag{4}$$

$$0 \le \Delta P_{di} \le \Delta P_{di}^{max}, \quad i = 1, 2, \ldots, N \tag{5}$$

$$\Delta P_d = \sum_{i=1}^{N} \Delta P_{di} \tag{6}$$

3) The ISO/RTO's Model

$$\min_{P_{gi}} \sum_{i=1}^{G} C_i(P_{gi}) \tag{7}$$

$$s.t. \qquad \sum_{i=1}^{G} P_{gi} = \sum_{j=1}^{N} (P_{dj} - \Delta P_{dj}) \tag{8}$$

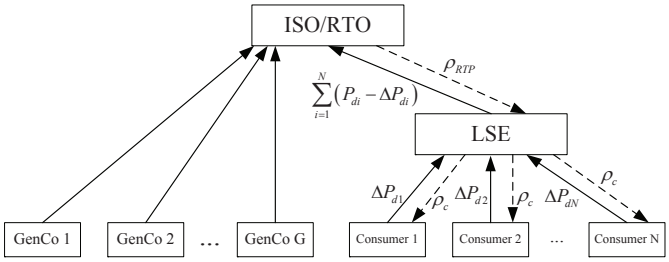

Fig. 1. Proposed three-layer information exchange structure for CIDR implementation

TABLE I
Comparisons Of Different Pricing Schemes

	Case 1: Flat Rate	Case 2: RTP	Case 3: CIDR
Demand Response(MW)	0	92	968
LSE's Profit($)	-101523	0	-49943
Price Consumers Face($/MWh)	100	104.61	100
Consumer's Rebate($)	0	0	49943
Social welfare(million $)	10.9137	10.9139	10.8928

$$P_{gi}^{min} \le P_{gi} \le P_{gi}^{max}, \quad i = 1, 2, \ldots, G \tag{9}$$

The aggregated cost function is:

$$C = a(P_d - \Delta P_d)^2 + b(P_d - \Delta P_d) + const \tag{10}$$

Based on the first order KKT condition, the optimal coupon price can be obtained.

$$\rho_c = \frac{k[-\rho_{RR} + 4aP_d + (b + \Delta b)]}{2k + 4a} \tag{11}$$

II. Key Figures

The information exchange structure is designed (shown in Fig. 1).

III. Key Results

The key results are shown in Table I. The optimal coupon price is $48.39/MWh. The social welfare under CIDR scheme is very close with RTP scheme.

Emission Pricing and Locational Signal Impact on Generation Portfolio in Large Scale Queensland Network

Kazi Nazmul Hasan, Tapan Kumar Saha, and Mehdi Eghbal
University of Queensland, Brisbane, Queensland 4072, Australia

***Abstract*--The evolving generation planning paradigm has been shifting from *reliability-driven* to *market-driven*, and further to *environment-driven* arena, while cumulatively adding up these consecutive objectives. This study evaluates the '*screening-curve based*' least-cost generation entry along with the '*market-based*' profit-maximizing generation investment. A *Markov Chain Monte Carlo* based scheme is implemented in the abovementioned algorithms to capture the uncertainty of electricity price. The *locational signals* of the generation resources are also included in the model. This paper analyzes possible impacts on the *generation portfolio* and *electricity price* that may emerge due to the employment of the '*Clean Energy Bill, 2011*' in the *Australian National Electricity Market (NEM)*. An analytical study is presented in this paper, simulating the proposed framework to the *Queensland network* of the *Australian NEM*. Simulation results show *market signals* for generation investments, highlighting considerable change in the *energy matrix* and *electricity price* in the coming decade.**

I. Key Equations

A. Screening-Curve Approach

Annual revenue requirement (ARR) is obtained as below,

i. Business-As-Usual

$$ARR = FC + cf \times VC \quad (1)$$

ii. Emission Price Impact

$$ARR = FC + cf \times VC \times ef \times EC \quad (2)$$

iii. Locational Signal Impact

$$ARR = FC + FC_T + cf \times (VC + VC_T) \quad (3)$$

B. Market-Driven Approach

Annual Required Return on Capital (ARRC) and annual revenue (AR) is calculated as formulated below,

i. Business-As-Usual

$$ARRC_i = \left(Cap_i + O\&M_i + Tax_i\right) \times G_i \times 8760 \times cf_i \times \left(1 - Aux_i\right) \quad (4)$$

$$AR_i = \sum_T \left\{p(t) - SRMC_i\right\} \times G_i(t) \quad (5)$$

ii. Emission Price Impact

$$AR_i = \sum_T \left\{p(t) - SRMC^{EC}{}_i\right\} \times G_i(t) \quad (6)$$

iii. Locational Signal Impact

$$ARRC_i = \left[\begin{matrix}\left(Cap_i + O\&M_i + Tax_i\right) \\ \times cf_i \times \left(1 - Aux_i\right) + ef_i \times EC\end{matrix}\right] \times G_i \times 8760 + \left(TCap + TO\&M\right) \times T_i \quad (7)$$

$$AR_i = \sum_T \left\{p(t) - SRMC^{TC}{}_i\right\} \times G_i(t) \quad (8)$$

II. Key Results

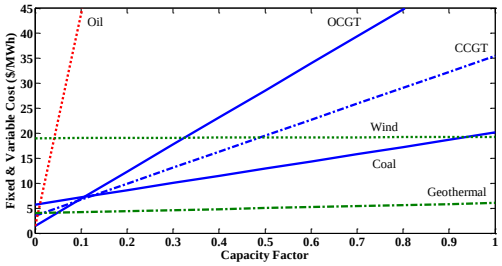

Fig.1 Screening curves to obtain optimum Queensland generation mix.

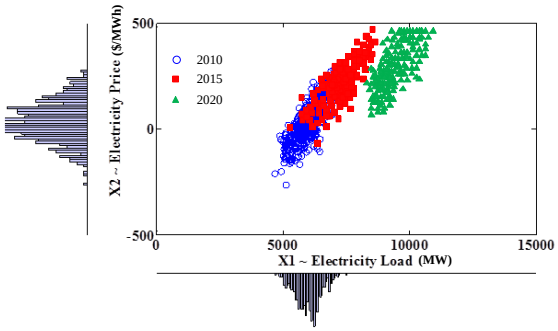

Fig.2 Simulated electricity price for 2010 (historical), 2015 and 2020 for Queensland electricity market.

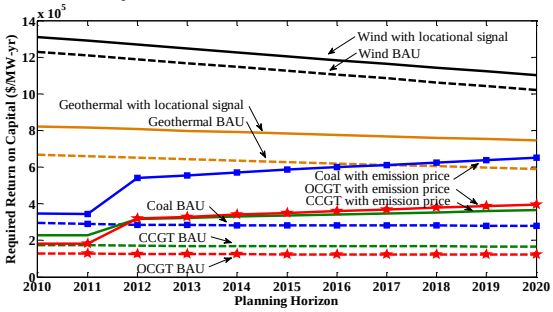

Fig.3 ARRC with emission cost and locational signals for QLD generation.

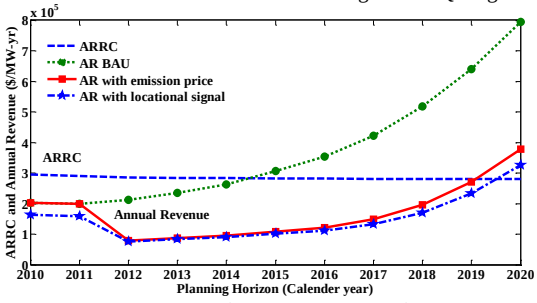

Fig.4 ARRC and annual revenue for coal generators of Queensland.

A Balance Between Stochastic and Deterministic Unit Commitment Formulations

Garret LaBove and Kory Hedman
School of Electrical, Computer and Energy Engineering
Arizona State University, Tempe, AZ, 85287, USA
Email: garret@asu.edu and kory.hedman@asu.edu

***Abstract*— As interest grows in power generation from sustainable and intermittent resources such as wind and solar, today's arbitrary and static security policies will become increasingly insufficient to address issues of supply-side uncertainty. The complexities involved in managing renewable power generation precipitate new approaches to better manage power system operations in order to protect the balance between high reliability and low cost for all market participants. Stochastic unit commitment has previously been demonstrated to improve preparation of thermal generation assets in the day-ahead market; however, such improvements require substantial computational burden and, for large systems like those managed by ISOs, may be intractable. This document proposes a balanced approach between stochastic and deterministic formulations to improve solution quality while maintaining computational efficiency. This involves a multi-stage process, beginning with a scenario-based unit commitment phase over a subset of scenarios of realized intermittent generation to commit slow-starting generation. Then, using the slow generation as fixed input, a deterministic unit commitment phase follows, with an objective to minimize load shedding for each of the available scenarios. The load shedding at all points in the network is cataloged for each scenario, and the expected value of load shedding at each bus is then added as a virtual load. This virtual load is then applied in addition to the demand of the initial scenario based unit commitment stage, which is re-solved in order to improve reserve levels in the network. This technique will result in higher quality solutions for the day-ahead unit commitment allocation while maintaining the computational tractability of deterministic methods necessary for analysis in large scale networks. This work will lead to an investigation into the tradeoffs, both in computational time and utility of solution, inherent in the number of chosen scenarios to model for the first stage.**

I. Key Equations

The first stage of the proposed technique is defined as follows.

$$\min \sum_g \sum_t C_g(P^0_{g,t}) + C_{SU}(SU_{g,t}) + C_{NL}(u_{g,t}) \quad (1)$$

Subject to

$$u_{g,t}P^{min}_g \le P^0_{g,t} \le u_{g,t}P^{max}_g \quad (2)$$
$$u_{g,t}P^{min}_g \le P_{g,t,s} \le u_{g,t}P^{max}_g \quad (3)$$
$$P^0_{g,t} - P_{g,t,s} \le R^{10}_g u_{g,t} \quad (4)$$
$$P_{g,t,s} - P^0_{g,t} \le R^{10}_g u_{g,t} \quad (5)$$
$$SU_{g,t} - SD_{g,t} = u_{g,t} - u_{g,t-1} \quad (6)$$
$$\sum_r^t SU_{g,r} \le u_{g,t} \quad \text{where } r = t - UT_g + 1 \quad (7)$$
$$\sum_s^t SD_{g,s} \le 1 - u_{g,t} \quad \text{where } s = t - DT_g + 1 \quad (8)$$
$$SR_t = \sum_g SR_{g,t} \quad (9)$$
$$SR_{g,t} \le (u_{g,t}) \min\left(P^{max}_g - P^0_{g,t}, R^{10}_g\right) \quad (10)$$
$$NSR_t = \sum_g NSR_{g,t} \quad (11)$$
$$NSR_{g,t} \le (1 - u_{g,t}) \min\left(P^{max}_g, R^{10}_g\right) \quad (12)$$
$$SR_t + NSR_t \ge SR_{min} + NSR_{min} \quad (13)$$
$$P^0_{g,t} - P^0_{g,t-1} \le R^+_g u_{g,t-1} + R^{SU}_g SU_{g,t} \quad (14)$$
$$P^0_{g,t-1} - P^0_{g,t} \le R^-_g u_{g,t} + R^{SD}_g SD_{g,t} \quad (15)$$
$$u_{g,t} \in \{0,1\} \quad (16)$$
$$0 \le \{SU_{g,t}, SD_{g,t}\} \le 1 \quad (17)$$

In addition to (2)-(17) are standard OPF constraints.

II. Key Figure

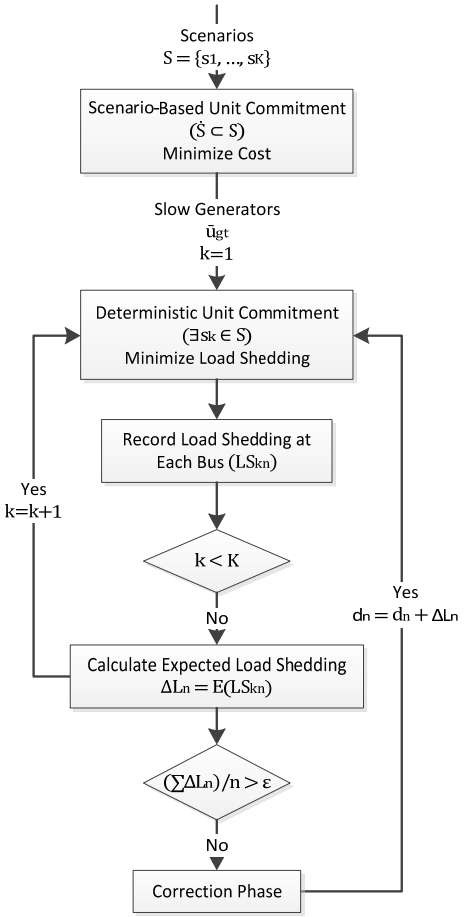

Figure 1. Flow chart of presented technique.

Day-Ahead electricity price forecasting using a hybrid non-linear model

Christian Geidel
Department of Electrical Engineering and Computer Sciences
Technische Universitaet Berlin
Berlin, Germany
Email: cgeidel@ucalgary.ca

Amir Motamedi
Alberta Electric System Operator (AESO)
Calgary, Canada
Email: motamedi.amir@yahoo.com

Hamidreza Zareipour
Department of Electrical and Computer Engineering
University of Calgary
Calgary, Canada
Email: h.zareipour@ucalgary.ca

I. Abstract

All over the world electricity markets are in the process of changing from government owned and regulated towards competitive markets. In most competitive markets, the independent system operator determines the price equilibrium of all submitted bids from both producers and consumers on a day ahead basis. In recent years, many markets have been affected by an increasing amount of energy produced by renewable sources, especially wind [1]. This is due to the movement of governments around the world towards a greener society in an effort to tackle climate change. However, these renewable energy sources are not always available and only predictable to some degree. At a large scale integration this uncertainty has a significant affect on market prices and makes its prediction much more complex than it used to be.

Many models have been developed in order to improve price forecasting accuracy such as time series-models [2] and neural networks [3]. In [4], an absolute negative correlation between price and wind power was found and [5] includes wind power to enhance the short-term forecasting performance in Denmark. Despite these results, models that take advantage of wind power are limited to linear models.

To the authors knowledge, wind power used as an explanatory variable in a non-linear model is limited to [6], however, the used model is relatively simple. Therefore, this research focuses on developing an advanced hybrid non-linear model which applies data mining techniques in order to capture the effect of wind on market prices and provide accurate short-term electricity price forecasts. The model is a hybrid between SVM and ANN models. SVM-based models were chosen because they do not require a long period of data for training, and thus the very short-term and dynamic patterns of electricity prices are expected to be captured using them [7]. Comparatively, ANN-based models require relatively long period of data for training and therefore, the longer term patterns of electricity prices can be captured using them [8]. In order to evaluate the forecasting performance using wind power as input for a non-linear model, the outcomes of the following input sets are compared:

$$CS_1 = \{D_{t-h}, ..., D_{t-2}, D_{t-1}, D_t^f, D_{t+1}^f, ..., D_{t+23}^f, D_{t+24}^f\},$$
$$CS_2 = \{D_{t-h}, ..., D_{t-2}, D_{t-1}, WP_{t-h}, ..., WP_{t-1}, D_t^f, D_{t+1}^f, ..., D_{t+24}^f, WP_t^f, WP_{t+1}^f, ..., WP_{t+24}^f\}.$$

Where, demand and wind power at hour t are represented by D and WP, respectively. The forecast values are represented using superscript f. In addition, h represents the last historical hour under consideration. Fig.1 shows the proposed price forecasting model.

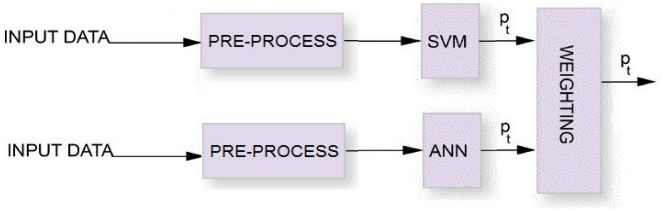

Fig. 1. The Proposed Electricity Price Forecasting Framework

References

[1] J. Morales, A. Conejo, and J. Perez-Ruiz, "Simulating the impact of wind production on locational marginal prices," *IEEE Transactions on Power Systems*, vol. 26, no. 2, pp. 820 – 828, May 2011.

[2] A. Conejo, M. Plazas, R. Espinola, and A. Molina, "Day-ahead electricity price forecasting using the wavelet transform and ARIMA models," *IEEE Transactions on Power Systems*, vol. 20, no. 2, pp. 1035 – 1042, May 2005.

[3] N. Pindoriya, S. Singh, and S. Singh, "An adaptive wavelet neural network-based energy price forecasting in electricity markets," *IEEE Transactions on Power Systems*, vol. 23, no. 3, pp. 1423 – 1432, 2008.

[4] G. Saenz de Miera, P. del Rio Gonzalez, and I. Vizcaino, "Analysing the impact of renewable electricity support schemes on power prices: the case of wind electricity in spain," *Energy Policy*, vol. 36, no. 9, pp. 3345 – 3359, 2008.

[5] J. Tryggvi, *Forecasting of Electricity Prices Accounting for Wind Power Predictions*. Master Thesis, Technical University of Denmark, 2008.

[6] J. L. Z. R. E. Alberto Cruz, Antonio Munoz, "The effect of wind generation and weekday on spanish electricity spot price forecasting," *Electric Power Systems Research*, vol. 81, no. 10, pp. 1924 – 1935, October 2011.

[7] C. Gao, E. Bompard, R. Napoli, and H. Cheng, "Price forecast in the competitive electricity market by support vector machine," *Physica A*, vol. 382, no. 1, pp. 98 – 113, August 2007.

[8] N. Amjady and A. Daraeepour, "Mixed price and load forecasting of electricity markets by a new iterative prediction method," *Electric Power Systems Research*, vol. 79, no. 9, pp. 1329 – 1336, September 2009.

Multiobjective Based Energy and Ancillary Service Markets Clearing

Amin Kargarian and Yong Fu
Department of Electrical and Computer Engineering, Mississippi State University, Mississippi State, 39762, USA
Email: *ak836@msstate.edu*, *fu@ece.msstate.edu*

Abstract—In certain electricity markets, the system operator clears both energy and ancillary services markets in a sequential manner. Due to some power system constraints, scheduling one market may cause some deviations in the other market. In this paper, a coupled energy and ancillary service market is presented. The proposed model is a multiobjective based optimization problem which minimizes market payment, transmission congestion, and power system emission, and maximizes voltage security margin and reactive power reserve. An IEEE 24-bus power system is used to show the effectiveness of the proposed algorithm.

I. Key Equations

1. Minimize total market payment:

$$Min \quad TMP = \sum_{\forall i \in gen} c_{p,i} + b_{p,i} P_i + a_{p,i} P_i^2 + \sum_{\forall i \in gen} CSP_i \times SP_i$$

2. Maximize voltage security margin:

$$Min \quad WLI = Max\left(\frac{4X\,Q_r}{[V_m \sin(\theta - \delta_m + \delta_n)]^2}\right)$$

3. Minimize transmission congestion:

$$Min \quad WTLC = Max\left(\left(\frac{S_i}{S_{i^{\max}}}\right)^2\right) \quad \forall i \in Transmission\ lines$$

4. Minimize power system emission:

$$Min \quad PSE = \sum_{i \in SM} 10^{-2}(c_{e,i} + b_{e,i} P_i + a_{e,i} P_i^2) + \zeta_i \exp(\lambda_i P_i)$$

5. Maximize reactive power reserve:

$$Max \quad RPR = \sum_{i \in SM} Q_{res,i}$$

Prevailing constraints are as follow:

$$P_{Gi} - P_{Di} = \sum_{j=1}^{nb} V_i V_j Y_{ij} \cos(\theta_{ij} + \delta_j - \delta_i) \quad \forall i$$

$$Q_{Gi} + Q_{Ci} - Q_{Di} = -\sum_{j=1}^{nb} V_i V_j Y_{ij} \sin(\theta_{ij} + \delta_j - \delta_i) \quad \forall i$$

$$0 \le SP_i \le \min(SP_i^{\max}, MT * UR_i) \quad \forall i \in gen$$

$$\sum_{\forall i \in g_m} SP_i \le SP_m \quad \forall m \in System zone$$

$$P_i^{\min} \le P_{Gi} + SP_i \le P_i^{\max} \quad \forall i \in gen$$

$$Q_i^{\min} \le Q_{Gi} \le Q_i^{\max} \quad \forall i \in SM$$

$$S_i \le S_i^{\max} \quad \forall i \in SM$$

$$Q_{Ci}^{\min} \le Q_{Ci} \le Q_{Ci}^{\max} \quad \forall i \in SC$$

$$V_i^{\min} \le V_i \le V_i^{\max} \quad \forall i$$

$$\left|S_j(V,\delta)\right| \le S_j^{\max} \quad \forall j$$

$$LI_j \le \nu \quad \forall j$$

6. Multiobjective optimization using compromise programming:

$$Min \quad \left\{\left(\frac{TMP}{TMP*}\right)^2 + \eta\left(\frac{WLI}{WLI}\right)^2 + \gamma\left(\frac{WTLC}{WTLC*}\right)^2 + \mu\left(\frac{RPR*}{RPR}\right)^2 + \psi\left(\frac{PSE}{PSE*}\right)^2\right\}^{0.5}$$

II. Key Results

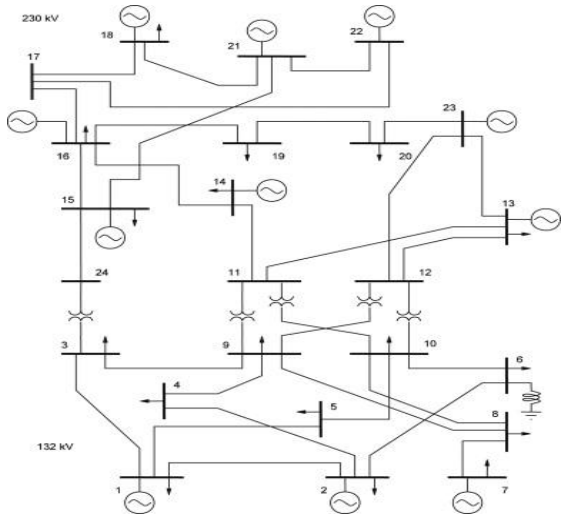

Fig.1. IEEE 24 bus test system

Table I
Power Market Clearing Results on IEEE 24 Bus Test System

Providers	At Bus	P(pu)	Q(pu)	Spinning (pu)
G1	1	1.45	-0.10	0.47
G2	2	1.66	-0.25	0.28
G3	7	2.42	0.46	0.61
G4	13	5.45	0.15	0.47
G5	15	1.96	1.11	0.22
G6	16	1.10	0.42	0.49
G7	18	3.30	0.27	0.72
G8	21	3.36	0.02	0.67
G9	22	2.30	0.14	0.72
G10	23	5.70	0.43	0.92
Condenser	14	0	0.53	0

Optimal Investment Decisions in a Smart Grid

Chin Yen Tee, *Student Member, IEEE,* Marija Ilic, *Member, IEEE,*
Carnegie Mellon University

***Abstract*—The future electricity grid is envisioned to be one that is characterized by an increased diversity of resources made possible by smart control, sensing, and communication infrastructures. With the proliferation of these new technologies, the traditional investment decision making framework in the electric power industry will need to evolve to account for the competing and complementary nature of these technologies. In order to ensure optimal investment in the future electricity grid, a framework needs to be designed to enable decision makers to compare various technological options and to evaluate the value of smart technologies in the grid. In this poster, a preliminary framework for evaluating optimal investment decisions in the electricity grid is introduced.**

The proposed framework is a welfare maximization framework modeled after the peak-load pricing investment decision making approach introduced by Crew and Kleindorfer [1]. Unlike the least cost planning framework which assumes that demand in inelastic, this modeling framework allows us to account for the flexibility of consumer demand for both electricity and reliability. The modeling framework can be adapted to allow us to compare various technologies in the grid and to determine the optimal investment decision for these technologies. In addition, it can also be adapted to account for the potential value added by IT-enabled coordination and distributed decision-making in the electricity grid.

In this poster, the proposed framework is applied to evaluate the optimal investment decision in transmission expansion/enhancement. An optimization model is developed to determine the optimal decision to build a new line vs. installing FACTS devices in the system. The Karush - Kuhn - Tucker (KKT) conditions of the model is determined to provide insights into the optimal decision making rule and to determine the optimal compensation framework for transmission technologies. The model is then applied on simple test system to demonstrate the potential implications of such models on the system.

This model can be adapted and extended to account for variation in industry structure and also to account for uncertainties in the system.

I. Key Equations

The general framework for making optimal investment decision is in the form of:

$$\begin{aligned} \max \quad & \text{Social Welfare} \\ \text{s.t.} \quad & \text{Operational and Investment Constraints} \end{aligned}$$

For the transmission investment example presented in this poster, the objective function is given as:

$$\min \sum_{y=1}^{Y} \frac{1}{e^{ry}} [\sum_{t=1}^{T} \sum_{n=1}^{Nbus} c_g(P_{n,t,y}) + \sum_{l=1}^{L} (c_l(K_{l,y}) + c_f(x_{f,l,y}))] \tag{1}$$

where c_g represents the nodal cost of electricity and c_l and c_f represents the cost of investment in new transmission line and Thyristor Controlled Series Compensator (TCSC) respectively.

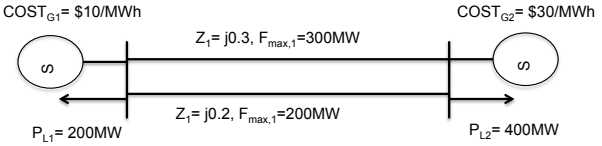

Fig. 1. Simple Two Bus Toy Example

	Flow L_1	**Flow L_2**	**Flow L_{New}**	**System Cost**
Base Case	133.3MW	200MW	-	$7334
New Line	114.3MW	171.4MW	114.2MW	$6326
TCSC in Line 1	200MW	200MW	-	$6257

TABLE I
Results of Simple Example

The DC power flow constraints and line capacity constraints are:

$$-(\mathbf{F_{max}} + \sum_{\mathbf{i=1}}^{\mathbf{y-b_l}} \mathbf{K_i}) \leq \mathbf{F_{line}} = \mathbf{HP} \leq (\mathbf{F_{max}} + \sum_{\mathbf{i=1}}^{\mathbf{y-b_l}} \mathbf{K_i}) \tag{2}$$

The power balance and generation constraints are:

$$\sum_{n=1}^{N_{bus}} P_{n,t,y} = 0 \quad \forall\, t, y \tag{3}$$

$$0 \leq P_{n,t,y} \leq P_{n,max} \quad \forall\, t, y \tag{4}$$

The TCSC investment constraints are:

$$0 \leq \sum_{i=1}^{y} x_{f,l,i} \leq 0.4 x_{base,l} \quad \forall\, l, y \tag{5}$$

$$x_{f,l,y} \geq 0 \quad \forall\, l, y \tag{6}$$

Lastly, the TCSC Operaional Constraints are:

$$o \leq x_{opt,l,t,y} \leq \sum_{i=1}^{y-b_f} x_{f,l,i} \quad \forall\, l, t, y \tag{7}$$

II. Key Results

Preliminary results on a simple 2 bus toy example (Fig. 1) yields the results shown in Table II. The model will be applied to a larger test system to obtain more substantial results for the poster.

References

[1] M. A. Crew and P. R. Kleindorfer, "Peak load pricing with a diverse technology," *The Bell Journal of Economics*, vol. 7, no. 1, pp. pp. 207–231, 1976. [Online]. Available: http://www.jstor.org/stable/3003197

Load and Risk Based Maintenance Management of Wind Turbines

Pramod Bangalore and Lina Bertling Tjernberg
Department of Energy and Environment, Chalmers University of Technology, Gothenburg, 41296, Sweden,
Email: *Pramod.bangalore@.chalmers.se and lina.bertling@chalmers.se*

Abstract— Over the lifetime of a wind turbine, the cost for operation and maintenance sums up to a considerable portion of its life cycle cost. Experience has shown a direct impact of service maintenance intervals on wind turbine availability on the one hand, and a correlation between the operating environment and failure frequency of wind turbines on the other hand. This project aims to predict failures in the wind turbine using the environmental correlations and available SCADA/CMS signals and thereby achieve optimized targeted maintenance. The RCAM approach has been proposed to be used for this and is described in the paper.

I. KEY FIGURES

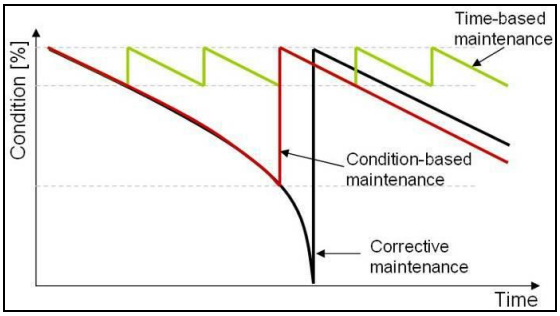

Figure 1. Different maintenance strategies

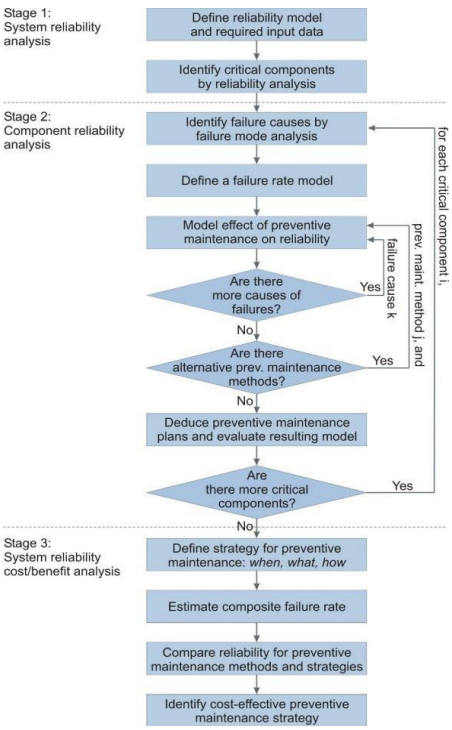

Figure 2. Proposed RCAM methodology

Reference: L. Bertling, R. Allan, R. Eriksson, "A reliability-centered asset maintenance method for assessing the impact of maintenance in power distribution systems", IEEE Transaction on Power Systems, 20(1):75- 82, 2005.

II. KEY RESULTS

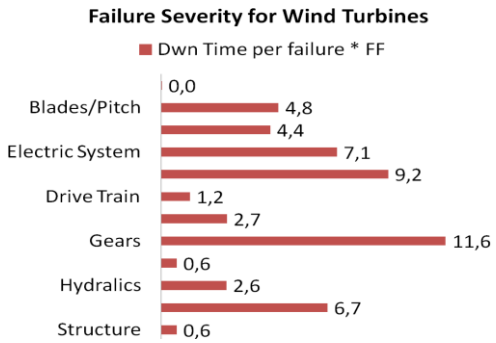

Figure 3 Severity of failures based on failure frequency and associated downtimes per turbine per year. Results from survey in Sweden between 1997-2005.

Reference: J. Ribrant and L.M. Bertling, "Survey of failures in wind power systems with focus on Swedish wind power plants during 1997-2005", IEEE Transaction on Energy Conversion, 2007, 22(1):167-173

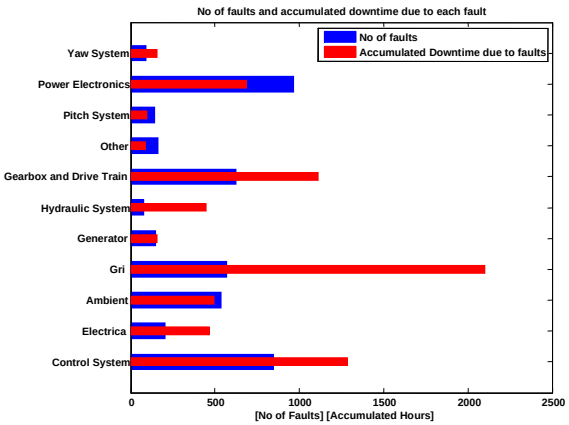

Figure 4. Number of faults and the accumulated downtime due to each category of fault for the wind turbines under consideration.

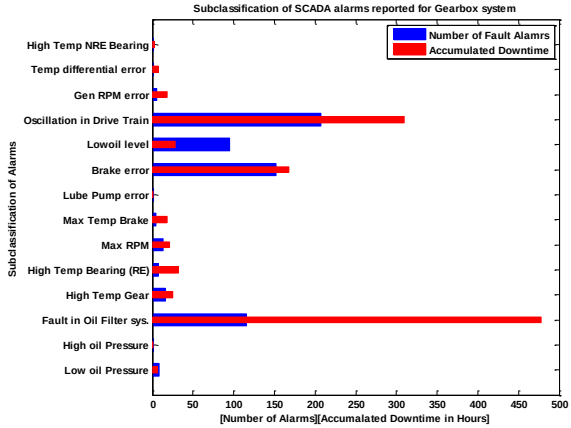

Figure 5. Number of faults and the accumulated downtime for faults in the gearbox system for the selected set of wind turbines.

A Review of ERCOT's Nodal Market

Its First Year of Performance

Sruti Nuthalapati, IEEE Student Member
Undergraduate Freshmen
Department of Electrical and Computer Engineering
University of Texas at Austin
Austin, USA
nsruti@utexas.edu

Mentors:
Dr. Ross Baldick, University of Texas at Austin
Thuy Huynh, Potomac Economics
Austin, USA
Emails: *baldick@ece.utexas.edu*
thuynh@potomaceconomics.com

***Abstract*— The Electric Reliability Council of Texas (ERCOT) is an independent system operator (ISO) for the electricity grid of the majority of Texas. It manages the deregulated market for 85% of the state's electric load, which includes 23 million customers, connects 40,500 miles of transmission lines and more than 550 generation units. An independent system operator is a non-profit entity that does not own generation or transmission assets but manages requests for transmission services, allocation of scarce transmission capacity and network expansions; essentially an ISO operates the power system reliably. It also manages the energy market.**

One of the most important roles of an ISO, as a reliable operator of the power network, is the re-dispatching of generation when congestion occurs in transmission.

ERCOT, as an ISO, previously used a zonal design. In order to efficiently deal with transmission congestion, it divided its region into zones, called congestion management zones. Each zone has different market prices when transmission congestion occurs. In a zonal market, this congestion is defined when it occurs between specific transmission lines between two zones. These specific transmission lines are called commercially significant constraints (CSCs). Thus, the energy market was balanced through price changes (re-dispatching) in each zone when congestion occurred at CSCs across two zones. This, in general terms, allows the price of energy to be on a portfolio (group of generators in the same zone) basis, rather than generator specific at each bus. Also significant to note, is that this energy balancing was done every fifteen minutes. This may result in inefficient prices at some buses. ERCOT operated on this zonal model until December 2010.

Now, ERCOT operates on a nodal market model. The nodal market will deal with more efficiently managing transmission congestion. In the nodal design, there exist four thousand nodes, to replace the congestion management zones (from zonal market). The price is determined to be different at each node (called nodal locational marginal pricing). Through this, the ERCOT nodal market was expected to improve dispatch efficiencies. The dispatch structure is expected to run every five minutes, instead of the zonal fifteen minute settlement.

My poster will present the outcome of my research into nodal's first year of performance.

Scheduling of Plug-in Electric Vehicle Charging and Effects on Day-ahead Market Price

Pavan Balram, Le Anh Tuan, Lina Bertling Tjernberg
Department of Energy and Environment, Chalmers University of Technology, Gothenburg, 41296, Sweden,
Email: *pavan.balram@chalmers.se, tuan.le@chalmers.se, lina.bertling@chalmers.se*

***Abstract*—The introduction of a large number of Plug-in electric vehicles (EV) and their charging from the electricity network would likely pose challenges towards the operation of power systems and influence the outcome of power markets. This paper investigates how the charge scheduling strategies of a fleet of EVs would affect the day-ahead electricity market price, at different levels of EV penetration. EV participation is modeled as flexible demand in the day-ahead market. Two different market modeling approaches are proposed and applied in the two case studies with the IEEE-30 bus test system and the Nordic electricity market [1].**

I. KEY EQUATIONS

1. The objective of the market model is:

$$min \quad J \tag{1}$$

where J is the total system cost.

2. The objective of the Aggregator model is:

$$min \left(\sum_{\forall t \in T} \pi_m^t * E^t \right) \tag{2}$$

where π_m^t is the estimated day-ahead market price for electricity by the Aggregator and E^t is the EV charging energy to be scheduled at time $t \in (1,2,\dots,T)$.

3. Subject to the following EV constraints:
   a. Minimum energy requirement
   b. Charging period limit
   c. Battery state
   d. Battery energy limit

II. KEY FIGURES

The two modeling approaches proposed are:

1. Joint scheduling model
2. Aggregator scheduling model

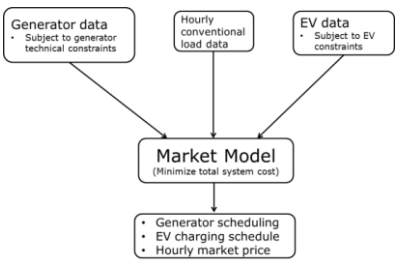

Figure 1. Joint scheduling model flowchart

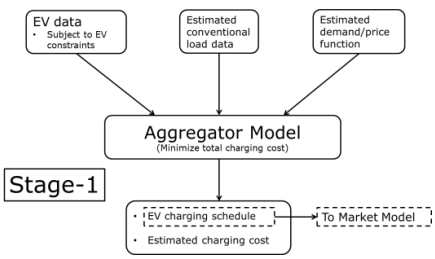

Figure 2. Stage-1 of Aggregator scheduling model

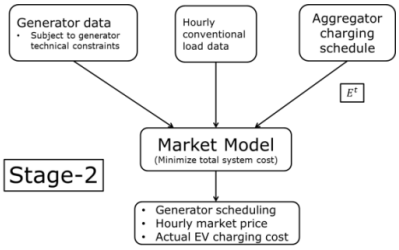

Figure 3. Stage-2 of Aggregator scheduling model

III. KEY RESULTS

Key results for the IEEE-30 bus system are shown in the figures below.

A fixed period charging model is used as a reference case and is compared with the two proposed approaches. From the Fig. 4 and 5 it can be seen that it is necessary to use advanced methods of control for the scheduling of EVs at higher penetration levels. It can also be seen that the Aggregator scheduling model bring about an increase in market price compared to the Joint scheduling model during certain hours. This can be directly related to how accurately the Aggregator estimates the demand/price function.

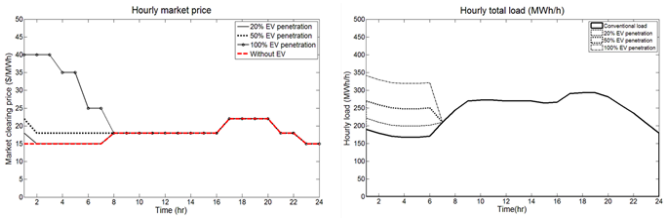

Figure 4. Scheduling at different EV penetration levels- Fixed period charging model.

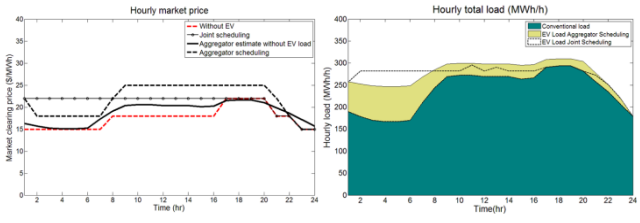

Figure 5. Scheduling at 100% EV penetration- Joint and Aggregator scheduling models.

IV. REFERENCE

[1] P. Balram, L. A. Tuan, L. Bertling Tjernberg, "Effects of Plug-in Electric Vehicle Charge Scheduling on the Day-ahead Electricity Market Price," *Innovative Smart Grid Technologies Europe (ISGT), IEEE PES, Berlin, October 2012*. Submitted for review.

Distribution-class Locational Marginal Pricing Index

Oluwaseyi Akinbode and Kory W. Hedman
School of Electrical, Computer, and Energy Engineering, Arizona State University, Tempe, AZ 85287-5206, USA,
Email: oakinbod@asu.edu and kory.hedman@asu.edu

Abstract*—Increased penetration of intermittent resources at the bulk energy level is a source of concern for power system operators. Intermittent resources in the form of renewable generation have relatively low variable costs and can potentially displace dispatchable and more controllable generators. Dispatchable generation is one of the main traditional control elements in power systems operations. The partial loss of this control element, as a result of operating with high levels of intermittent resources, could negatively impact system reliability. To maintain high system reliability with high levels of variable resources, the operational paradigm of bulk energy systems may have to evolve to include increased load management. Programs such as demand response (DR) are already implemented by some system operators. Likewise, new control technologies, developed as part of the smart grid initiative, are further enabling price responsive demand. This research focuses on developing a new distribution system pricing index to act as a control signal for the price responsive loads and resources that may emerge in substantial quantities in the distribution system. The price signal is termed the Distribution-class Locational Marginal Pricing Index (DLMP). It is analogous to the Locational Marginal Pricing (LMP) concept in the transmission system. The research investigates the potential impact of the use of a DLMP on transmission system operation and the transmission system optimal power flow (OPF). Particularly, the potential impact of a DLMP on economic modeling of loads for transmission system operations and OPF formulation is studied. The DLMP is expected to improve upon distribution system rates structures by coupling prices in the transmission and the distribution to reflect conditions in both systems. Deploying a DLMP in the distribution system will incentivize appropriate consumption by responsive loads and production by generation resources. This paper defines the DLMP and formulates its DCOPF problem. The DCOPF problem for the DLMP is a lossy formulation that enables the DLMP to inherently capture the cost of the impact of marginal consumption on system losses. The formulation is tested on numerical examples and the results are discussed.

I. Key Equations

Equation (1) is the node balance constraint of the DLMP's lossy DCOPF formulation developed in this research. In order to keep the formulation linear, the quadratic-shaped non-linear part of the loss term in (1) is approximated by Equation (2) and the piecewise linear representation in Figure 1. The linearized real power losses are associated with line flows obtained from the DC power-flow equation in (3).

$$\sum_{\forall k(n,;)} P_k - \sum_{\forall k(;,n)} P_k + \sum_{g \in G_n} P_g = D_n + P_{Loss}^n \quad (1)$$

$$\left(\theta_n - \theta_m\right) = \sum_{\forall i} \theta_k^{i+} - \sum_{\forall i} \theta_k^{i-} \quad (2)$$

$$B_k\left(\theta_n - \theta_m\right) - P_k = 0 \quad (3)$$

II. Key Figures

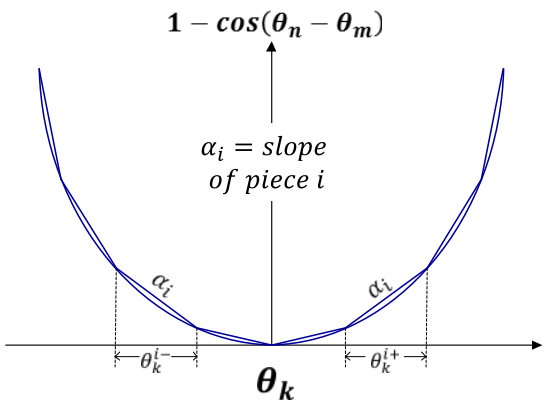

FIGURE 1. PIECEWISE LINEARIZATION OF LOSSES

Figure 2 illustrates the two-part optimization process used to calculate the DLMP. In the first part, the transmission system OPF is solved and transmission system LMPs are calculated. The transmission system LMPs are inputs to the distribution system DCOPF solved in the second part to calculate the DLMP. The DLMP act a control signal for the local resources expected to emerge in the distribution system.

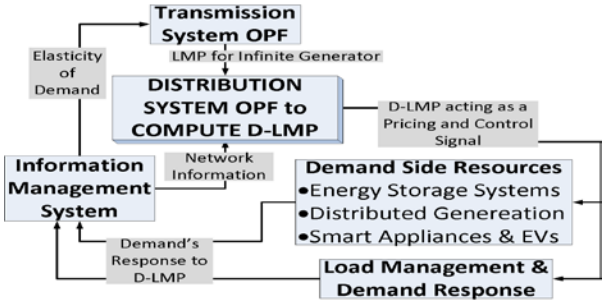

FIGURE 2. DLMP CALCULATION AND APPLICATION FRAMEWORK

Zonal Supply Curve Estimation in Transmission-Constrained Electricity Markets

Mostafa Sahraei-Ardakani, Seth Blumsack and Andrew Kleit
John and Willie Leone Family Department of Energy and Mineral Engineering
The Pennsylvania State University

Abstract:

Many important policy initiatives, such as renewable fuels mandates, would directly affect the operation of electric power networks. Evaluating such policies often requires models of how the proposed policy will impact system operations. Predictive modeling of electric transmission systems, particularly in the face of transmission constraints, is difficult unless the analyst possesses a detailed network model. Further, policy analysis must often be performed under time constraints, which may prevent the use of complex engineering models.

Our motivation in this paper is to develop a method for estimating zonal supply curves in transmission-constrained electricity markets that can be implemented quickly by policy analysts with training in statistical methods (but not necessarily engineering) and with publicly-available data. We develop a nonlinear statistical model that uses fuel prices and zonal electric loads to determine piecewise supply curves, each segment of which represents the influence of a particular fuel type on the zonal electricity price. Our problem thus requires the simultaneous estimation of the slope of each supply-curve segment, as well as the thresholds that define the endpoints of each segment.

We illustrate our methodology by estimating zonal supply curves for the seventeen utility zones in the PJM system. The estimated supply curves are robust to several different model specifications. We use then our supply curves to estimate regional impacts of Pennsylvania's legislative requirement that utilities in Pennsylvania to reduce annual and peak electric load. For most utilities in Pennsylvania, successful implementation of this requirement would reduce the influence of natural gas on electricity price formation and increase the influence of coal. We also find evidence of mixed pecuniary effects on utility zones outside of Pennsylvania; the reduction of electricity demand in Pennsylvania reduces electricity prices in most other regions, but increases prices in the Virginia and Washington, D.C. areas.

Using Demand Response to Reduce Price Variations

Ailin Asadinejad Kevin Tomsovic Fran Li
Department of Electrical Engineering and Computer Science
University of Tennessee
Knoxville, Tennessee
aasadine@utk.edu

***Abstract*— Excessive price variation induces stress to the power system. Demand elasticity in today's electricity markets is generally insufficient to avoid price volatility. We investigate the proper market incentives to avoid critical load levels where prices jump significantly. By investigating the primary factors impacting demand responsiveness, an optimal incentive payment is designed. This payment is to be paid to the consumer as an effective capacity payment. The contribution of such incentive payments on price volatility is investigated.**

***Keywords*— critical load levels, demand response, electricity markets, incentive payments, price volatility.**

I. INTRODUCTION

Excessive price variation induces stress on the power system and can lead to inefficient operation. To reduce the price jumps, one can try to avoid the so-called critical load levels (CLL) [1]. Natural elasticity of demand is not sufficient to avoid these price variations. Consequently, an incentive demand response program is proposed. In most recent research, only the effect of one or two different categories of incentives are examined. We investigate a combination of types in appropriate time frames to assist operations.

II. ANALYSIS NATURAL ELASTICITY OF DEMAND

Elasticity is the proportion of demand change to price change. It can also be represented as load participation factor and high and low price in each point. For the following price/load curve, the elasticity at each critical point is calculated. The elasticity is large and does not correspond to normal elasticity of demand that is less than 1% according to NYISO reports.

$$\varepsilon=-(\Delta D/D)/(\Delta\pi/\pi)$$

$$\varepsilon=-D_R/D_F*\pi_L/(\pi_H-\pi_L)$$

Interval 1) ε=-0.42%, Interval 2) ε=-2.22%, Interval 3) ε=-2.00%

III. ANALYSIS OF LOAD AND PRICE DATA IN NORTH REGION OF NYISO

Load and price curve for real time actual data and hourly forecast load data are shown below (1). Correlation factors show that LMPB is mostly related to hourly forecast load data. Correlation factor between price and different factors like time of day, day of month, fuel cost and so on has to be done. This information helps to determine which type of demand response is appropriate in each price range.

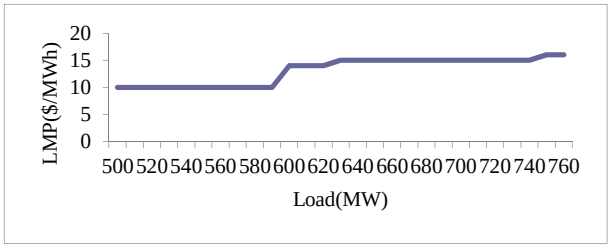

Figure 1: price/load curve for elasticity analysis

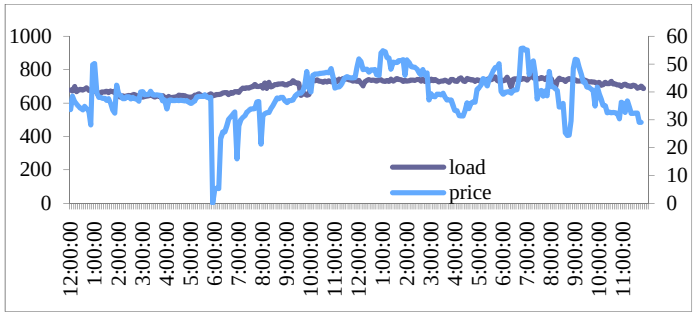

Figure 2: real time price/load curve 10/1/2011 north

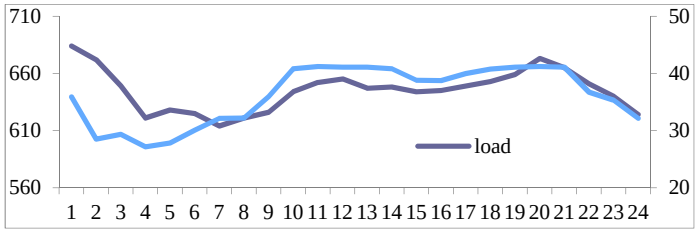

Figure 2: hourly forecast price/load curve 10/1/2011 north

A Novel Power Management Control Strategy for a Renewable Stand-Alone Power System

Abu Mohammad Osman Haruni, Michael Negnevitsky, Md. Enamul Haque, and Ameen Gargoom
School of Engineering, University of Tasmania, Hobart, Tas 7001, Australia.

***Abstract*—This paper proposes an overall power management control strategy of a stand-alone power supply system consisting of wind turbine and battery storage system. The overall control strategy consists of two layer structure. The upper layer is overall power management controller that generates the reference signal for the local controller. Based on reference signal, the local controllers control the wind energy conversion system and energy storage system.**

I. PROPOSED SYSTEM AND CONTROL STRATEGY

The proposed system is shown in Fig. 1.

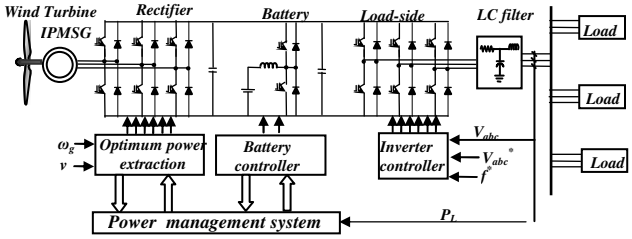

Fig. 1 Structure of proposed hybrid power generation system.

1. *Power Management Controller (PMC)*

The PMC predicts the wind and load profile for a period of time. Based on the prediction and the status of energy reserve, the PMC schedules the maximum load that can be connected to the system. The PMC also determines the operating condition of each sub-system.

2. *Individual System Control:*

Based on the signal from PMC, the individual system is controlled by local controller. The local wind turbine, battery controller and inverter controller is shown in Fig. 2 and Fig. 3. The aim of the wind turbine controller is to obtain the maximum power from the wind, while the battery controller regulates the dc-link voltage.

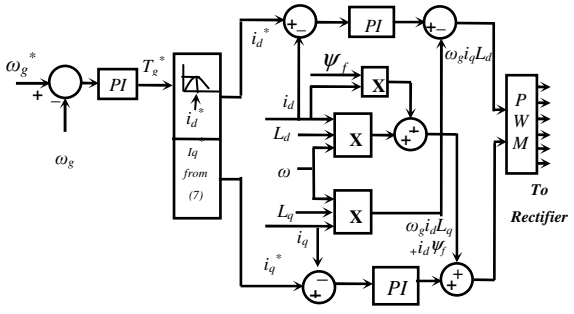

Fig. 2. Machine side converter controller.

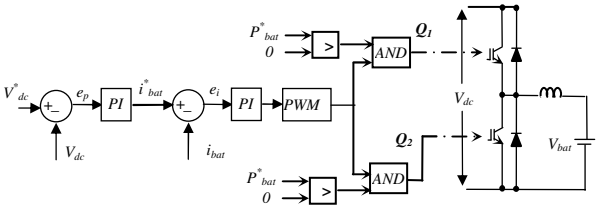

Fig. 3. The battery charger/discharger controller.

II. SIMULATION SYSTEM OPERATION AND PERFORMANCE

A simulation study is shown to verify the performance of the PMC as shown in Fig. 4-6.

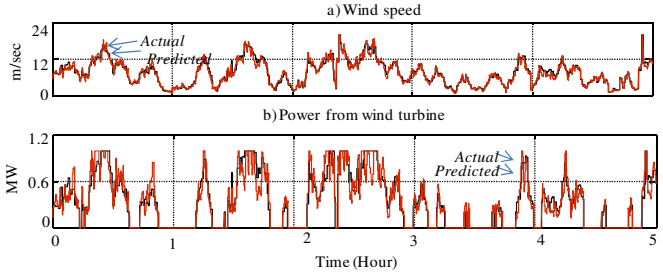

Fig. 4. Wind condition.

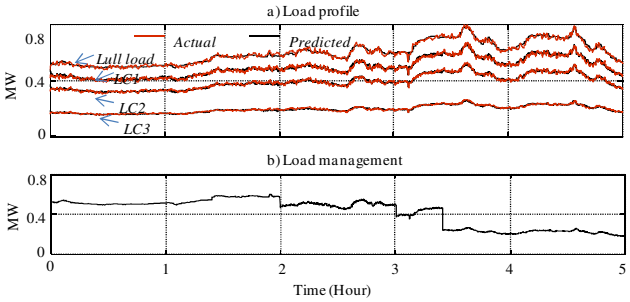

Fig. 5. Load condition.

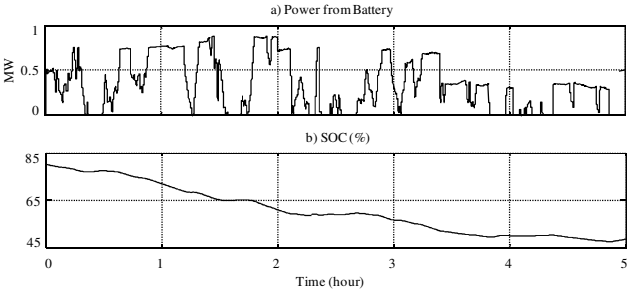

Fig. 6. Battery power and SOC.

III. CONCLUSION

The results of proposed PMC are presented. The PMC ensures a continuous operation of hybrid renewable energy based power system by proper energy and load management.

Controllers Parameter Variation Effects on a Multi-Converter based Microgrid

Juan C. Jimenez and Chika O. Nwankpa
Center for Electric Power Engineering, Department of Electrical and Computer Engineering, Drexel University
Philadelphia, PA 19104, USA,
Email: jcj26@drexel.edu and con22@drexel.edu

***Abstract*—A large variety of dynamic and static interactions are possible in a system with multi-converters and electromechanical equipment. It is known that converter controllers, proprietary in nature, are designed to be local without consideration of underlying coupling dependencies with other segments of the system. One of the issues raised are inherent cross-regulation behavior – when converter outputs, each regulated via feedback control affect each other's outputs through their common bus. Harmful operational situations may arise leading to cascading of controller limit violations with the overall goal and quality of maintaining load supply being seriously affected. This work will present a developed system model of a buck-boost converter based microgrid where of interest are the converters' dynamics and analyze the system wide effects of independently operated converter's controller parameter changes through simulation.**

I. KEY EQUATIONS

The general model used to investigate power system dynamics is that of the Differential Algebraic Equations (DAE) type:

$$\begin{aligned} \dot{x} &= f(x,u,N) \\ 0 &= g(x,u,N) \end{aligned} \tag{1}$$

In general the DAE model of the system, when converters' dynamics are of interest, is given by (2)

$$\left.\begin{aligned} v_i^{'} &= f_i\left(v_i,i_i\right) \\ i_i^{'} &= f_i\left(v_i,i_i\right) \end{aligned}\right\} \text{load converters}$$

$$v_1^{'} = f_1\left(i_i,i_j\right)\Big\} \text{DC bus} \tag{2}$$

$$i_j^{'} = f_j\left(v_j,i_j\right)\Big\} \text{source converters}$$

$$\left.\begin{aligned} P_i &= f_i\left(\omega_i,v_i,i_i\right) \\ P_j &= f_j\left(\omega_j,v_j,i_j\right) \end{aligned}\right\} \text{Power at load and generator buses}$$

Independently operated converter controllers duty ratio is described by (3),

$$d(t) = V_{ref} - k_1 i_L - k_2 v_C \tag{3}$$

II. KEY FIGURES

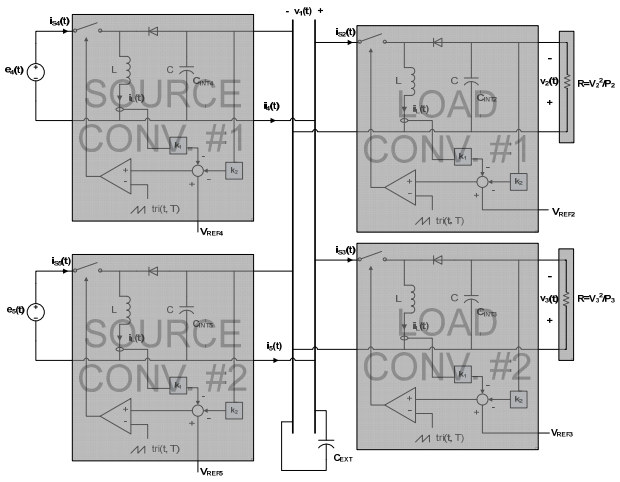

Figure 1. Buck-boost multi-converter based microgrid

III. KEY RESULTS

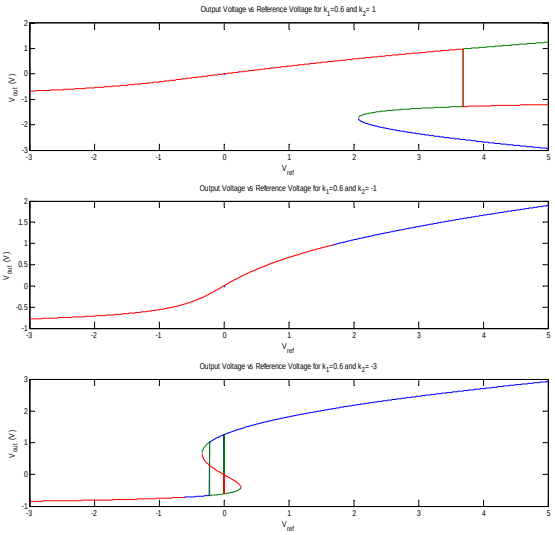

Figure 2. Output voltage vs reference voltage for a single converter

Application of Stochastic Differential Equations to Feasibility Studies of Converter Systems in the Presence of Communication Network Delay

Sachi Jayasuriya and Chika O. Nwankpa
Electrical and Computer Engineering Department, Drexel University, Philadelphia, PA
Email: *sj336@drexel.edu, chika@coe.drexel.edu*

***Abstract*—This work presents the probabilistic analysis of the behavior of remotely monitored system states of a DC-DC buck-boost converter system in the presence of communication network delay. The system is modeled using stochastic differential equations (SDEs) and simulated to identify conditions under which the system model becomes infeasible. This work is motivated by the need to develop a metric that accounts for the inherent transport time delay in communication networks and is descriptive of the amount of leeway the network control system has in order to take corrective measures in the event of a fault.**

I. Key Equations

Conventional averaged model of the buck-boost converter:

$$\left.\begin{aligned}\frac{di}{dt} &= \frac{1}{L}\left[-v + V_{ref}v - k_1 iv - k_2 v^2 + V_{ref}E - k_1 iE - k_2 vE\right] \\ \frac{dv}{dt} &= \frac{1}{C}\left[i - V_{ref}i + k_1 i^2 + k_2 iv - \frac{v}{R}\right]\end{aligned}\right\} \quad (1)$$

Exponential white noise network model:

$$\left.\begin{aligned}\frac{di_m}{dt} &= s\left(i - i_m\right) + \sqrt{2LC\varepsilon}\left(i - i_m\right)\dot{w}_i \\ \frac{dv_m}{dt} &= s\left(v - v_m\right) + \sqrt{2LC\varepsilon}\left(v - v_m\right)\dot{w}_v\end{aligned}\right\} \quad (2)$$

II. Key Figures

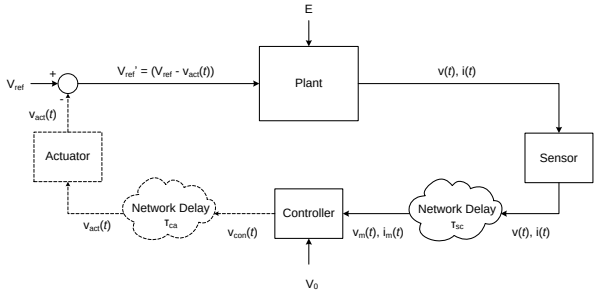

Figure 1. Network controlled DC-DC buck-boost converter system in the presence of communication network delay

III. Key Results

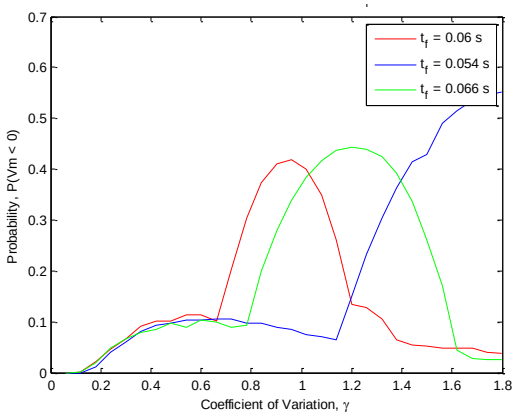

Figure 2. Probability that the measured voltage is infeasible at times (t_f) 0.06, 0.054 and 0.066 s as a function of the coefficient of variation γ for a given delay r of 0.06 s

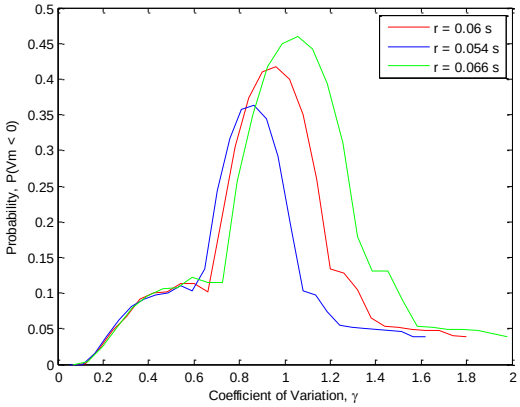

Figure 3. Probability that the measured voltage is infeasible at time t_f = 0.06 s as a function of the coefficient of variation γ for delays (r) of 0.06, 0.054 and 0.066 s

Predictive Control of a Modular Multilevel Converter for a Back-to-Back HVDC System

Jiangchao Qin
School of Electrical and Computer Engineering
Purdue University,
West Lafayette, IN, USA
qinj@purdue.edu

Maryam Saeedifard
School of Electrical and Computer Engineering
Purdue University
West Lafayette, IN, USA
maryam@purdue.edu

I. ABSTRACT

The voltage-sourced converter (VSC)-based high-voltage direct current (HVDC) transmission technology has been widely accepted for either back-to-back or point-to-point bulk power transmission. Various classes of high power converter topologies including the conventional two level converter with series-connected semiconductor devices, multilevel converters, multi-module converters, and the recently introduced modular multilevel converter (MMC) have been proposed and investigated for VSC-HVDC applications. Among all of the converter topologies, the MMC is the most promising topology due to its inherent salient features, i.e., its modularity and scalability.

One of the main technical challenges associated with the control of an MMC is to simultaneously keep the sub-module capacitor voltages balanced and eliminate/minimize the circulating currents flowing through the three phases of the converter. Similar to multilevel converter topologies, proper operation of an MMC necessitates an active voltage balancing technique to maintain the sub-module capacitor at their nominal values. The circulating currents, if not properly eliminated /minimized, increase the amplitude of the capacitor voltages ripples, rating values of the converter components, and converter losses. The capacitor voltage balancing of an MMC has been extensively investigated and reported in the technical literature, and correspondingly, various remedial measures, mainly based on multi-carrier PWM techniques, have been proposed/implemented. However, elimination of the circulating currents has not been comprehensively investigated. The existing methods to eliminate the circulating currents are not straightforward and, practically, add to the system cost and complexity, particularly at high voltage/power levels.

This poster proposes a simple model predictive control (MPC) strategy for back-to-back MMC units which are used as an HVDC converter station. The MPC strategy is a promising control strategy to control power electronic converter systems due to its fast dynamic response, flexibility to include constrains and nonlinearities of the system, and ease in digital implementation. The poster takes the advantages of the features of MPC strategy and develops a discrete-time predictive model of an MMC-based HVDC system. The discrete model is used to minimize a defined cost function associated with the internal control objectives of an MMC, i.e., capacitor voltages balancing and circulating currents elimination/minimization, and external control objective, i.e., ac-side currents control. Based on the developed model, an MPC strategy is proposed which enables:

• capacitor voltage balancing of the MMC units through the use of redundant switching states,

• elimination/minimization of the circulating currents,

• overall HVDC converter station control, i.e., regulated power flow control,

• easy and straightforward implementation procedure.

The effectiveness of the proposed MPC strategy in terms of capacitor voltage balancing, circulating current control, and power flow regulation, for a five-level MMC-based back-to-back HVDC converter station is presented. The studies are carried out based on time domain simulations in the PSCAD/EMTDC environment under various study cases which include circulating current control, real power flow reversal, frequency conversion, and single-phase-to-ground fault.

The study results highlight satisfactory performance of the proposed control strategy in terms of capability to carry out the voltage balancing task, elimination of circulating currents, and regulation of power flow for a back-to-back MMC-HVDC system, under various operating conditions. The proposed MPC strategy, developments and conclusions of the paper are equally valid for the point-to-point MMC-HVDC systems The results and conclusions of this poster, presented for an MMC-based back-to-back HVDC system, are equally valid for an MMC-based point-to-point HVDC system.

Real-Time Parameter Identification of DFIG Using Online Measurement

Shaotong GUO and Anjan BOSE
Department of Electrical Engineering and Computer Science, Washington State University, Pullman, WA 99163, USA,
Email: sguo@eecs.wsu.edu and bose@wsu.edu

***Abstract*— Doubly-feed Induction Generators (DFIG) are increasingly used in wind farms and better operational tools are needed to control this renewable generation. This project mainly focuses on identifying both the types of wind turbines and the number of each type in operation, by using online measurement data from PMUs. The poster would present results using Model Reference Adaptive Control (MRAC) algorithm, Extended Kalman Filter (EKF) algorithm, and Random Search algorithm for parameter identification process. Models were built to provide source data for the algorithms in Simulink as well as DigSILENT. Several cases were tested on different scenarios such as wind speed changes and number of DFIGs in ON status changes during simulation. Further work would focus on the algorithm comparison and also simulate on power systems with more buses and DFIGs.**

I. KEY EQUATIONS

The 5th order DFIG model used for parameter Identification is:

$$\dot{x}(t) = A(t)*f(x(t)) + B(t)*u(t)$$

where

$$u(t)=\begin{bmatrix} u_{ds}(t) \\ u_{qs}(t) \\ u_{dr}(t) \\ u_{qr}(t) \end{bmatrix} \quad x(t)=\begin{bmatrix} I_{ds}(t) \\ I_{qs}(t) \\ I_{dr}(t) \\ I_{qr}(t) \\ pw_r(t) \end{bmatrix} \quad f(x(t))=\begin{bmatrix} I_{ds}(t) \\ I_{qs}(t) \\ I_{dr}(t) \\ I_{qr}(t) \\ pw_r(t) \\ I_{ds}(t)I_{qr}(t) \\ I_{ds}(t)pw_r(t) \\ I_{qs}(t)I_{dr}(t) \\ I_{qs}(t)pw_r(t) \\ I_{dr}(t)pw_r(t) \\ I_{qr}(t)pw_r(t) \end{bmatrix}$$

$$A(t)=\begin{bmatrix} A_{1,1} & 0 & A_{1,3} & 0 & 0 & 0 & 0 & 0 & A_{1,9} & 0 & A_{1,11} \\ 0 & A_{2,2} & 0 & A_{2,4} & 0 & 0 & A_{2,7} & 0 & 0 & A_{2,10} & 0 \\ A_{3,1} & 0 & A_{3,3} & 0 & 0 & 0 & 0 & 0 & A_{3,9} & 0 & A_{3,11} \\ 0 & A_{4,2} & 0 & A_{4,4} & 0 & 0 & A_{4,7} & 0 & 0 & A_{4,10} & 0 \\ 1 & 1 & 1 & 1 & 1 & 1 & 1 & 1 & 1 & 1 & 1 \end{bmatrix}$$

$$A_{1,1}=\frac{-Rs}{M*Ls}=A_{2,2} \qquad A_{1,3}=\frac{Lh*Rr}{M*Ls*Lr}=A_{2,4}$$

$$A_{1,9}=\frac{Lh^2}{M*Lr*Ls}=-A_{2,7} \qquad A_{1,11}=\frac{Lh}{M*Ls}=-A_{2,10} \qquad A_{3,1}=\frac{-Rr}{M*Lr}=A_{4,2}$$

$$B(t)=\begin{bmatrix} B_{1,1} & 0 & B_{1,3} & 0 \\ 0 & B_{2,2} & 0 & B_{2,4} \\ B_{3,1} & 0 & B_{3,3} & 0 \\ 0 & B_{4,2} & 0 & B_{4,4} \\ 1 & 1 & 1 & 1 \end{bmatrix}$$

$$B_{1,1}=\frac{1}{M*Ls}=B_{2,2}$$

$$B_{1,3}=\frac{-Lh}{M*Ls*Lr}=B_{2,4}=B_{3,1}=B_{4,2}$$

$$B_{3,3}=\frac{1}{M*Lr}=B_{4,4}$$

II. KEY FIGURES

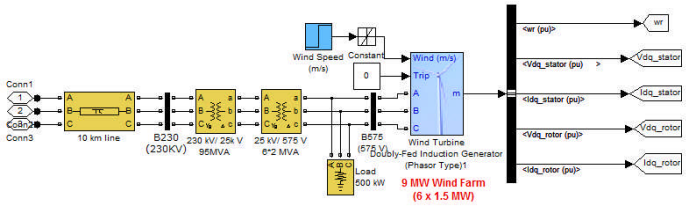

Figure 1. DFIG subsystem which is in-cooperate into Kundur's 2area system

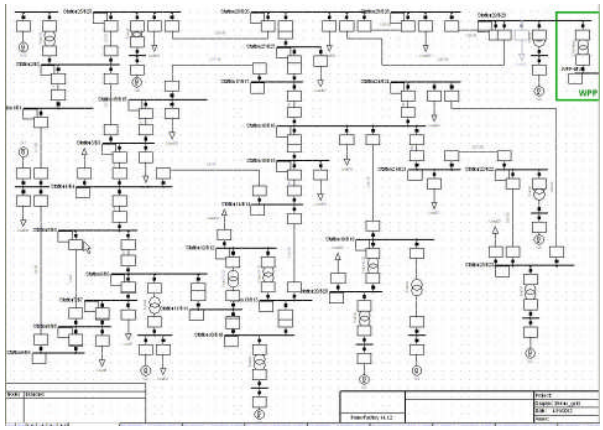

Figure 2. 168DFIG connected into IEEE-39Bus System in DigSILENT

III. KEY RESULTS

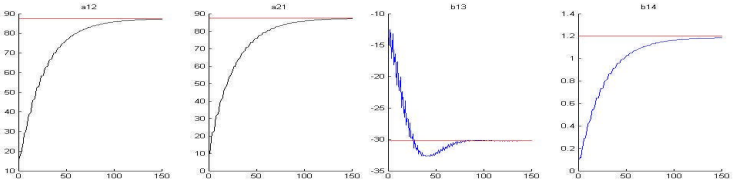

Figure 3. Estimate A12, A21,B13,B14 using Model Reference Adaptive Control (MARC) Method

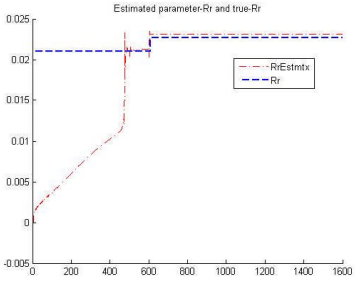

Figure 4. Estimate Rr by Extended Kalman Filter method (3rd order model) while Wr constant, working condition of DFIG changes

Stochastic Optimization of a Microgrid with Solar Power Generation

Robin Broder Hytowitz and Kory Hedman
School of Electrical, Computer and Energy Engineering, Arizona State University, Tempe, AZ 85281, USA
Email: robin.hytowitz@asu.edu and kory.hedman@asu.edu

***Abstract*— As renewable energy becomes more prevalent in both transmission and distribution systems, it is vital to understand the uncertainty and variability that accompany these resources. Microgrids have the potential to mitigate the effects of generation uncertainty caused by renewable energy resources. With the ability to exist in either an islanded mode or maintain connections with the main grid, a microgrid can increase reliability, defer T&D infrastructure and effectively utilize demand response. Microgrids can further control system operations and increase value to consumers when used in conjunction with transmission switching. Transmission switching would allow the microgrid to open one or many intertie lines connecting the microgrid to the main grid. Such transmission switching can be used to reduce loop flow, which may cause unnecessary congestion or losses within the microgrid. This study presents a co-optimization framework for a microgrid with solar photovoltaic (PV) generation, emergency generation, and transmission switching. Today unit commitment models ensure reliability with deterministic criteria, which are either insufficient to ensure reliability or can degrade economic efficiency for a microgrid that uses a large penetration of variable renewable resources. A stochastic mixed integer linear program for a day-ahead unit commitment model is proposed to account for uncertainty inherent in PV generation. The model incorporates the ability to trade energy and ancillary services with the main grid, including the designation of firm and non-firm imports, which captures the ability to allow for reserve sharing between the two systems. Emergency generators are included as part of the microgrid in order to ensure reliability. Model results demonstrate the ability for the microgrid to adapt to varying solar generation scenarios. Future studies will also consider the impacts of energy storage and electric vehicles on the microgrid.**

I. Key Figure

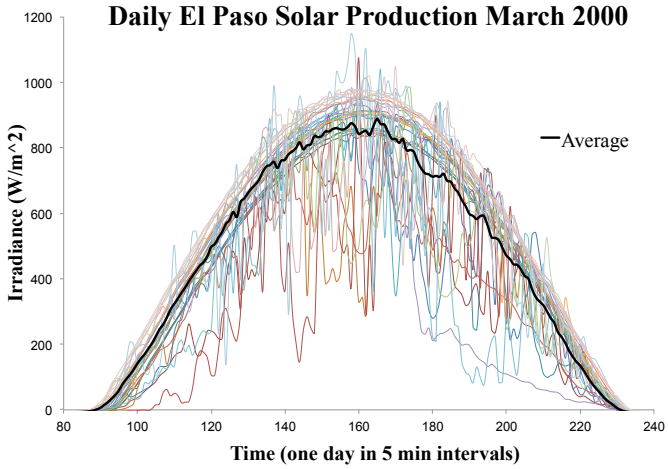

Figure 1 Solar production over the course of one day at 5-minute intervals. Each series represents a single day in March 2000 for El Paso, TX.

II. Key Equation

The model used is a day-ahead unit commitment model, whose objective is minimization of total operation cost:

$$\min \sum_{t\in Time}\sum_{c\in Scen}\rho_c\Bigg(\sum_{g\in Gen}\left(c_g P_{g,t,c}+c_g^{SU}SU_{g,t,c}+c_g^{NL}u_{g,t,c}\right)+\left(c_t^{-F}PI_{t,c}^{-F}+c_t^{-NF}PI_{t,c}^{-NF}\right)-\left(c_t^{+F}PI_{t,c}^{+F}+c_t^{+NF}PI_{t,c}^{+NF}\right)\Bigg)$$

where

ρ_c	Probability of scenario c
c_g	Cost of generator g
c_g^{SU}	Start up cost of generator g
c_g^{NL}	No load cost of generator g
c_t^{+F}	Cost to sell firm imports to the main grid in period t
c_t^{-F}	Cost to purchase firm imports from the main grid in period t
c_t^{+NF}	Cost to sell non-firm imports to the main grid in period t
c_t^{-NF}	Cost to purchase non-firm imports from the main grid in period t
$P_{g,t,c}$	Power output from generator g in period t for scenario c
$PI_{t,c}^{+F}$	Net firm power sold to the main grid in period t for scenario c
$PI_{t,c}^{-F}$	Net firm power purchased from the main grid in period t for scenario c
$PI_{t,c}^{+NF}$	Net non-firm power sold to the main grid in period t for scenario c
$PI_{t,c}^{-NF}$	Net non-firm power purchased from the main grid in period t for scenario c
$SU_{g,t,c}$	Startup commitment of generator g in period t for scenario c
$u_{g,t,c}$	Online commitment of generator g (binary) in period t for scenario c

Interval Arithmetic for Short-Circuit Computation in MV Radial Networks with Distributed Generation

W. C. Briceño Vicente, R. Caire, N. Hadjsaid,
Grenoble Electrical Engineering laboratory, ENSE3 bat D, 38402 St Martin d'Hères Cedex, FRANCE
Email: wendy.briceno-vicente@g2elab.grenoble-inpg.fr

Abstract-- The short-circuit computations determine fault currents and voltages. The interconnection of Distributed Generation (DG) increases the short-circuit currents. At the same time, the increment of renewable energy sources and other forms of DG, introduces uncertainties to the network. This issue has motivated the development of methodologies to evaluate the effects of DG on distribution networks. The fuzzy sets theory is implemented to evaluate the impact of uncertainties on fault levels considering the IEC Standard 60909. The solution is compared to Monte-Carlo Simulation (MCS) the most usual simulation used to solve stochastic problems.

***Index Terms*—Short-circuit currents, Fault currents, Distributed power generation, Monte-Carlo simulation, Interval arithmetic, Wind power generation.**

I. Possibilistic Background

A fuzzy set $\tilde{A} \in \tilde{A}(\Re): [0,1]$ is a superset of Boolean logic sets $\{0,1\}$ and handles the concept of partial truth. It models the uncertainty of natural language where human estimation is influential. $\tilde{A}$ is normal and convex; there is a close interval for any α-cut of the membership function $\{x/\mu_{\tilde{A}}(x) \geq \alpha\}$ called interval of confidence. A trapezoidal $A = [a_1, a_2, a_3, a_4]$ fuzzy number (FN) can be represented in terms of its α-cuts as $A_\alpha = [a_1 + \alpha(a_2 - a_1), a_4 - \alpha(a_4 - a_3)] \quad \forall \alpha \in [0,1]$. The interval arithmetic (IA) extends the basic arithmetic to the α-cuts intervals $a = [\underline{a}, \bar{a}] = \{a \in \Re / \underline{a} \leq a \leq \bar{a}\}$ pointed out here:

$$[\underline{a}, \bar{a}] + [\underline{b}, \bar{b}] = [\underline{a} + \underline{b}, \bar{a} + \bar{b}] \quad (1)$$

$$[\underline{a}, \bar{a}] - [\underline{b}, \bar{b}] = [\underline{a} - \bar{b}, \bar{a} - \underline{b}] \quad (2)$$

$$[\underline{a}, \bar{a}] \times [\underline{b}, \bar{b}] = [\underline{a} \times \underline{b}, \bar{a} \times \bar{b}] \quad (3)$$

$$[\underline{a}, \bar{a}] \div [\underline{b}, \bar{b}] = [\underline{a}, \bar{a}] \times [1/\bar{b}, 1/\underline{b}] \text{ if } 0 \notin [\underline{b}, \bar{b}] \quad (4)$$

A probability density function (PDF) can be transformed into a possibility distribution function (PODF) by Possibility-Probability Consistency Principle (PPCP) with a specified consistent degree between both of them.

II. Case Study and Results

The case study is a distribution network with four types of DG. Three-phase fault current is calculated by IEC 60909 methodology. Network impedances ($\underline{Z}$) and pre-fault sources ($\underline{V}$, $\underline{I}$) uncertainties were of 5% and modeled by a normal PDF and trapezoidal PODF. It was considered PPCP, to establish a comparison between the MCS and FN arithmetic

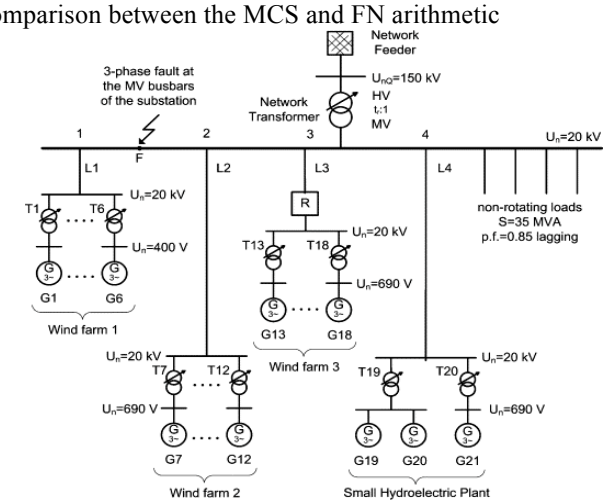

Fig. 1. Study case MV distribution network.

The deterministic short circuit power at the MV bus bar 2 was of 300 MVA. MCS was tested over 1200 samplings, with an error margin of 0.0475 and a confidence level of 99%. MCS results were compared with those results obtained by IA.

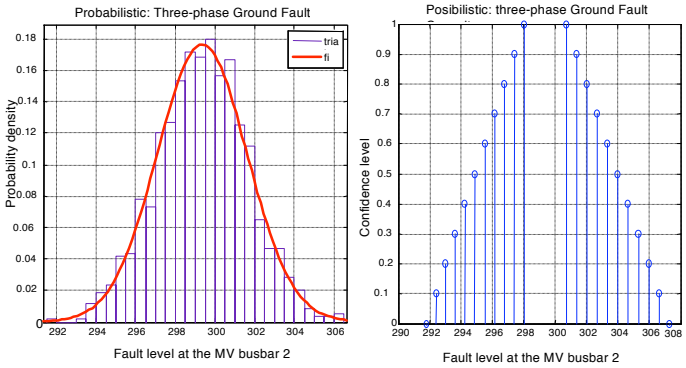

Fig. 2. Probabilistic and possibilistic three-phase ground fault current.

III. Conclusions

IA offers a better and simple alternative from MCS, which requires a large number of trials. IA is useful whenever it is necessary to solve problems of arithmetical operations with uncertainties. IA has been used in the past in load flow and reliability studies. PPCP transforms a probability into a possibilistic representation.

Online Risk-based Security-Constrained OPF in Power System and Market Operation

Qin Wang and James D. McCalley
Department of Electrical and Computer Engineering, Iowa State University, Ames, IA 50010, USA,
Email: wangqin@iastate.edu and jdm@iastate.edu

***Abstract*— The work presented here was motivated by a perceived increase in the frequency at which the power system operators are encountering higher stressing operation conditions, especially with the increasing uncertainties in power system due to the integration of renewable resources and price responsive demand. To deal with the emerging challenges, we propose a novel risk-based security-constrained optimal power flow (RB-SCOPF) for the online operation of power system. The RB-SCOPF can be operated under both preventive and corrective modes. Computational strategies have been developed to solve large-scale RB-SCOPF problems. Test results based on ISO New England system illustrate the effectiveness of the proposed method, and demonstrate the benefits of RB-SCOPF over traditional SCOPF.**

I. KEY EQUATIONS

The compact forms of preventive and corrective RB-SCOPF models are shown in (1) and (2), respectively:

$$\begin{aligned} &\text{Min}\left\{ f(\underline{P}_0)\right\} \\ &\textit{Subject to}: \\ &\underline{h}(\underline{P}_0)=\underline{0} \\ &\underline{g}_{\min} \le \underline{g}(\underline{P}_0) \le \underline{g}_{\max} \\ &K_C\,\underline{g}'_{\min} \le \underline{g}_k(\underline{P}_0) \le K_C\,\underline{g}'_{\max}, k=1,...,NC \\ &0 \le Risk(\underline{g}_1(\underline{P}_0),...\underline{g}_{NC}(\underline{P}_0)) \le K_R Risk_{\max} \end{aligned} \quad (1)$$

$$\begin{aligned} &\text{Min}\left\{ f(\underline{P}_0)\right\} \\ &\textit{Subject to}: \\ &\underline{h}(\underline{P}_k)=\underline{0}, k=1,...,NC \\ &\underline{g}_{\min} \le \underline{g}(\underline{P}_k) \le \underline{g}_{\max}, k=1,...,NC \\ &K_C\,\underline{g}'_{\min} \le \underline{g}_k(\underline{P}_k) \le K_C\,\underline{g}'_{\max}, k=1,...,NC \\ &\left|\underline{P}_0-\underline{P}_k\right| \le \Delta\underline{P}, k=1,...,NC \\ &0 \le Risk(\underline{g}_1(\underline{P}_0),...\underline{g}_{NC}(\underline{P}_0)) \le K_R Risk_{\max} \end{aligned} \quad (2)$$

II. KEY FIGURES

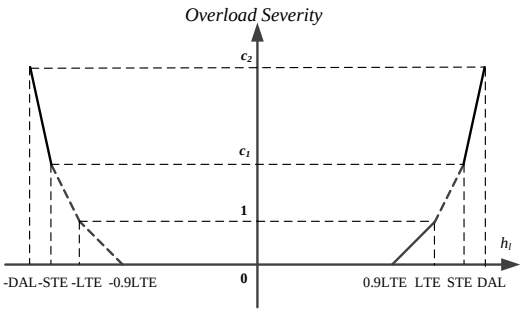

Fig.1. Multi-layer Benders decomposition to solve RBSCOPF

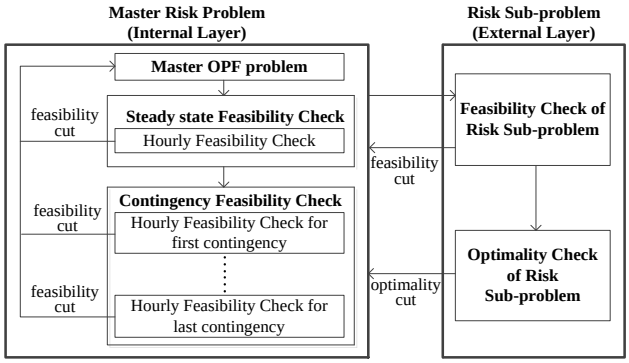

Fig. 2. Decomposition strategy of the preventive RB-SCOPF

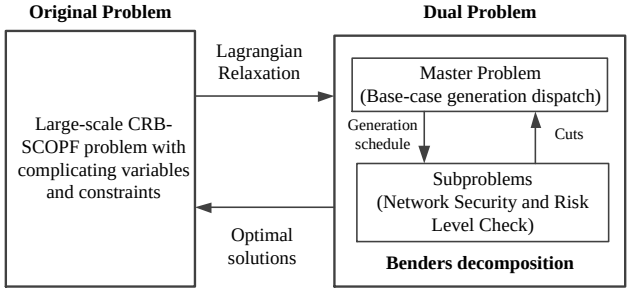

Fig. 3. Decomposition strategy of the corrective RB-SCOPF

III. KEY RESULTS

Table 1
Comparison of Computing Results for ISO-NE System

Options		Iterations to converge	No. of circuit with flow over 90% *limit*	
			normal state	*contig.* states
SCOPF		7	33	8183
RBOPF		43	26	6411
RBSCOPF	HSM	33	28	6819
	ESM	49	22	5388
	EESM	26	23	5678

Table 2
Number of Circuits with Flow Over 90% Limits in Various Cases Based on ISO New England Bulk System

approach		no. of circuits with flow over 90% *limit*	
		normal state	*contingency* states
CSCOPF		30	7201
CRB-SCOPF	HSM	21	5876
	ESM	19	5019
	EESM	18	4963

Table 3. Comparison of various OPF results

Constra.	**SCOPF**		**RBOPF**	**Preventive RB-SCOPF**			**Corrective RB-SCOPF**		
	Preventive	**Corrective**		**HSM** (K_C=1, K_R= 0.5)	**ESM** (K_C =1.05, K_R= 0.5)	**HEM** (K_C =1.20, K_R= 0.5)	**HSM** (K_C=1, K_R= 0.5)	**ESM** (K_C =1.05, K_R= 0.5)	**HEM** (K_C =1.20, K_R= 0.5)
Risk	18.2690	18.24	9.1345	9.1345	9.1345	9.1345	9.12	9.12	9.12
Cost($/hr)	684642.50	616172.1	605407.32	728899.10	610611.54	605542.08	678654.3	608672.2	593676.6

Sensitivity Analysis of Load-Damping Characteristic in Power System Frequency Control

Hao Huang and Fangxing Li
The Department of Electrical Engineering and Computer Science, The University of Tennessee (UT), Knoxville, TN 37996
E-mail: hhuang11@utk.edu, and fli6@utk.edu

***Abstract*-- The smart grid initiative leads to growing interests in demand responses which call the need to investigate the load models, especially the frequency-sensitive loads such as motors. The reason is that a high-penetration controllable load may have substantial impact to system frequency response (SFR). Many recent efforts are focused on the impact of frequency-sensitive load on the system frequency. However, the effect of the frequency-related load-damping coefficient is still not completely understood. This paper presents an analytical model based on the typical SFR model to investigate the effect of frequency-sensitive load on system frequency. Transfer functions are used in theoretic analysis which shows that the inaccurate load-damping coefficient has very trivial impact when the power system is essentially stable. However, it could accelerate system frequency deviation when a power system is unstable after disturbance. The largest dip of frequency drop by a perturbation and the corresponding critical time can be derived by Laplace inverse transformation, respectively. Multiple-machine cases and AGC are also included in the analysis. The simulation results show validity and effectiveness of the proposed analysis. The conclusion can be a useful indication for power system operators for decision-making of load control or interruption.**

I. KEY EQUATIONS

A. *Single Machine (SISO) System - Without AGC:*

$$\frac{\Delta\Omega(s)}{-\Delta P_L(s)} = \frac{(1+\tau_g s)(1+\tau_T s)}{(2Hs+D)(1+\tau_g s)(1+\tau_T s)+1/R} \quad (1)$$

$$\frac{\partial\Delta\Omega(s)}{\partial D} = \Delta P_L(s)\left[\frac{(1+\tau_g s)(1+\tau_T s)}{(2Hs+D)(1+\tau_g s)(1+\tau_T s)+1/R}\right]^2 \quad (2)$$

$$= \left[\frac{\Delta\Omega(s)}{\Delta P_L(s)}\right]^2 \Delta P_L(s)$$

B. *Multiple-Machine System – AGC*

$$\Delta\Omega(s) = -\Delta P_L(s)\frac{1}{(2Hs+D)+\frac{K_I}{s}+\sum_{i=1}^{N}\frac{1}{R_i(1+\tau_{g_i}s)(1+\tau_{T_i}s)}} \quad (3)$$

$$\frac{\partial\Delta\Omega(s)}{\partial D} = \Delta P_L(s)\frac{1}{\left[(2Hs+D)+\frac{K_I}{s}+\sum_{i=1}^{N}\frac{1}{R_i(1+\tau_{g_i}s)(1+\tau_{T_i}s)}\right]^2} \quad (4)$$

$$= \left[\frac{\Delta\Omega(s)}{\Delta P_L(s)}\right]^2 \Delta P_L(s)$$

II. KEY FIGURES AND RESULTS

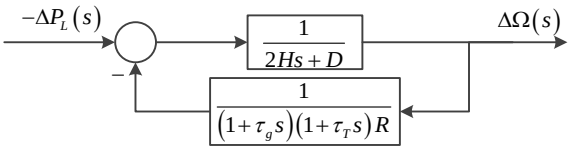

Fig. 1. Load frequency control diagram with input $\Delta P_L(s)$ and output $\Delta\Omega(s)$

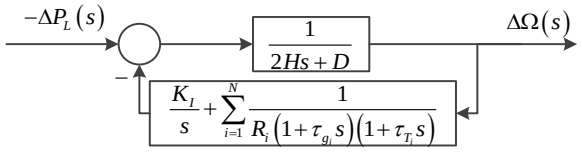

Fig. 2. The equivalent block diagram of AGC for an isolated power system with multiple generation machines case

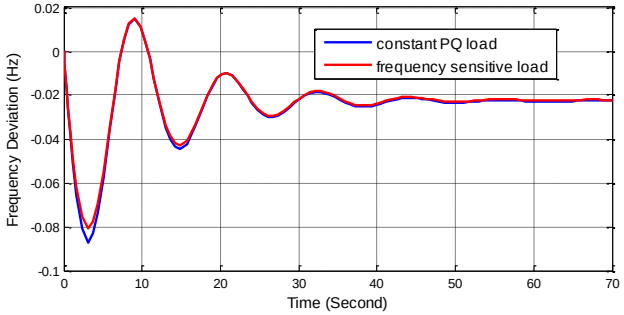

Fig. 3. $\Delta f(t)$ curve when power system stable

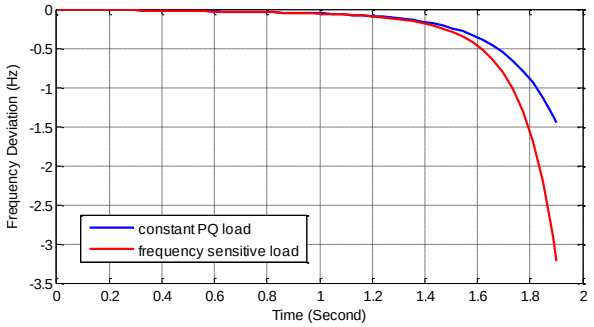

Fig. 4. $\Delta f(t)$ curve when power system unstable

Short Circuit Modeling of Wind Turbine Generators

Sriram Chandrasekar, Rama Gokaraju and Mohindar Sachdev
Department of Electrical and Computer Engineering, University of Saskatchewan, Saskatoon, Canada
Email: *src385@mail.usask.ca, rama.krishna@usask.ca and sachdev@sasktel.net*

***Abstract*— Short circuit faults in a power system can result in severe equipment damage and considerable degradation of the system performance if left undetected. Short circuit analysis and consecutive fault modeling have been used to find typical fault current values for determining switch gear settings, equipment ratings and protection coordination. Short circuit analysis of wind generators has drawn considerable attention due to the significant increase in the amount of wind power integration. As far as Wind Turbine Generators are concerned (especially Type 3), there is a lack of generic fault models that can be used by power operators to calculate and predict fault currents with confidence. This can be attributed to the modeling complexities introduced by the complex controls used for variable speed wind energy generation and the proprietary nature of control algorithms used by different manufacturers.**

Fault studies on Type 1 and Type 2 generators using network solution and EMTP simulations (envelope detection) reveal that they can be adequately represented by a voltage behind transient reactance. However this is not true for Type 3 generators utilizing a doubly fed asynchronous generator (DFAG) with back-to-back PWM converters in the rotor circuit. This paper explores the influence of control complexities on fault current contribution of Type-3 Wind Turbine Generators and how to model them adequately. A generic mathematical model of the system is developed and validated using electromagnetic transient simulations performed in PSCAD on a detailed Type 3 Wind Generator model.

I. KEY FIGURES

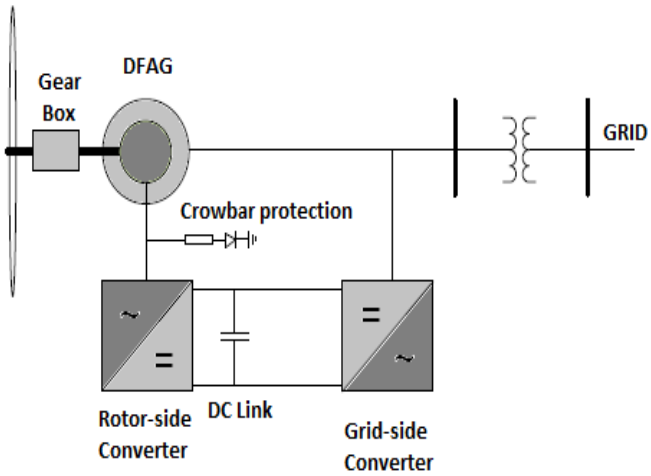

Fig. 1 - Doubly Fed Asynchronous Generator

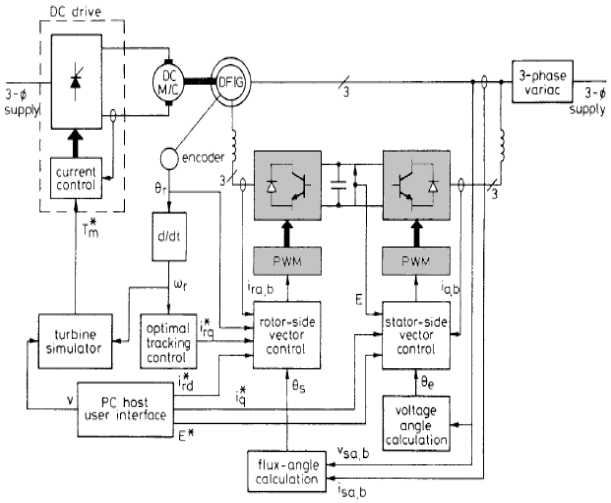

Fig. 2 – Schematic of PWM control of a Doubly Fed Asynchronous Generator

II. KEY RESULTS

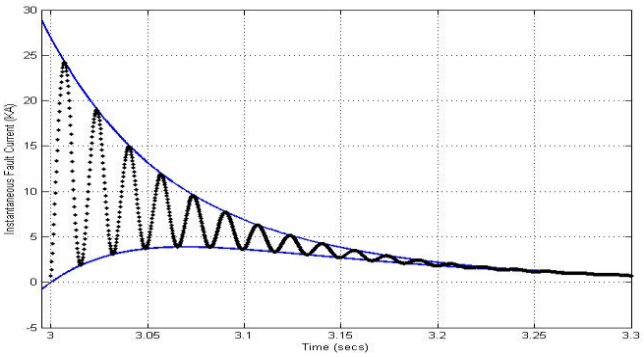

Fig. 3 - Fault Current Envelope Detection for a 3-ph fault at the terminals of a Type-1 WTG

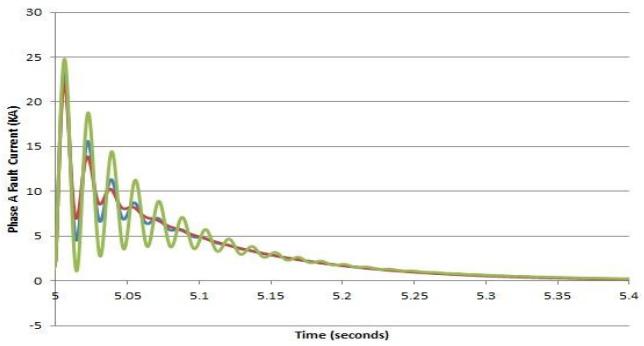

Fig. 4 – Phase-A fault currents for a Type 2 WTG (3-ph Fault) for different values of rotor external resistance

Transient Stability Studies on Large Power Systems

P. Sharma, *Student Member, IEEE,* G. Ramakrishna, *Member, IEEE*
Department of Electrical and Computer Engineering, University of Saskatchewan, SK, Canada
Email: pas609@mail.usask.ca, rama.krishna@usask.ca

Abstract- The disturbance in power system leads to oscillations of the synchronous machine because of the imbalance in power produced and the power consumed. This power swing, if severe, can lead to the loss of synchronism and in the worst case scenario can eventually lead to system blackout. A severe disturbance can cause greater excursion on the machine rotor angle. In a large power system machines form a coherent group and swing together. In previous works large power system is divided into two coherent areas for transient stability assessment. This work explores the transient stability assessment of the power system when there are three coherent areas. The coherency is determined based on the generator internal voltage angle and the aggregation is performed to represent the areas by equivalent machine. The stability analysis of the equivalent power system is done using State Plane Analysis (SPA) whereby mathematical model governing power swings is represented by a graphical plot. The proposed method is tested in IEEE 39 bus test system using electromagnetic transient simulation tool (PSCAD/EMTDC).

I. KEY EQUATIONS

The classical swing equation for the three-machine system as shown in figure 1 take the form

$$M_1 \frac{d^2\delta_3}{dt^2} = Pm_1 - E_1E_2Y_1 \sin(\delta_1 - \delta_2) - E_1E_3Y_3 \sin(\delta_1 - \delta_3)$$

$$M_2 \frac{d^2\delta_2}{dt^2} = Pm_2 - E_1E_2Y_1 \sin(\delta_2 - \delta_{1)} - E_2E_3Y_2 \sin(\delta_2 - \delta_3)$$

$$M_3 \frac{d^2\delta_3}{dt^2} = Pm_3 - E_1E_3Y_3 \sin(\delta_3 - \delta_{1)} - E_2E_3Y_2 \sin(\delta_3 - \delta_2)$$

II. KEY FIGURES

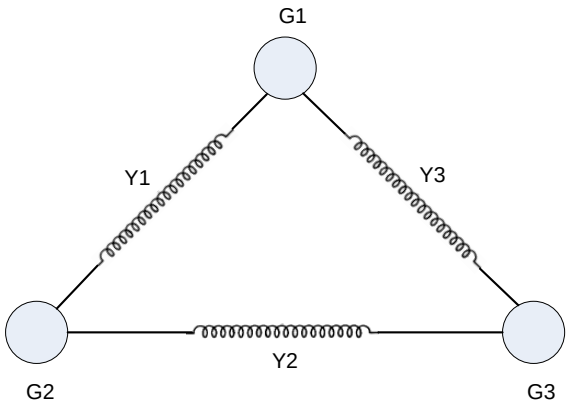

Figure 1. Equivalent three-area system

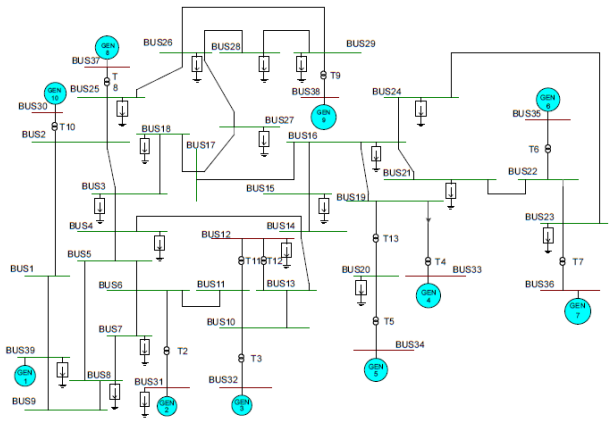

Figure 2. IEEE 39 Bus Test System

Reserve Zone Determination and Analysis

F. Wang, *Student Member, IEEE* and K. W. Hedman, *Member, IEEE*
School of Electrical, Computer, and Energy Engineering, Arizona State University, Tempe, AZ 85287, USA
Email: *fengyu.wang@asu.edu* and *kory.hedman@asu.edu*

***Abstract*— Reserve requirements help ensure system reliability. Typically, attention is given to the quantity of reserve that is required to ensure system reliability in the face of uncertainties and contingencies. However, due to congestion, the location of reserve is also critical to ensure system reliability. Reserve zones help ensure that there are sufficient local reserves where needed. A required amount of spinning reserve level should be satisfied for every period t and every zone k: $\sum_{g\in Z_k} r_g^t \geq SR_k^t$, where r_g^t is the spinning reserve supplied by generator g at period t, and SR_k^t is the spinning reserve requirements during period t for reserve zone k. Proper partition of reserve zones may benefit both market efficiency and system reliability. Today's reserve zones determination methods are mainly based on ad-hoc rules, such as utilities ownership, geographical boundaries, or key transmission lines. Today's reserve determination criteria assume that the location of the reserves within the reserve zone is irrelevant as the mathematical representation of reserves in unit commitment does not account for congestion, so the reserve (locations and quantity) are "blindly" chosen inside the reserve zones. Theoretical and systematic methods are needed to determine reserve zones to improve the deliverability of reserves. Statistical clustering techniques are employed to determine the reserve zones based on the power transfer distribution factor differences (PTDFD) and electrical distances (ED). This work will also examine the importance of reserve zones for systems with variable renewable resources.**

I. Key Equations

Mathematical expression of PTDFDs, weighed PTDFD, and ED.

$$PTDFD_{ij} = \frac{\sum_{k=1}^{N}\left|PTDF_{k,i}^{R} - PTDF_{k,j}^{R}\right|}{N} \quad (1)$$

$$WPTDFD_{ij} = \frac{\sum_{k=1}^{N} w_k\left|PTDF_{k,i}^{R} - PTDF_{k,j}^{R}\right|}{N} \quad (2)$$

$$D_{i,j} = Z_{ii} + Z_{jj} - 2Z_{ij} \quad (3)$$

II. Key Results

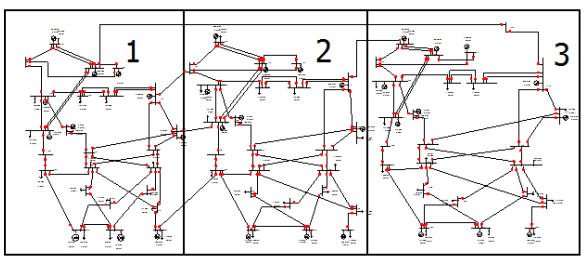

Fig.. 1. K-means zonal clustering results using PTDFDs for the RTS96 system

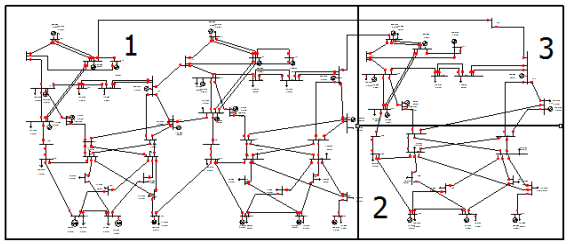

Fig. 2. K-means zonal clustering results using ED for the RTS96 system

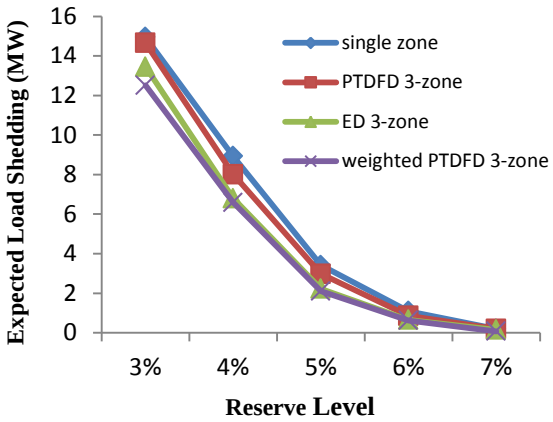

Fig. 3. Expected total load shedding (MW) in the RTS96 system for single reserve zone, PTDFD 3-zone, ED 3-zone, and weighted PTDFD 3-zone results

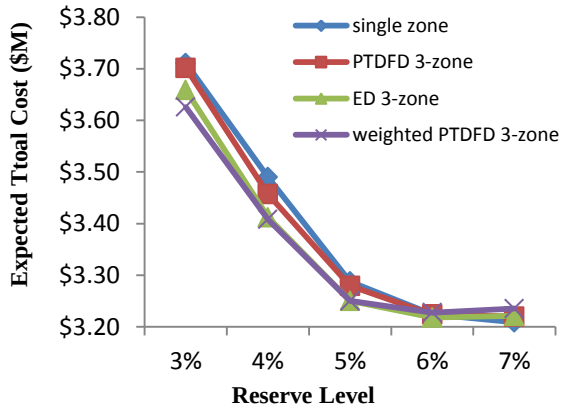

Fig. 4. Expected total cost (Million dollars) for the RTS96 system with single reserve zone, PTDFD 3-zone, ED 3-zone, and weighted PTDFD 3-zone results with the value of lost load at $40,000/MWh

Multi-level state estimation utilizing synchronized phasor measurements

Lin Zhang and Anjan Bose
School of Electrical Engineering and Computer Science
Washington State University
Pullman, WA, USA
lin.zhang@wsu.edu

***Abstract*—with the advent of synchronized phasor measurement, state estimation becomes non-iterative and more efficient. However, so much PMU streaming data flush into one control center; it will be a challenge for communication. In this poster, we propose a multi-level state estimation to mitigate the impact of too much streaming PMU data. This is a continuation of our two-level state estimation. In two-level state estimation, only local state estimation (LSE) and control center state estimation (CCSE) may not be adequate to track down the states of a very large-scale power system. We can divide the whole grid into a couple of sub-sites, which runs the intermediate level regional state estimation (RSE) between LSE and CCSE. RSE use the measurements from outputs of LSE and run its own state estimator (linear or nonlinear). The advantage of doing this is that the measurements have been filtered out first in LSE, so results of RSE should be more accurate. So does CCSE.**

I. KEY IDEAS

It's known that the communication is expensive rather than PMUs. Therefore, from the perspective of communication, if in future with so many PMU data streaming into one control center, it could be a huge challenge for the requirement of QoS e.g. latency, deadline, rate, criticality, geography and quantity. Hence if TSE is already accurate due to the filtering effect of substation level SE, CCSE can be run relatively slower than TSE. And it can also save much communication resources.

So far, in practical there are not enough PMU completely installed at the very large-scale power grid for linear SE. It's known that the PMU are being installed mostly at the highest level voltage buses. So we could run a RSE among those buses with PMUs. The benefit of doing this is that normally more attention is paid on the highest voltage buses. The highest voltage level substations are the most important infrastructures in power grid. The second benefit is that the sampling rate of PMU can let our linear SE running 6 times/second or even faster 30 times/second. And also we can get more accurate outputs of the SE and let us get better real time model of the core of power grid. The third benefit is that with the help of Gridstat, the output of the linear SE at one site could be sent to other TSE as pseudo measurements so as to increase the accuracy of their SE.

II. KEY FIGURES

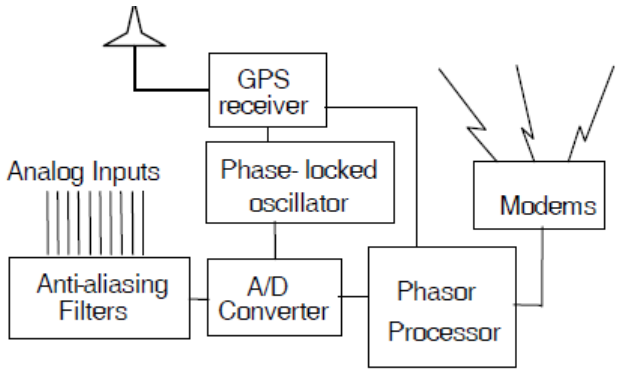

Figure 1. Synchronized phasor measurement

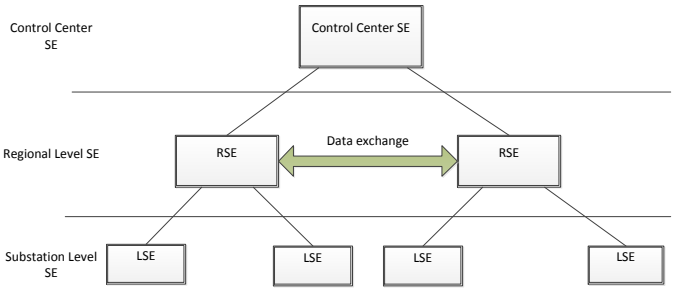

Figure 2. Multi-level state estimation

III. KEY RESULTS

Not yet established, will be completed before July 22, 2012

Identify applicable sponsor/s here. *(sponsors)*

Modeling and Stability Analysis of Distributed Generation

Ehsan Nasr Azadani, *Student Member,IEEE*, Claudio Canizares, *Fellow, IEEE*, Kankar Bhattacharya, *Senior Member, IEEE*

Power and Energy System Group, Department of Electrical and Computer Engineering,
University of Waterloo, CANADA

***Abstract*— There are many technical aspects and challenges of Distributed Generation (DG) that are still not properly understood and addressed. Since most of these studies have to be carried out based on simulations, adequate static and dynamic models for DG units are required. The objective of this work is the dynamic and static modeling of various DG technologies for stability analysis. These models allow studying systems with DGs both in the long- and short-term; thus, differential and algebraic equations of various DGs are formulated and discussed based on models found in the literature in order to integrate these models into a system representation. The presented and discussed models are generally based on well-known dynamic models of different DGs for stability studies considering the dynamics of the primary governor, generators and their interfaces and controls. The results of applying these models for voltage and angle stability studies of a realistic distribution system are presented and compared, demonstrating the typical application of the presented models.**

***Keywords*- Modeling, distributed generation, voltage stability, angle stability.**

I. KEY FIGURES

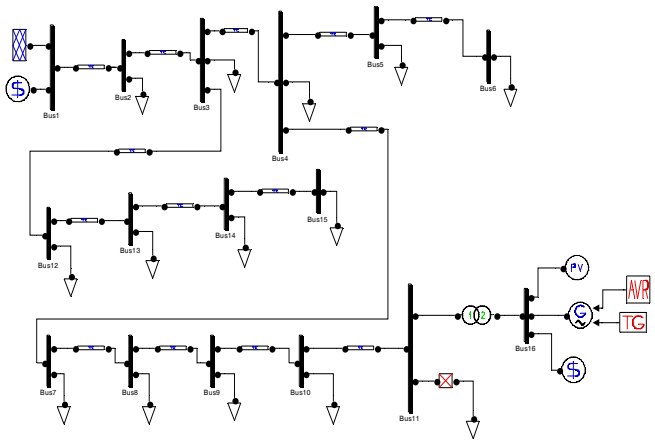

Fig. 1. Kumamoto distribution test system simulated in PSAT.

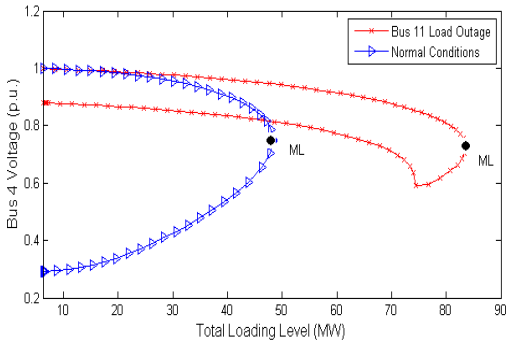

Fig 2. P-V curve for test system with PV model.

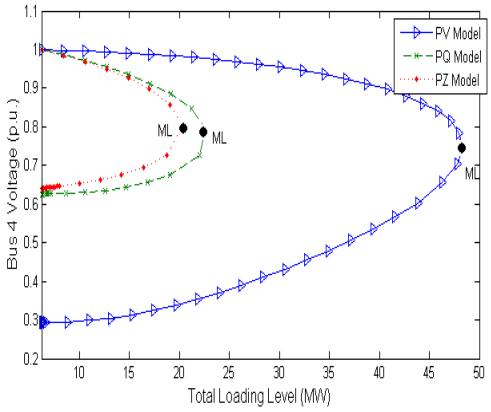

Fig. 3. P-V curves for different static models.

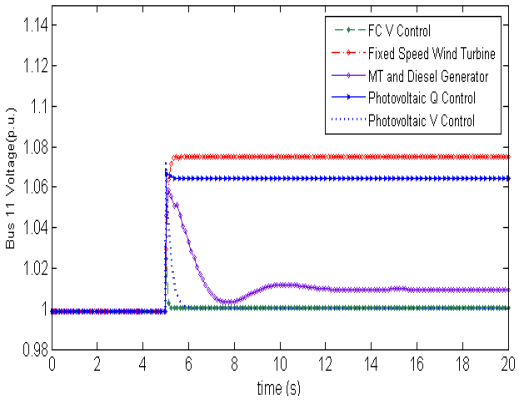

Fig. 4. Comparison of the time domain simulations for a load outage at Bus 11 for the test system with different DGs.

Title:
Experience of Implementing controller-in-the-Loop with Over-current Relay Example by Using cRIO, PXI and RTDS

Abstract
To study the performance of new control or protection methods for power systems, time domain simulation is widely used. One of the time domain simulation methods is controller-in-the-loop (CIL) simulation, which includes a real time simulator and an embedded controller. In this work, the experience of implementing CIL is presented. The methodology of implementation to increase the success rate is described. Some practical issues such as real-time programming issues, task allocation, synchronization issues, and debugging methods are addressed. To validate these methods and concepts, a simple overcurrent relay example was implemented. A three-phase ground fault was applied and the simulation results were compared and analyzed. These results are found to be satisfactory, which validates the concepts and methods shared in this paper.

Long-term effect of relay protection operation on cascading failures in growing scale-free small-world power grid

Yudong Zhang, Zhejing Bao and Yijia Cao, *Member, IEEE*

***Index Terms*—Cascading failure, Relay protection, Topology evolution, Scale-free, Small-world, OPA model.**

Electric power transmission systems are a key infrastructure in modern power system, and the relay protection device is one of the most important components of a power system. Analyses of topology and blackout data of real power systems indicate that many real power systems possess complex networks' characteristics like scale-free or small-world and blackouts behave as a complex dynamical system. Moreover, the topology evolution is a significant characteristic of the network. Therefore, we use an ORNL-PSerc-Alaska (OPA) model considering topology evolution to investigate how these complex system dynamics impact on the assessment of measures for improving relay protection. The flowchart of the improved OPA model is shown in Fig.1.

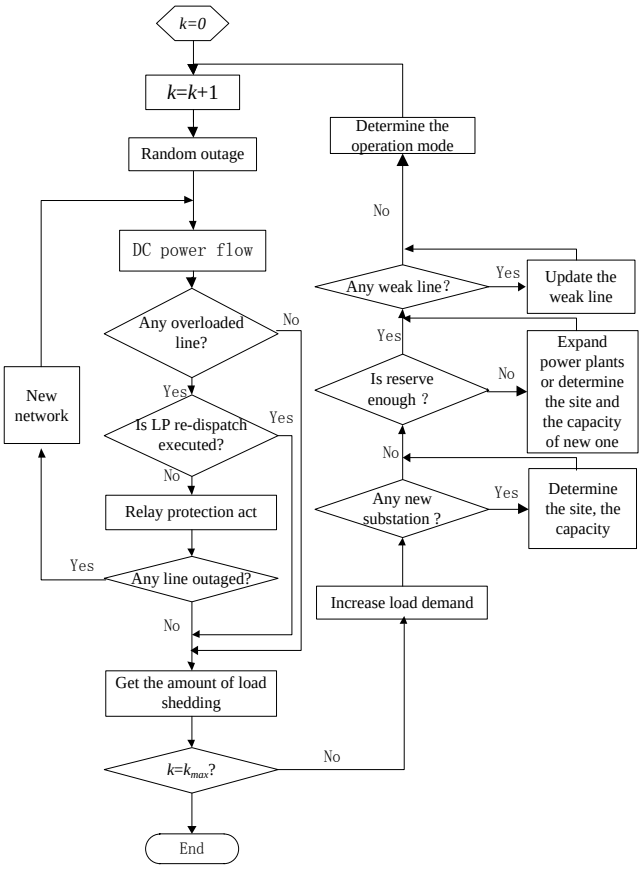

Fig.1. Flowchart of the improved OPA model

In this paper, we assume that the power grid grows in scale-free small-world way. That is, when a new node (a new substation or a new power) is added to a system, the edges of the new node which will be attached to an existing node should be chosen in a particular rule called scale-free small-world way.

Two types of improving measures are considered in this paper as follows:

1) Dependability improvement: That is reducing the probability of failure to operate relay protection, α. When $\alpha = 0$, the protection is 100% dependable.
2) Security improvement: That is reducing the probability of unwanted operation of relay protection, β. When $\beta = 0$, the protection is 100% secure.

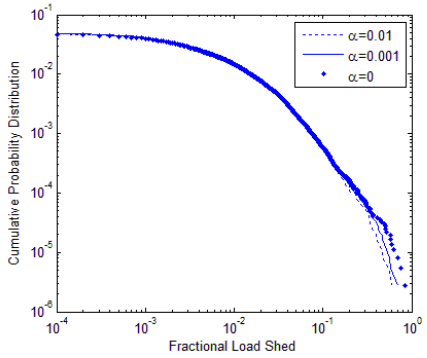

Fig.2. Blackout distribution of scale-free small-world growth way with different α (other parameters are the same as the initial ones)

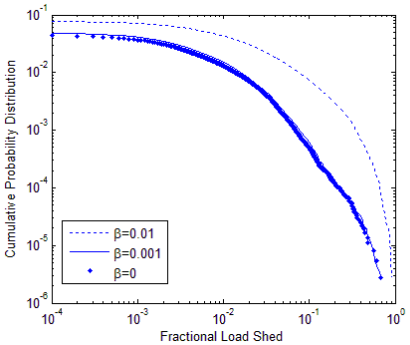

Fig.3. Blackout distribution of scale-free small-world growth way with different β (other parameters are the same as the initial ones)

Simulation results show that a decrease in the probability of failure to operate relay protection does not reduce the probability of large blackouts in the growing scale-free small-world power grid, but increases that instead, and unwanted operation of relay protection is more harmful to the system. The mitigation of failures of relay protection in complex systems needs to be approached with care.

A Novel Method for Solving the Divergence of Power Flow and Controlling Voltage in Integrated Distributed Generators Network

Hung Nguyen Dinh and Yong Tae Yoon
Electrical Engineering and Computer Science Department, Seoul National University, Seoul, Korea
Email: hunghtd@snu.ac.kr and ytyoon@ee.snu.ac.kr

***Abstract*—In this paper, a new method for solving the divergence of power flow is proposed. The salient feature of the new method is that instead of focusing on computation techniques as in prevalent methods, physical conditions of networks are changed to overcome problem of divergence, i.e. reallocating reactive power compensations. Since incongruous distribution of reactive power may lead to divergence of load flow, switched shunts are controlled to re-appropriate reactive power in power systems. As a result, mismatch decreases over iterations of Newton-Raphson method and power flow quickly converges. Thereby, power flow solvability is restored. The most important contribution of the proposed method is ability to prevent voltage collapse. Numerical test on a large scale electric power system is analyzed.**

Moreover, an approach to derive a simple formula to control voltage at some heavy load bus is presented. The reactive power source used in this research is the distributed generator which is adjacent to the heavy load. Linearizing the power network using Power Transfer Distribution Factors is a simple method with accepted errors. A new value of voltage at the distributed generator terminal is computed in terms of the voltage deviation of load buses. In this approach, solving the entire system is unnecessary.

I. KEY EQUATIONS

PTDF of the reactive power through the line l_{ij} is obtained as:

$$p_{ij-k} = \frac{dQ_{l(ij)}}{dQ_k} =$$

$$= -B_{ij}.(2V_i - V_j\cos\delta_{ij})\frac{1}{\frac{\partial Q_k}{\partial V_i}} + B_{ij}V_i(\frac{\cos\delta_{ij}}{\frac{\partial Q_k}{\partial V_j}} - V_j\sin\delta_{ij}(\frac{1}{\frac{\partial Q_k}{\partial \delta_i}} - \frac{1}{\frac{\partial Q_k}{\partial \delta_j}})) \quad (1)$$

The mismatch of reactive power at bus i where switched shunt (SS) resides can be represented as:

$$\Delta Q_i = \left[p^i\right]\left[\Delta Q_k\right] \quad (2)$$

$$\Delta Q_{l(ij)} = \Delta Q_i \sum_{j\in\Omega_l, k\in\Omega_N} p_{ij-k}u_k = h_{ki}\Delta Q_i \quad (3)$$

$$\Delta' = \Delta + H\Delta ss \quad (4)$$

$$\Delta ss = \left(\left[-H\right]^T\left[-H\right]\right)^{-1}\left[-H\right]^T\Delta \quad (5)$$

$$\begin{bmatrix} \Delta V_{DG} \\ \Delta V_j \\ \dots \\ \Delta V_k \\ \dots \\ \Delta V_{j+ni-1} \end{bmatrix} = \left[J_V\right]^{-1}\begin{bmatrix} 1 \\ U \end{bmatrix} * \Delta Q_{DG} \quad (6)$$

$$\Delta V_{DG} = \frac{d_{DG}}{d_j}(0.95 - V_j) = \alpha\Delta V_j \quad (7)$$

II. KEY FIGURES

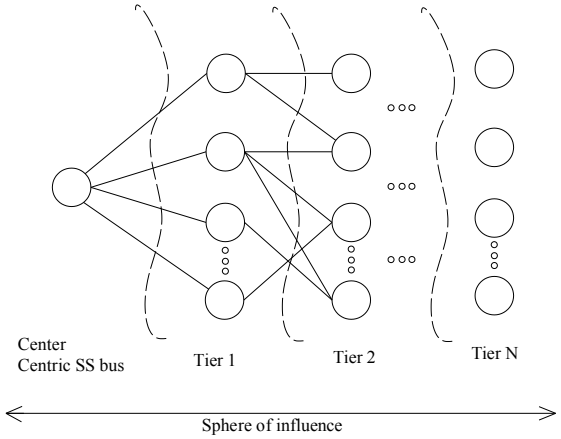

Fig.1. The sphere of influence.

III. KEY RESULTS

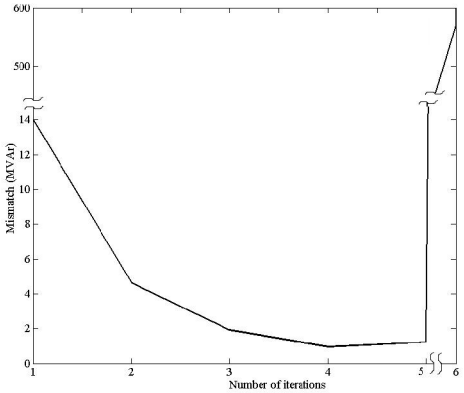

Fig. 2. Convergence characteristic of original problem

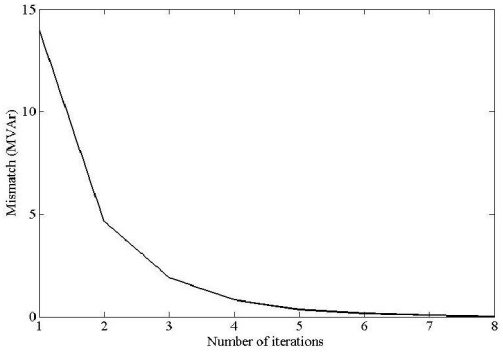

Fig. 3. Convergence characteristic of power flow with controlled SS

Automated Topology Processing for Conventional, Phasor-Assisted and Phasor-Only State Estimators

Mostafa Farrokhabadi
Department of Electrical and Computer Engineering
University of Waterloo
Waterloo, Ontario, Canada
Mostafaf@kth.se

Luigi Vanfretti
Electric Power Systems Division
KTH Royal Institute of Technology
Stockholm, Sweden
Luigiv@kth.se

***Abstract*—Topology processing is a crucial step necessary for most EMS applications to properly function (particularly state estimation). However, the openly available documented evidence on the implementation of current topology processors (TP) and associated research shows a lack of rigor in the description of the available algorithms. This paper encompasses the development of a robust network topology processor which can be used for both traditional and PMU-based state estimators. Building on top of the state of the art, an algorithm is proposed in a way to cover the limitations of current approaches and to suggest new features. The topology processor was coded in MATLAB and tested over two different power networks; a fictitious test system and a modified version of the IEEE Reliability Test System 1996. As the topology processor is designed to supply network topologies to a PMU-based Sate Estimator, the IEEE Reliability Test System 1996 is simulated in real-time to provide synthetic data as PMU measurements. Real-time simulation is performed using the eMegaSim Opal-RT real-time simulator which is part of "SmarTS Lab" at KTH Royal Institute of Technology. Different test scenarios are carried out and the inclusion of PMU measurements is analysed. Through test results it is shown that the proposed topology processor is fast and robust enough to support PMU-only state estimators, as well as conventional or phasor-assisted state estimators.**

Keywords-component; State Estimator, Topology Processor, Real-Time Simulation, Phasor Measurement Unit

I. KEY ALGORITHM

The algorithm is divided into six different steps:

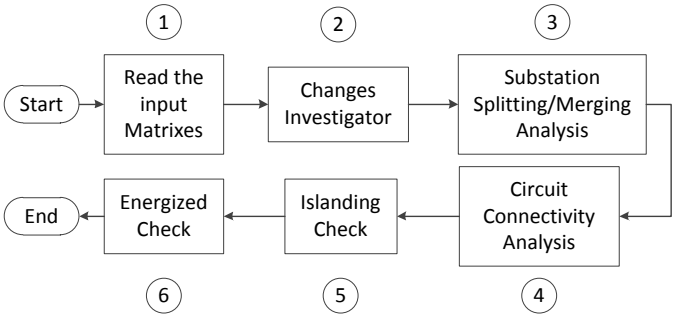

Figure 1. TP General Algorithm

II. KEY FIGURES

A. *Fictitious Test System*

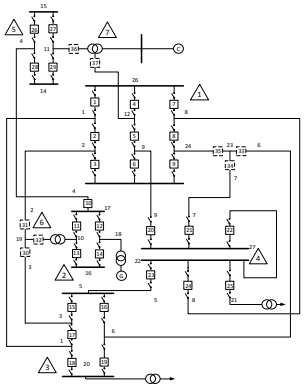

Figure 2. Fictitious Test System

B. *IEEE Reliability Test System 1996 (modified)*

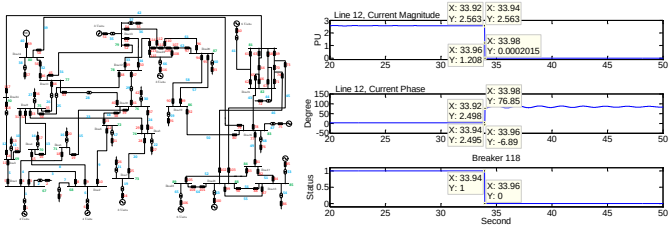

Figure 3. IEEE Reliability Test System 1996 (modified), and a Sample Real-Time Simulation Results

III. SAMPLE RESULT

TABLE I. SAMPLE RESULT

Scenario	Description	Results
1	5 switches are opened simultaneously. 2 Stations suffer changes inside.	All the changes identified and reported correctly. Computation time: 5.4 ms

A Statistical Study on Impact of PHEVs Charging on Power grid

Zahra Darabi and Mehdi Ferdowsi
Department of Electrical and Computer Engineering, Missouri University of Science and Technology
Emails: *zd8r4@mst.edu*, *ferdowsi@mst.edu*

Abstract— This poster extracts and analyses the data that are available through national household travel surveys (NHTS) and based on 40,000 vehicle trips, probability distribution functions for arriving time and required energy of PHEVs are extracted. Also, the probabilistic and deterministic PHEV charging load profiles are built and compared.

I. Key Data

Three key questions:

- when each vehicle begins to be charged,
- how much energy is required to charge it,
- what level of charge is available.

Statistical Study:

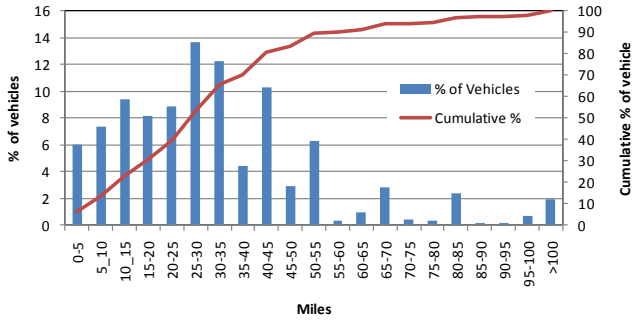

Fig. 1. Percentages of vehicles vs. daily miles driven

TABLE I
NUMBER AND PERCENTAGE OF EACH TYPE OF VEHICLES IN NHTS

Vehicle Type	1	2	3	4
Number	23,818	4,686	5,139	5,536
Percentage	60.85%	11.94%	13.1%	14.11%

TABLE II
ENERGY REQUIREMENT FOR FOUR TYPES OF PHEV30

Type	Total kWh	kWh/mile
Compact Sedan	9.765	0.3255
Mid-size Sedan	10.815	0.3605
Mid-size SUV	13.125	0.4375
Full-size SUV	15.225	0.5075

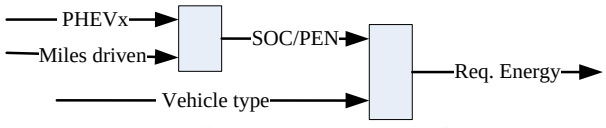

Fig. 2. The procedure of obtaining required energy for each vehicle

II. Key Results

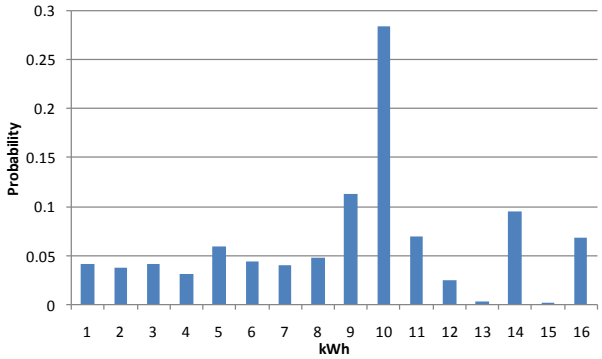

Fig. 6. Required energy probability distribution based on PHEV30

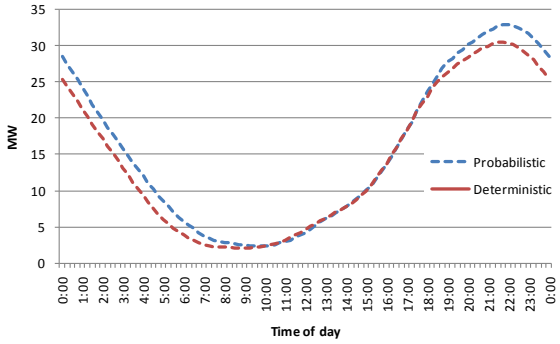

Fig. 7. Deterministic and probabilistic PCLP curves

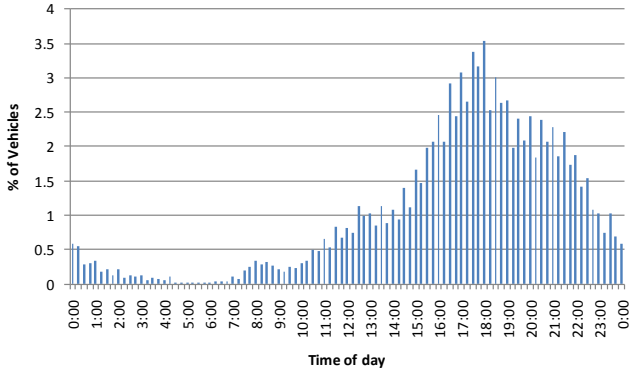

Fig. 2. Probabilistic percentages of vehicles vs. arriving time

Effect of Shield Thickness on Braided-Shield Cables Crosstalk

Miguel Penagos and Pablo Moreno
Center for Research and Advanced Studies (CINVESTAV), Guadalajara, Jalisco 45019, México,
Email: mpenagos@gdl.cinvestav.mx and pmoreno@gdl.cinvestav.mx

***Abstract*—A basic unshielded-shielded configuration is modeled as a MTL and the shield thickness effect on the frequency domain and time domain crosstalk is investigated. The initial shield thickness is equal to the diameter of the wires making up the braid (2 r_{braid}). The shield is grounded at the near and far ends and the generator wire is driven with a sinusoidal source in a frequency range from 10 Hz to 100 MHz. The non ideal ground return path is modeled with the complex images method. The frequency dependence of the distributed series impedance is modeled with the Wedepohl and Wilcox approximations for the surface and transfer impedances [1]. Pigtail sections are taken into account with conductors connected at the ends of the generator and receptor wires and modeled as MTL. In order to incorporate the transfer impedance to the model, voltages and currents are defined as loop variables and afterwards they are converted to conductor variables (voltages with respect to ground and currents returning through ground). The time domain crosstalk analysis is performed by the implementation of the Numerical Laplace Transform technique.**

I. Reference

[1]. L.M. Wedepohl and D.J. Wilcox, "Transient analysis of underground power-transmission systems. System-model and wave-propagation characteristics, "*Proceedings of the IEEE*, 120(2), pp. 253-260, Feb. 1973

II. Key Equations

The transfer impedance is approximated with the Wedepohl and Wilcox expressions proposed in [1]:

$$Z_T = \frac{\rho\gamma}{2\pi(a+b)}\cosh\left(\gamma(b-a)\right) \qquad (1)$$

Voltages and currents can be related by the **AB** parameters using modal analysis. For each MTL section:

$$\begin{bmatrix}\mathbf{I}(0,s)\\ \mathbf{I}(\mathcal{L},s)\end{bmatrix}=\begin{bmatrix}\mathbf{A} & -\mathbf{B}\\ -\mathbf{B} & \mathbf{A}\end{bmatrix}\begin{bmatrix}\mathbf{V}(0,s)\\ \mathbf{V}(\mathcal{L},s)\end{bmatrix} \qquad (2)$$

III. Key Figures

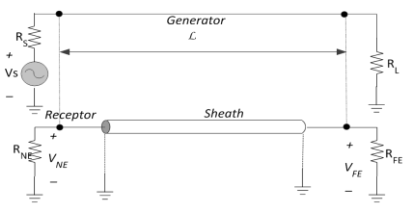

Figure 1. Unshielded-shielded configuration.

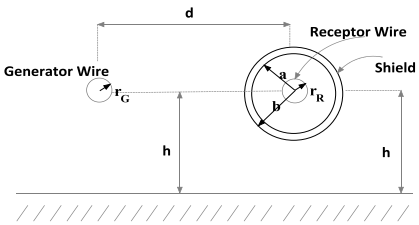

Figure 2. Dimensions of the cross section.

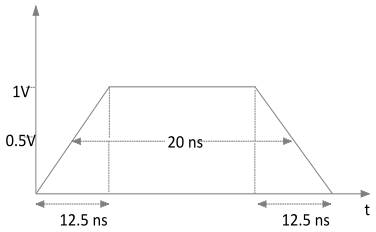

Figure 3. Voltage Source for the time domain Crosstalk Analysis.

IV. Key Results

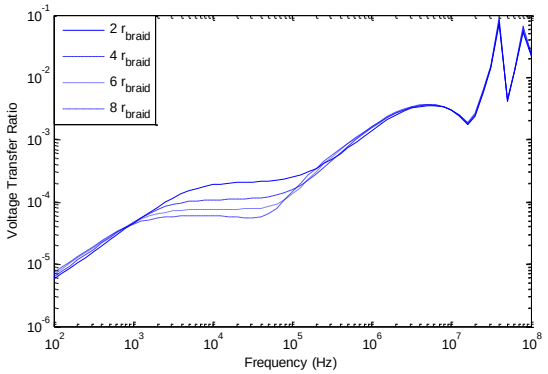

Figure 4. Frequency Domain Crosstalk V_{NE}/V_S

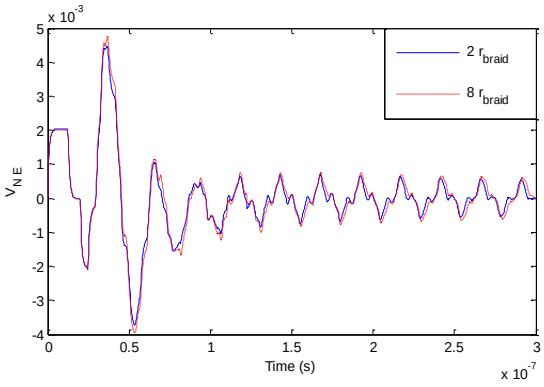

Figure 5. Time Domain Crosstalk at near end

A Dynamic Equivalent Model for Wind Power Plants with Type-4 Units

Dalia N. Hussein, and Reza Iravani
Department of Electrical and Computer Engineering, University of Toronto, Toronto, ON M5S 3G4, Canada
Email: dalia.hussein@ieee.org, and iravani@ecf.utoronto.ca

***Abstract*—With the increased penetration of wind power into the power system, modeling of wind Power Plants (WPPs) becomes an essential issue to study their impact on the power system during system transients. Detailed modeling of WPPs is not a desirable option since a typical WPP consists of hundreds of components including tens or even hundreds of wind turbine generator units, the collector network, and the WPP central controller. Detailed modeling of all these components is complex, time consuming, and not practical; therefore, there is a need to develop computationally efficient and accurate equivalent models of WPPs.**

This paper proposes a novel dynamic, reduced-order equivalent model of WPPs. The proposed equivalent is developed to model the terminal behavior of the WPPs in response to electromagnetic transients (EMTs) that take place in the power system external to the WPPs. The proposed equivalent deals with the limitations of the existing WPP equivalent models and considerably reduces the complexity and the computational burden associated with detailed modeling of WPPs without compromising the accuracy or numerical stability. The novelty of the proposed equivalent is that it is a simple, reduced-order, frequency-dependent equivalent model that fully represent both (i) the frequency response of the WPP passive network in the desired frequency range, e.g., DC to 50 kHz, and (ii) the dynamics of the active components of the WPP in response to EMTs in the host power system. The accuracy of the proposed equivalent is validated by comparing the time-domain simulation results of the proposed equivalent with those of the detailed system model in the PSCAD/EMTDC simulation environment.

I. Key Figures

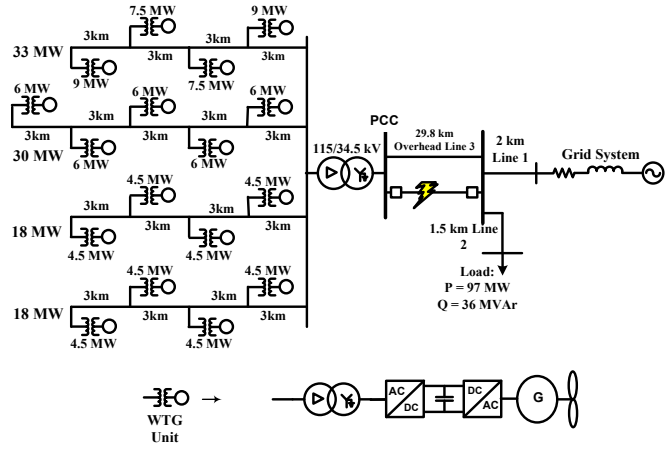

Fig. 1. Schematic Diagram of the Modified version of Lake Erie Shores WPP

II. Key Results

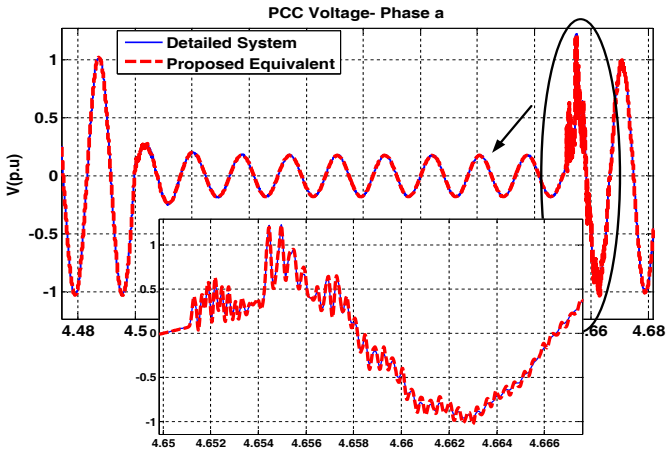

Fig. 2. The PCC Voltage (phase-a) of the Detailed Network and the Developed Equivalent During an External 3ph Fault

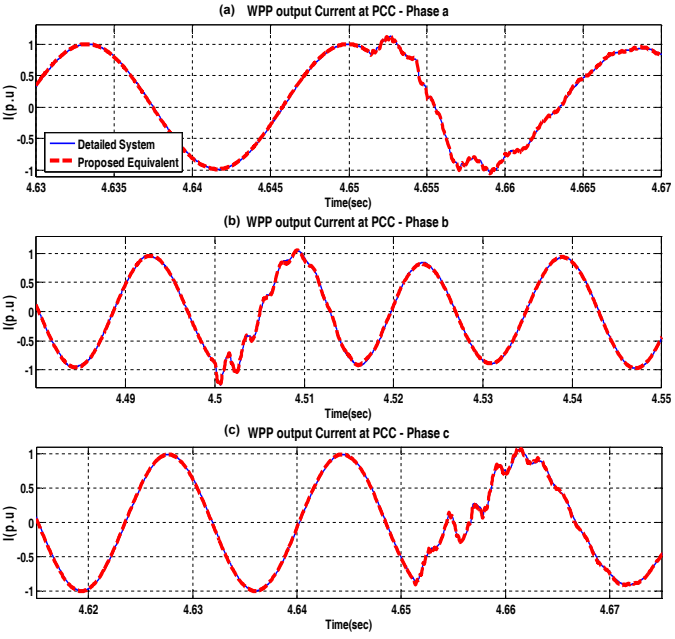

Fig. 3. The WPP Output Currents at the PCC of the Detailed Network and the Developed Equivalent. (a) phase-a (b) phase-b (c) phase-c

Towards Sustainable Intra-Dispatch Real Power Balancing

Nipun Popli *Student Member, IEEE* and Marija D.Ilić *Fellow, IEEE*

***Abstract*—Power systems are composed of heterogeneous energy resources, broadly categorized as controllable conventional generators and intermittent renewable resources. The generation output of the later consists of fluctuations and persistent variations over multiple time-scales. Consequently, it is critical to balance supply and demand in real-time once the system is dispatched, i.e. before the operator re-schedules additional conventional resources. A classificatory approach is needed for planning resources for namely two intra-dispatch control actions, stabilization for small but fast fluctuations and load-following/regulation for slow but sustained deviations. Our objective is to balance sustained/persistent intra-dispatch real power variations. In [1] and [2], a quasi-stationary model has been derived which explicitly states the inter-dependence between the real power generation as states and the non-zero mean wind variations as disturbances. The proposed control framework is an automated function to follow sustained intra-dispatch real-power imbalances in the system. Conventionally, the ramp rates of the power plants are measured as scalars, reflecting the amount by which they can ramp-up or ramp-down between consecutive dispatch interval. However, for balancing of large intra-dispatch wind-power variations, such scalar values may not hold good. We propose a dynamic ramp-rate based control framework for generating real power needed to follow the sustained wind power deviations within each dispatch interval, taking into account the energy conversion dynamics. We aim to achieve higher degree of efficiency by aligning natural response characteristics of conventional balancing resources with the time-scales of power imbalances in the system.**

***Index Terms*—Load Following, Ramp-Rates, Tertiary Control**

I. Preliminary Simulations

The linearized model for two different types of stand-alone conventional units, coal-based steam plant and dam-based hydro plant. The plants were subjected to disturbance for two possible cases. For the case when energy-dynamics was taken into account (blue-curve) and when it was not (red-curve). The work in progress includes the control design for non-linear models of the plant in an interconnected system. This is critical for dynamic efficiency of the network for the purpose of following load as well wind variations.

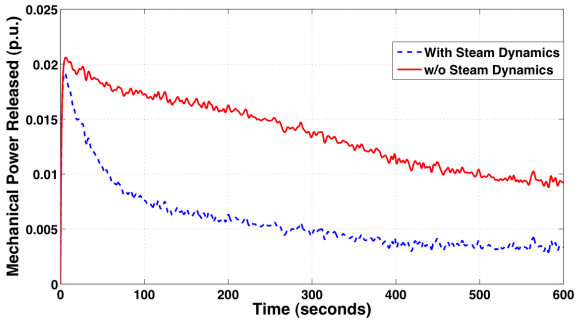

Fig. 1. Mechanical Power released by the Coal-based Steam Plant

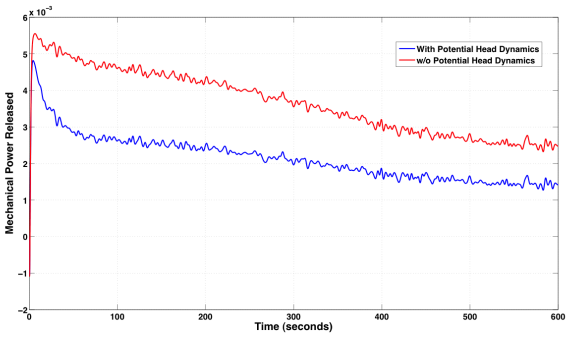

Fig. 2. Mechanical Power released by the Dam-based Hydro Plant

References

[1] M. Ilić , N. Popli, J. Y. Joo, and Y. Hou, *A Possible Engineering and Economic Framework for Implementing Demand Side Participation in Frequency Regulation at Value*, IEEE Power Engineering Society General Meeting, July 2011

[2] L. Xie, P. M. S. Carvalho, L. A. F. M. Ferreira, J. Liu, B. Krogh, N. Popli, and M. D. Ilić, *Wind energy integration in power systems: operational challenges and possible solutions*, Proceedings of IEEE: Special Issue on Network Systems Engineering for Meeting the Energy and Environment Dream (Invited). Vol. 99, No. 1, pp. 214 - 232, January 2011

Nipun Popli is with Carnegie Mellon University, Pittsburgh, PA, USA (email: npopli@andrew.cmu.edu).

Marija D. Ilić is with Carnegie Mellon University, Pittsburgh, PA, USA, and Delft University of Technology, Delft, The Netherlands (email: milic@ece.cmu.edu).

Identification of Power System Inter-area Oscillation by Analytic Wavelet Transforms

Daham Min
School of Electrical and Electronic Engineering, Yonsei University, Seoul, South Korea,
Email: gockachu@gmail.com

***Abstract*—This poster presents an improved damping estimation technique that can track the temporal variations in the inter-area oscillation. Damping of electro-mechanical oscillations is considered useful indicator for system operation. Based on bandpass theory and analytic wavelet transforms, the proposed technique is suitable in tracing damping of oscillation with synchronized phasor measurements at a high sampling rate. This will focus on modes of our interest and avoid unnecessary computational burden. Also, this method is able to estimate time-varying damping ratios of the selected modes. Case studies on a 179-bus power system and real measurement data show that estimated system damping can be utilized to investigate the potential separation boundaries.**

I. Key Equation

The mother wavelet of AWT is defined as

$$\psi(t) = g(t)\exp(j\eta t) \tag{1}$$

Inter-area oscillation which are observed in a power system are usually modeled, $v(t)$ as $v(t) = \alpha(t)cos\theta(t) = \alpha e^{-\zeta\omega_n t}\cos(\omega_d t + \phi)$. In the case of such a signal, its AWT can be obtained as follows:

$$Wv(u,s) = \frac{1}{2}\alpha(u)\hat{\psi}_{u,s}(\omega(u),\sigma,\eta)\,e^{j\theta(u)} + \varepsilon(\alpha'(t),\omega') \tag{2}$$

$$\ln\left(\frac{2|Wv(u,s(u))|}{(4\pi\sigma^2 s(u)^2)^{1/4}}\right) \approx -\zeta\omega_d u + \ln\alpha \tag{3}$$

By substituting t for u, (3) can be rewritten in the form of time-varying damping ratio ζ_i.

II. Key Result

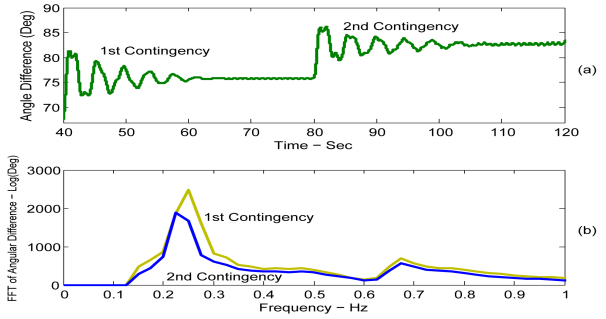

Fig. 1. (a) Angle differences between directly connected elementary coherent groups and (b) FFT analysis of the each contingency.

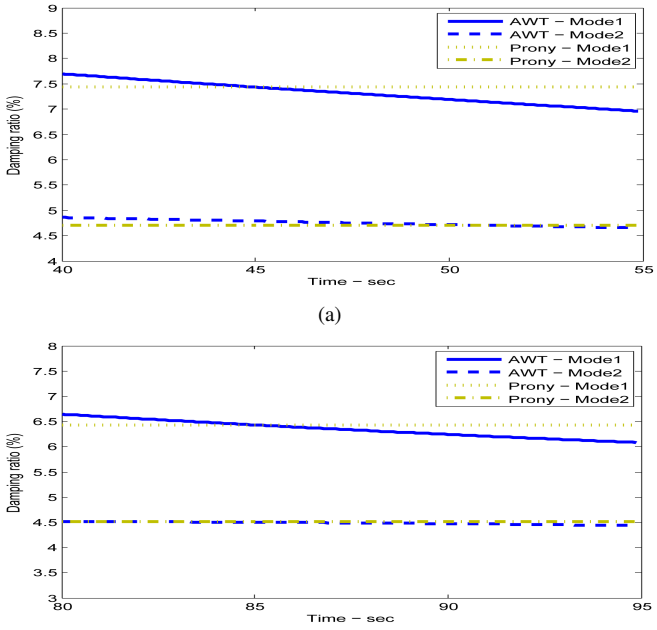

Fig. 2. (a) Damping ratio plot of AWT method and Prony analysis in the 1st contingency and (b) 2nd contingency.

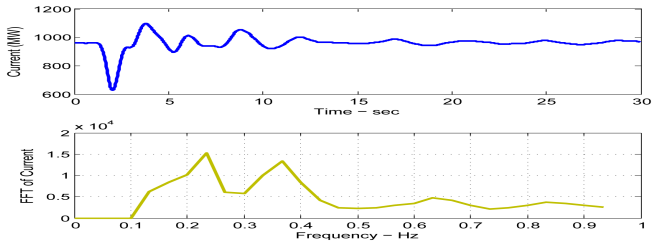

Fig. 3. (a) Maln-Round Mountain 1 current - June 24, 2004 and (b) FFT analysis of the current.

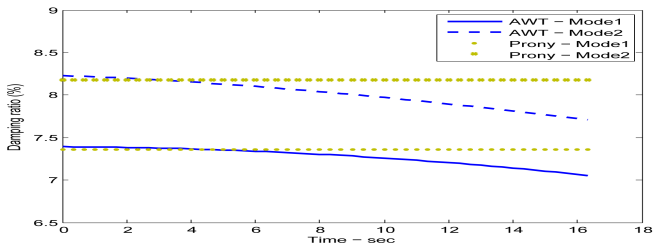

Fig. 4. Estimated time-varying damping ratio of MALN-Round Mountain on June 24, 2004.

Comprehensive Evaluation of Power Reversal Action of LCC- and VSC-HVDC Transmission

Hee Jin Kim
School of Electrical and Electronic Engineering, Yonsei University, Seoul, South Korea,
Email: jimmykim07@gmail.com

***Abstract*— This poster presents detailed discussion on the power reversal procedure and operational issues for line commutated converter (LCC) and voltage sourced converter (VSC) based high voltage direct current (HVDC) transmission system. Increasing penetration of intermittent renewable energy sources may increase the need of power reversal operation for HVDC, e.g. Skagerrak HVDC in Europe and HVDC #3 planned in Jeju Island, Korea. Power reversal of LCC-HVDC is obtained by changing polarity of DC voltages at both ends. It generally requires four steps to reverse power direction for LCC-HVDC. Also, power reversal of LCC-HVDC requires transformer tap change and filtering action. On the other hand, power direction of VSC-HVDC can be more flexibly reversed with controlling current direction. Developing detailed time-domain electromagnetic models for LCC-and VSC-HVDC and control schemes, we comprehensively investigate transient responses of LCC- and VSC-HVDC during power reversal. We also compare transient responses of LCC- and VSC-HVDC for AC fault. Finally, we examine transient responses of multi-infeed HVDC transmission, comprising both LCC- and VSC-HVDC system for various operating conditions, which may be the case for the interconnection between Jeju island and main land of Korea.**

***Index Terms*—LCC HVDC, VSC HVDC, Multi-infeed HVDC, Power Reversal, DC Fault, AC Fault.**

I. KEY FIGURE

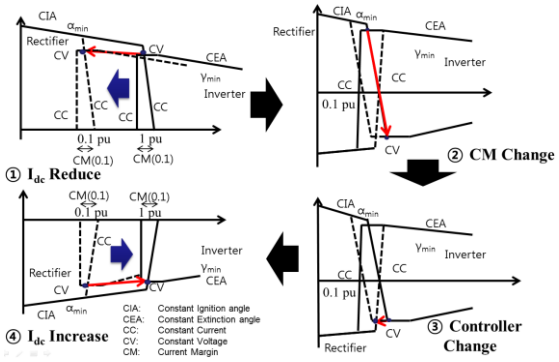

Fig. 1. Four Steps to Reverse Power Direction for LCC-HVDC.

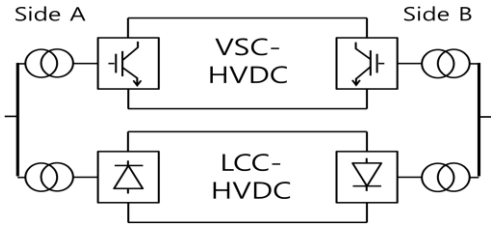

Fig. 2. Configuration of Multi-infeed HVDC which Consists of LCC-HVDC and VSC-HVDC.

II. KEY RESULTS

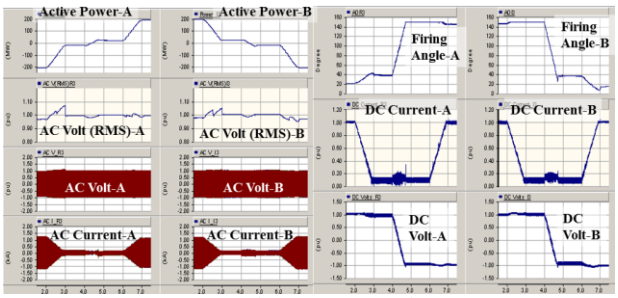

Fig. 3. Transient Response of Power Reversal for LCC-HVDC.

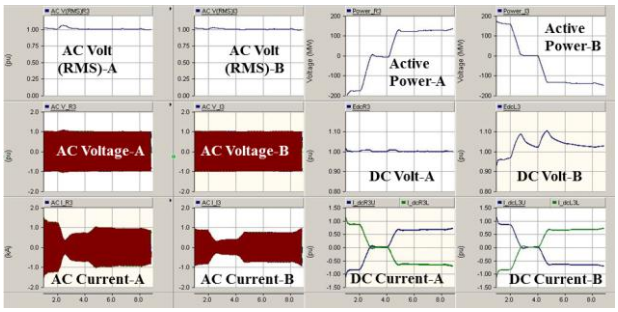

Fig. 4. Transient Response of Power Reversal for VSC-HVDC.

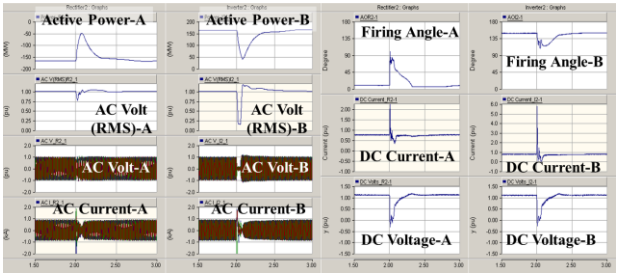

Fig. 5. Transient Response of LCC-HVDC in Multi-infeed HVDC during AC fault at Inverter Side (B).

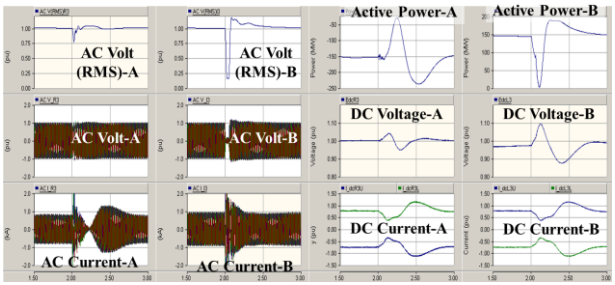

Fig. 6. Transient Response of VSC-HVDC in Multi-infeed HVDC during AC fault at Inverter Side (B).

Multistage Stochastic Optimal Operation of Energy-Efficiency Building with CHP System

Ping Liu and Yong Fu
Department of Electrical and Computer Engineering, Mississippi State University, Mississippi State, 39762, USA
Email: *pl266@ msstate.edu*, *fu@ece.msstate.edu*

Abstract—Given the operation of energy buildings, it's necessary to determine power productions from various energy sources, resulting in operating cost and possible energy import expenses. This paper presented a multistage stochastic programming model for the optimal operation of energy building systems with consideration of controllable electric and heat loads. The proposed algorithm will take into account the uncertainties of non-controllable electric and heat loads and solar power production. The rolling scheduling method is also introduced to decide the hourly operation status and power output of electric grid, charging and discharging power from battery, power output of CHP with boiler, which will make sure the efficient operation of energy buildings. The simulation results can offer a cost-effective solution by providing a sequence of decisions within the scheduling horizon.

I. Key Equations

Objective function

$$\min \sum_{t=1}^{T}\sum_{j=1}^{J_t} \rho_j^t \cdot [p_{l,j}^t \cdot pr_l^t + p_{g,j}^t \cdot pr_g^t + (F_{c,j}^t + F_{b,j}^t) \cdot pr_n^t] \cdot T_d$$

$$\sum_{j=1}^{J_t} \rho_j^t = 1, t = 1,2,...,T$$

Electric and heat power balances

$$p_{l,j}^t + p_{g,j}^t + p_{c,j}^t + p_{bat,j}^t + p_{solar,j}^t = p_{NC,j}^t + P_{CNTR,j}^t \cdot x_{ele,j}^t$$

$$H_{\sup,j}^t = \eta_{hc}(H_{c,j}^t + H_{boiler,j}^t) = H_{load,j}^t = H_{NC,j}^t + H_{CNTR,j}^t \cdot x_{heat,j}^t$$

Constraints for power from utility grid

$$0 \le p_{l,j}^t \le p_l^{t,\max} \cdot x_{l,j}^t$$

$$p_g^{t,\min} \cdot x_{g,j}^t \le p_{g,j}^t \le 0$$

$$x_{l,j}^t + x_{g,j}^t \le 1$$

Constraints for power from battery

$$p_{bat}^{\min} \cdot x_{bat,j}^t \le p_{bat,j}^t \le p_{bat}^{\max} \cdot x_{bat,j}^t$$

$$0 \le x_{bat,j}^t \le 1$$

$$s_{bat,j}^{t+1} = s_{bat,j}^t + p_{bat,j}^{t+1} \cdot T_d / c_{bat}^{\max}, \ j = 1,2,...,J_t; t = 0,1,...T$$

$$s_{bat}^{t,\min} \le s_{bat,j}^t \le s_{bat}^{t,\max}$$

Constraints for power from CHP with boiler

$$p_c^{\min} \cdot x_{c,j}^t \le p_{c,j}^t \le p_c^{\max} \cdot x_{c,j}^t$$

$$F_{c,j}^t = a \cdot p_{c,j}^t + b \cdot x_{c,j}^t$$

$$H_{boiler}^{\min} \cdot x_{boiler,j}^t \le H_{boiler,j}^t \le H_{boiler}^{\max} \cdot x_{boiler,j}^t$$

Constraints for controllable electrical and heat loads

$$\sum_{t=k}^{k+T_{ON}-1} x_j^t \ge T_{ON} \cdot (x_j^k - x_j^{k-1}), k = 1:(T - T_{ON} + 1)$$

$$E_j^{t,\min} \le \sum_{t=1}^{T} p_j^t \cdot x_j^t \le E_j^{t,\max}$$

II. Key Diagram

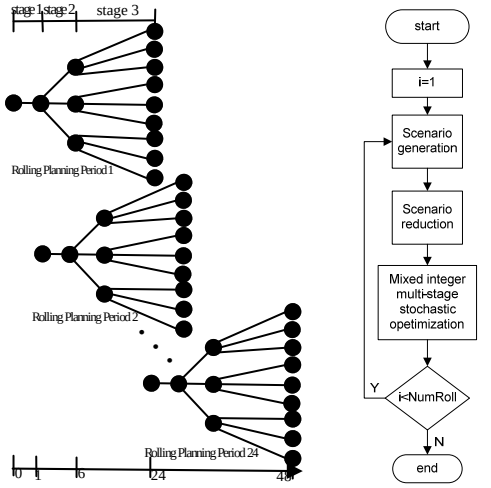

(a) Decision structure (b) Flow chart

Fig. 1 Diagram of rolling scheduling

III. Key Results

TABLE I
CASES DEVELOPED FOR ANALYSIS

Case		1	2	3	4	5	6	7(Stochastic)
Power Generation	Electric Grid	✓	✓	✓	✓	✓	✓	✓
	Solar	×	✓	✓	✓	✓	✓	✓
	Battery	×	×	✓	✓	✓	✓	✓
	CHP	×	×	×	×	×	✓	✓
	Boiler	×	×	×	×	✓	✓	✓
Household Loads	NC Electric Loads	✓	✓	✓	✓	✓	✓	✓
	Controllable Electric Loads	---	---	---	…	…	…	…
	NC Heat Loads	×	×	×	×	✓	✓	✓
	Controllable Heat Loads	×	×	×	×	…	…	…

'✓' means candidate; '×'mean non-candidate; '--'means fixed status; '…' means unfixed status

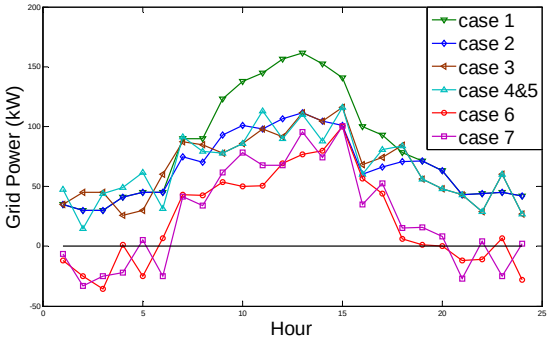

Fig. 2 Power output of grid

Stochastic Economic Dispatching for Wind Penetrated Power System

A.H.Shahirinia[1], D.C.Yu[1], E.Soofi[2]
1- Department of Electrical and Computer Engineering,
2- Sheldon B Lubar School of Business
University of Wisconsin–Milwaukee, Kenwood Blvd. Milwaukee, WI 53201-0413
Email: shahiri2@uwm.edu, yu@uwm.edu and esoofi@uwm.edu

***Abstract*—** This research is an entirely new approach to analyzing economic dispatching problems for wind penetrated power systems. We have developed new MATLAB compatible software specifically for this purpose known as the Stochastic Economic Dispatcher (SEconD). This software is able to find the optimal solution using the Dynamic Programming Method. Since wind speed is unknown we use a random variable described by a Weibull distribution. This is inserted into a Monte Carlo simulation to produce the wind power distribution, which is also uncertain. The goal, therefore, is to determine the optimal distribution of output power for each generator, the distribution of power transmission loss, the related costs and total costs based on these distributions as shown in Fig. 1. The many inequality constraints and non-linear equations complicate this system eliminating the possibility of the closed-form solution. A uniqueness of SEconD is the ability to analyze the effects on output of even trivial changes to the input. For example, we have demonstrated the ability to optimize generator outputs given variable fuel costs in this research. Another uniqueness of SEconD is the ability to analyze outputs with different confidence boundary about wind speed, of which we will show 95% and 90%.

Key Equations:

$$\text{Minimize } C_{tot} = \sum_{i=1}^{n} c_i * P_i^2 + b_i * P_i + a_i \quad (1)$$

$$\text{Subject to } P_d + P_{loss} = \sum_{i=1}^{n} P_i \quad (2)$$

$$\sum_{i=1}^{n}\sum_{j=1}^{n} B_{ij} * P_i * P_j + \sum_{i=1}^{n} B_{0i} * P_i + B_{00} \quad (3)$$

$$P_{\min.i} \le P_i \le P_{\max,i} \quad (4)$$

Key Results:

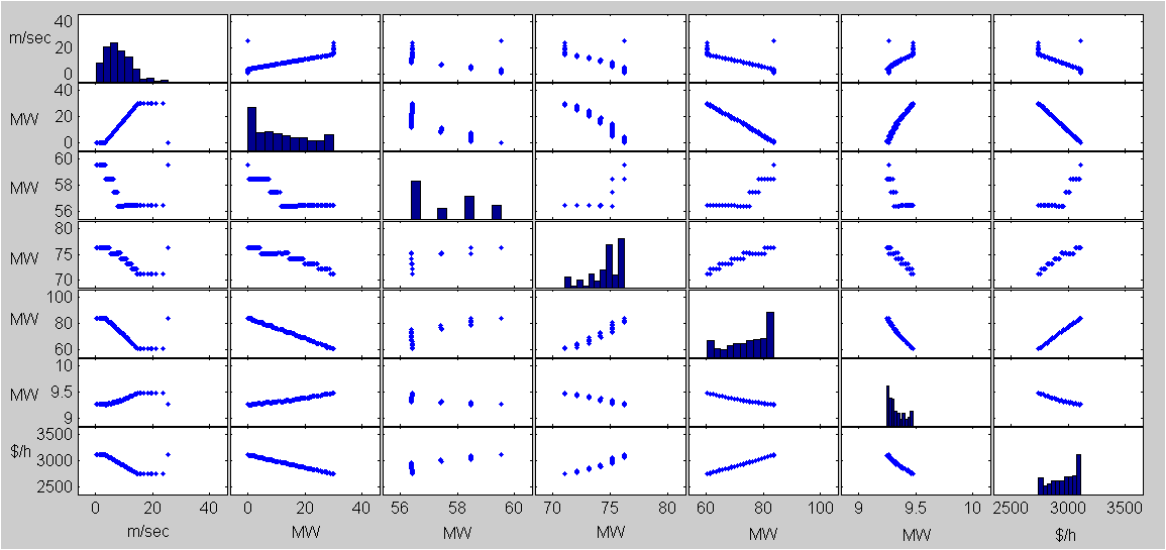

Fig. 1. Matrix plot for the optimal output solutions for powers, loss and total cost with their related marginal distribution

Capturing Electro-Thermal Dynamics in Power System Models with Building Loads

Mohammed Muthalib
Department of Electrical and Computer Engineering
Drexel University
Philadelphia, PA USA
mkm46@drexel.edu

Chika Nwankpa
Department of Electrical and Computer Engineering
Drexel University
Philadelphia, PA USA
con22@drexel.edu

***Abstract*— The electrical load of a building is largely determined by the energy requirements of the HVAC equipment. By studying the electro-thermal relationships that exist within buildings engineers have been able to estimate the corresponding electrical load. In the realm of electrical power distribution, building loads have been considered static loads which can be attributed to the slow reacting nature of the mechanical loads. However, enhanced metering and actuating capabilities brought about by the "Smart Grid" update have made it possible to re-evaluate building loads to reflect their true dynamic nature. The building dynamics, however, do not exist in isolation from the electrical power grid and the effect of varying the building load on the grid needs to be quantified. The presented work does this by using an equivalent energy circuit model to represent the building load and using an equivalent transformation to examine the causality of load variation on the grid side.**

I. Background and Motivation

Effectively capturing the building load dynamics is essential for improved participation of buildings in the energy market. By participating in demand response programs buildings can act as alternate resources to serve the purpose of flattening load profiles or contributing to frequency regulation. The dynamic load model presented in [1] uses equivalent energy circuit analysis to create a circuit model that represents the dynamic building load. A circuit model is easily integrated into power flow studies as shown in Fig. 1 thereby allowing building models to be used in both planning and operational analysis. The dynamic building equation (1) presented in [1] captures the effect on building temperature ψ due to temperature control input ψ_B and corresponding building electrical load P_{L3}. It should be noted that electric voltage dynamics at the building interface are ignored in this setup.

$$\frac{d\psi}{dt} = \frac{1}{R^{Th}C^{Th}}\left(\psi_B - \psi\right) - \frac{P_{L3}}{C^{Th}} \qquad (1)$$

II. Problem Formulation

The work proposed is to incorporate the building bus voltage dynamics using structure preserving models similar to the work done in [2] and [3]. A goal is a presentation of differential-algebraic equation set capturing both building temperature and network voltage dynamics.

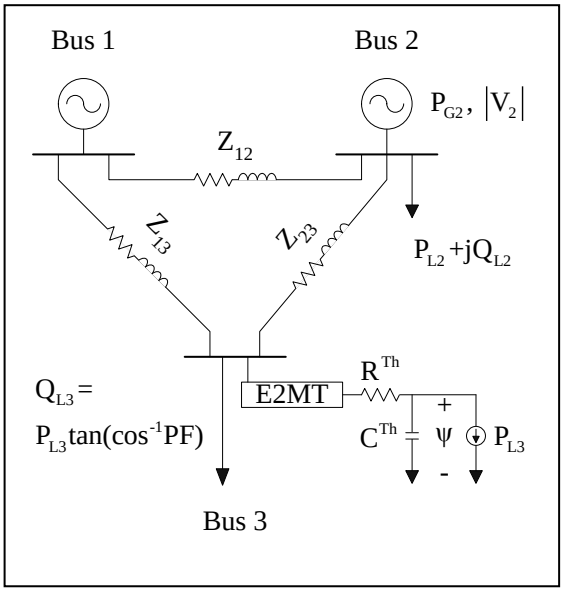

Figure 1 – Example 3-bus Power system with dynamic building load

References

[1] M. Muthalib, C. Nwankpa "Dynamic characterization of building electrical loads by equivalent energy circuit analysis," The IEEE International Symposium on Circuits and Systems, 2012

[2] A. R. Bergen, D. J. Hill, "A Structure Preserving Model for Power System Stability Analysis," *Power Apparatus and Systems, IEEE Transactions on* , vol.PAS-100, no.1, pp.25-35, Jan. 1981

[3] Y. Liang, C. Nwankpa, R. Fischl, A. DeVito, S. Readinger, "Dynamic reactive load model," *Power Systems, IEEE Transactions on* , vol.13, no.4, pp.1365-1372, Nov 1998

[4] IEEE Task Force on Load Representation for Dynamic Performance, "Standard load models for power flow and dynamic performance simulation," *Power Systems, IEEE Transactions on* , vol.10, no.3, pp.1302-1313, Aug

[5] J. Berardino and C. Nwankpa, "Dynamic Load Modeling of an HVAC Chiller for Demand Response Applications," *IEEE Smart Grid Communications Conference*, Gaithersburg, MD, Oct. 2010.

Quantifying Economic, Operational, and Environmental Impacts of Adoption of Plug-in Hybrid Electric Vehicle on California Electricity Grid

Jingjie Xiao and Andrew L. Liu
School of Industrial Engineering, Purdue University
315 N. Grant Street, West Lafayette, IN 47907
xiaoj@purdue.edu, andrewliu@purdue.edu

Abstract-The concerns of the global climate change and heavily fluctuated oil prices have generated enormous amount of interests and efforts in developing and marketing the plug-in hybrid electric vehicle (PHEV). The major challenge that the system operators or utilities are facing is to meet the potential new load associated with the battery charging at the lowest net costs. And, the fact that the timing of the use of the electricity can possibly be controlled and optimized (e.g. charging during off-peak hours) is worth of a close look at. The study is designed to evaluate the potential shift in the use of electricity and the operation of electric power systems represented by the use of PHEVs. First, insights are provided through simulations on when the potential new load for the battery charging is consumed during the day for different charging scenarios. Second, a two-stage stochastic unit commitment model is formulated to assess the system economics through optimizing the on/off and generation level of California's hundreds of natural gas plants and reserve requirement when the large-scale wind energy is present. Moreover, the emissions associated with PHEVs from both the transportation and electricity generation sectors are examined.

I Key Figures

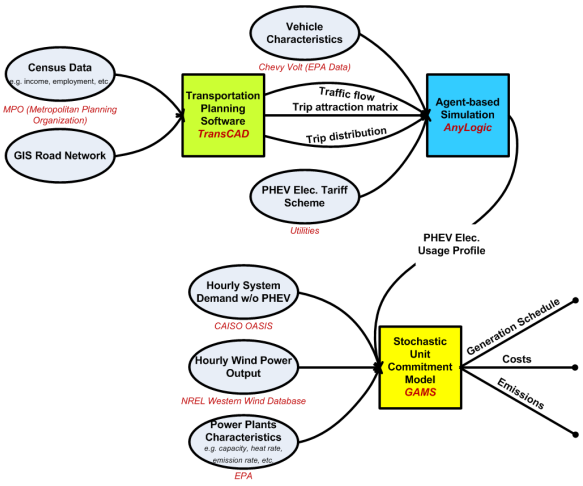

II Key Equations

$t = 1, \ldots, T$ RTM dispatch time periods
$n = 1, \ldots, N$ slow-start generating units
$m = 1, \ldots, M$ fast-start generating units

DAM Planning Decision
$z_{t,n}(z_{t,m})$ binary on-line generator
$x_{t,n}$ (MW) output of generator
$s_{t,n}$ (MW) scheduled spinning reserve
$r_{t,m}$ (MW) scheduled non-spinning reserve

Estimate of Random Outcome
μ_t (MW) forecast wind output

Cost Incurred in DAM Generation Planning
= slow-start units (start-up cost, fixed cost, variable fuel and O&M cost, and offer cost for contracting spinning reserve)
+ fast-start units (start-up cost, fixed cost, and offer cost for contracting non-spinning reserve)

Day-Ahead Market Constraints
Power Balance in period t ($t \geq 1$)
total generation = demand − forecast wind output

Operation Limits in period t ($t \geq 1$)
generation ≥ slow generator min output
generation + spinning rsv ≤ slow generator max output
non-spinning rsv ≤ fast generator max output

Start-up Costs
Minimum up and down Times
Ramping rates

$k = 1, \ldots, K$ realizations of wind outputs

RTM Dispatch Decision
v_t^k (MW) unsatisfied demand
$s_{t,n}^k$ (MW) actual spinning reserve
$r_{t,m}^k$ (MW) actual non-spinning reserve

Random Outcome
w_t^k (MW) kth realization of wind output
p_t^k prob. for kth realization

Expected Cost Incurred in RTM Dispatch
= expected cost for unsatisfied demand
+ slow-start units (expected variable fuel and O& M cost for providing spinning reserve)
+ fast-start units (expected variable fuel and O& M cost for providing non-spinning reserve)

Real-Time Market Constraints
Real-time Power Balance in period t and realization k
unsatisfied demand = max (0, demand − RT wind output − (generation + RT spinning rsv. + RT non-spinning rsv.))

Real-time Operation Limits in period t and realization k
RT spinning rsv. ≤ scheduled spinning rsv.
RT non-spinning rsv. ≤ scheduled non-spinning rsv.

III Key Results

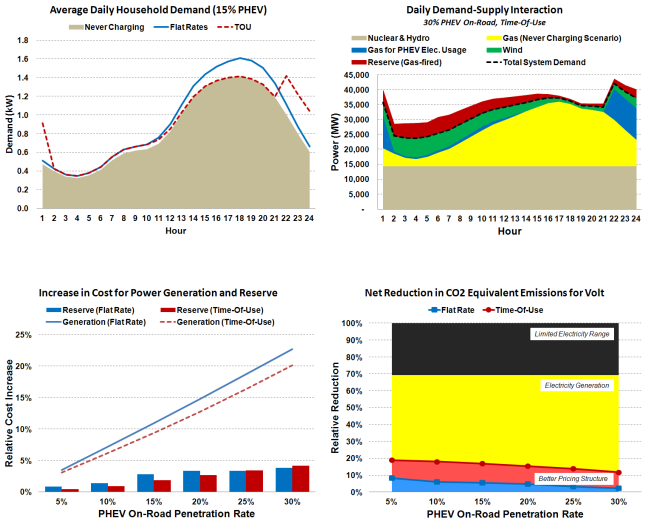

Modeling an Islanded Microgrid Addressing Power Quality Assessment

Q. Fu[1], L. F. Montoya[1], A. Solanki[1], A. Nasiri[1], V. Bhavaraju[2], and D. Yu[1]
University of Wisconsin – Milwaukee[1], Milwaukee, WI, 53201, USA[1]
Eaton Corporation Innovation Center, Milwaukee, WI 53216, USA[2]

***Abstract*— Microgrids are receiving a lot of attention to utilize distributed generations in a sub-system and provide higher efficiency and reliability and support local loads. In the poster, the standard IEEE 34 bus is selected and regarded as an islanded microgrid. The system parameters are scaled down to 12kV level and two renewable sources including solar PV and wind turbine, as well as two energy storage devices and a diesel generator have been added to the system. The system is modeled using PSCAD software and practical constraints of the components are considered. The monitoring requirements of the microgrid and control requirements for these Distributed Generations (DG) are managed to maintain the power quality of the system when loads are varied and the renewable sources are modeled with annual variation at different locations. The microgrid is monitored at number of buses and the power quality issues are measured and indexes are calculated.**

I. KEY FIGURES

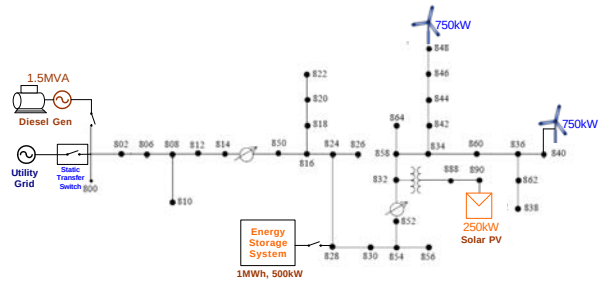

Figure 1. The configuration of the microgrid

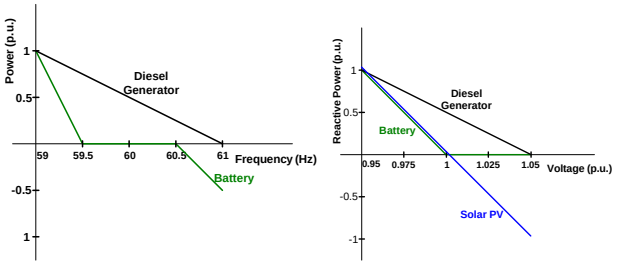

Figure 2. The droop mechanism

$$SAIDI = \frac{\text{Sum of all customer interruption durations}}{\text{Number of customers served}} \quad (1)$$

$$SAIFI = \frac{\text{Total number of customer interruptions}}{\text{Total number of customers served}} \quad (2)$$

$$CAIDI = \frac{\text{Sum of all customer interruption durations}}{\text{Total number of customer interruptions}} \quad (3)$$

II. KEY RESULTS

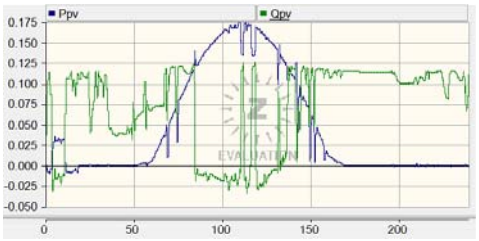

Figure 3. Active and reactive power delivered by 0.25MW solar PV.

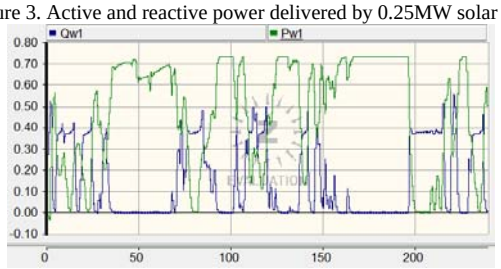

Figure 4. Active and reactive power delivered by one of the wind turbines

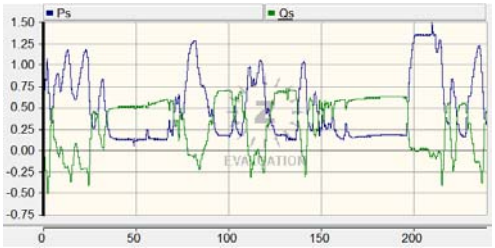

Figure 5. Active and reactive power delivered by the diesel generator.

Figure 6. Voltage profile of all sources in the system.

Table 1. Power quality parameters for three cases of the system

	Original Case 1	Case 2	Case 3
SAIDI (hrs)	3.25	0.91	0
SAIFI	166	796	0
CAIDI (hrs)	0.0196	0.0011	0

Risk Assessment Based on Information Entropy of Cascading Failure in Power Systems

Youwei Jia, *IEEE Student Member*, Zhao Xu, *Member, IEEE*

***Abstract*—Along with the high pace of power network interconnection development in recent years, power system operational uncertainty is increasing rapidly and system dynamic behavior is becoming more and more complicated, which makes the risk assessment of cascading failures and catastrophic events in power systems more challenging. Therefore advanced methods of high reliability to assess risks of cascading failures under various power systems operation conditions need to be developed. In this paper, a risk assessment framework for cascading failures based on the information entropy principle has been developed. The developed method aims at identifying the worst case cascading development among all other possibilities to support system operators in preparing countermeasures accordingly beforehand. A case study of cascading failure analysis for IEEE 30-bus system is carried out in details. *N-1* contingencies are selected as the initiating events of cascading failures. The weighting factors of all types of severity (i.e. transmission line overload, bus voltage violation, real/reactive power violation of generators) are determined by entropy principle, as compared with conventional methods which use fixed values according to expertise information with different focus. Finally, the feasibility and effectiveness of this proposed approach are demonstrated through MATLAB. The results show a high potential of this proposed method for further research and application.**

I. KEY EQUATIONS

- Entropy weight

The entropy of an index is defined as:

$$H_i = -k\sum_{j=1}^{n} f_{ij} \ln f_{ij} \qquad i = 1, 2, \cdots, m \tag{1}$$

The entropy weight of the i^{th} index is defined as:

$$\omega_i = \frac{1 - H_i}{m - \sum_{i=1}^{m} H_i} \tag{4}$$

- Severity of violation

i) Transmission line overload

$$Sev(L) = \begin{cases} \sum_i \left(\frac{F_{ki} - F^s_{k\,i}}{F^s_{k\,i}}\right)^{2m} & F_{ki} > 1.4F^s_{k\,i} \\ 0 & F_{ki} < 1.4F^s_{k\,i} \end{cases} \tag{5}$$

ii) High-limit/low-limit bus voltage violation

$$Sev(V_H) = \begin{cases} \sum_i \left(\frac{\Delta V_i}{V_{i-upper}}\right)^2 & V_i > V_{upper} \\ 0 & V_i < V_{upper} \end{cases} \tag{6}$$

$$Sev(V_L) = \begin{cases} \sum_i \left(\frac{\Delta V_i}{V_{i-lower}}\right)^2 & V_i < V_{lower} \\ 0 & V_i > V_{lower} \end{cases} \tag{7}$$

iii) Active/reactive power violation of generators

$$Sev(P) = \begin{cases} \sum_i \left(\frac{\Delta P_i}{P_{i-margin}}\right)^2 & P_i < P_{\min} or P_i > P_i > P_{\max} \\ 0 & P_{\min} \le P_i \le P_{\max} \end{cases} \tag{8}$$

$$Sev(Q) = \begin{cases} \sum_i \left(\frac{\Delta Q_i}{Q_{i-margin}}\right)^2 & Q_i < Q_{\min} or Q_i > Q_i > Q_{\max} \\ 0 & Q_{\min} \le Q_i \le Q_{\max} \end{cases} \tag{9}$$

- Risk assessment based on entropy weight

$$Sev = w_L Sev(L) + w_{V_H} Sev(V_H) + w_{V_L} Sev(V_L) + w_P Sev(P) + w_Q Sev(Q) \tag{10}$$

$$R(X) = P(X) \cdot Sev(X) \tag{11}$$

II. KEY FIGURE

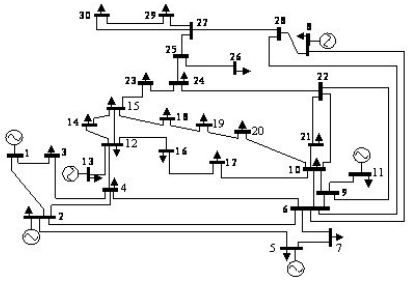

Fig. 1. Schematics of IEEE 30-bus system

III. KEY RESULTS

TABLE I. RISK RANKING OF CASCADING CHAINS

Ranking	Outage chains	Total risk	Load shedding
1	6,7,5,15,19,21	0.9397	251.45MW
2	6,7,18,15,19,21	0.2484	82.34MW
3	6,7,1,15,19,21	0.1953	32.12MW
4	6,3,2	0.1762	0
5	6,3,4	0.1718	0

The total load loss was taken as the severity criterion, the resulted risk based ranking matched the load loss based in Table I, which demonstrates the effectiveness of the proposed risk assessment approach.

An Affine Arithmetic Method to Solve the Stochastic Power Flow Problem Based on a Mixed Complementarity Formulation

Mehrdad Pirnia[1], Claudio Canizares[1], Kankar Bhattacharya[1] and Alfredo Vaccaro[2]
[1]Department of Electrical and Computer Engineering, University of Waterloo, Ontario, Canada, N2L 3G1
[2]Department of Engineering, University of Sannio, Benevento, Italy
Email: mpirnia@uwaterloo.ca , ccanizares@uwaterloo.ca , kankar@uwaterloo.ca , vaccaro@unisannio.it

***Abstract*— The Affine-Arithmetic (AA) method is applied to an optimization based power flow model to solve the stochastic power flow analysis problem. This model is used to obtain operational intervals for power flow variables considering active and reactive power demand uncertainties. The proposed AA-based algorithm is tested on a 14-bus test system and the results are then compared with the Monte-Carlo Simulation (MCS) results. The AA-based method shows slightly more conservative bounds; however, it is faster and does not need any information on statistical distributions of random variables.**

I. Key Equations

If the sources of uncertainties are assumed to be the real and reactive power injections, the affine forms of the real $\tilde{e}_i$ and imaginary $\tilde{f}_i$ components of the bus voltage magnitude can be presented as follows:

$$\tilde{e}_i = e_{i,0} + \sum_{j \epsilon N} e^P_{i,j}\, \varepsilon_{P_j} + \sum_{j \epsilon N} e^Q_{i,j}\, \varepsilon_{Q_j} \qquad \forall i,j \in N \quad (1)$$

$$\tilde{f}_i = f_{i,0} + \sum_{j \epsilon N} f^P_{i,j}\, \varepsilon_{P_j} + \sum_{j \epsilon N} f^Q_{i,j}\, \varepsilon_{Q_j} \qquad \forall i,j \in N \quad (2)$$

Using the above AA forms of real and imaginary bus voltages, affine forms of the real and reactive power can be obtained. Fig. 1 demonstrates the method to obtain operational intervals for power flow variables. Center values represent the value of a variable considering the given deterministic case, i.e., when uncertainties are neglected; and noise magnitudes represent deviations of the power flow variables due to the uncertainties. There is also a probability (ε) associated with each noise magnitude.

Fig. 2 demonstratesA a comparison between the bounds for bus voltage magnitudes, obtained from the AA-based approach and the MCS method. As shown above, the AA-based approach generates slightly more conservative bounds.

This work was supported by a grant from ABB Corporate Research, USA and MITACS Canada

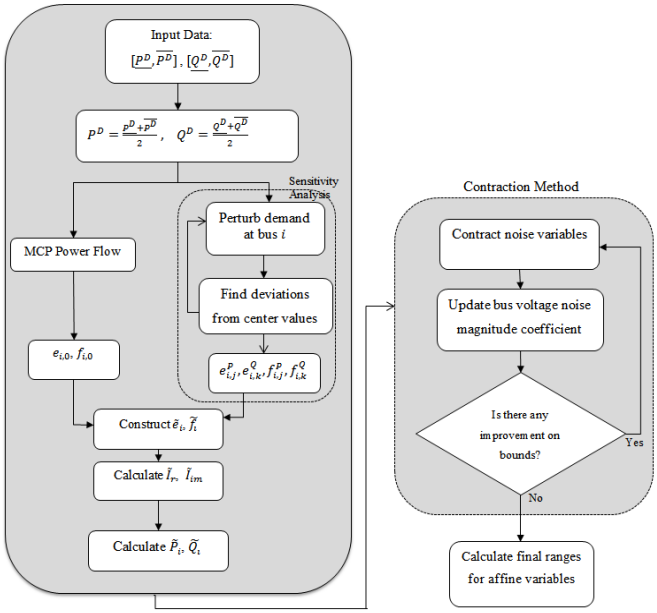

Figure 1. Algorithm to Calculate Operational Intervals for Power Flow Variables

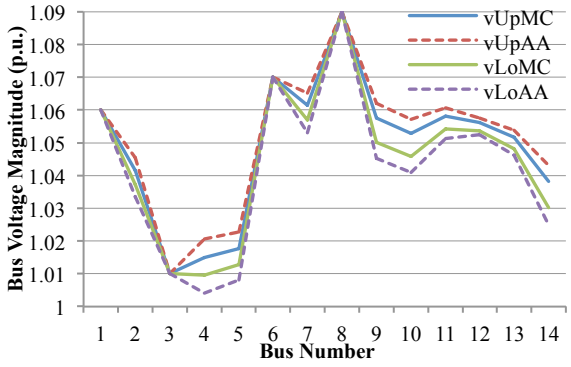

Figure 2. Bus Voltage Magnitude Bounds Using AA and MCS

II. Conclusion

The stochastic power flow problem is solved using the AA-based method. This approach does not rely on random variables' probability distribution functions, and is not an iterative-based method. Thus, it is solved much faster than the MCS method and is computationally less complicated than other suggested stochastic approaches. The obtained results from this approach are very close to the MCS method.

Assigning Weights for PMU Measurements: Two Alternative Methods

Liuxi Zhang, *Student Member, IEEE*, and Ali Abur, *Fellow, IEEE*
Department of Electrical and Computer Engineering
Northeastern University, Boston, MA, USA
Email: lzhang@ece.neu.edu and abur@ece.neu.edu

***Abstract*—Assignment of proper weights to measurements remains an important problem in power system state estimation. The weights are commonly specified by users based on assumed accuracies of conventional measurements. Since such historical information may not be available for new kinds of measurements such as those received from Phasor Measurement Units (PMUs), weight assignment for such measurements becomes a challenge. This paper investigates possible alternatives and suggests two different approaches to address this problem. Simulated scenarios using IEEE 14-bus system as well as laboratory tests are used to illustrate the application of suggested approaches.**

Keywords- PMU measurement system, measurement weight, measurement accuracy

I. KEY EQUATIONS

The measurement equation formulated in power system state estimation is in the form of

$$z = \begin{bmatrix} z_1 \\ z_2 \\ \vdots \\ z_m \end{bmatrix} = \begin{bmatrix} h_1(x_1, x_2, \dots, x_n) \\ h_2(x_1, x_2, \dots, x_n) \\ \vdots \\ h_m(x_1, x_2, \dots, x_n) \end{bmatrix} + \begin{bmatrix} e_1 \\ e_2 \\ \vdots \\ e_m \end{bmatrix} = h(x) + e \quad (1)$$

The measurement errors are normally assumed with following characteristics:

1) The mean of measurement error is zero:

$$E(e_i) = 0, \quad i = 1, 2, \dots, m \quad (2)$$

2) Errors of measurements are independent so that

$$cov(e) = E(e \cdot e^T) = R = \begin{bmatrix} \sigma_1^2 & & & \\ & \sigma_2^2 & & \\ & & \ddots & \\ & & & \sigma_m^2 \end{bmatrix} \quad (3)$$

The measurement residuals can be calculated as below:

$$r = Se \quad (4)$$

The covariance matrix of measurement residuals is derived from (4):

$$\begin{aligned} R_r &= cov(r) \\ &= S \cdot cov(e) \cdot S^T \\ &= S \cdot R \cdot S^T \\ &= S \cdot R \end{aligned} \quad (5)$$

Only considering the diagonal elements, since R is diagonal as shown in (3), equation (5) can be reformulated as follows:

$$R(i,i) = \frac{R_r(i,i)}{S(i,i)} \quad (6)$$

II. KEY FIGURES

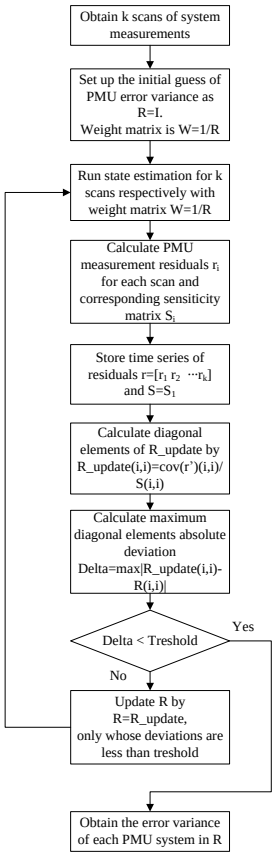

Fig.1. Flow chart of estimating accuracies through state estimator

III. KEY RESUTLS

TABLE I
RESULTS OF PMU ACCURACY TEST THROUGH METHOD A IN IEEE 14-BUS SYSTEM (VARIANCES GIVEN IN RADIAN^2)

PMU	*R_perfect*	*R_origin*	*R_result*	*R_actual*
θ_2	10^{-6}	1	2.61×10^{-6}	2.3×10^{-6}
θ_3	10^{-6}	1	9.68×10^{-7}	4×10^{-7}
θ_4	10^{-6}	1	7.49×10^{-7}	2.4×10^{-6}
θ_5	10^{-6}	1	8.28×10^{-7}	1.8×10^{-6}
θ_6	10^{-6}	1	1.72×10^{-7}	6×10^{-7}
θ_7	10^{-2}	1	0.0148	0.0148
θ_8	10^{-6}	1	3.78×10^{-6}	1.5×10^{-6}
θ_9	10^{-6}	1	9.16×10^{-7}	4×10^{-7}

This paper is based on work that was supported in part by the Power Systems Engineering Research Center.

Development of an Agent-Based Distribution Test Feeder with Smart-Grid Functionality

Pedram Jahangiri, *Student Member, IEEE,* Di Wu, *Student Member, IEEE,* Wanning Li, *Student Member, IEEE,* Dionysios C. Aliprantis, *Senior Member, IEEE,* and Leigh Tesfatsion, *Member, IEEE*

***Abstract*—This poster reports on the development of an agent-based distribution test feeder with smart-grid functionality. The test feeder is based on an actual distribution feeder with various additional features incorporated, including rooftop photovoltaic generation and price-responsive loads (e.g., plug-in electric vehicles and intelligent air-conditioning systems). This work aims to enable the integrated study of wholesale electric power markets coupled with detailed representations of the retail-side distribution systems.**

***Index Terms*—Air conditioning, electric vehicles, multi-agent systems, photovoltaic systems, power distribution, smart grid.**

Pedram Jahangiri (S'10) received the B.S. and M.S. degrees in electrical engineering from Isfahan University of Technology and Sharif University of Technology, Iran, in 2006 and 2008, respectively. He is currently working toward the Ph.D. degree in the Department of Electrical and Computer Engineering at Iowa State University, with research emphasis on smart distribution systems. He has been previously employed as a researcher by the Electric Ship Research and Development Consortium, Mississippi State University, MS, USA, and by the Automation of Complex Power Systems Center, RWTH University, Aachen, Germany.

Di Wu (S'08) received the B.S. and M.S. degrees in electrical engineering from Shanghai Jiao Tong University, China, in 2003 and 2006, respectively. He is currently a Ph.D. candidate in the Department of Electrical and Computer Engineering at Iowa State University. His research interests include impacts of plug-in electric vehicles on power systems; planning of national energy and transportation infrastructures; power electronics, with applications in hybrid electric vehicles and wind energy conversion systems.

Wanning Li (S'12) received the B.S. degree in electrical engineering from Harbin Institute of Technology, China, in 2011. She is currently working toward the Ph.D. degree in the Department of Electrical and Computer Engineering at Iowa State University. Her research interest lies in energy market risk management, and market efficiency assessment.

Dionysios C. Aliprantis (SM'09) received the Diploma in electrical and computer engineering from the National Technical University of Athens, Greece, in 1999, and the Ph.D. from Purdue University, West Lafayette, IN, in 2003. He is currently an Assistant Professor of Electrical and Computer Engineering at Iowa State University. He was a recipient of the NSF CAREER award in 2009. He serves as an Associate Editor for the *IEEE Power Engineering Letters*, and the *IEEE Transactions on Energy Conversion*. His research interests are related to electromechanical energy conversion and the analysis of power systems. More recently his work has focused on technologies that enable the integration of renewable energy sources in the electric power system, and the electrification of transportation.

Leigh Tesfatsion (M'05) received the Ph.D. degree in economics from the University of Minnesota in 1975. She is Professor of Economics, Mathematics, and Electrical and Computer Engineering at Iowa State University. Her principal research area is agent-based test bed development, with a particular focus on restructured electricity markets. She is an active participant in IEEE PES working groups and task forces focusing on power economics issues. She serves as associate editor for a number of journals, including *J. of Energy Markets*.

Modeling and Planning of EV Fast Charging Station in Power Grid

Champa Hemamali Dharmakeerthi, Nadarajah Mithulananthan and Tapan Kumar Saha.
The University of Queensland, Brisbane, Queensland 4072, Australia

***Abstract*- Introduction of the electric vehicle (EV) to the transport sector is greatly anticipated considering numerous environmental and socio-economical benefits. Consideration of their charging impact on electricity networks is of major importance to power system engineers under such circumstances. A number of system studies can be found in the literature describing different aspects of EV charging on power grid. However, scant attention has been paid to the issue of power system stability due to EV charging. Practicality of the power system stability studies is mainly determined by the accuracy of the models used to represent the EV load. However, EV load modeling for system stability studies has not yet been considered in the literature. Hence, for this study, a static load model has been developed for a universal input battery charger at the first stage. The second phase of the study considers static voltage stability margins, system losses, the regulatory voltage limits, and the cable flow ratings for appropriate placement of EV fast charging stations in electricity grid. Further, the maximum allowable charging station capacity at a network point is evaluated based on reliable and stable grid operation.**

I. KEY EQUATIONS

Power consumption of the charger is given by,

$$P = V_B i_B + r{i_B}^2 + \frac{2}{3}\left({Ri_B}^2 k^2 / {D_d}^2 \right) \quad (1)$$

where,

$$k = (V_B + ri_B)/V_r \quad (2)$$

and

$$D_d = \frac{V_d \pm \sqrt{{V_d}^2 - \frac{8}{3} R i_B V_r k}}{2V_r} \quad (3)$$

For R=0.1 Ω and 0.01 Ω, the load models are given by (4), (5).

$$P/P_o = 0.9061 + 0.0939\left(V/V_o\right)^{-3.715} \quad (4)$$

$$P/P_o \approx \left(V/V_o\right)^0 \approx 1 \quad (5)$$

Charging station placement considers system loading margin(LM), Generator reactive power limits, total system losses, voltage regulatory limits, and cable MVA flow limits as given in (6)- (10).

$$\text{LM} = \lambda_* - \lambda_0 \quad (6)$$

Where λ_*-loading parameter at collapse point

λ_0-loading parameter for the based case

$$Q_i^{gmin} \le Q_i^g \le Q_i^{gmax} \quad i = 1,2 \ldots . n_g \quad (7)$$

$$V_i^{reg.min} \le V_i^l \le V_i^{reg.max} \quad i = 1,2 \ldots . n_l \quad (8)$$

$$P_L = \sum_i^n \sum_j^m -G_{ij}({V_i}^2 + {V_j}^2 - 2V_i V_j cos\emptyset_{ij}) \quad (9)$$

$$|S_{ij}| \le S_{ij}\,\text{max} \quad (10)$$

I. KEY RESULTS

TABLE I
SIMULATION RESULTS FOR DIFFERENT CHARGING STATION PLACEMENTS

Con-nec-cted Bus	CONSTANT POWER LOAD MODEL			CONST. POWER & VOLTAGE DEPENDENT LOAD MODEL		
	Power Losses /(MW)	Most significant line Loading	Loading Margin	Power Losses /(MW)	Most significant line Loading	Loading Margin
Base	0.1411	-	2.876	0.1411	-	2.876
5	0.1641	3-5-63.1%	2.401	0.1648	3-5 -63.5%	1.870
6	0.1650	3-6-75.7%	2.396	0.1657	3-6–76.1%	1.862
8	0.1793	4-8-84.7%	2.345	0.1801	4-8-85.2%	1.721
9	0.1650	3-9-57.5%	2.394	0.1657	3-9-57.9%	1.860
15	0.1812	4-15-70.3%	2.327	0.1821	4-15-70.5%	1.860
24	0.1790	4-24-66.9%	2.342	0.1798	4-24-67.2%	1.810
27	0.1789	4-7-61.92%	2.342	0.1797	4-7-62.34%	1.808
16	0.1789	4-7-61.92%	2.339	0.1797	4-7-62.34%	1.802
26	0.1642	3-26-40.9%	2.399	0.1650	3-26-41.3%	1.865

TABLE II
CONSEQUENCES OF INCREASING CHARGING STATION CAPACITY FOR CONSTANT POWER LOAD MODELING

No of Charging spaces	Consequences of charging
25	Voltage at connected bus 0.89 p.u., Cable 3-9 loaded 99% MVA rating. (Upgraded by adding similar cable in Parallel). Load Margin-0.8608
28	Voltage at connected bus 0. 88 p.u., Cable 9-25 loaded 102.6% MVA rating. (Upgraded by adding similar cable in Parallel) Load Margin-0.5748
46	Voltage at connected bus 0. 85 p.u., Load Margin-0.0078
47	Unstable operating point. Voltage collapsed due to reactive power limit induced Bifurcation at bus 50.

TABLE III
CONSEQUENCES OF INCREASING CHARGING STATION CAPACITY FOR CONSTANT POWER AND VOLTAGE DEPENDENT LOAD MODELING

No of Charging spaces	Consequences of charging
22	Cable 3-9 loaded 99.3% MVA rating. (Upgraded by adding similar cable in Parallel). Load Margin-0.507
24	Voltage at connected bus 0.89 p.u., Load Margin-0.4028
26	Voltage at connected bus 0. 88 p.u., Cable 9-25 loaded 100.5% MVA rating. (Upgraded by adding similar cable in Parallel) Load Margin-0. 305
35	Voltage at connected bus 0. 76 p.u., Load Margin-0.0092
36	Unstable operating point. Voltage collapsed due to reactive power limit induced Bifurcation at bus 50.

Topology Comparison of 3-Phase Solid State Transformers based on Efficiency and Control

Sachin Madhusoodhanan, *Student Member, IEEE*

FREEDM Systems Center, Department of Electrical and Computer Engineering, North Carolina State University, Raleigh, NC 27606, USA,

Email: sachin@ncsu.edu

Abstract – **There is a need for a 3-phase interface at the substations between the transmission and the distribution grids for controlling the power flow. Traditionally the line frequency transformers have been used for this purpose which has certain limitations. They are bulky in size and weight. They don't have a provision for improving the quality of power drawn from the grid. They only allow unidirectional power flow. They have improper voltage regulation and offer lesser flexibility in control. So an alternative is needed to replace these conventional transformers. What is being proposed in this poster is to replace these transformers with semiconductor devices based 3-phase Solid State Transformers (SST). Concept of solid state transformers has been developed sometime back. But because of unavailability of Silicon based semiconductor devices which can block such a high level of voltage, it never got materialized. Recently, with the development of Silicon Carbide (SiC) based devices with higher voltage blocking capability of up to 15kV, this is feasible. Also the high frequency Pulse Width Modulation based switching of these devices offers a considerable reduction in size and weight. These switching devices offer a greater flexibility in control. This results in a 3-phase SST with bidirectional power flow capability. Through control of these devices it is possible to maintain unity power factor at the grid, thus improving the power quality. Also it will be possible to improve the grid voltage profile under necessary conditions such as fault, voltage sag etc. through reactive power compensation. All these features are achievable at efficiency very close to that of the conventional transformers.**

I. KEY FIGURES

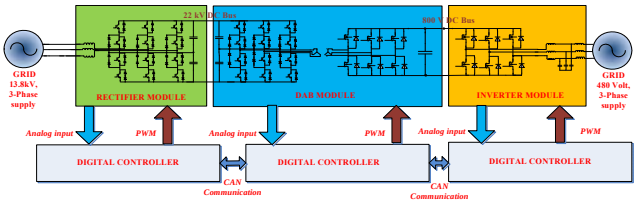

Figure 1: Block diagram of voltage source based 3-phase SST

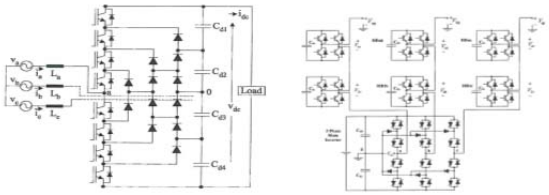

(a) (b)

Figure 2: Possible Front End Converters for voltage source based 3-Phase SST (a) 5-Level Rectifier (b) Series Active Filter

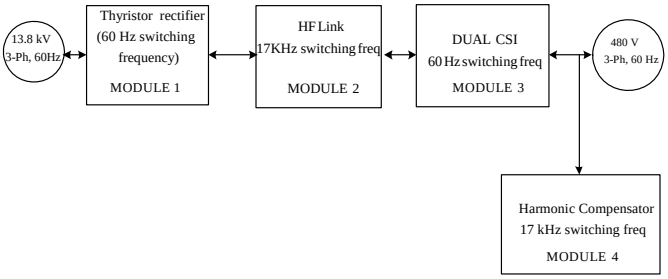

Figure 3: Block diagram of current source based 3-phase SST

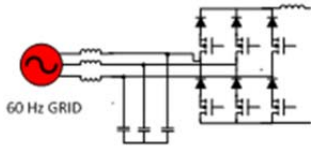

Figure 4: Buck Rectifier as the Front End Converter for current source based 3-Phase SST

II. KEY RESULTS

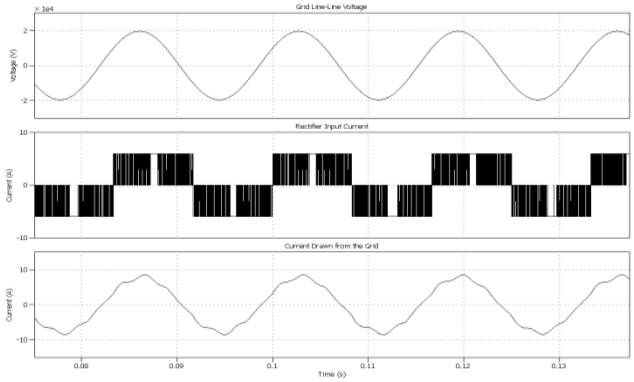

Figure 5: Buck Rectifier simulation results showing Grid Voltage, Rectifier Input Current and Filtered Grid Current for a 13.8 kV, 100 kVA system

Test Condition (100KVA, 3-Level NPC)		f_{sw}**=3kHz,** ***UPF Mode***	
Device		**Si IGBT**	**SiC MOSFET**
Total Loss (W)		1830.54	325.53
Efficiency (η%)		98.17	99.67
Middle Device	**Switching Loss (W)**	260.5	8.655
	Conduction loss (W)	21.29	22.3
Top/Bottom Device	**Switching Loss (W)**	0	0
	Conduction loss (W)	18.8	18.8
Clamping diode (W)		4.5	4.5

Figure 6: Efficiency Estimation done with a 3-level NPC using 6.5 kV Si IGBT and 10 kV SiC MOSFET

Effects of Price-Responsive Residential Demand on Retail and Wholesale Power Market Operations

Auswin George Thomas[a], *Chengrui Cai*[b], *Pedram Jahangiri*[c],
Dr. Di Wu[d], *Dr. Huan Zhao*[e], *Prof. Leigh Tesfatsion*[f], *Prof. Dionysios Aliprantis*[g]
Department of Electrical and Computer Engineering {a,b,c,g} and Department of Economics{f}
Iowa State University, Ames, IA, USA, Email: *(agthomas, ccai, pedramj, tesfatsi, dali)@iastate.edu*
Pacific Northwest National Laboratory[d], Richland, WA, USA, Email: *Di.Wu@pnnl.gov*
ISO-New England[e], Holyoke, MA, USA, Email: *hzhao@iso-ne.com*

***Abstract*— In this project, a novel intelligent residential air-conditioning (A/C) system controller with smart grid functionality has been developed. The qualifier "intelligent" means the A/C system has advanced computational capabilities and uses an array of environmental and occupancy parameters in order to provide optimal intertemporal comfort/cost trade-offs for the resident, conditional on anticipated retail energy prices. The term "smart-grid functionality" means that retail energy prices can depend on wholesale energy prices. Simulation studies are used to demonstrate the capabilities of the proposed A/C system controller. To implement these studies, a computational platform using AMES (agent-based power market simulation software) and a distribution system modeling software has been developed for studying integrated retail and wholesale power market operations. An example is provided below to illustrate the dynamic feedback loop connecting residential A/C load, the energy prices determined at wholesale conditional on A/C load, and the retail energy prices offered to residential A/C consumers by wholesale energy buyers.**

I. KEY FIGURES

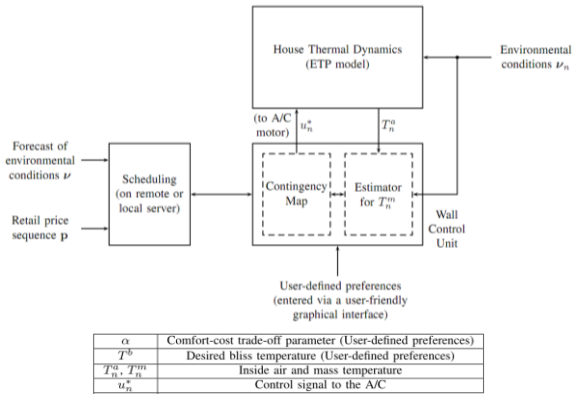

α	Comfort-cost trade-off parameter (User-defined preferences)
T^b	Desired bliss temperature (User-defined preferences)
T_n^a, T_n^m	Inside air and mass temperature
u_n^*	Control signal to the A/C

Figure 1. Structure of the Intelligent A/C Controller

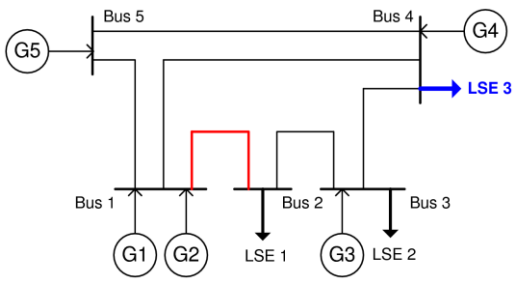

Figure 2. Five Bus Test Case with LSE 3's load determined by the intelligent A/C load. (LSE 1 and LSE 2 have arbitrary loads)

II. KEY RESULTS

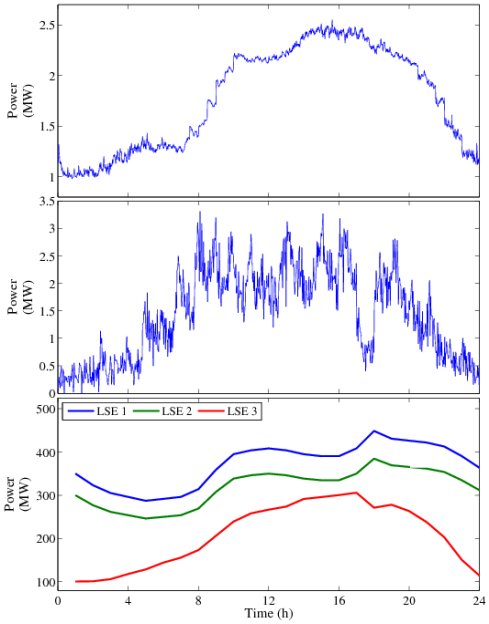

Figure 3. a) Non-price-responsive load in the distribution feeder; b) Intelligent A/C load in the distribution feeder; c) Daily load profiles for the LSEs, averaged by hour.

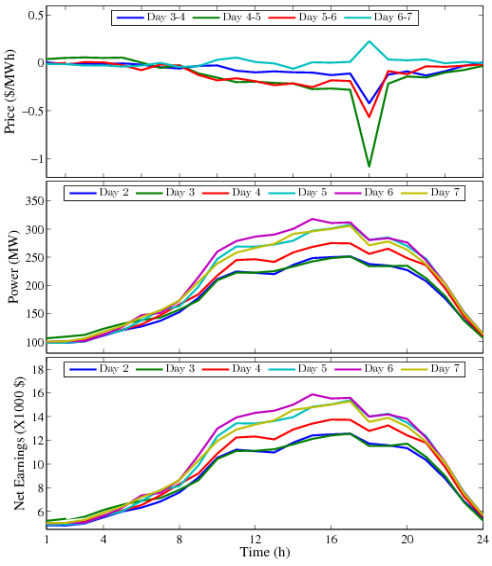

Figure 4. a) Differences between day-ahead and real-time LMPs; b) The aggregated load profile at bus 4; c) Hourly net earnings of LSE 3 from the two-settlement system.

Different Classes of Oscillation Monitoring systems: Advantages and Disadvantages

S. Arash Nezam Sarmadi and Mani V. Venkatasubramanian
School of Electrical Engineering and Computer Science
Washington State University
Pullman, WA 99163
Email: snezamsa@eecs.wsu.edu, mani@eecs.wsu.edu

Abstract— **One of the fundamental part of reliable operation and control of power system is the accurate knowledge and estimation of the low-frequency electromechanical oscillations [1]. This mode estimation basically can be done with two different approaches: using the system model and linearizing it about the equilibrium operating points or using mode estimation methods based on the measurement data [2]. The later is known as oscillation monitoring system which can monitor oscillations in real-time. Measurement based approaches also divide into three different methods: Block processing, Recursive and Prony methods. In the block processing methods we use a time window and estimate modes in that fixed size window and then we can update our window whenever we want and a new calculation can be done completely independent of the previous window. But in the recursive methods, estimated modes are updated with each new sample of data so the mode estimation updates based on the new sample and previous estimation.**

There are two different types of measurement data: ringdown data and ambient data. A ringdown data is the response to a sudden disturbance in power system such as outage of a generator or line tripping which result in a significant oscillation. But under the ambient data condition, power system is operating at its steady state condition and the system input is the continuous change of loads and other small variations which can be assumed as a white noise. Some of the measurement based methods can estimate the modes only for one of these types while others can be applied on both of them. Since these ambient data are always available and they act as non-intrusive, the algorithms which can be applied on the ambient data are more attractive [3]. Fig. 1 Shows the general classification of the mode estimation methods in power system.

For each of these methods different algorithms have introduced to do the mode estimation or specifically to find the mode's frequencies and damping ratios but since each of these methods has some advantages and disadvantages, more research need to be done to estimate the modes correctly with the least error. Hence one of the most crucial things we need to consider before developing an algorithm is to recognize and understand these advantages and disadvantages and exploit the best and appropriate one.

This poster introduces the advantages and disadvantages of these methods and some algorithms within each method. It also compares them in terms of different factors using simulated PMU data and archived PMU data.

Keywords- block processing; electromechanical oscillations; mode estimation; oscillation monitorin; recursive methods

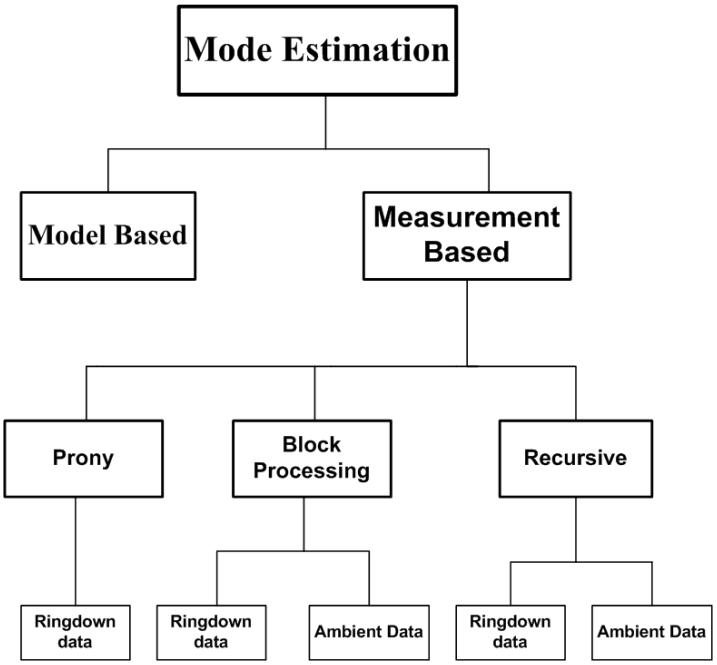

Figure 1. General Classification of the mode estimation methods.

REFERENCES

[1] J. W. Pierre, D. J. Trudnowski and M. K. Donnely, "Initial Results in Electromechanical Mode Identification from Ambient Dat," *IEEE trans. on power syst.*, vol.12, no.3, pp. 1245-1250, Aug. 1997.

[2] P. Kundur, *Power System Stability and Control*, New York: McGraw-Hill, Inc., 1994.

[3] G. Liu and V. Venkatasubramanin, "Oscillation Monitoring from Ambient PMU measurements by Frequency Domain Decomposition," IEEE international symposium on circuit and systems, May 2008, pp. 2821-2824.

Real-Time Intelligent Operation of Hybrid AC/DC Smart Grids

Ahmed Mohamed, *Student Members*, *IEEE* and Osama Mohammed, *Fellow*, *IEEE*

***Abstract*—This paper presents a real-time energy management algorithm for hybrid AC/DC microgrids involving sustainable energy and hybrid energy storage. This hybrid storage system consists of super capacitors (SC) for ultra-fast load matching beside lithium-ion batteries for relatively long term load buffering. The energy management algorithm aims mainly at managing the energy within the system such that the effect of pulse (short duration) loads on the power system stability is minimized. Moreover, an average annual saving of around 7% is achieved by shifting loads to off-peak hours. The expected energy needed during a future peak, the time of its occurrence and the current state of charge of both elements of the hybrid storage system are all examples of the inputs to the algorithm. A non-linear regression technique is used to obtain mathematical models for the uncertain quantities including load and sustainable energy curves. The results show a significant improvement for the system in terms of voltage and power stability by applying the proposed algorithm.**

I. Real-Time Energy Management Algorithm

The main objective of the real time energy management algorithm developed in this paper is to mitigate pulse loads. Besides, the total cost of energy is to be reduced using this algorithm by minimizing the energy drawn from the main grid and/or shifting it to off-peak hours. Therefore, we can define two main modes of operation namely; the pulse load mitigation mode and the normal operation or cost minimization mode. A fuzzy agent is employed as a part of the developed management algorithm.

II. Key Results and Figures

In order to evaluate the performance of the algorithm under normal and pulse loads, an example hybrid AC/DC system was simulated. Fig. 1 shows the PV and load data of the 24 hours at a certain day (D1=200) of the year. As can be seen, by using the developed algorithm (*Algorithm 1*) to handle the battery's energy, we save money by shifting the energy highlighted in the figure (E_{PK}) as compared to the conventional operation (*Algorithm 2*). Figures 2 and 3 show the response of the system to a series of pulse loads. If the developed algorithm is used, the batteries/SC set is ready to supply the pulsed loads and mitigate its effect on the rest of the system. Therefore, the DC bus voltage and the frequency oscillations are within limits. Fig. 3 shows this situation using the conventional algorithm. After the second pulse, the battery injected power is zero, and then the AC generators are totally responsible for the next two pulses. As can be seen, there are large oscillations in AC generation levels and the super capacitor's power. The DC bus voltage drops to 0.82 p.u.

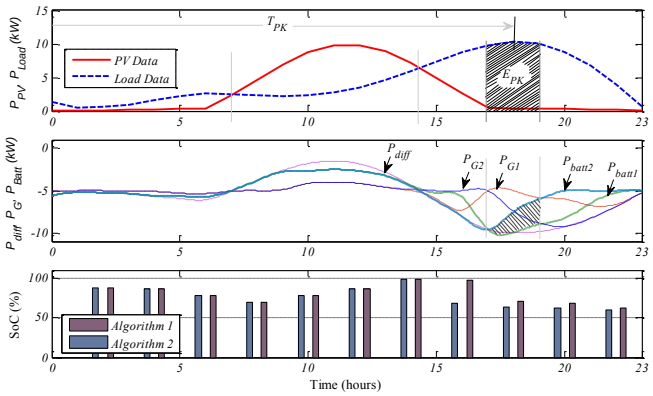

Fig. 1. Operation of the system for a 24 hours interval, while applying *Algorithms 1* and *2*.

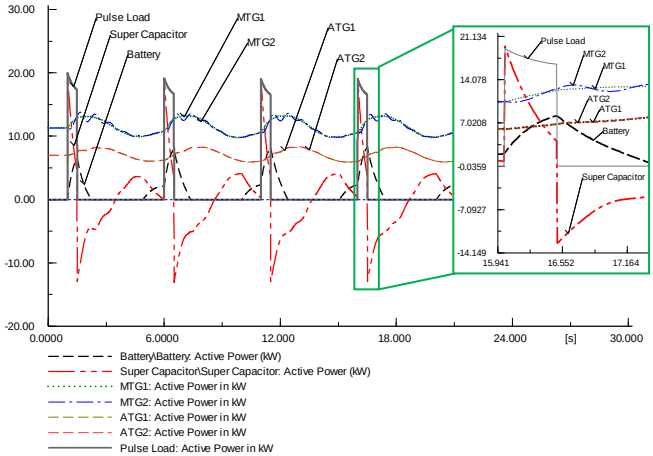

Fig. 2. Active power of the pulsed loads and the power sharing among AC generators, super capacitor and full-charged battery (*Algorithm 1*)

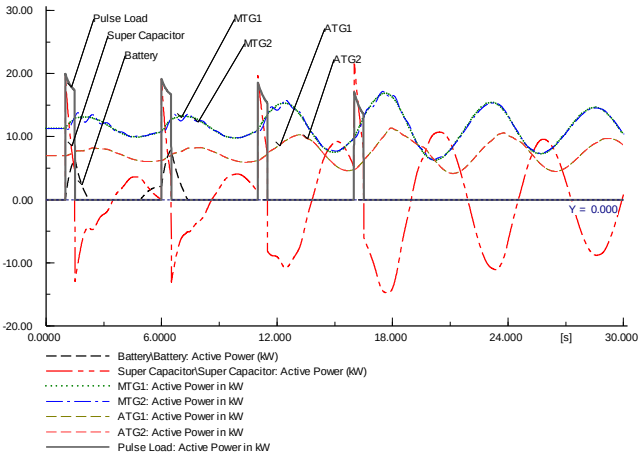

Fig. 3. Active power of the pulsed loads and the power sharing among AC generators, super capacitor and half-charged battery (*Algorithm 2*).

Voltage Unbalance Analysis of Distribution Systems Using a Three-Phase Power Flow and a Genetic Algorithm for PEV Fleets Scheduling

Alejandra Jiménez, *Student Member, IEEE,* and Norberto García, *Member, IEEE*

***Abstract*—A powerful blend based on a three-phase distribution power flow method and a Genetic Algorithm for plug-in electric vehicular fleets scheduling is proposed in this paper. The Genetic Algorithm optimizes the number of charging and discharging plug-in electric vehicles in order to efficiently manage voltage unbalances and power losses. The plug-in electric vehicle based on a voltage controlled representation is incorporated into a power flow formulation suitable for radial and unbalance distribution network. The PEV model comprises a voltage source converted (VSC) and a battery pack. While active power is regulated at the storage device according to the charging and discharging status of battery, the voltage magnitude at the point of common coupling is regulated by the VSC. Furthermore, a comprehensive VSC-based PEV equivalent model that accurately reflects the behavior of a distributed vehicular fleet is proposed in this work to carry-out efficient steady-state analyses. The impact of a plug-in vehicular fleet in the voltage unbalance of the IEEE 13-node test feeder is optimized with a multiobjective genetic algorithm, where each PEV is modeled as a Tesla Roadster EV with a lithium-ion battery pack.**

I. Key Equations.

In order to evaluate the effects of the PEVs on the distribution feeder, the Genetic Algorithm evaluates each proposed solution using a three-phases distribution power flow method is based on the relationship between the bus injections to branch currents and the branch currents to bus voltages,

$$\mathbf{i_b} = \mathbf{A_{BIBC}} \cdot \mathbf{i} \tag{1}$$

$$\mathbf{v}_0 - \mathbf{v} = \mathbf{\Delta v} = \mathbf{A_{BCBV}} \cdot \mathbf{i_b} \tag{2}$$

The mismatches at the bus voltages caused by the variations at current injections are obtained by combining (1) and (2),

$$\Delta \mathbf{v} = \mathbf{A_{BIBC}} \cdot \mathbf{A_{BCBV}} \cdot \mathbf{i} = \mathbf{A_{DLF}} \cdot \mathbf{i} \tag{3}$$

The distribution power flow iterative process is given by,

$$\Delta \mathbf{v}^{k+1} = \mathbf{A_{DLF}} \cdot \mathbf{i}^k \tag{4}$$

$$\mathbf{v}^{k+1} = \mathbf{v}_0 + \triangle \mathbf{v}^{k+1} \tag{5}$$

$$I_i^k = \left(\frac{P_i + jQ_i}{V_i^k} \right)^* \tag{6}$$

Assuming $\hat{V}_{EV}$ is the desired voltage at PEV controlled voltage node, then the voltage mismatch is defined as,

$$\Delta V_{EV} = \left| \hat{V}_{EV} \right|^2 - \left| V_{EV}^{k,l} \right|^2 \tag{7}$$

Then the reactive power error in terms of the voltage mismatch is given by,

$$\Delta Q_{EV}^{k.l} = \frac{\Delta V_{EV}}{2 \boldsymbol{X}_{EV}} \tag{8}$$

where

$$\boldsymbol{X}_{EV} = im \left(\mathbf{A_{BCBV}}(i,:) \cdot \mathbf{A_{BIBC}}(:,i) \right) \tag{9}$$

II. Key Figures and Results.

A. Charging from the grid

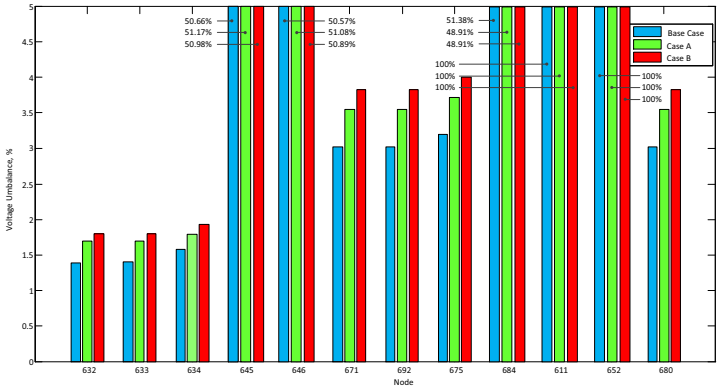

Figure 1. Percent of voltage unbalance for PEV fleet demanding active power.

B. Discharging to the grid

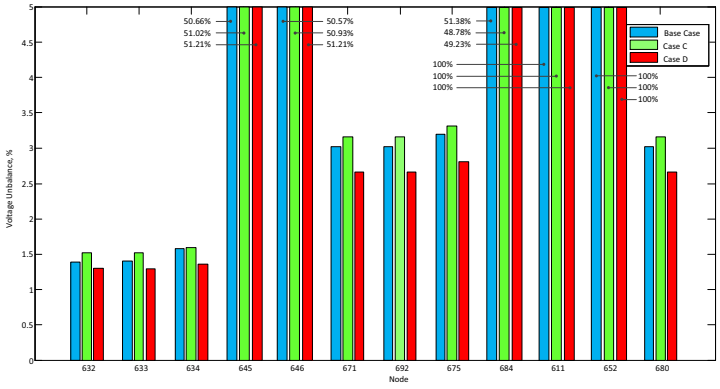

Figure 2. Percent of voltage unbalance for PEV providing active power.

Developing Smart Grid Demonstrations and Experiments

Authors: Abderrahmane Elandaloussi, Dr. Noel Schulz
Department of Electrical and Computer Engineering
Kansas State University Manhattan, KS USA
Email: aelanda1@ksu.edu

Currently, most lab experiences in the power curriculum of many universities deal with subjects such as power electronics, renewable energy, and power conversion. However, lab experiments concerning the new concept of the smart grid and its complex set of topics including communications, networking, and cyber-security are just starting to evolve. Kansas State University developed a smart grid laboratory class that worked to involve graduate students in the development of demonstrations and experiments to highlight features and capabilities related to smart grid applications. This course addresses the education as well as industrial perspectives of the smart grid concept. Six graduate students and the professor worked together in developing the initial lab demonstrations and experiments. It is a new approach to help students have a better grasp of what constitutes a smart grid on a basic level. This course was a very interactive course where the students and the professor worked together to devise a plan on developing a smart grid laboratory. The educational aspect of this class involves going through multiple steps in order to devise labs that demonstrate electric power protection and communication techniques in a smart grid setting. The industrial aspect of the lab provides the students with hands on experience with real protection and communication devices, reading reference manuals, and communicating with engineers from industry; providing the students with a better understanding of how to apply theory in the real world. This poster will involve an overview of the process taken in the class to create labs that represent components of the smart grid. It will include the labs that were constructed in the class and explain how each of them relates to the field of smart grid. The objective is to enable students interested in the upcoming field of smart grid to have a practical approach on the subject rather than just pure theory.

Air Conditioner Optimal Scheduling Using Best Response Techniques

J. Dang, *Student Member, IEEE,* and Ronald G. Harley, *Fellow, IEEE*
School of Electrical and Computer Engineering
Georgia Institute of Technology
Atlanta, GA, 30332 USA
jdang3@gatech.edu, rharley@gatech.edu

Abstract—**With the development of demand side management (DSM) for future smart grid applications, residential loads are expected to provide elastic response to fluctuating generation. In this paper, an air conditioner (AC) schedule optimization algorithm, for the smart meter energy consumption scheduler (ECS), using best response technique, is proposed. The performance and improvement of this algorithm, with optimal customer and utility benefits, is also presented at the end of the paper.**

Keywords-Demand side management, air conditioner, schedule optimization

I. INTRODUCTION

For residential customers, DSM can be implemented by smart meters, which control the household appliances, and in this paper, only AC is considered. The ECS of a smart meter analyzes the information of outside temperature and other customers' energy usage, and synthesizes the optimal day-ahead schedule for the AC it controls. In this paper, the best response technique in game theory is employed to propose a schedule-optimization algorithm.

II. AC SCHEDULING MODEL

A. Energy Cost Model

In this section, the analysis investigates m customers for n hours in a day. The energy cost of each house is modeled as a function of the day-ahead scheduled indoor temperature. The energy consumption for customer i and hour j is $P_{i,j} = \frac{T_{i,j} - T_{i,j-1} - \alpha \cdot (T_{out\_j} - T_{i,j-1})}{\beta_i}$, and the total energy cost function is assumed to be quadratic with the form of $C_{total} = \sum_{j=1}^{n} c \cdot E_j^{\,2} = \sum_{i=1}^{m} C_i$, where E_j denotes the total energy consumption in this area in hour j.

The optimization problem is defined as: given the outside temperature and other customers' energy usage, find the optimal value of $T_i = [T_{i,1}, T_{i,2}, \ldots, T_{i,n}]$ to minimize C_i.

B. Best Response Optimization

The derivative of energy cost C_i respect to $T_{i,j}$ is $\frac{dC_i}{dT_{i,j}} = \frac{P_{i,j} + E_j}{\beta_i} - \frac{(1-\alpha)\cdot(P_{i,j+1} + E_{j+1})}{\beta_i}$. Because $dC_i / dT_{i,j}$ is negative, the algorithm replaces $T_{i,j}$ by $T_{i,j} + 1$, so the cost C_i decreases for the AC operating in a cooling state until no more cost reduction is possible by changing $T_{i,j}$. Then the algorithm optimizes the next customer's schedule, according to the change in previous customers' schedules. Finally, all the customers' temperature settings T are optimized with individual minimum cost.

III. SIMULATION RESULT

To illustrate the algorithm, the results of a typical case with 3 customers and 13 hours (8 am – 9 pm) in a day (m=3, n=13) are presented in Fig. 1. The energy costs of the optimized schedule are compared with those without optimization, and the savings are presented in Table I.

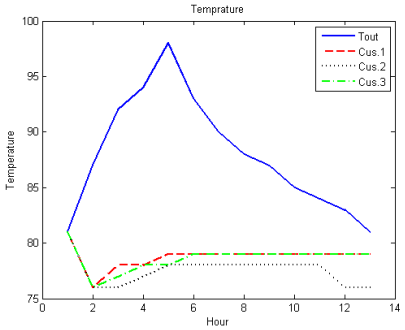

Fig. 1. Temperature optimization result with minimum energy cost.

TABLE I
COST COMPARISON W/ AND W/O SCHEDULE OPTIMIZATION

T_i Setting	Energy Cost	Saving
$(T_{\min} + T_{\max})/2$	\$7.495	8.8%
rand $(T_{\min}, T_{\max})$	\$10.644	35.78%
Optimal Result	\$6.835	

IV. CONCLUSION

The method proposed in this paper can be integrated in the smart meter ECS function to schedule the air-conditioning (AC) usage one day ahead to achieve minimum energy cost. The simulation results show that the energy cost of each customer is less than the cost of setting the AC temperature at one fixed point, or randomly within a certain range, with an improvement of 8.8% or 35.78% respectively.

DC Fault Interruption Using Reactor-Assisted AC Circuit Breaker

Saurabh Kulkarni, *Student Member, IEEE,* and Surya Santoso, *Senior Member, IEEE*

***Abstract*—A fault on an MVDC distribution system results in a fault current with no zero crossings. This makes clearing such faults challenging using any traditional interruption techniques. Furthermore, for faults with low fault resistance (or even bolted faults) the transient DC fault current has a high magnitude impulse and a short rise time. To maintain continuity of supply to healthy parts of the power system and to prevent damage to any equipment, it is essential to limit the fault current magnitude and physically isolate the faulted section as soon as possible. However, DC circuit breakers for MVDC applications are still in the research and development stage. An innovative concept of using a reactor assisted AC circuit breaker to interrupt DC faults at the terminals of a phase-controlled rectifier will be demonstrated. The addition of the reactor causes the rising fault current to oscillate and have zero crossings which are inherently absent from DC systems. A conventional AC circuit breaker can then be employed to interrupt the fault current during the first zero crossing. Using the proposed scheme for the example case, the fault current magnitude is reduced from 56 kA to 14 kA, while the interruption time is reduced from 44 ms to 25 ms.**

I. Key Figures

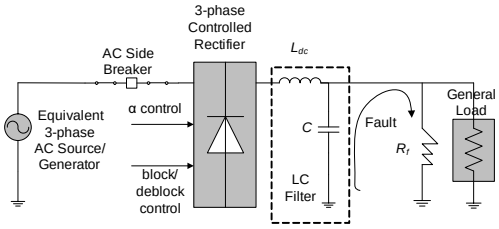

Fig. 1. Controlled Rectifier with Fault at the Terminals

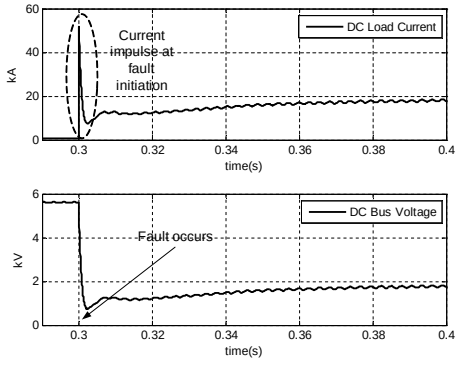

Fig. 2. Fault Voltage and Current Profile for Circuit shown in Fig. 1

II. Key Equation

S. Kulkarni and S. Santoso are with the Department of Electrical and Computer Engineering at the University of Texas at Austin.

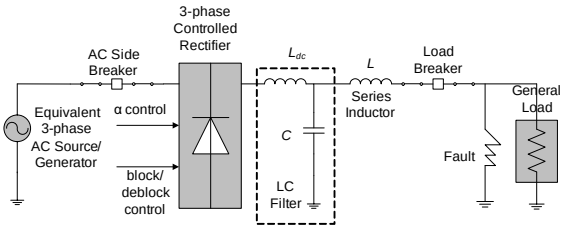

Fig. 3. Controlled Rectifier with Series Inductor and AC Breaker

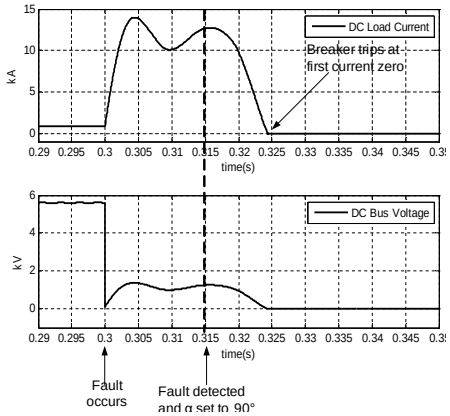

Fig. 4. Fast Fault Current Interruption Using AC Circuit Breaker

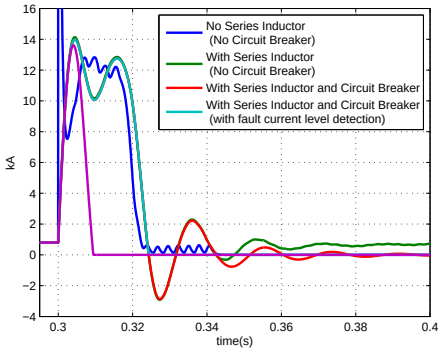

Fig. 5. Comparison of Fault Current Interruption Techniques

TABLE I
Quantities for Mode 1 Operation of Rectifier, $\alpha = 0$

μ (radian)	$-\alpha + \arccos\left(\cos(\alpha) - \frac{2\omega L_c i_{dc0}}{\sqrt{3}E_m}\right)$
$\bar{V}_{dc}(t)$	$\frac{3\sqrt{3}E_m}{\pi}\cos(\alpha) - i_{dc0}\left(\frac{3\omega L_c}{\pi}\right) - L_c\frac{d\bar{i}_{dc}}{dt}\left(2 - \frac{3u}{2\pi}\right)$
$\frac{d\bar{i}_{dc}}{dt}$	$\frac{\frac{3\sqrt{3}E_m}{\pi}\cos(\alpha) - i_{dc0}\left(R_{dc} + \frac{3\omega L_c}{\pi}\right) - e_{dc}}{L_{dc} + L_c\left(2 - \frac{3u}{2\pi}\right)}$

Integrating Distribution System Operational Constraints into Demand Side Management

B. Moradzadeh, *Student Member, IEEE*, and K. Tomsovic, *Fellow, IEEE*

***Abstract*--Demand Side Management (DSM) is one of the key components of the future smart grid. DSM helps to reduce peak load and adapt elastic demand to fluctuating generation from renewables. This paper suggests a decentralized optimization of energy consumption of residential customers. The objective of the optimization is to reduce peak load as well as costs for the customers while taking customer satisfaction into account. As an important feature, distribution system constraints such as equipment capacity, line flow limits, and voltage constraints are taken into account. Local agents in the houses interact with the energy provider's agent to arrive at a real time price, which reflects the aggregated load on the substation. Different customers and appliances have different disutility functions based on the detailed model of the load. In addition, the agents use different optimization tools to schedule the energy consumption.**

***Index Terms*-- Demand Side Management (DSM), Multi-Agent Optimization, Dual Decomposition, Real-Time Pricing (RTP).**

I. Key Equations

The general form of the optimization model for optimal operation of residential energy hubs is as follows:

min ***F***

s.t. Network constraints

Appliances constraints

where ***F*** is the objective function based on social welfare which is the cost imposed to the utility company as well as customer dissatisfaction. Since the centralized optimization suffers from many issues, a decentralized approach is developed based on dual decomposition of the Lagrangian multiplier.

II. Key Figures

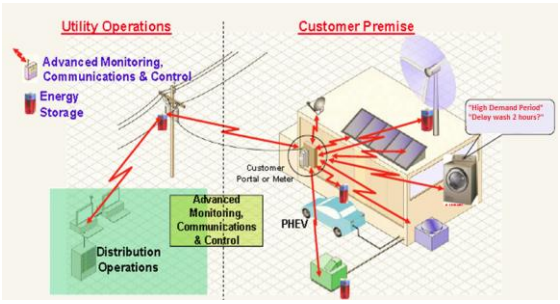

Figure 1. Interaction between HANs and utility company

III. Key Results

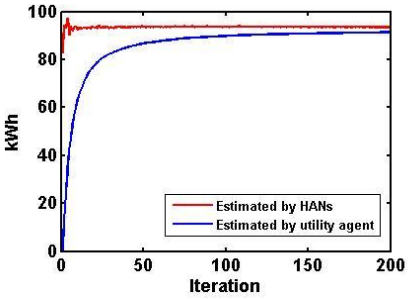

Figure 2. Convergence of the algorithm at the aggregator

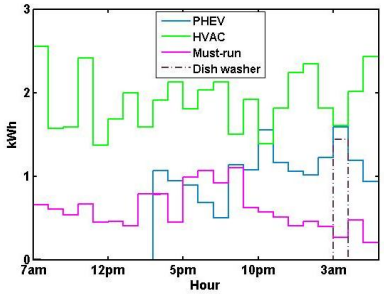

Figure 3. Energy consumption of different appliances in a house

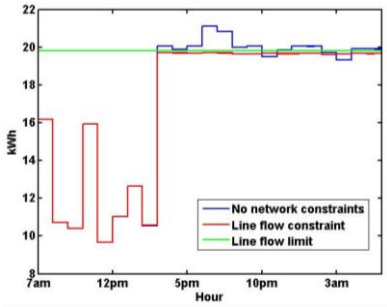

Figure 4. Effect of network constraints on appliance scheduling

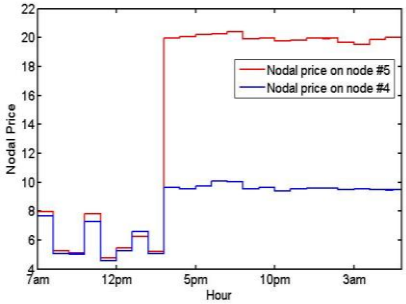

Figure 5. Effect of network constraints on nodal prices

Identification of Power System Inter-area Oscillation by Analytic Wavelet Transforms

Daham Min
School of Electrical and Electronic Engineering, Yonsei University, Seoul, South Korea,
Email: gockachu@gmail.com

***Abstract*—This poster presents an improved damping estimation technique that can track the temporal variations in the inter-area oscillation. Damping of electro-mechanical oscillations is considered useful indicator for system operation. Based on bandpass theory and analytic wavelet transforms, the proposed technique is suitable in tracing damping of oscillation with synchronized phasor measurements at a high sampling rate. This will focus on modes of our interest and avoid unnecessary computational burden. Also, this method is able to estimate time-varying damping ratios of the selected modes. Case studies on a 179-bus power system and real measurement data show that estimated system damping can be utilized to investigate the potential separation boundaries.**

I. Key Equation

The mother wavelet of AWT is defined as

$$\psi(t) = g(t)\exp(j\eta t) \tag{1}$$

Inter-area oscillation which are observed in a power system are usually modeled, $v(t)$ as $v(t) = \alpha(t)cos\theta(t) = \alpha e^{-\zeta\omega_n t}\cos(\omega_d t + \phi)$. In the case of such a signal, its AWT can be obtained as follows:

$$Wv(u,s) = \frac{1}{2}\alpha(u)\hat{\psi}_{u,s}(\omega(u),\sigma,\eta)\,e^{j\theta(u)} + \varepsilon(\alpha'(t),\omega') \tag{2}$$

$$\ln\left(\frac{2|Wv(u,s(u))|}{(4\pi\sigma^2 s(u)^2)^{1/4}}\right) \approx -\zeta\omega_d u + \ln\alpha \tag{3}$$

By substituting t for u, (3) can be rewritten in the form of time-varying damping ratio ζ_i.

II. Key Result

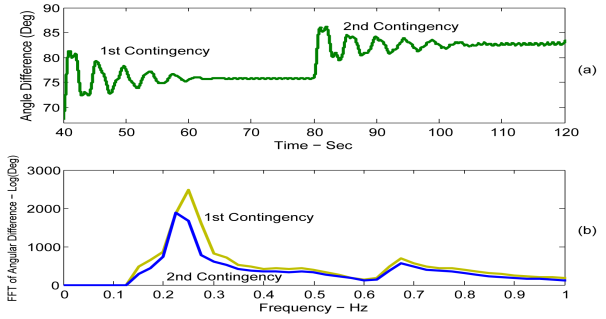

Fig. 1. (a) Angle differences between directly connected elementary coherent groups and (b) FFT analysis of the each contingency.

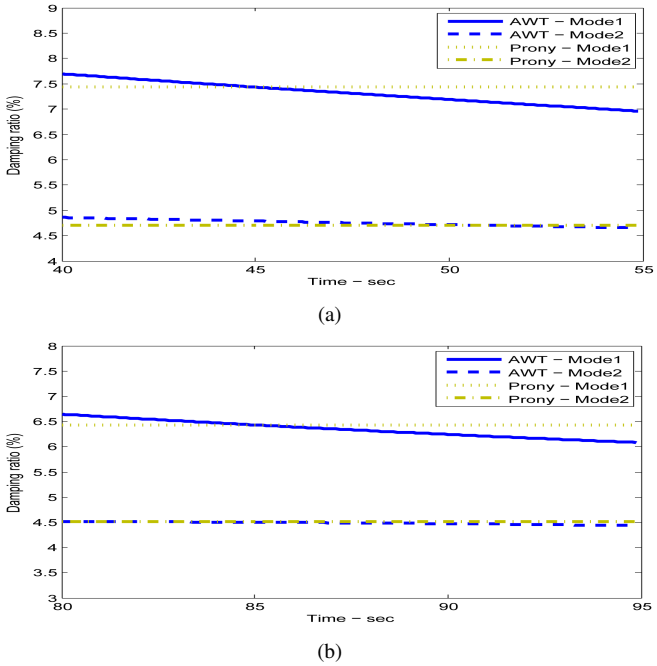

Fig. 2. (a) Damping ratio plot of AWT method and Prony analysis in the 1st contingency and (b) 2nd contingency.

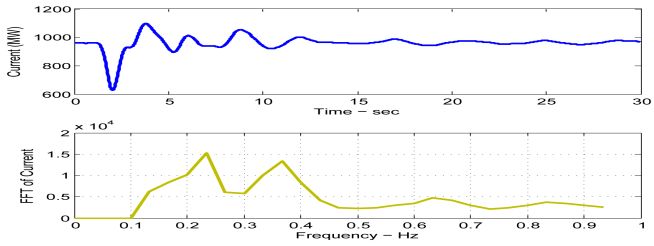

Fig. 3. (a) Maln-Round Mountain 1 current - June 24, 2004 and (b) FFT analysis of the current.

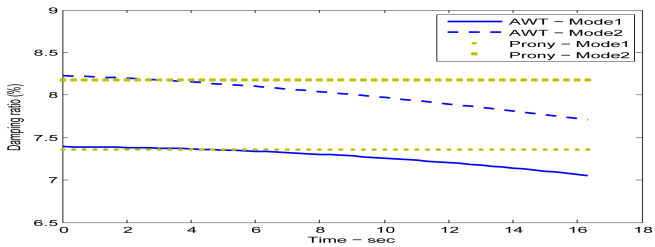

Fig. 4. Estimated time-varying damping ratio of MALN-Round Mountain on June 24, 2004.

A Stochastic Dynamic Programming Method for Optimizing Vehicle-to-Grid Frequency Regulation

Jonathan Donadee and Marija Ilic
Department of Electrical and Computer Engineering
Carnegie Mellon University
5000 Forbes Avenue, Pittsburgh, PA 15213
Email: jdonadee@andrew.cmu.edu, milic@ece.cmu.edu

***Abstract*— Smart electrical grid infrastructure, such as advanced metering, will enable demand side participation in electrical energy and ancillary services markets. Deterministic optimization models have been proposed for minimizing the cost of charging individual and fleets of Electric Vehicles (EVs) within market settings. These models include revenues that EVs could earn by providing ancillary services such as secondary frequency regulation. Providing regulation makes future state of charge (SOC) uncertain. If a vehicle is providing unidirectional regulation, it is possible that the SOC can reach the battery maximum, ceasing to provide regulation and violating the regulation contract. Also, the wrong choice of charging and regulation decisions could leave a high probability that the EV will not be completely charged by the driver's desired departure time. Optimization models in the literature do not appropriately value the risks of providing regulation, but instead impose arbitrary constraints on charging and regulation decisions. We propose a stochastic dynamic programming method for optimizing EV charging and unidirectional regulation decisions. First we formulate a stochastic deterministic equivalent integer linear program(DEP) which properly values the risks of providing frequency regulation for one hour given a state of charge. Our method proceeds by strategically solving many of these problems at the final decision time before the EV unplugs given many possible SOCs. The results are used to create an approximate, convex, piecewise-linear optimal value function (OVF) of SOC at that decision time. This OVF of SOC is then added to problems of the next, earlier, decision period in a backwards recursion. The process is repeated until arriving at the initial decision time, where the current SOC is known. Optimal decisions can then be made and implemented while correctly valuing the risks of providing regulation. Simulations demonstrate the benefit of charging an EV with our method over an expected value dynamic programming scheme.**

I. Key Equations

The objective function to be minimized when making the final decision before the EV unplugs is shown below in (1) and (2).

$$V_H(E_{i,H}) = \min_{P_{i,H},\,B_{i,H}} \; c_H P_{i,H} - r_H B_{i,H} + \theta \qquad (1)$$

$$\theta = \frac{1}{N}\sum_{\omega\in\Omega_N}\Big(c_H \sum_{t=1}^{t_f-1}\left(-B_{i,H}\cdot R_t^{\omega}\cdot \Delta t - s_t^{\omega}\right) + \cdots \qquad (2)$$

$$Q\cdot\Delta t\cdot B_{i,H}\cdot\textstyle\sum_t u_t^{\omega} + L\cdot T^{\omega} + c_{H+1}(E_{max} - e_{t_f}^{\omega})\Big)$$

The objective function to be minimized when making earlier decisions is shown below nearly the same as above but with (3) replaced by the OVF of future decisions shown in (4).

$$L\cdot T^{\omega} + c_{H+1}(E_{max} - e_{t_f}^{\omega}) \qquad (3)$$

$$V_{h+1}\left(e_{t_f}^{\omega}\right) \qquad (4)$$

II. Key Figures

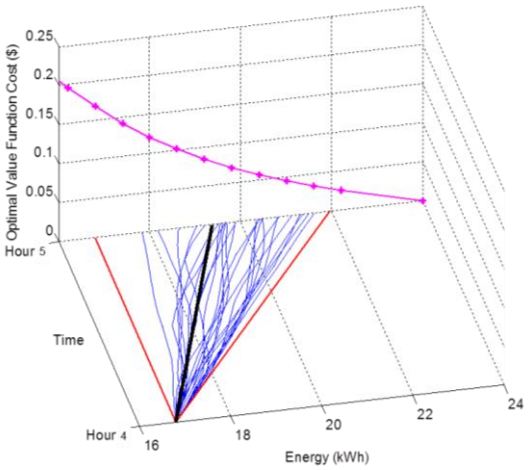

Figure 1. SOC in 30 sample realizations of the DEP with OVF in magenta

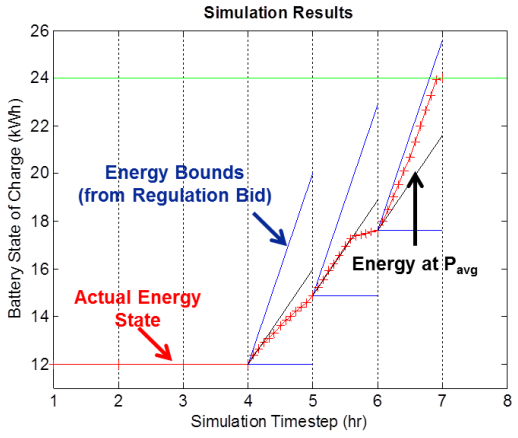

Figure 2. Example resulting SOC path and bid decisions from implementing the proposed method

A Novel Method of Wireless Power Supply and Charging for Appliances in Smart Houses

Jinchi Han, Jianmin Ding and Zhaoguang Pan
Department of Electrical Engineering, Tsinghua University, Beijing, 100084, China
Email: hanjc09@mails.tsinghua.edu.cn , djm09thu@gmail.com and panzg09@163.com

Abstract — **With the development of smart grid technologies, smart appliances in smart houses become more and more essential and required. People are seeking for convenient and flexible power supply and charging method for facilities. In this work, we introduce a novel method for WPT, which might provide a better choice for the smart appliances in smart houses.**

With the discovery of the giant magnetoelectric (ME) effect, the detection of magnetic signals based on it is receiving more and more concern. A ME composite is comprised of two layers of magnetostrictive materials outside and one layer of piezoelectric material inside. The magnetostrictive materials are forced to deform under the AC magnetic field, and the piezoelectric material is also forced to deform. As a result, the piezoelectric material generates electric charges, which accumulate at the poles. We assume that if better materials are used and the strength of magnetic field is enlarged, this method could possibly be used to transmit power.

Our work consists of three parts: magnetic field generator, ME composites, and simple management of the power transmitted for appliances. The generator could produce 0.65mT magnetic field in the middle of the notch with $1A_{pp}$ current. A Sandwich-Structure ME composite is comprised of two layers of magnetostrictive materials (Metglas) outside and one layer of piezoelectric material (PFC) inside. The resonant frequency is quite determined by the length of the composites. The voltage and current generated are sinusoidal with a double frequency of the primary current. The power transmitted are rectified and regulated before it is used to drive loads. We present two general applications: direct power supply and charging.

I. KEY FIGURES

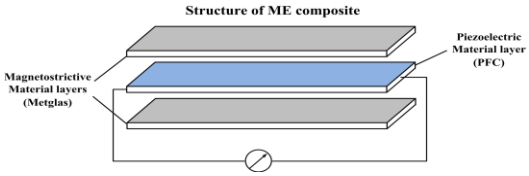

FIG.1. Structure of ME composites

II. KEY RESULTS

power characteristics

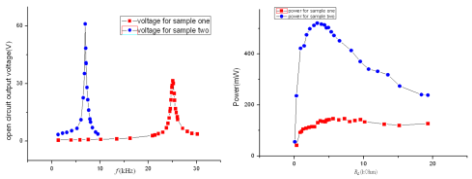

FIG.2. The power characteristics of a single composite

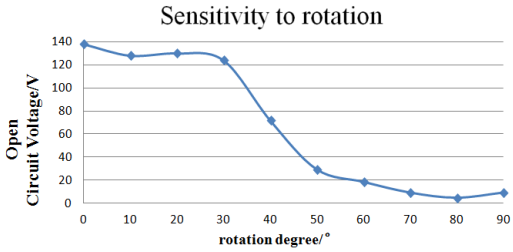

FIG.3. The sensitivity to rotation

Residential Energy Management using multi-resolution Moving Window Algorithm

M. Beaudin, *Student Member, IEEE* , H. Zareipour *Member, IEEE*, A. Schellenberg, *Member, IEEE*

***Abstract*—Residential energy management is an attractive research topic due to the opportunities offered by the coming of Smart Grid, and increasing concern of greenhouse gas emissions. An automated technology that can economically improve residential load management on behalf of the consumer are power schedulers, by influencing energy consumption and production schedules for a single dwelling. However, it can be difficult to create a high resolution schedule without significant adverse effects from shortsightedness and forecast errors. This work presents a multi-resolution moving window algorithm (MWA) that can address both issues. It builds on the moving window topology in [1], on the physical system presented in [2], which includes the systems in Figure 1 under time of use pricing and daily peak demand charge. The Moving Window Algorithm (MWA) is compared to a baseline model, and the impact of timing parameters such as rescheduling interval and scheduling window size are evaluated and discussed. The Moving Window Algorithm outperforms the baseline in all cases, and is shown to be more robust to forecasting errors.**

I. Key Figures

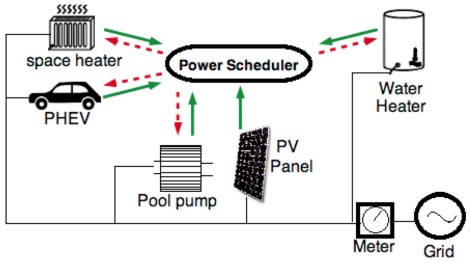

Fig. 1. Energy Optimizer high-level operations

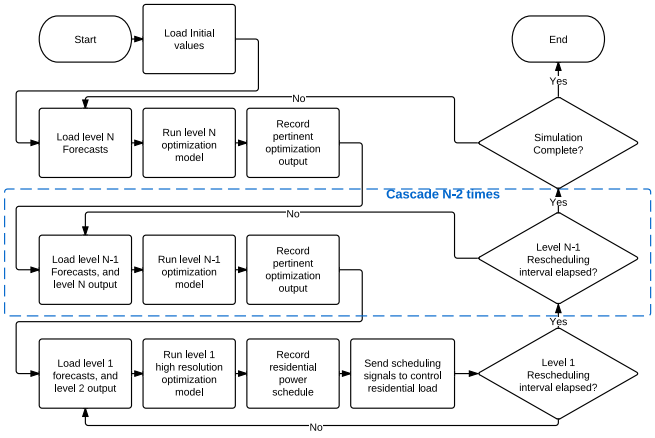

Fig. 2. Flowchart of Moving Window Algorithm

TABLE I
Value of Energy Services over 1-year simulation ($\times$ 1000 $)

Model	Base, No forecast error	MWA, No forecast error	Base, forecast error	MWA forecast error
Total Value	29.447	30.160	27.733	30.144
Electricity Cost	1.2287	1.3504	1.2358	1.3597
Space heater	4.0191	4.6594	2.5968	4.6592
Water heater	6.0922	6.2564	5.7781	6.2487
PHEV	2.1462	2.1462	2.1458	2.1476

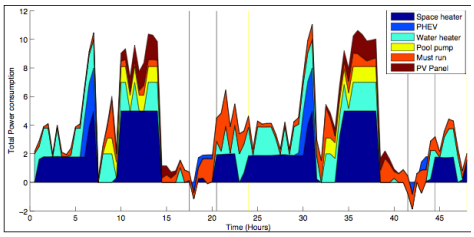

Fig. 3. Power consumption (kW) over two day simulation

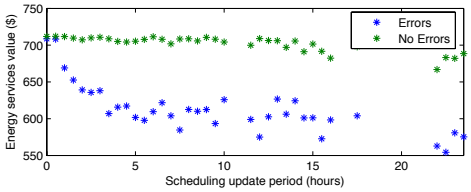

Fig. 4. Value of Energy Services vs. Rescheduling Interval

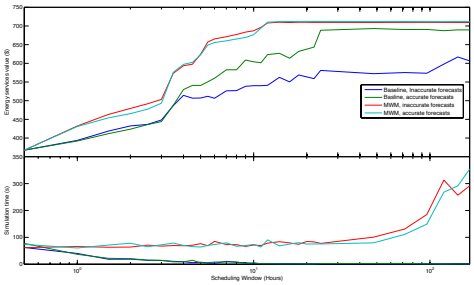

Fig. 5. Value of energy services vs. Scheduling Window size

References

[1] D. Livengood and R. Larson, "The energy box: Locally automated optimal control of residential electricity usage," *Service Science*, 2009.

[2] M. A. A. Pedrasa, T. D. Spooner, and I. F. MacGill, "Coordinated scheduling of residential distributed energy resources to optimize smart home energy services," *Smart Grid, IEEE Transactions on*, vol. 1, no. 2, pp. 134 –143, sep. 2010.

Synchrophasor Data Quality

Karl Reinhard
Department of Electrical and Computer Engineering, University of Illinois at Urbana-Champaign (UIUC) Urbana, IL 61802
reinhrd2@illinois.edu

***Abstract*—This poster describes efforts by the Trustworthy Cyber Infrastructure for the Power Grid (TCIPG) research project and the Midwest Independent Transmission System Operator (MISO) to investigate and characterize synchrophasor data quality. The poster outlines the research approach, describes MISO's observed synchrophasor data errors, and makes an initial effort to classify the error types.**

I. INTRODUCTION

United States 'Smart Grid' initiatives envision high-quality, complete, and timely synchrophasor data as a cornerstone for improving electric power grid efficiency and reliability. However through early 2012, power system operators report that synchrophasor data availability falls well short of levels required to realize the vision. UIUC's TCIPG is developing a research partnership with MISO to pursue a fundamental understanding of real-time synchrophasor measurement challenges, PMU data quality measures (error, availability, and reliability), methods for detecting faulty PMU data, and the implications of and remedies for defective PMU data.

II. SYNCHROPHASOR DATA QUALITY CHARACTERIZATION

A. *Data Characterization*

The TCIPG/MISO research collaboration seeks to isolate the sources and corresponding frequencies of defective synchrophasor data. The model at Fig 1. depicts nominal data flow from the point of measurement to the control room and data archive with four levels and connecting transmission paths. Each level has an identifiable role in generating, processing, and forwarding data to meet power system requirements – and as such becomes a possible point of failure. Attributing defective synchrophasor data sources and corresponding error rates is key to prioritizing efforts to improve data quality.

B. *Identified Error Sources and Proposed Error Type Classification*

MISO has been studying the synchrophasor data received from its stakeholders to identify error sources. Table 1 is a sampling of the identified error sources; the table also classifies the errors by type and identifies levels within the synchrophasor data flow that the error can occur. Future work will include data-mining synchrophasor archives to identify the frequency at which each error is occurring and attributing errors to specific locations in the synchrophasor system.

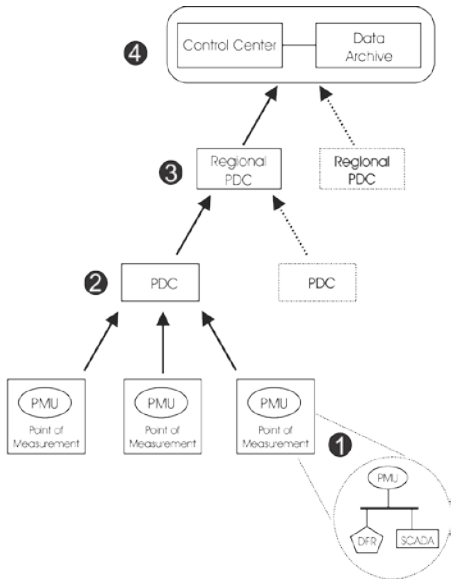

Figure 1. Nominal synchrophasor data flow from the point of measurement to the Control Center and Data Archive

TABLE I. Identified Error Sources and Proposed Error Type Classifications

Error Source	Level(s)	Error Type
Status Code Errors	1,2,3	Data Processing
Data streams disordered / shifted in processing	1,2,3	Data Processing
Loss of PDC Configuration	2,3,4	Data Processing
Improperly configured PMUs (window length/ windowing method)	1	Digital Signal Processing
Frequency calculation discrepancies (C37.118.2005)	1	Digital Signal Processing
Quality of Metering	1	Equipment Specification
Accuracy Issues (CT/PTs not properly rated for application)	1	Equipment Specification
Calculation Uncertainty -- Vendor Equipment operating differences	1	Equipment Specification
Metering Locations Separated by Breakers	1	Installation
Meters not installed at recorded locations	1	Installation
PMU data not named IAW policies	1	Installation
Asynchronous local behaviors (e.g. DC bias injections during solar storm)	1	Measurement
Malformed Network Packets	2,3,4	Network Failure
Network Data Loss	2,3,4	Network Failure
Mislabeled Phasor Data Streams	1,2,3	PMU Configuration
Differences between PMU Manufacturer calculation approaches	1	PMU Standards

Advisor: Dr Peter Sauer, University of Illinois at Urbana-Champaign, psauer@illinois.edu
Kevin Frankeny, Midwest Independent Transmission System Operator (MISO), kfrankeny@misoenergy.org

Comparison of Interval-Specific Building Load Forecasting Models for Demand Resource Planning

Jonathan Berardino and Chika Nwankpa,
Center for Electric Power Engineering, Electrical and Computer Engineering Department, Drexel University, Philadelphia, PA 19104, USA,
Email: jnb38@drexel.edu, nwankpa@ece.drexel.edu,

***Abstract*— This poster presents a method of load forecasting specifically for predicting a building's electrical load for demand resource planning. This forecasting method allows the manager of a controllable load to assess his or her risk and capabilities when participating in the energy market. A general problem formulation for building-specific load forecasting is presented. The several aspects of the model can be allowed to vary over each forecast interval. The variability of these factors is the focus of this work, with particular attention given to finding the optimal model structure at each interval to forecast future building demand most accurately. Correlation studies are performed using demand data at Drexel University in order to identify important factors that drive the electrical demand of the building and create the proposed forecast models. Using this collected demand data, the forecasting method presented here is tested and the results compared to that of a basic forecaster.**

I. KEY EQUATIONS

A general building load forecast model is formulated as shown below:

$$P_i = f_i\left(k_i\left(\Delta\tau_i\right)\right) \qquad (1)$$

where
P_i – Building demand (kW) for interval i
k_i – Chosen functional relationship
$\Delta\tau_i$ – Time shift (minutes) for demand
i – Number of intervals each day is broken down into

In this form, building demand P_i is a function of one driving factor or functional relationship k_i (i.e. – outside air temperature) and subject to a time shift. Impact of varying this model on the forecast accuracy is the focus of this work.

For example, if the selected parameter of interest is the outside air temperature (OAT), to forecast model takes form shown in (2).

$$P_i = f_i\left(OAT_i\left(\Delta\tau_i\right)\right) \qquad (2)$$

II. KEY RESULTS

TABLE 1. OVERALL FIT RESULTS - WEEKDAYS

Interval	*R^2 Value*	*Shift(min)*	*Relation*
1	0.707	35	OAT
2	0.734	0	OAT-Temp
3	0.403	60	OAT
4	0.557	60	OAT-Stpt
5	0.659	60	OAT-Temp
6	0.797	15	OAT-Temp
7	0.805	25	OAT-Temp
8	0.837	0	OAT-Temp
9	0.798	0	OAT
10	0.613	50	OAT-Temp
11	0.590	50	OAT-Temp
12	0.625	0	OAT-Temp
13	0.490	0	OAT-Temp
14	0.474	25	OAT-Temp
15	0.556	0	OAT-Temp
16	0.483	0	OAT-Temp
17	0.450	60	OAT-Temp
18	0.484	25	OAT-Temp
19	0.440	60	OAT-Temp
20	0.489	20	OAT-Temp
21	0.476	0	OAT-Temp
22	0.436	55	OAT-Temp
23	0.499	60	OAT
24	0.611	0	OAT-Temp

TABLE 2. ERROR ANALYSIS – WEEKDAY FORECAST

	RMSE (kW)	
Interval	*Variable*	*Fixed*
1	10.502	10.502
2	10.122	10.162
3	30.987	29.351
4	21.038	18.900
5	20.684	14.205
6	19.557	15.978
7	12.456	11.759
8	10.638	9.590
9	19.732	19.570
10	17.819	18.912
11	18.335	16.853
12	23.580	22.759
13	25.909	24.808
14	28.504	27.229
15	27.519	25.599
16	26.529	24.7106
17	24.406	22.726
18	23.174	21.078
19	21.122	18.855
20	22.548	19.644
21	21.475	17.526
22	16.953	14.746
23	14.439	14.071
24	13.026	12.827

Measurement-based Load Modeling at Distribution Level with Complete Model Structure

Jia Hou, Zhao Xu and Zhaoyang Dong

Department of Electrical Engineering, Hong Kong Polytechnic University, China

Email:houjia06@gmail.com

***Abstract*—In this paper, our research work will focus on load modeling at distribution level. In order to capture specific load characteristics of various load components, a complete load model at distribution level with equivalent capacitor, large motor and small motor is applied. In case study, the measurements and simulated model outputs are demonstrated. For comparison purpose, three load models are used to access model accuracy, which are respectively complete load model at distribution level, composite load model at transmission level and dynamic load model in PowerFactory at distribution level. By contrast, the complete load model proved to have better performance in transient conditions. By splitting the induction motor into two parts, some issues are introduced at the same time. Future work will focus on the generalization capability of this compete load model.**

I. KEY EQUATIONS

The equations of a third order induction motor which represents the dynamic part of the load are:

$$\begin{cases} \dfrac{dw}{dt} = -\dfrac{1}{2H}\left[(Aw^2 + Bw + C)T_0 - (E'_d I_d + E'_q I_q)\right] \\ \dfrac{dE'_q}{dt} = -\dfrac{1}{T'}\left[E'_q - (X - X')I_d\right] + (w-1)E'_d \\ \dfrac{dE'_d}{dt} = -\dfrac{1}{T'}\left[E'_d + (X - X')I_q\right] - (w-1)E'_q \end{cases} \quad (1)$$

$$\begin{cases} I_d = \dfrac{1}{R_s^2 + X'^2}\left[R_s(U_d - E'_d) + X'(U_q - E'_q)\right] \\ I_q = \dfrac{1}{R_s^2 + X'^2}\left[R_s(U_q - E'_q) - X'(U_d - E'_d)\right] \end{cases} \quad (2)$$

The static part of the load can be represented by polynomial load model:

$$P = P_0[a_p(\frac{V}{V_0})^2 + b_p(\frac{V}{V_0}) + c_p] \quad (3)$$

$$Q = Q_0[a_q(\frac{V}{V_0})^2 + b_q(\frac{V}{V_0}) + c_q] \quad (4)$$

II. KEY FIGURES

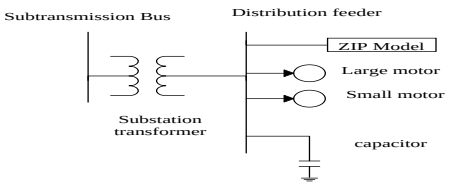

Fig. 1Complete load model structure at distribution level

III. KEY RESULTS

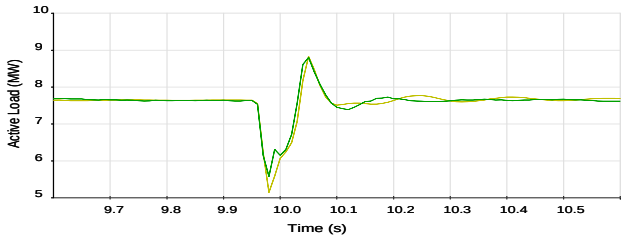

Fig. 2 Measured and simulated active load of complete load model at 22kV level

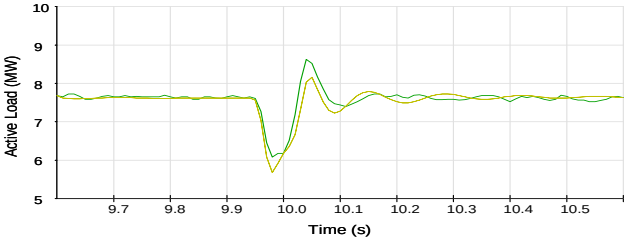

Fig. 3 Measured and simulated active load of composite load model at 132kV level

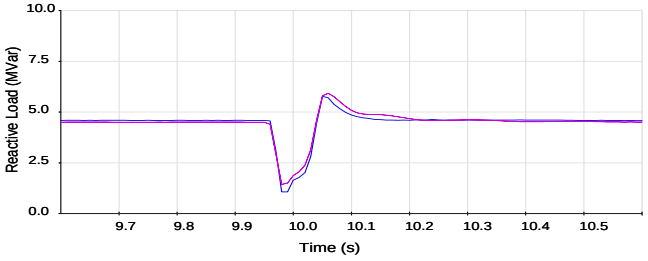

Fig. 4 Measured and simulated reactive load of complete load model at 22kV level

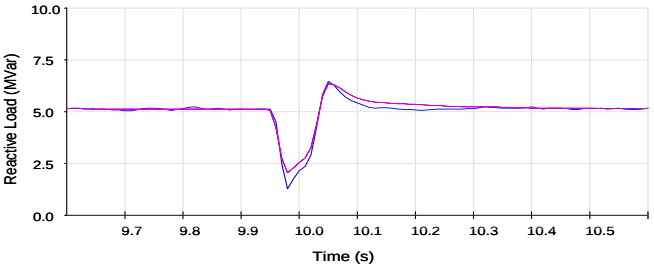

Fig. 5 Measured and simulated reactive load of composite load model at 132kV level

Zinc-Bromine Flow Batteries in Residential Electricity Supply: Two Case Studies

Mio Nakatsuji-Mather (Author)
School of IT and Electrical Engineering
University of Queensland
Brisbane, Australia

Prof. Tapan Saha (Author)
School of IT and Electrical Engineering
University of Queensland
Brisbane, Australia

***Abstract*— Electricity utilities are increasingly faced with the problems associated with rising electricity demand and the intermittency of renewable energy sources. Energy storage can provide an effective solution to these problems. This study investigates the use of zinc-bromine (ZB) batteries in Australian residential electricity supply. A grid-connected suburban house in Sydney showed that it is possible to dramatically reduce grid power import, especially during peak times, and reduce overall grid import to less than two per cent of the time. Furthermore, an-off grid application in rural Victoria showed the significant reductions in diesel generator run time that can be achieved. The financial case for implementing such projects on a wide scale was also investigated. It was concluded that ZB batteries are very effective when used in residential electricity supply and in conjunction with embedded generation, but that an appropriate battery management system must be used in order to attain successful results.**

Keywords- Batteries, distributed power generation, energy storage, power demand

I. BACKGROUND

There has been a general trend towards increasing electricity usage worldwide, both in terms of actual consumption and in gaps between base and peak loads. This results in costly infrastructure upgrades, environmental concerns, and the power quality and grid stability issues associated with intermittent renewable energy that has a growing presence in contemporary grids.

Zinc-bromine (ZB) battery-based energy storage presents a viable solution to the aforementioned problems facing electricity utilities now and even more so into the future.

This paper provides insight into research undertaken to evaluate the feasibility of using ZB batteries, in particular, those produced by RedFlow, in residential electricity supply, as well as in conjunction with embedded generation. In doing so, it investigates the Newington Smart Home project as a grid-supported application and the Energy Safe Victoria (ESV) project as an off-grid application. Both trials were conducted in Australia using varied Australian household loads and sizes of embedded generation.

II. RESULTS

The major findings between the two projects were similar. Firstly, there was the significance of solar exposure to solar panel outputs, and the importance of optimal placement of panels to capture exposure. Optimum solar power output resulted in minimal need for non-renewable electricity sources such as the grid and diesel generators.

The second major finding was that while each of these projects fulfilled the needs of the household loads as the first priority, both systems were more able to achieve their respective goals when residents reduced their energy load consumption. This stressed the behaviour changes that may be required during participation in such trials.

The third major finding was that both projects used storage capacity that was too great for each application. Increasing the size of solar panels would also improve the return on investment (ROI) periods.

The last major finding was the importance of an effective battery management system (BMS) and energy management system (EMS) that optimally control power flows and charging and discharging of storage to best fulfil the aims of each project. While BMS for more conventional energy storage such as lead-acid batteries are well advanced, more work is needed in investigating how best to control ZB batteries to allow them to operate to their full potential.

It should also be noted that after conducting a preliminary financial analysis, the current cost of ZB batteries and associated circuitry is not viable for wide-scale implementation.

In conclusion, despite problems with losses, and the cost of ZB batteries, they are effective in aiding residential electricity supply, especially when used in conjunction with embedded generation. As electricity prices rise and capital costs fall, systems similar to those studied in this paper will become more financially and commercially viable.

Modeling and Impacts of Smart Charging PEVs in Residential Distribution Systems

Isha Sharma Claudio A. Cañizares Kankar Bhattacharya
Department of Electrical and Computer Engineering
University of Waterloo, Waterloo, Ontario, N2L 3G1, CANADA,
Email: *{i4sharma, ccanizar, kankar}@uwaterloo.ca*

***Abstract*— This work presents a new modeling framework for inclusion of charging operations of Plug-in Electric Vehicles (PEVs) within a three-phase unbalanced, residential, distribution system. Coordinated charging of PEVs is proposed to minimize the total energy drawn from substation, total losses in the system and the total PEV charging cost. The impact of PEVs on load profiles, feeder currents, voltages, taps and capacitor switching are examined. A practical distribution test feeder is used to demonstrate the features of the proposed model.**

I. THREE-PHASE DOPF WITH PEV CONSTRAINTS

A three-phase Distribution Optimal Power Flow (DOPF) model is formulated to determine the optimal charging schedule of Plug-in Electric Vehicles (PEVs), taking into account the specified range of charging periods and grid constraints. The following cases are considered:

a. Case 1: Minimize total energy drawn from the substation:

$$J = \sum_h Real(V_{ss} I_{ss}^*) \quad (1)$$

b. Case 2: Minimize total feeder losses:

$$J = \sum_h \sum_n Real(VI_s^* - VI_r^*) \quad (2)$$

c. Case 3: Minimize the total cost of charging PEVs:

$$J = \sum_h \sum_L (E\ TOU) \quad (3)$$

The constraints of the DOPF model are as follows:

- Series components are modeled using ABCD parameters [1]:

$$\begin{bmatrix} \overline{V}_s \\ \overline{I}_s \end{bmatrix} = \begin{bmatrix} A & B \\ C & D \end{bmatrix} \begin{bmatrix} \overline{V}_r \\ \overline{I}_r \end{bmatrix} \quad \forall l \quad (4)$$

- The A and D parameters of the LTCs are modeled using the following equations:

$$A = \begin{bmatrix} 1 + \Delta S\ tap_a & 0 & 0 \\ 0 & 1 + \Delta S\ tap_b & 0 \\ 0 & 0 & 1 + \Delta S\ tap_c \end{bmatrix} \quad (5)$$

$$D = A^{-1} \quad (6)$$

- Wye-connected impedance loads on a per-phase basis:

$$V_{p,L} = Z_{p,L} I_{p,L} \quad \forall p, \forall L \quad (7)$$

- The PEV controlled current load on a per-phase:

$$|I_p|(\angle V_{p,L} - \angle I_{p,L}) = |Io_{p,L}|\angle\theta_{p,L} \quad \forall p, \forall L \quad (8)$$

- The total energy drawn by the PEV battery:

$$\sum_h E_{p,EV} = C_{p,L}^{max} \quad \forall p, \forall EV \quad (9)$$

- The maximum power drawn by the charger:

$$P_{h,p,EV} \le MaxW \quad \forall h, \forall p, \forall EV \quad (10)$$

The model is validated using IEEE 13-node test feeder [2]. Table 1 presents a summary comparison of the case studies carried out. The results in Fig. 1 show that PEV charging takes place in the early morning hours and late night hours when the demand is low, as expected.

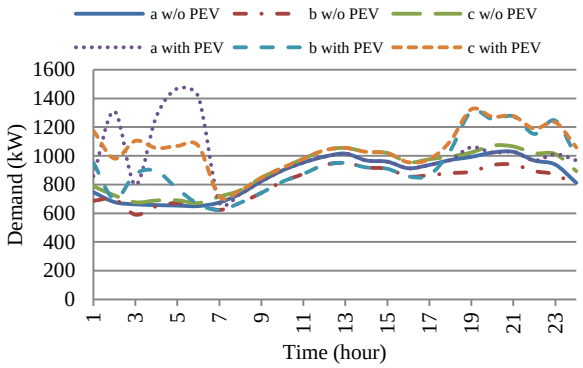

Fig. 1. System load profile with 90% penetration and without PEV.

TABLE I
SUMMARY FOR 90% PENETRATION

	Total Energy Drawn (kWh)	Total Losses (kW)	Total Cost for charging PEVs ($/day)
No PEV	62,966.6 (Min energy)	1,512.4 (Min losses)	0
Case 1	73,126.2	2,040.6	593.5
Case 2	73,322.6	1,962.7	597.0
Case 3	77,130.6	2,344.8	585.5

II. CONCLUSIONS

This work presented the modeling of PEVs within a three-phase unbalanced distribution optimal power flow framework. Smart charging of the PEVs was achieved considering various objective functions, both from the perspective of the utility and the customer.

III. REFERENCES

[1] S. Paudyal, C. A. Cañizares and K. Bhattacharya, "Optimal Operation of Distribution Feeders in Smart Grids," *IEEE Trans. Ind. Electron.*, vol. 58, no. 10, pp. 4495-4503, Oct. 2011.

[2] W. H. Kersting, "Radial distribution test feeders," *Proc. IEEE PES Winter Meeting*, vol. 2, pp. 908-912, 2001.

Control and Operation of Multiple Microsources in a Microgrid

M. Rasheduzzaman, *Student Member IEEE*, Shyam N. Bhaskara *Student Member IEEE* and Badrul H. Chowdhury, *Senior Member IEEE*
Department of Electrical and Computer Engineering
Missouri University of Science and Technology, Rolla, MO 65409, USA,
Email: *mr6x7@mst.edu, sbhxf@mst.edu and bchow@ieee.org*

***Abstract*—Synchronous machine based generators when used in combination with the inverter based sources in a microgrid enhance the system stability during transients. For operating synchronous machines in a microgrid, different control strategies have to be adopted during grid connected and islanded modes. In grid connected mode, the synchronous machines can be commanded to generate power to share the loads in the microgrid. The power flow in the system decides the voltage at various buses. The frequency is decided by the grid which translates into the shaft speed for the synchronous machines. In islanded mode, droop control may be adopted for active and reactive power. The controlling parameters for the synchronous machine are field voltage and shaft torque applied to the machine. A laboratory test bench is setup for demonstrating the controller operation. LabVIEW software and NI data acquisition systems are used for communicating with hardware and also for building controllers for different modes of operations.**

I. Design of Controllers and Test Results

Real and reactive power droop

$$\omega_{rm}^{*} = \omega_{rm0}\left(1 - \frac{D_{pf}}{100} \times \frac{P_{gen}}{P_{gen,rated}}\right); \quad V_s^{*} = V_{s0}\left(1 - \frac{D_{qv}}{100} \times \frac{Q_{gen}}{Q_{gen,rated}}\right)$$

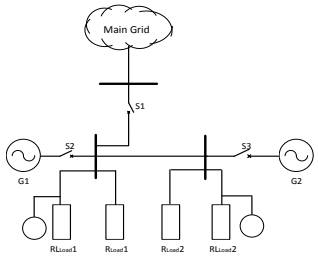

Figure 1. Test setup

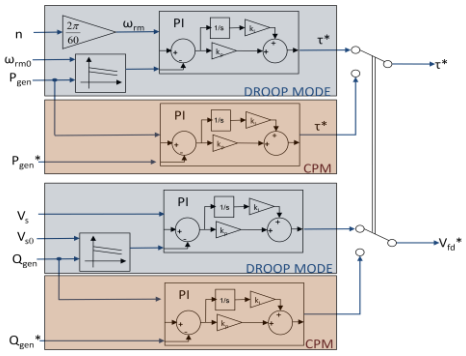

Figure 2. Control scheme

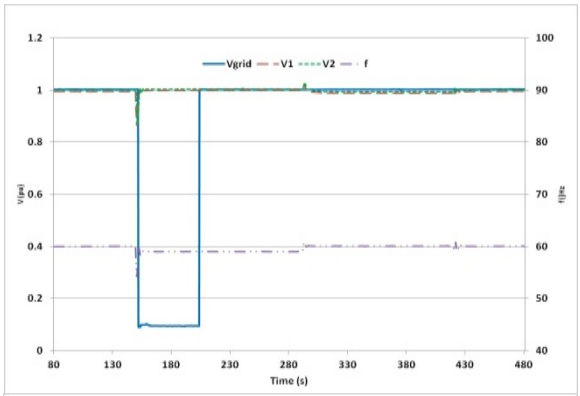

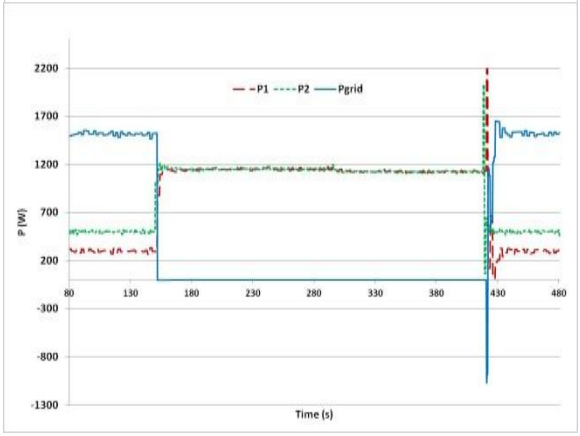

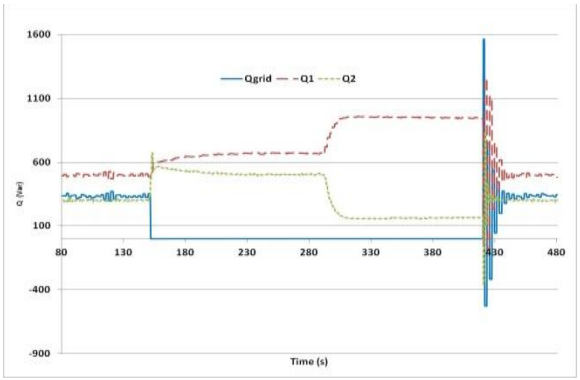

Figure 3. Experiment results

III. Conclusion

- The system can run with and without grid support
- Loads are served at nominal voltage and frequency in all cases
- Generating units share the load in the system
- All generators are stable at all times

Detection, Identification, and Correction of Bad Sensor Measurements for Fault Location

Mert Korkalı and Ali Abur
Department of Electrical and Computer Engineering
Northeastern University
Boston, MA 02115-5000 USA
Email: {mkorkali, abur}@ece.neu.edu

***Abstract*—We initially review the readily devised methodology for transmission-grid disturbance location employing measurements from strategically deployed sensors. Later, we introduce one viable procedure for bad measurement detection and identification in order to accurately localize power system faults, thereby to enhance the practicality of the developed method. Furthermore, subsequent elimination of the errors resulting from bad sensor measurements will yield significantly enhanced fault-location accuracy. Simulated data regarding a particular fault scenario are illustrated using the modified IEEE 30-bus test grid.**

I. Key Equations

$$\zeta_{k\ell}(\alpha) = \min\left\{\mathcal{D}_{k\ell}^{(o)} + \alpha D_\ell,\ \mathcal{D}_{k\ell}^{(t)} + (1-\alpha)D_\ell\right\} \tag{1}$$

$$\mathbf{T} = \begin{bmatrix} T_1 & T_2 & \cdots & T_K \end{bmatrix}^{\mathrm{T}} \tag{2}$$

$$\boldsymbol{\eta} = \begin{bmatrix} 1 & 1 & \cdots & 1 \end{bmatrix}_{K\times 1}^{\mathrm{T}} \tag{3}$$

$$\boldsymbol{\zeta_\ell(\alpha)} = \begin{bmatrix} \zeta_{1,\ell}(\alpha) & \zeta_{2,\ell}(\alpha) & \cdots & \zeta_{K,\ell}(\alpha) \end{bmatrix}^{\mathrm{T}} \tag{4}$$

$$\underset{\{\ell,\ \alpha,\ T_0\}}{\text{minimize}} \quad \left\|\mathbf{T} - T_0\boldsymbol{\eta} - \boldsymbol{\zeta_\ell(\alpha)}\right\| \tag{5a}$$

$$\text{subject to} \quad 0 \le \alpha \le 1; \quad \ell \in \{1, 2, \cdots, L\}. \tag{5b}$$

$$\mathcal{J}_\ell = \left\|\boldsymbol{\mathcal{D}}_\ell + \psi^{(\ell)}\mathbf{S}_\ell - \mathbf{T} + T_0^{(\ell)}\boldsymbol{\eta}\right\|_2^2, \tag{6a}$$

where

$$\boldsymbol{\mathcal{D}}_\ell = \begin{bmatrix} \mathcal{D}_{1,\ell}^{(o)} & \mathcal{D}_{2,\ell}^{(o)} & \cdots & \mathcal{D}_{K,\ell}^{(o)} \end{bmatrix}^{\mathrm{T}} \tag{6b}$$

$$\mathbf{S}_\ell = \begin{bmatrix} S_{1,\ell} & S_{2,\ell} & \cdots & S_{K,\ell} \end{bmatrix}^{\mathrm{T}} \tag{6c}$$

$$\mathbf{r}^{(\ell)} = \boldsymbol{\Delta}\mathbf{T}^{(\ell)} - \boldsymbol{\Delta}\widehat{\mathbf{T}}^{(\ell)} \tag{7}$$

$$\mathbf{T}_j^{(\ell)} \approx \boldsymbol{\Delta}\mathbf{T}_j^{(\ell),\mathrm{bad}} + \mathcal{D}_{j\ell}^{(o)} - \frac{\mathbf{r}_j^{(\ell),\mathrm{bad}}}{\boldsymbol{\Omega}_{jj}^{(\ell)}} \tag{8}$$

II. Key Figures & Results

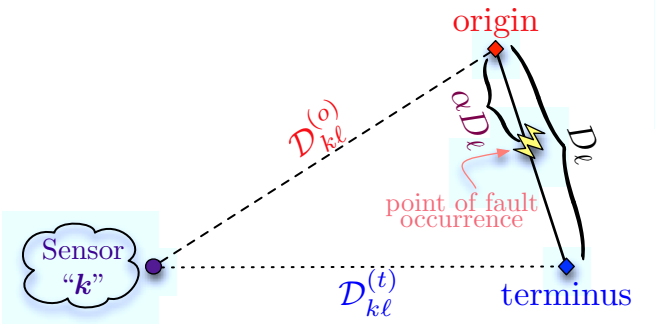

Fig. 1. Visual depiction of the terms "origin" and "terminus" as well as the delays, $\mathcal{D}_{k\ell}^{(o)}$ and $\mathcal{D}_{k\ell}^{(t)}$, with regard to Sensor "k".

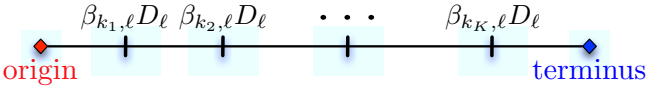

Fig. 2. The fictitious buses generated at the points "$\beta_{k_i,\ell}D_\ell$".

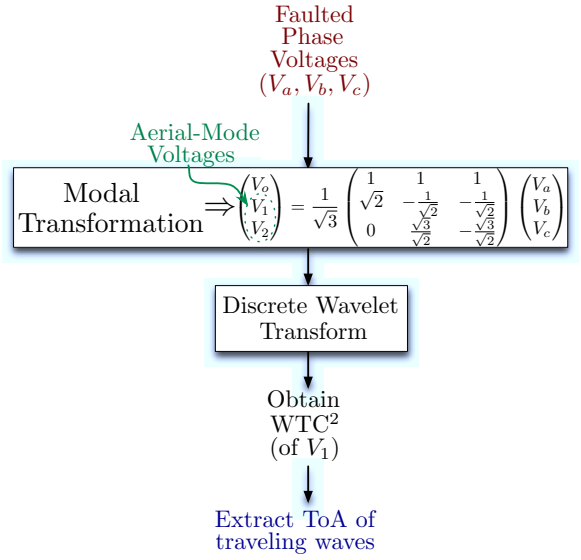

Fig. 3. Computational stages of the devised fault-location algorithm.

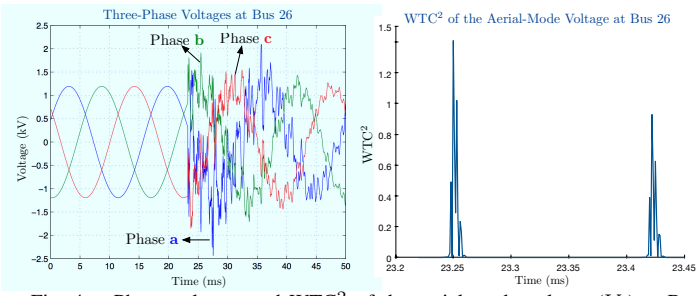

Fig. 4. Phase voltages and WTC^2 of the aerial-mode voltage (V_1) at Bus 26 after the occurrence of a short-circuit fault on Line 2-6.

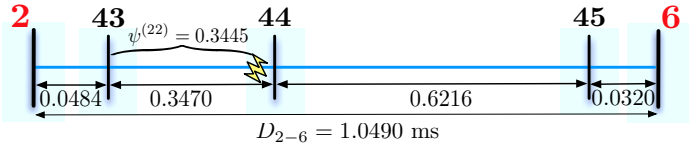

Fig. 5. Value of $\psi^{(\ell)}$ for the short-circuit fault occurring on Line 2-6.

Monitoring the Energy Consumptions of Home Appliances Using Smart Meter Data

Ming Dong
Department of Electrical and Computer Engineering
University of Alberta
Edmonton, Canada
mdong@ualberta.ca

***Abstract*—Smart meter is probably the most visible symbol of the future smart grid. Industry hopes that more energy conservation behaviors will be induced if customers can access their own energy data from the smart meters. However, existing smart meters are not sufficient for providing households with the feedback needed to achieve effective energy saving. This poster presents techniques that have the potential to make the smart meters truly smart in term of metering capability – the tracking of the energy consumptions of home appliances.**

***Keywords*-Load management, Load signatures, Time-of-Use Price, Demand response, Nonintrusive Load Monitoring.**

I. INTRODUCTION

The smart meter, a device for utilities to measure a customer's energy consumption, is probably the most recognized symbol of the future smart electric grid. However, current smart meters are not really smart. They essentially are digital versions of the traditional mechanical meter enhanced with telecommunication capability. Many of the benefits brought by the smart meters are actually attributable to their communication capability, not metering capability. Therefore, a huge opportunity exists for innovations that can harness the meters' measurement capabilities such as identifying and monitoring activities and energy consumptions of individual appliances.

Is smart meter truly smart?

-Yes. A smart meter can measure real-time power and communicate with other devices.

-No, it does not offer any additional information to help ordinary customers "smartly" use energy.

Our mission is to bring real intelligence to smart meter based on existing metering and communication functions.

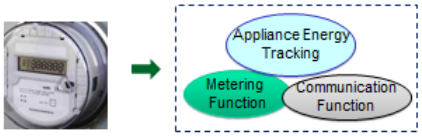

Fig.1. Stucture of smart meters with appliance monitoring fuctions

II. APPLIANCE' DNA

If we can identify appliance's events such as turning ON/OFF, we can monitor their energy consumptions with only total power curve known from meter. This is based on appliance's signatures. Each appliance has its unique "DNA".

- DNA 1---Edge Signature

When you switch ON/OFF an appliance, meter side will see a rising/falling power edge on top of original total power. This edge is determined by the electrical characteristics of appliances. Those characteristics include active power P, reactive power Q and waveform shape W. Those edge signatures are fixed values and will stay roughly the same every time when you switch ON/OFF it.

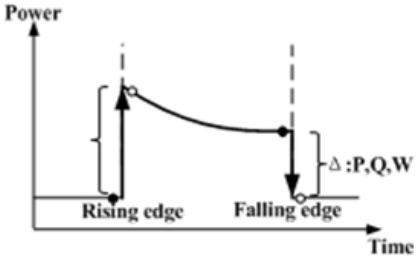

Appliance	*P_ON (W)*	*Q_ON (Var)*	*P_OFF (W)*	*Q_OFF (Var)*	*Waveform*
Fridge	*160*	*65*	*135*	*38*	
Desktop PC	*120*	*12*	*115*	*15*	
…	….	…	…	…	…

Fig.2. Edge signatures of appliances

- DNA 2---Power Pattern Signature

Different appliances have different working cycles. For simple appliances, there is only an ON edge and an OFF edge in its working cycle. However, for complicated appliances, specific power change patterns can be found. Generally speaking, there are three types of power patterns as below:

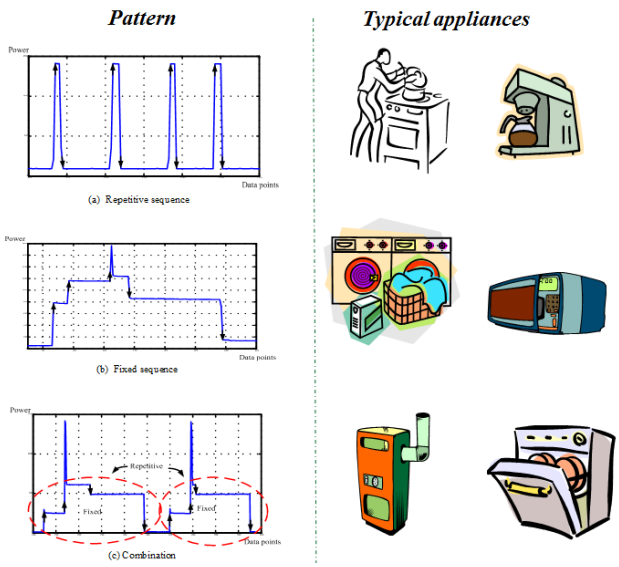

Fig.3. Power pattern signatures of appliances

- DNA 3---Power Trend Signatures

Similar to DNA 2, some appliances experience unique distortions on their power trends. Those distortions are not edges. However, they can be identified based on their power slope pattern.

Type	Curve example	Power slope feature
Rising spike		A large negative slope following a larger positive slope
Falling spike		A large positive slope following a large negative slope
Pulses		Continuous pairs of large slopes

Fig.4. Power Trend Signatures of appliances

- DNA 4---Phase Signatures

In North America, residential house has two 120V hot wires. Some appliances are connected to Phase A and neutral; some are connected to Phase B and neutral; some are connected between Phase A and B to gain a 240V voltage. Thus, CTs inside meter can tell us which appliances it could be simply by its connection.

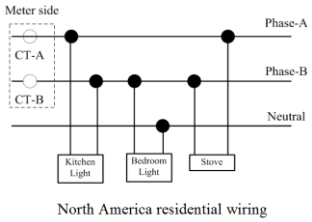

Fig.5. Phase signatures of appliances

III. System Implementation

To identify appliances, all edges of power are firstly captured. Those edges will form different event windows. Each event window represents a possible appliance's working cycle. Then the signatures of these working cycles are extracted and compared with appliance signature database.

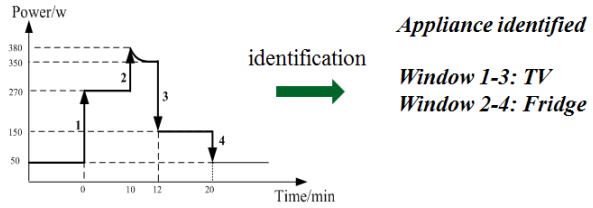

Fig.6. Identification of appliances

After activities of appliances are identified, their energy consumptions can thus be further extracted as below:

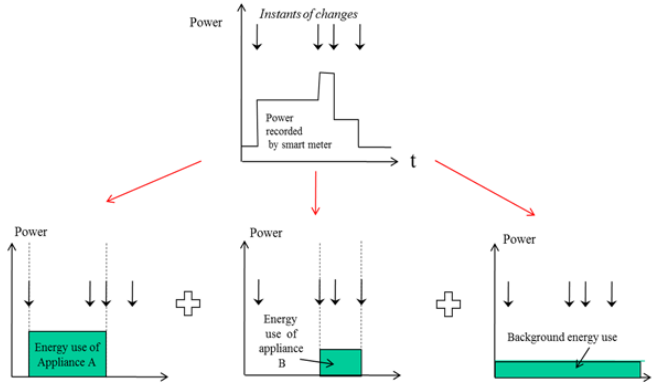

Fig.7. Energy estimation of appliances

IV. Sample Results

In the end electricity bill can be broken down to appliance level and provided to customers. A pie chart illustrating the composition of energy can be given as below:

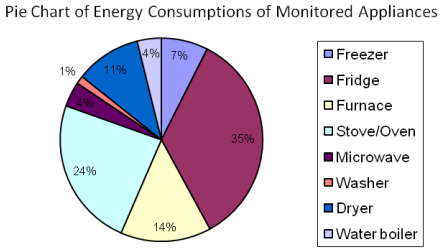

Fig.8. Pie chart of energy consumtpions of appliances

Also, user can obtain a more detailed usage pattern with time as reference shown like below:

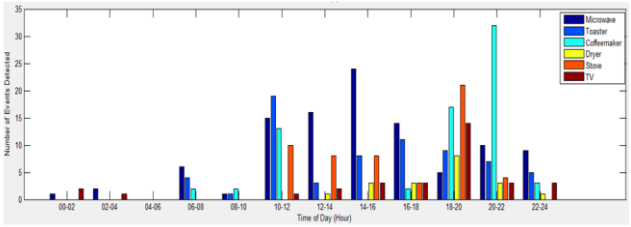

Fig.9. Pie chart of energy consumtpions of appliances

This type of information is especially useful for users to adapt load shifting---shift their electricity use from expensive hours to cheaper hours based on Time-Of-Use prices.

V. System Implementation

Different smart meters will send their metering signals to a central utility sever which has above algorithm installed. Then this server can track specific appliances of connected houses. Customer can interact with the sever on-line through internet browser. The entire system works as a cloud in smart grid.

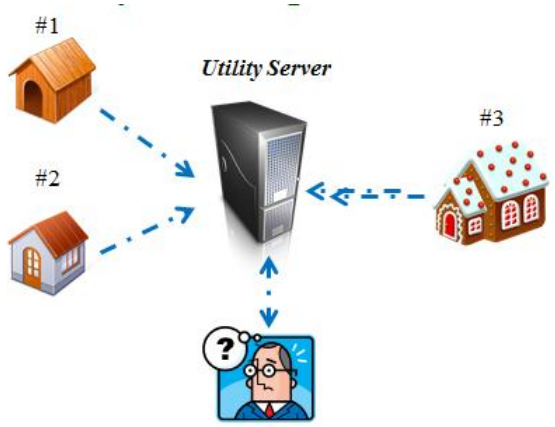

Fig.10. System implementation

References

[1] S. Massoud Amin and Bruce F. Wollenberg, "Toward a Smart Grid", IEEE Power & Energy Magazine, Sept/Oct 2005, pp. 34-41.

[2] H. Farhangi, "The Path of the Smart Grid", IEEE Power & Energy Magazine, Jan/Feb 2010, pp. 18-28.

[3] United States Department of Energy. *The Smart Grid: An Introduction.* [On-line].Available:www.oe.energy.gov/SmartGridIntroduction.htm [Apr 16,2011].

[4] Litos Strategic Communication, "The Smart Grid: An Introduction", United States Department of Energy, 2004.

[5] S. Rahman, "Smart Grid Expectations", IEEE Power & Energy Magazine, Sept/Oct 2009, pp. 83-85.

[6] David Schatsky and Clint Wheelock, *Home Energy Management*. [On-line]. Available: www.pikeresearch.com/research/ [Jan 22,2011].

[7] A. Mahmood, M. Aamir and M.I. Anis, "Design and Implementation of AMR Smart Grid System", IEEE Electrical Power and Energy Conference, 2008, pp. 1-6.

[8] Wilsun Xu, Alex Nassif, and Jing Yong "Harmonic Current Characteristics of Home Appliances", Report to CEATI International Inc., 60 pages, March 2009.

[9] Ming Dong and Wilsun Xu, "Load Signature based Home Appliance Identification Method", Internal research report of Dept. of ECE, University of Alberta, 50 pages, May 2009.

[10] A.B. Nassif, J. Yong, Wilsun Xu and C.Y. Chung, "Comparative Harmonic Characteristics of Home Appliances", submitted to IEEE Transactions on Power Delivery.

[11] Hart, G.W. , "Non-intrusive Appliance Load Monitoring", Proceedings of the IEEE, vol. 80, No 12, December, pp. 1870 - 1891,1992

[12] Norford L.K., Leeb S.B., "Non-intrusive Electrical Load Monitoring in Commercial Buildings based on Steady-state and Transient Load-detection Algorithms". Energy and Buildings 24, pp. 51 – 64,1996

[13] Baranski, M.; Voss, J.," Genetic algorithm for pattern detection in NIALM systems", Systems, Man and Cybernetics, 2004 IEEE International Conference on, Volume 4, 10-13 Oct. 2004, Page(s):3462 - 3468 vol.4

[14] Suzuki, K.; Inagaki, S.; Suzuki, T.; Nakamura, H.; Ito, K., "Nonintrusive appliance load monitoring based on integer programming", SICE Annual Conference, 2008, 20-22 Aug. 2008, Page(s):2742 – 2747

[15] Duan, J.; Czarkowski, D.; Zabar, Z., "Neural network approach for estimation of load composition", Circuits and Systems, 2004. ISCAS '04. Proceedings of the 2004 International Symposium on, Volume 5, 23-26 May 2004 ,Page(s):V-988 - V-991 Vol.5

[16] Srinivasan, D.; Ng, W.S.; Liew, A.C., "Neural-network-based signature recognition for harmonic source identification", Power Delivery, IEEE Transactions on, Volume 21, Issue 1, Jan. 2006 ,Page(s):398 – 405

[17] A. Capasso, W. Grattieri, R. Lamedica and A. Prudenzi, "A bottom-up approach to residential load modeling," *Power Systems, IEEE Transactions on*, vol. 9, no. 2, 1994, pp. 957-964.

[18] S.W. Heunis, and R. Herman, "A probabilistic model for residential consumer loads," *Power Systems, IEEE Transactions on*, vol. 17, no. 3, 2002, pp. 621-625.

[19] BlueLine Electricity Power Cost Monitor, http://www.blueline innovations.com/Products/PowerCost-Monitor/

Ming Dong (S'08) received his B.Eng. degree in Electrical Engineering from Xian Jiaotong University, China in 2008. He is currently pursuing his Ph.D. degree with Electrical and Computer Engineering, University of Alberta, Canada. His research covers smart grid and power quality.

Effect of Network Packet-Dropout on the Control Performance of Power Systems

Singh, Abhinav Kumar
Department Electrical and Electronic Engineering
Imperial College London
London, United Kingdom
a.singh11@imperial.ac.uk

Majumdar, Ankur
Department of Electrical and Electronic Engineering
Imperial College London
London, United Kingdom
ankur.majumdar@imperial.ac.uk

Pal, Dr. Bikash C.
Department of Electrical and Electronic Engineering
Imperial College London
London, United Kingdom
b.pal@imperial.ac.uk

***Abstract*—With the introduction of wide area measurement systems (WAMSs) and flexible AC transmission systems (FACTS) in Power Technology, remote signals need to be transmitted over distances as large as even hundreds of kilometers to centralized or distributed controllers. Presently, dedicated channels are used for the transmission of these signals. The number of such signals and controllers is bound to increase with an increase in the complexity of power systems as they are going to operate closer to their operating limits and also become larger by integration of more and varied sources of energy. The introduction of a packet based network is soon going to be indispensable for the communication of such a 'smart' grid. This poster aims to study the effect of packet-dropout rate on the stability of such a networked controlled power system, specifically on the stability of the damping control using a thyristor controlled series capacitor (TCSC). To this end, we have used a representative 16-machine, 68-bus, 5-area power system. The open loop system needs to be damped in the frequency range 0-1 hertz. The reason for the poor damping is large inter-area power flow over the tie-line between two areas. A TCSC is used to control the impedance of this tie line and using modal and residual analysis of the open-loop system it is found that power flow signals from two remote transmission lines as an input to the TCSC-controller are enough to adequately damp the system. For the controller design purpose, first it is assumed that there is no packet loss in the transmission of the two signals. After the controller design, a packet-dropout rate is introduced in the system, which follows a Bernoulli process. The sampling period of the network is assumed to be constant and we consider network delay in our analysis only in as much as it relates to dropping packets due to an extensive delay. The effect on the damping of the system with varying packet-dropout rate is studied and a threshold value for the dropout rate is found out so that the system remains adequately damped. MATLAB is used for the modeling and simulation of the system. The machines are modeled using sub-transient dynamics while the loads are modeled as constant impedance loads. The study and results presented in this poster are intended to form a foundation for a further and more detailed analysis of damping control of networked controlled power systems and subsequent controller design for such a system.**

Keywords-smart grid; damping control; wide-area power systems (WAPSs); networked control systems (NCSs); packet-drop; flexible AC Transmission systems (FACTS); thyristor controlled series capacitor (TCSC)

I. KEY FIGURES

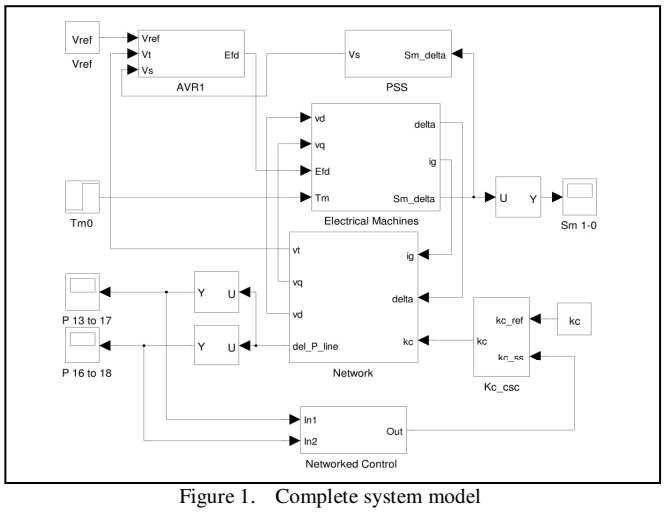

Figure 1. Complete system model

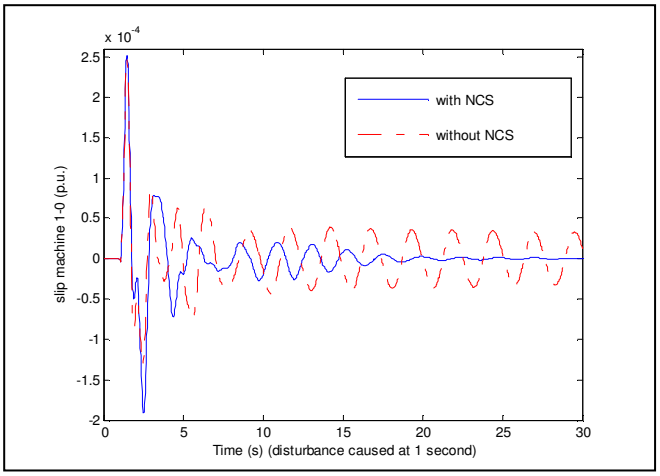

Figure 2. Damping response of the system

II. KEY REFERENCES

[1] Shaobu Wang; Xiangyu Meng; Tongwen Chen; , "Wide-Area Control of Power Systems Through Delayed Network Communication," *Control Systems Technology, IEEE Transactions on* , vol.20, no.2, pp.495-503, March 2012

[2] Azimi-Sadjadi, B.; "Stability of networked control systems in the presence of packet losses," *Decision and Control, 2003. Proceedings. 42nd IEEE Conference on* , vol.1, no., pp. 676-681 Vol.1, 9-12 Dec. 2003

Vulnerabilities in Coupled Control and Communication Systems with Power Grids and Their Effects on Cascading Failures

Mahshid Rahnamay-Naeini*‡, Zhuoyao Wang*, Shahin Abdollahy*, Andrea Mammoli†, and Majeed M. Hayat*‡
*Department of Electrical and Computer Engineering, University of New Mexico, Albuquerque, NM, USA
† Department of Mechanical Engineering, University of New Mexico, Albuquerque, NM, USA
‡ Center for High Technology Materials, University of New Mexico, Albuquerque, NM, USA
Email: mrahnama@ece.unm.edu, {zywang, shahinab, mammoli}@unm.edu, hayat@ece.unm.edu

***Abstract*—Modern power grids rely heavily on their control systems, which operate over communication networks to mitigate the adverse effects of stress in the grid. Nonetheless, large cascading failures do occur in transmission grids, triggered by a combination of initial failures in the power system and lack of proper corrective actions in a timely manner. Inefficiencies in the corrective actions can be due to system vulnerabilities such as failures or delays in the communication and control systems. They can also be due to physical limitations of devices as well as marketing policies, which together affect the control procedure. Conversely, contingencies in the power system may affect the control/communication systems through lack of power supply and possible overloading of communication components because of high volumes of control and monitoring message exchanges.**

In this poster the vulnerabilities in the interdependent control/communication systems and power grids are coupled with the load-shedding mechanism and modeled by formulating an optimization problem with new constraints. MATPower is used to simulate the power system and solve the optimization problem. The cascading failure behavior of the grid is investigated considering the coupled effects of failures in the control and communication systems, as well as the topological location of the failures. Furthermore, the effect of response-time behavior of load buses in implementing load-shedding control signals on systems working under stress is also investigated. Load buses may have different temporal-response behaviors to load-shedding control signals due to possible delays in the communication network, physical device restrictions on reducing the load or marketing policies. The results confirm our intuition that due to certain vulnerabilities, such as losing full or partial control over the load buses and delay in performing load shedding, the power grid becomes prone to cascading failures. The insights drawn from this work can be valuable in designing future reliable power grids along with their control/communication systems.

I. KEY EQUATIONS

The notation L_i represents the total initial load on bus i. The parameter c_i represents the ratio of the controllable load over the total load of a load bus, say i, where $0 \leq c_i \leq 1$. Here, $c_i = 0$ means that no load shedding is possible on the bus i and $c_i = 1$ means that all the loads in bus i can be controlled. Each load bus has a dispatchable load (controllable load), ${L^d}_i = c_i L_i$, and a fix-load load part with value ${L^f}_i = (1 - c_i)L_i$. We calculate the optimal power flow and the optimal load shedding by minimizing the cost defined as

$$\text{Cost} = \sum_{i \in \mathcal{G}} {w^g}_i g_i + \sum_{i \in \mathcal{L}} {w^\ell}_i \ell_i. \qquad (1)$$

The constraints for this optimization are listed below.

(a) Generators power: $0 \leq g_i \leq {G_i}^{\max}$, $i \in \mathcal{G}$.
(b) Controllable loads: ${L^d}_i \leq \ell_i \leq 0$, $i \in L$.
(c) Line power flows: $|F_{ij}| \leq {F_{ij}}^{\max}$.
(d) Power balance: $\sum_{i \in \mathcal{G}} g_i + \sum_{i \in \mathcal{L}} (\ell_i + {L^f}_i) = 0$.

We define $r_{c/t} \triangleq (\sum_{i \in \mathcal{L}} c_i L_i) / \sum_{i \in \mathcal{L}} L_i$.

II. KEY RESULTS

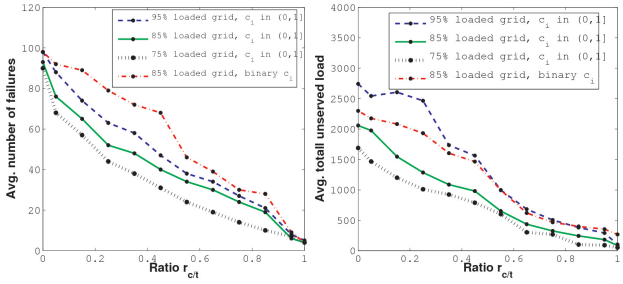

Fig. 1. Average number of failed lines, and total unserved load, due to cascading failures as a function of $r_{c/t}$.

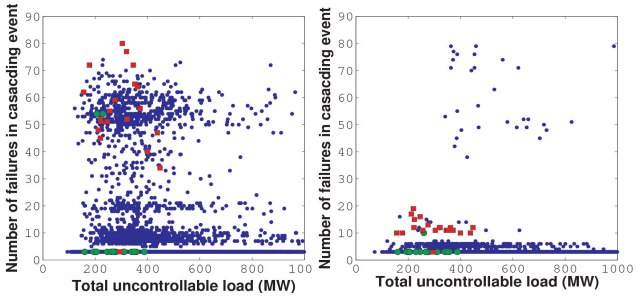

Fig. 2. Cascading behavior of the grid for distributions of load buses with uncontrollable loads over the grid for two scenarios of initial failures.

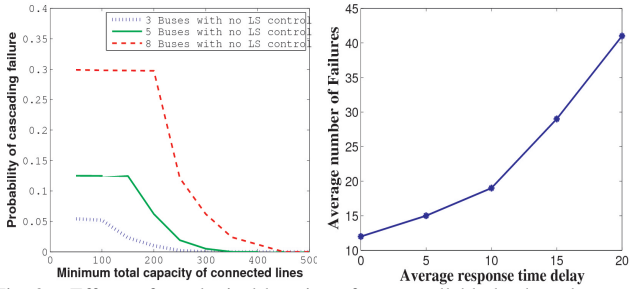

Fig. 3. Effects of topological location of uncontrollable loads and response-time delay in load shedding on cascading failures.

A Partitioning Method for Distributed Capacitor Control of Electric Power Distribution Systems

Michael Kleinberg Karen Miu
Electrical and Computer Engineering Department, Drexel University, Philadelphia, PA 19104, USA
Email: *mrk26@drexel.edu, karen@coe.drexel.edu*

***Abstract*— With the renewed investment in advanced capacitor control systems, the potential for online distributed control is increasing. In this work, an analytical partitioning method based on capacitor reactive power domains is presented. Boundaries of the computed reactive power domains are used as natural decoupling points for distributed analysis and control. Once partitioned, a distributed control algorithm is employed to support distribution operation applications. Here, capacitor control for voltage spread reduction is investigated. Simulation results on a 20-bus test distribution network are presented and compared against a tradition centralized control scheme. Results show the proposed distributed control methodology is capable of producing high quality solutions to the capacitor control problem, and hence, may facilitate the deployment of advanced distribution automation.**

I. KEY EQUATIONS

Positive power flow direction is used to trace power back to a source and to allocate load and loss to several sources for common areas [1, 2]. For two directly connected buses, bus *i* and *j*, reactive power flows from bus *i* to bus *j* over phase *p*, if:

$$\mathrm{Im}(V_i^p I_{ij}^{p^*}) - \mathrm{Im}(V_j^p I_{ij}^{p^*}) > 0 \qquad (1)$$

Using positive power flow direction, reactive power commons may be identified as seen in Figure 1. Reactive power domains, consisting of one or more commons, are then used to partition the network into control areas [3], as seen in Figure 2. Here, capacitor control for voltage spread reduction (VSR) is investigated. For each control area *i*, the distributed VSR problem formulation may be stated as:

$$\min_{u_i \in U_i} \max_{\substack{j \in N_i \\ p \in a,b,c}} \left\| \left|V_{ref,i}^p\right| - \left|V_j^p\right| \right| \qquad (2)$$

subject to:

$$f(V_i, u_i) = 0 \qquad (3)$$

$$\left|I_k^p\right| \le I_k^{\max} \;\; \forall \; k \in N_i \qquad (4)$$

$$P_l^2 + Q_l^2 \le (S_l^{\max})^2 \;\; \forall \; l \in F_i \qquad (5)$$

$$V_k^{\min} \le \left|V_k^p\right| \le V_k^{\max} \;\; \forall \; k \in N_i, \; p \in a,b,c \qquad (6)$$

where:

F_i: set of all feeders, control area *i*
N_i: set of all buses, control area *i*
u_i: capacitor control scheme, control area *i*
U_i: set of all capacitor controls, control area *i*
V_i: vector of node voltages, control area
$\left|V_{ref,i}^p\right|$: distributed reference, control area *i*

II. KEY FIGURES

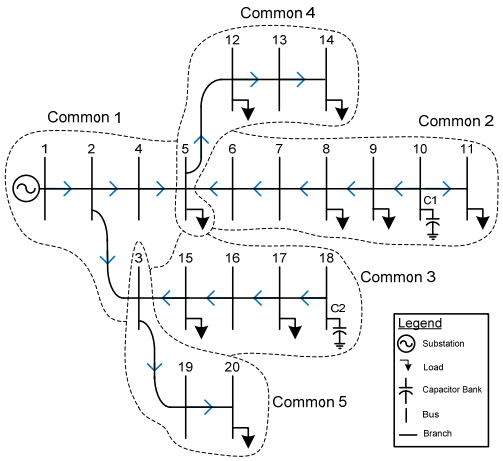

Figure 1: Single line diagram of a 20 bus distribution system with arrows indicating positive reactive power flow direction and reactive power commons highlighted for phase *a*

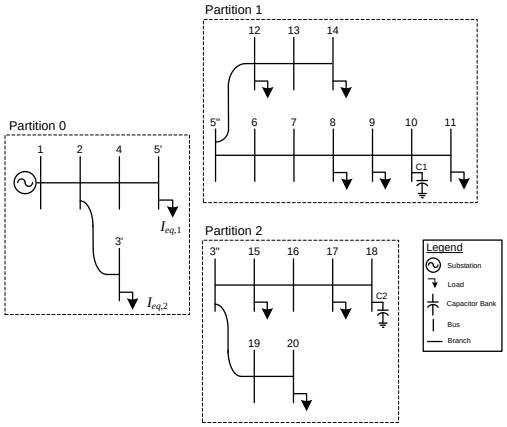

Figure 2: 20 bus distribution system partitioned based on reactive power domains shown in Figure 1

III. REFERENCES

[1] D. Kirschen, G. Strbac, "Tracing active and reactive power between generators and loads using real and imaginary currents," *IEEE Trans. on Power Systems*, vol. 14, no. 4, pp. 1212-1319, Nov. 1999.

[2] S. Tong, K. Miu, "A network-based distributed slack bus model for DGs in unbalanced power flow studies", *IEEE Trans. on Power Systems*, vol. 20, no. 2, pp. 835-842, May, 2005.

[3] M. Kleinberg, K. Miu, "A study of distribution capacitor control for electric power distribution networks," *Proceedings of the North American Power Symposium*, Boston, MA, Aug. 2011.

A Reliability Analysis for the Smart Grid Distribution Communications

Babak Karimi *(Author)*
Department of Electrical Engineering and Computer Science
Wichita State University
Wichita, KS USA
bxkarimi@wichita.edu

Parisa Nazaran
Department of Industrial and Manufacturing Engineering
Wichita State University
Wichita, KS USA
pxnazaran@wichita.edu

Vinod Namboodiri
Department of Electrical Engineering and Computer Science
Wichita State University
Wichita, KS USA
Vinod.namboodiri@wichita.edu

***Abstract*— Intelligent network is an important mean to achieve energy saving and promote renewable energy develop. With the technology of power electronics, IT, communications continuing to evolve, the smart grid will be an important direction of the electric power industry development. It has been always said that Smart Grid communication should be reliable but this has not been clarified why and how. Although there has been some basic analysis and works but a thorough reliability study of any proposed architecture is still missing. Briefly, the goal of this project is to demonstrate a reliability and security assessment process. To do so, we utilized the most common methods (Reliability Block Diagram and fault tree) to analyze the system using powerful tool, BlockSim7.**

Keywords-component; Smart Grid; Communication; Reliability; Availability

I. INTRODUCTION

Like other wireless networks in our daily life, it is substantial to have an ongoing network for Smart Grid. In other words frequent downtimes or system failures are not affordable. Smart Grid communications are categorized under Real-time systems that are now widely in service; like emergency rescue systems, accident notification systems and catastrophe monitoring systems. In such scenario the network is expected to maintain a high quality service as it remains reliable during operating time.

A. Reliability definition and analysis

Reliability is defined as the probability that a system or component will function over a specific period of time when used under stated operation conditions. Generally system failure behavior is divided into three regions during its life cycle. Starting with decreasing failure rates early in their life cycle (infant mortality) following by an almost constant failure rate making through with random failures (useful life), following by an increasing failure rate (wear out). Depending on what the failure rate for each region is, a different probability distribution can be derived regarding the region. The most known distributions pertaining reliability are Exponential, Weibull, Normal, Lognormal and Gamma distribution. Logically a constant failure rate is considered for a system on a long period of time when it is being studied on its steady-state, meaning that Exponential distribution is used.

II. DISTRIBUTION LEVEL RELIABILITY MODEL

In this model the end-to-end connectivity at any given time is the objective. It is assumed that there are three types of end-to-end connectivity. Control center to each pole on feeder, control center to aggregators and control center to home area network (HAN). So the reliability model represents only one out of many end-to-end connectivity of each type at a certain time.

Here is some of the component information which has critical impact on connection failure:

One of the most important cases that can endanger the network security is backhaul availability attacks. It's very first effects on the network are delayed data, disruption in communication and temporary network unavailability. This sort of security attacks, also known as malicious attacks or backhaul security attacks commonly happen nowadays.

Concentrator is designed to gather all the incoming data from Smart meters. Its failure is usually due to high load, electronic or firmware malfunctioning or short circuit and will result in lack of information at control center. Hence large area's communication is depending on operation of the correspondent data concentrator.

Smart meter is designed to communicate between Utility Backhaul Network and Home Area Network. If it fails home area access to or from grid will be cut off.

To make a system reliable at quantitative level, two set of numerical information is required. First, each component or sub-component's reliability information such as distribution function, meant time to failure, failure rate etc. In the following table there is a list of some important components with relative failure rates that we have used in analysis. In this project, we assumed that every component follows an exponential distribution with a constant failure rate.

Second, an operating time should be considered to run reliability analysis. For this paper it is assumed that every components failure rate was obtained in years. So, the system reliability analysis should also be reported in years. System's reliability will be discussed after first year, fifth year, tenth year and fiftieth year.

The outcomes of this phase are Reliability Block Diagram and System Fault Tree, which is probably the most important step towards analyzing reliability from qualitative point of view. Once the fault tree is constructed, minimal cut sets can be obtained as well. From this step forward, it's all about numerical variables to compute system reliability function and so on.

TABLE I. IMPORTANT COMPONENTS AND THEIR FAILURE MODE

Failure Mode	***Failure Rate (per year)***	***Mean Time to Failure***
Main power supply fails	1.53E-05	65231.57208
Control center communication infrastructure	0.003987	250.8151492
Wireless Link Availability Attacks	0.00788	126.9035533
Router physical damage	0.0019987	500
Pole-to-pole Sub-Net Availability Attacks	0.0019987	500.3252114
Home area power outage	0.0004	2500

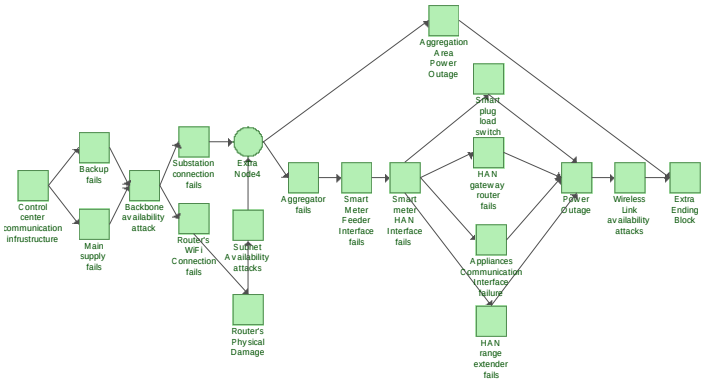

Figure 1. Reliability Block Diagram

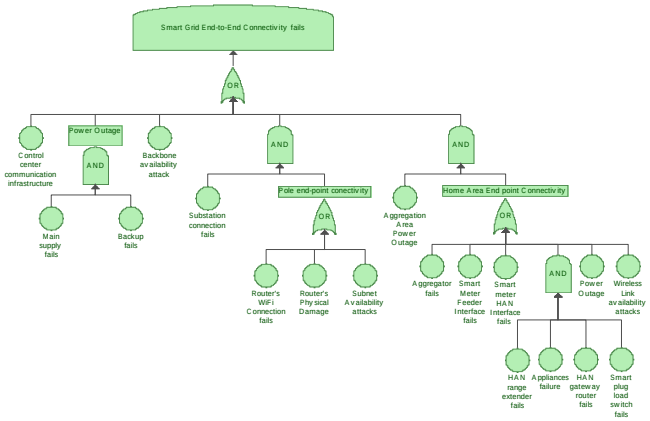

Figure 2. System Fault Tree diagram

III. CONCLUSIONS AND FUTURE WORKS

As a reliability point of view it can be concluded that the suppliers need to make sure of critical components availability either by preventive maintenance, repair, regular inspections, device replacements, software reconfiguration etc. In this study, software results show that the most two important components were backbone availability and control center. In other words, a secure and available backbone network and a trustworthy and operating control center which is monitoring and working on-line nonstop, is required to have a safe and satisfying network. It is noticeable that the quantitative results, such as reliability in several years, only represent the data that was assumed in this study. It is for sure that by considering real world data a more reliable report. Also, it is critical for the network to be always available, which leads to another study regarding availability analysis.

REFERENCES

[1] Babak Karimi, Vinod Namboodiri, Visvakumar Aravinthan, Ward Jewell, "'Feasibility, Challenges, and Performance of Wireless Multi-Hop Routing for Feeder Level Communication in a Smart Grid", In Proceedings of the 2nd International Conference on Energy-Efficient Computing and Networking (e-Energy), New York, USA, May 2011.

[2] Cheng-Min Lin; Hui-Kang Teng; Cheng-Chih Yang; Hwei-Li Weng; Ming-Cheng Chung; Chiu-Chiao Chung; , "A mesh network reliability analysis using reliability block diagram," Industrial Informatics (INDIN), 2010 8th IEEE International Conference on , vol., no., pp.975-979, 13-16 July 2010.

[3] Egeland, G.; Engelstad, P.; , "The availability and reliability of wireless multi-hop networks with stochastic link failures," Selected Areas in Communications, IEEE Journal on , vol.27, no.7, pp.1132-1146, September 2009.

[4] http://www.nist.gov/smartgrid/

[5] http://www.dlink.com/

[6] Hutchison, K.; Quigley, J.; Raza, M.; Walls, L.; "Empirical Bayes methodology for estimating equipment failure rates with application to power generation plants," Industrial Engineering and Engineering Management, 2008. IEEM 2008. IEEE International Conference on , vol., no., pp.1359-1364, 8-11 Dec. 2008.

[7] Koizumi, Y.; Yotsumoto, K.; "Power supply system reliability taking battery failure into account " Telecommunications Energy Conference, 1995. INTELEC '95., 17th International , vol., no., pp.53-58, 29 Oct-1 Nov 1995.

Hierarchical two-level Voltage Controller for Large Power Systems (Local Substation Level)

Hong Chun, *Member, IEEE*, Vaithianathan Venkatasubramanian, Javier Guerrero, Farrokh Habibi-Ashrafi and Armando Salazar.

I. Introduction

This document presents a two-level voltage controller for large power system emphasizing the local substation level. The local substation voltage controller is an automatic voltage controller which will automate the switching of discrete voltage control devices (shunt capacitor banks, shunt reactor banks and Under Tap Changers (ULTC) transformer banks. The substation Local Voltage Controller (SLVC) uses mostly local measurements at the substation with supervisory guidance from a central coordinator. The voltage references for substation voltage controllers will be determined by the central coordinator. The signals from central coordinator to local controllers are referred to as supervisory control signals (see Fig. 1) .The substation local controllers will do all internal control calculations mostly based on local PMU measurements along with possibly a few SCADA like measurements from control center as shown in (Fig. 1).

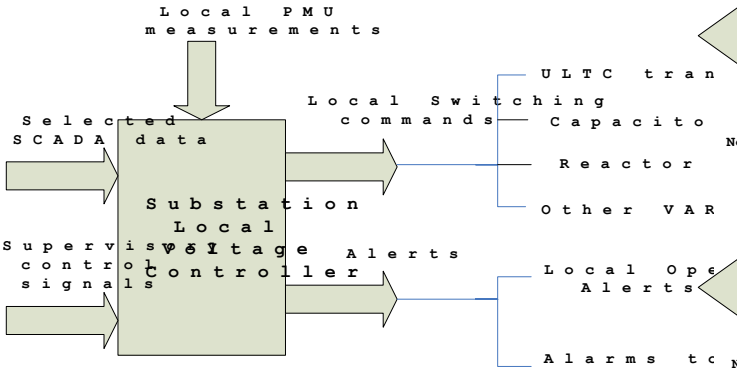

Fig.1 Substation Local Voltage Controller

II. Local Substation Voltage Controller (SLVC) Formulation

The primary responsibility of SLVC is to maintain the substation bus voltages close to specified voltage schedules. When all voltages are within acceptable tolerances, the controller will look into local VAR issues such as elimination of local circular VAR flows, maintenance of adequate VAR reserves at local SVC device as well as from local shunt VAR devices (see Fig. 2)

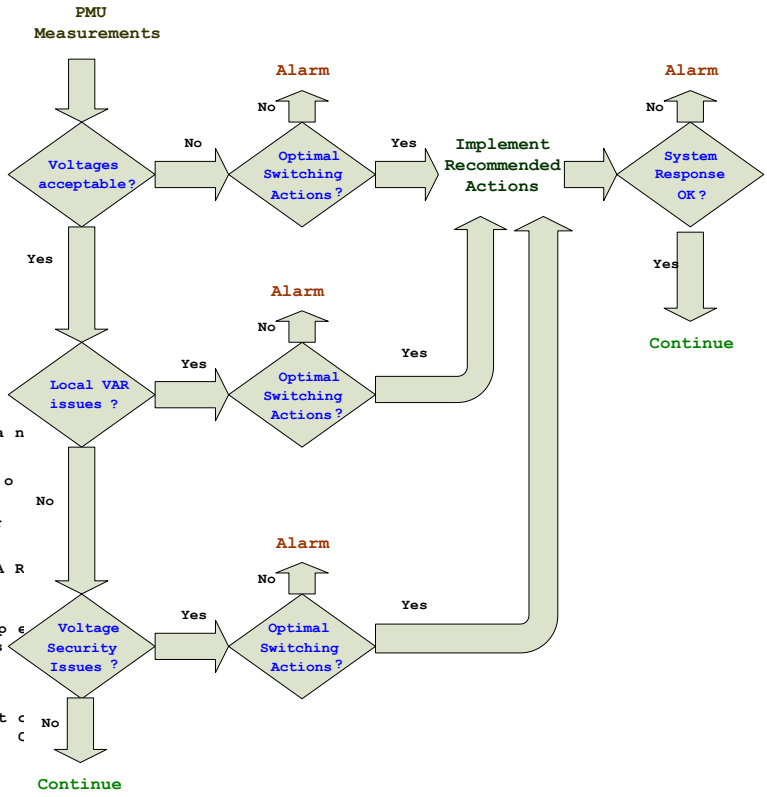

Fig.2 Overview of SLVC functions and flowchart

This work was supported in part by Southern California Edison Inc., Power System Engineering Research Center and US Department of Energy.

Mani V. Venkatasubramanian, Hong Chun and Javier Guerrero are with School of Electrical Engineering and Computer Science, Washington State University, Pullman, WA (email: mani@eecs.wsu.edu, hong.chun@email.su.edu, j.guerrerosedeno@email.wsu.edu).

Farrokh Habibi-Ashrafi and Armando Salazar are with Southern California Edison Inc., Los Angeles, CA.

III. References

[1] Vaithianathan "Mani" Venkatasubramanian, Hong Chun, Javier Guerrero, Farrokh Habibi-Ashrafi and Armando Salazar " Hierarchical two-level voltage controller for Southern California Edison," *IEEE PES GM 2012*, to be published.

Improved Harmonic Estimatation of Time-Varying Signals using RBFNN and ESPRIT

Sachin K. Jain and S. N. Singh
Department of Electrical Engineering, Indian Institute of Technology Kanpur, India
Email: *skjain@ieee.org*, *snsingh@iitk.ac.in*

***Abstract*—Future power system is expected to be dominated by the power electronics based components in generation, transmission and distribution sectors. The challenge in harmonic estimation of distorted power supply is increasing due to time-variation of the harmonics and interharmonics. Sliding-window concept has been applied on the existing techniques, e.g. short time Fourier transform (STFT), sliding-window estimation of signal parameters via rotational invariance technique (ESPRIT), etc. However, minimum window size is limited to 10 cycles or more due to accuracy and frequency resolution requirements. This poster paper presents a new approach to enhance the performance of the radial basis function neural network (RBFNN) that facilitates harmonic estimation of time-varying power supply signals with only half-cycle data sample size. The proposed method employs the high resolution ESPRIT to continuously update the free parameters of the RBFNN according to the varying input signal to provide more accurate and reliable estimates of harmonic amplitudes. New ESPRIT assisted online training scheme makes the RBFNN based harmonic estimation technique more versatile for stationary as well as time-varying power supply signals. The performance of the proposed method is investigated on the time-varying synthetic signal, which comprise of harmonics, interharmonics and white Gaussian noise of 26dB signal to noise ratio. A considerable improvement in the performance of the proposed method is observed and the mean total relative error reduces from 4% to 0.18%.**

I. Main Equations

The outputs of the three layer multiple outputs RBFNN can be defined as

$$y_k = \sum_{i=1}^{m} w_{ik} \cdot \Phi_i \tag{1}$$

where, Φ_i is the Gaussian radial basis function and w_{ik} is the connection weight between i^{th} hidden layer node to k^{th} output node. The total relative error E_T for K number of outputs with y_{dk} as the k^{th} desired output is defined as

$$E_T = \sum_{k=1}^{K} \left(\frac{y_{dk} - y_k}{y_{dk}} \right)^2 \tag{2}$$

II. Key Figures

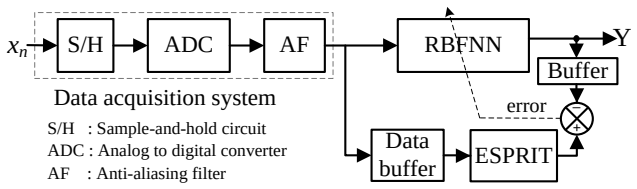

Fig. 1. Conceptual block diagram of the proposed method.

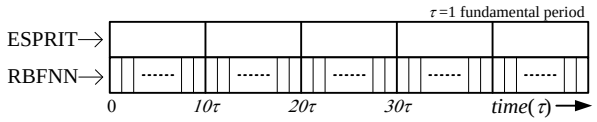

Fig. 2. Signal sampled data handling by two techniques.

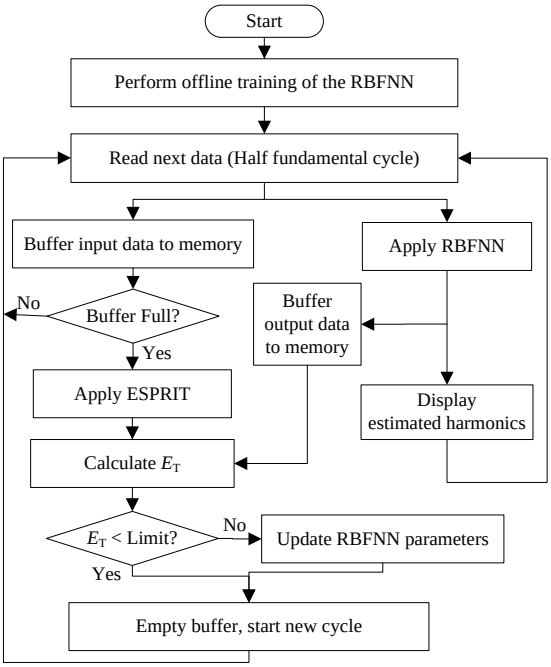

Fig. 3. Flowchart of the proposed method.

III. Important Results

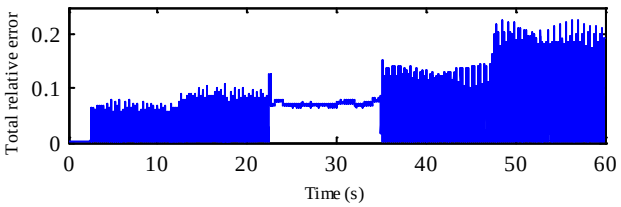

Fig. 4. The relative error for time-varying signal using RBFNN only.

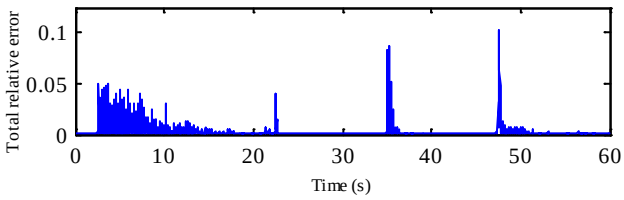

Fig. 5. The relative error with the proposed method.

Look-ahead Dispatch with Forecast Uncertianty and Infeasibility Mangagement

Yingzhong Gu, *Student Member, IEEE*, Le Xie, *Member, IEEE*
Department of Electrical and Computer Engineering, Texas A&M University, College Station, TX 77840, USA,
Email: *lxie@ece.tamu.edu*

***Abstract*— We propose a framework of look-ahead dispatch which considers forecast uncertainty and infeasibility management. Two major advantages of the framework have been demonstrated: 1) economic performance improvement under the presence of forecast uncertainty and 2) feasibility enhancement of the dispatch problem. In the look-ahead dispatch framework, Weighted Predictive Scheduling (WPS) technique is proposed to relieve the negative impacts on dispatch due to wind forecast uncertainty in future steps. Look-ahead Security Management (LSM) technique which could detect, quantify the potential infeasibility to the system scheduling problem in advance and work out optimal recovery plan is introduced. Finally, the proposed techniques are illustrated in a modified 24 Bus Reliability Test System.**

I. KEY EQUATIONS

A. Mathematical Formulation

The mathematical model of the look-ahead dispatch is presented as follows:

$$\max: f=\sum_{k=k_0}^{T}\sum_{i\in D}B_i\left(P_{Di}^k\right)-\sum_{k=k_0}^{T}\sum_{i\in G}C_i^G\left(P_{Gi}^k\right)+\sum_{i\in S}E_i^T\hat{\lambda}_i^T \quad (1)$$

The objective function (1) is to maximize the total social welfare (total customer benefits minus system operating costs). The problem is subject to various security constraints.

$$\sum_{i\in G}P_{Gi}^k=\sum_{i\in D}P_{D_i}^k \quad k=k_0,\cdots,T \quad (2)$$

$$E_i^{k-1}-E_i^k=\Delta t\cdot P_{Gi}^k \quad i\in S,k=k_0,\cdots,T \quad (3)$$

$$\left|\boldsymbol{F}^k\right|\le\boldsymbol{F}^{\max} \quad k=k_0,\cdots,T \quad (4)$$

$$\Delta t\left(P_{Gi}^k-P_{Gi}^{k-1}\right)\le P_i^{RMP} \quad i\in G,\ k=k_0,\cdots,T \quad (5)$$

$$E_i^{\min}\le E_i^k\le E_i^{\max},\ i\in S,\ k=k_0,\cdots,T \quad (6)$$

$$P_{Gi}^{\min}\le P_{Gi}^k\le P_{Gi}^{\max},\ k=k_0,\cdots,T \quad (7)$$

$$P_{Di}^{\min}\le P_{Di}^k\le P_{Di}^{\max},\ k=k_0,\cdots,T \quad (8)$$

In Weighted predictive scheduling formulation, all constraints from (2) to (8) are kept as the same. The objective function (1) is replaced with equation (9) with weight variables.

$$\max: \sum_{k=k_0}^{T}W_k\sum_{i\in D}B_i\left(P_{Di}^k\right)+\sum_{i\in S}W_TE_i^T\hat{\lambda}_i^T-\sum_{k=k_0}^{T}W_k\sum_{i\in G}C_i^G\left(P_{Gi}^k\right) \quad (9)$$

where W_k is the weight variables corresponding to benefit component over time step k.

II. KEY FIGURES

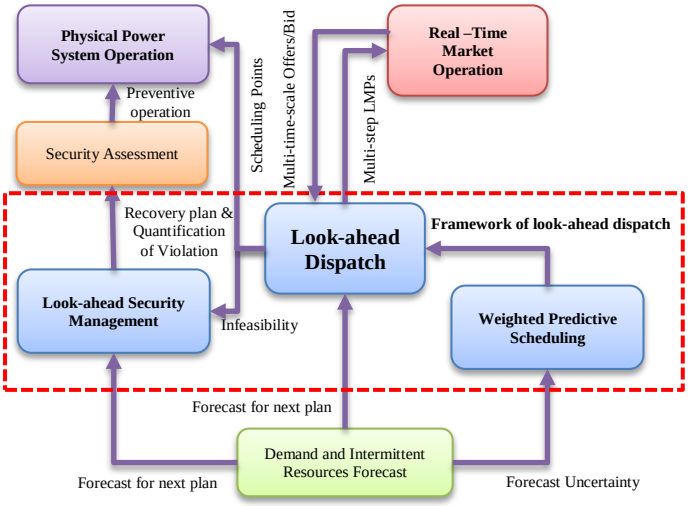

Fig. 1. Framework of look-ahead dispatch

III. KEY RESULTS

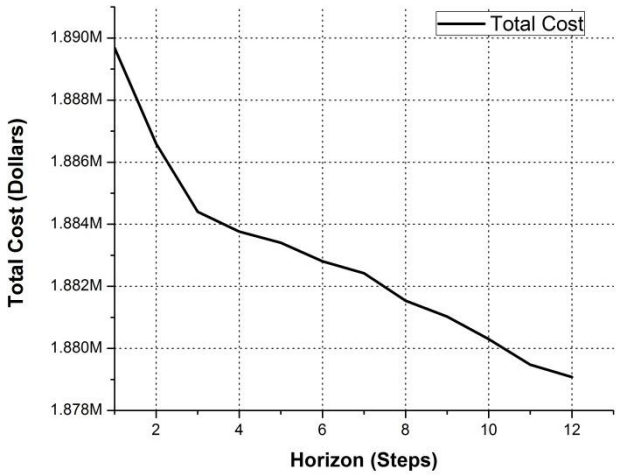

FIG. 2 TOTAL OPERATING COST OF DIFFERENT LOOK AHEAD HORIZON

Robust Corrective Transmission Switching Schemes for System Reliability

Akshay S. Korad, *Student Member, IEEE,* and Kory W. Hedman, *Member, IEEE*
School of Electrical, Computer, and Energy Engineering, Arizona State University, Tempe, AZ 85287, USA.
Email: akorad@asu.edu and Kory.Hedman@asu.edu

***Abstract*—The corrective transmission switching schemes are an essential part of grid operations. Traditionally, corrective transmission switching schemes are used to improve the reliability of the grid as well as the operational efficiency. Today, corrective transmission switching schemes are established based on the operator's past knowledge of the system as well as on some ad-hoc methods. The corrective transmission switching problem is a complex nonlinear, non-convex combinatorial network problem. These problems are very complex, they require long computational time, and they do not guarantee feasibility of the solution. Hence, real time corrective transmission switching is difficult to implement.**

The proposed robust corrective transmission switching scheme allows for the problem to be solved off-line since it guarantees the solution over multiple operating states (an uncertainty set). The proposed robust corrective transmission switching scheme will guarantee the feasibility of a solution and can be implemented in real time. The robust properties of the switching solution are obtained by constructing an uncertainty set around the system load. The solution is obtained such that it will work for all the load levels within the uncertainty set. This ensures that the switching action will work for various operating states. The complete corrective transmission switching problem is split into two parts: master problem and the sub-problem. The master problem is an Integer Problem (IP), which selects the switching action. The sub-problem is a Mixed Integer Problem (MIP), which evaluates the worst cast scenario of the particular topology. The solution is obtained by implementing a decomposition process between the master problem and the sub-problem. The resultant topology will be feasible for all the demand levels within the uncertainty set.

It should be noted that the proposed corrective action would also need to be confirmed with an AC power flow and stability models to ensure that the switching action is feasible.

I. KEY EQUATIONS

The basic mathematical model for corrective transmission switching for a fixed load, $\bar{d}$ is represented in (1)-(5).

$$\min_{x,y} \; C^T x + b^T y \tag{1}$$

$$\text{s.t.} \quad Fx \leq f, \; x \in \{0,1\} \tag{2}$$

$$Hy \leq h, \tag{3}$$

$$Ax + By \leq g, \tag{4}$$

$$I_u y = \bar{d}, \tag{5}$$

The presented formulation is a generic model with the objective as $C^T x + b^T y$. For this research, we investigate a feasibility problem where the objective is to find switching solutions in response to contingencies while not allowing any load shedding.

The two stage robust corrective switching formulation is given in (6)-(7). The objective function of two stage robust corrective switching formulation has two parts. The first part is a feasibility of transmission switching solution. The second part is worst case solution. The above corrective switching problem is solved by decomposing the problem into a master and sub-problem, which iteratively applies cuts to the master problem until optimality is achieved.

$$\min_{x} \left(C^T x + \max_{d \in \mathcal{D}} \; \min_{y \in \Omega(x,d)} b^T y \right) \tag{6}$$

$$\text{s.t.} \quad Fx \leq f, \; x \in \{0,1\} \tag{7}$$

where $\Omega(x,d) = \{y : Hy \leq h, \; Ax + By \leq g, \; I_u y = d, \; d \in \mathcal{D}\}$ is a set of feasible solutions for a fixed topology and demand d.

In (6), the $\max_{d \in \mathcal{D}} \min_{y \in \Omega(x,d)} b^T y$ part of problem can be combined together and the resultant problem is shown in (8)-(11).

$$R(x) = \max_{d,\varphi,\lambda,\eta} \; \lambda^T (Ax - g) - \varphi^T h + \eta^T d \tag{8}$$

$$\text{s.t.} \quad \lambda^T B - \varphi^T H + \eta^T I_u = b^T, \tag{9}$$

$$d \in \mathcal{D} \tag{10}$$

$$\lambda \geq 0, \varphi \geq 0, \eta \; free, \tag{11}$$

where $\varphi, \; \lambda$ and η are dual variables of constraints (3), (4) and, (5) respectively.

The above corrective switching problem is solved by decomposing the problem into a master and sub-problem which iteratively applies cuts to the master problem until the optimality is achieved. The resultant topology will be feasible for all the demand levels within the uncertainty set.

II. KEY FIGURES

The complete robust corrective switching scheme is presented in Fig. 1. The mathematical model presented above is a part of third block of Fig. 1.

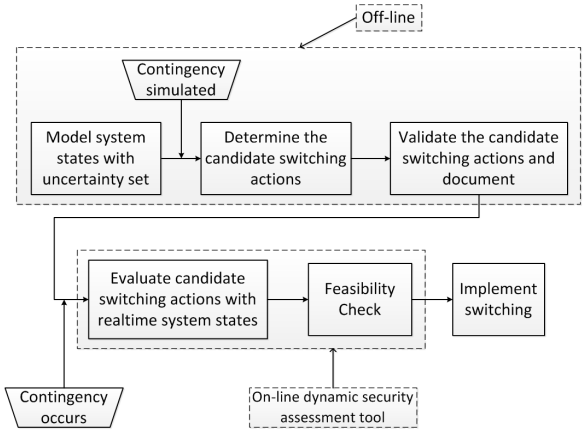

Fig. 1. Proposed robust corrective switching scheme.

Uncoordinated Charging Impacts of Electric Vehicles on Electric Distribution Grids: Normal and Fast Charging Comparison

E. Akhavan-Rezai, M. F. Shaaban, E. F. El-Saadany, A. Zidan
Department of Electrical and Computer Engineering, University of Waterloo
email: seakhava@uwaterloo.ca

***Abstract*-- Extra electrical loads due uncoordinated charging of electric vehicles have different impacts on the local distribution grid. This study proposes a method to evaluate the impacts of uncoordinated PEVs charging on the distribution grid during peak period. Two PEVs charging scenarios are studied, including normal and fast charging. The impact analysis is evaluated in terms of voltage, losses and line loading, which is implemented on a real distribution system in Canada. The results of the analysis indicate that there are significant impacts on distribution networks due to PEVs charging, which limits the accommodation of desired penetration levels of PEVs.**

I. Methodology

The grid performances are evaluated in terms of voltage, losses and line loading due to different PEVs penetration levels and normal/fast charging scenarios. The analysis starts with zero penetration of PEVs, and follows by increasing the PEVs penetration levels up to 30%. Consequently, the distribution grid performance is evaluated according to voltage violation and power losses, as well as, lines loading levels.

This process is applied to two different normal and fast charging scenarios to illustrate how different charging patterns might effect on system performance (see Fig. 1).

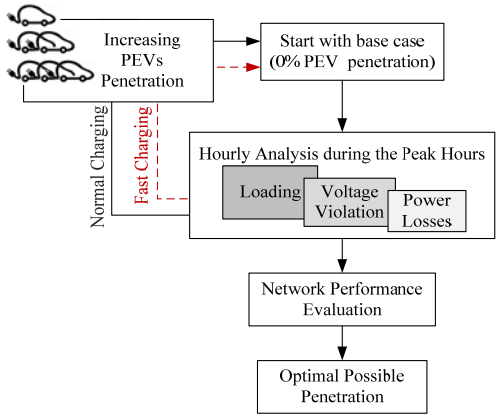

Fig. 1.Flowchart of the proposed method

II. Key Results

The proposed method is applied to a practical distribution system with a peak load of 16.18 MVA using Newton-Raphson load flow analysis. The analysis including two charging level scenario: 1st level (12A, 1.44 kW/h), and 2nd level (30A, 6 kW/h).The analysis considers the worst case of uncoordinated PEVs charging in peak demand only. Figs. 2 and 3 address the main results of the load flow analysis.

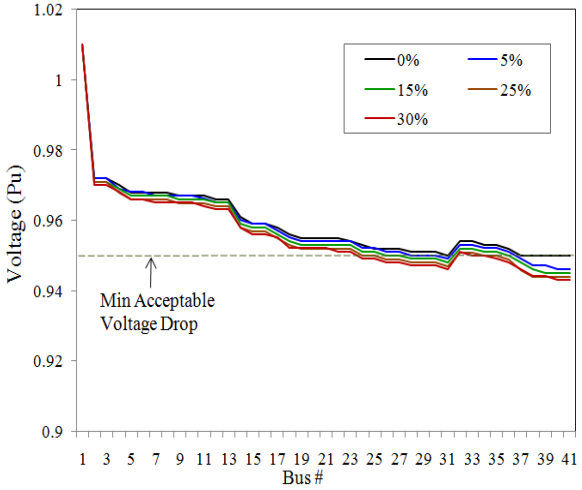

Fig. 2.Results of load flow analysis: Normal Charging Scenario

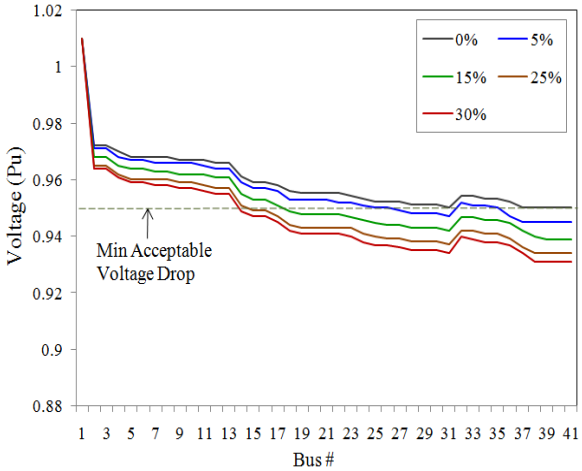

Fig. 3.Results of load flow analysis: Fast Charging Scenario

III. Conclusion

The results of the analysis illustrated that in high penetration of PEVs the uncoordinated charging violated system performance and it might not be applicable. The findings also highlighted the need for applying load management practices for residential PEV charging, to avoid excessive system stresses and losses.

Screening Algorithm for Event Detection in PMU Data

A. Allen, S.W. Sohn, S. Santoso, and W. Mack Grady
Department of Electrical and Computer Engineering, University of Texas at Austin, Austin, TX 78712, USA
Email: *aliciajallen@utexas.edu*

***Abstract*—This poster presents a screening algorithm for detecting power system events in PMU data and to illustrate the effectiveness of the algorithm through examples. The University of Texas at Austin has created a synchrophasor network to obtain real power system measurements for analysis, with measurements taken from single-phase, customer-level voltage (120 V). The network is continuously operating and recording voltage phasor data (magnitude, angle, and frequency) at 30 Hz. Because of the high volume of PMU data generated, an algorithm was created utilizing techniques to automatically screen for events. These techniques include the fast-Fourier transform, autoregressive Yule-Walker, Matrix-Pencil parameter estimates for damped sinusoids, and a simple technique to detect large swings in the data. The techniques are applied to a 10 second moving window of data. Peak amplitudes from each technique are saved. A possible event is detected based on statistical properties of peak amplitudes. An actual event is detected when two or more techniques detect possible events in the same window.**

To test the algorithm, PMU data from McDonald Observatory (West Texas) and UT-Austin (Central Texas), i.e., the McDonald frequency, UT-Austin frequency, and UT-Austin to McDonald voltage phase angle separation, are analyzed. At 23:33 UTC a generating unit tripped resulted in a loss of 810 MW of generation and a frequency decline to 59.8 Hz. The event was detected in both the frequencies and the voltage phase angle difference. The results from the algorithm applied to the voltage phase angle separation is in Fig. 1. All techniques detected the event. The PMU voltage phase angle during the event is in Fig. 2 and the PMU frequencies during the event are in Fig. 3.

A smaller disturbance was detected in the voltage phase angle difference and the McDonald frequency. The results from the algorithm applied to the McDonald frequency is in Fig. 4. A window of frequency data is in Fig. 5. The McDonald frequency (dotted line) contains damped oscillations that are not present in the UT-Austin frequency (solid line). The UT-Austin - McDonald PMU voltage phase angle for this series of events is in Fig. 6. The sudden change and return of the phase angle indicates multiple reclosing events. The examples presented here illustrate the effectiveness of the algorithm in detecting power system events.

I. Key Results

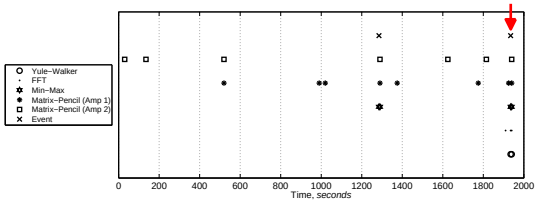

Fig. 1: Ex 1: Large disturbance detected in angle separation

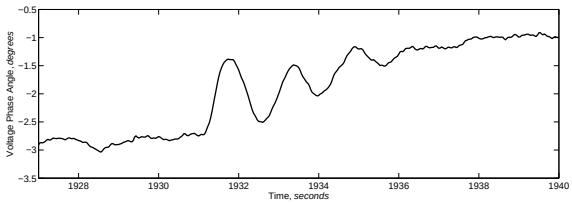

Fig. 2: Ex 1: Angle plot of the detected disturbance

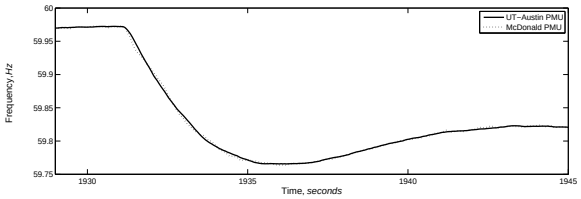

Fig. 3: Ex 1: Frequency plot of detected disturbance

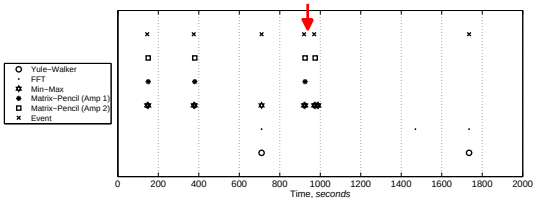

Fig. 4: Ex 2: Disturbance detected in McDonald frequency

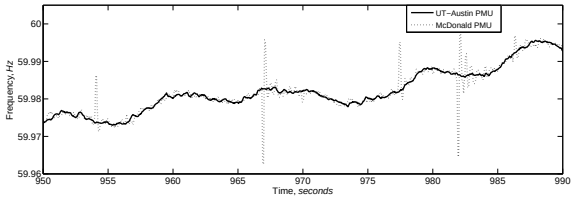

Fig. 5: Ex 2: Frequency plot of the disturbance

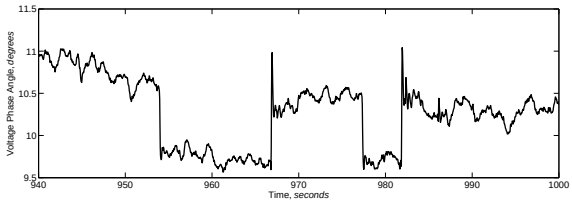

Fig. 6: Ex 2: Angle plot of disturbance

A Gaussian Mixture Model Based Prediction for Weather-Related Outages by EM Algorithm

Padmavathy Kankanala
Electrical and Computer Engineering
Kansas State University
Manhattan, KS 66502

Sanjoy Das
Electrical and Computer Engineering
Kansas State University
Manhattan, KS 66502

Anil Pahwa
Electrical and Computer Engineering
Kansas State University
Manhattan, KS 66502

***Abstract*— A Gaussian mixture models (GMMs) approach is presented for the prediction of weather-related outages in power distribution system. Outages in overhead distribution system caused by different environmental factors, such as weather, trees and animals significantly impact the reliability. Wind and lightning continue to be the major weather related causes of outages on overhead power distribution lines. The parameters of the GMMS are estimated by expectation-maximization (EM) algorithm. The drawback of EM for mixture fitting is the possibility of convergence toward a singular estimate at the boundary of the parameter space. A genetic algorithm (GA) and the EM algorithm (GA_EM) based approach which enables escaping from local optimal solutions is used. Results obtained are compared with observed outages to evaluate the performance of the model for estimating the outages. The results are also compared with previously studied regression, neural network and MFA models to determine an appropriate model to represent effects of wind and lightning on outages.**

Keywords- Gaussian Mixture Models, Power System Reliability, Power Distribution System, The Expectation-Maximization Algorithm, Weather Affects.

I. GAUSSIAN MIXTURE MODELS

Gaussian mixture models (GMMs) are among the most fundamental and widely used statistical models. GMMs are often used for probability density estimation in a variety of machine learning systems. The standard method used to estimate GMMs parameters to observed data optimally is the expectation-maximization (EM) algorithm, which converges to a maximum likelihood (ML) estimate of the mixture parameters. However, the EM algorithm for learning GMMs parameters has several drawbacks: It is a local method, thus sensitive to initialization; for certain types of mixtures, it may converge to the boundary of the parameter space leading to meaningless estimates. The EM algorithm is embedded in the framework of the GA in this research so that the properties of both algorithms are utilized.

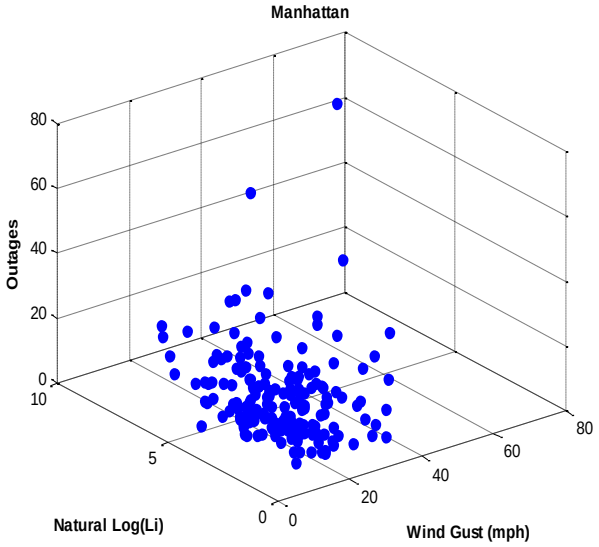

Fig. 1. 3d scatter plot of wind, natural log of lightning and outages for Manhattan

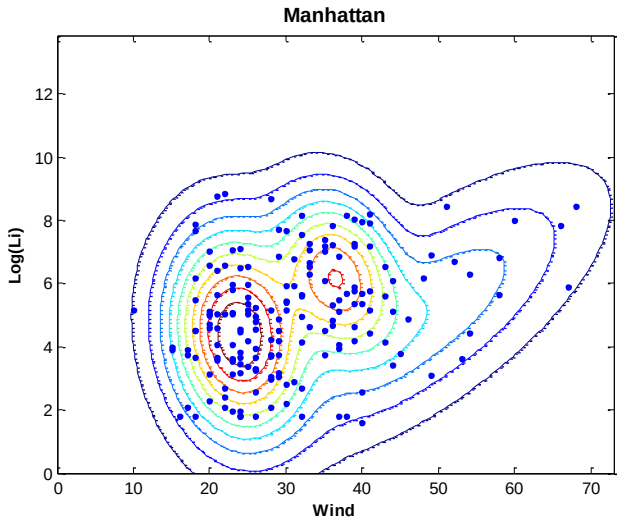

Fig. 2. Contour plot of probability of weather event occurring with three Gaussian mixtures for Manhattan area over the period of 2005-2009.

Stochastic Determination of PHEV Load Profiles with Recommendations for Charging Strategies

Maigha and Mariesa L.Crow
Department of Electrical and Computer Engineering,
Missouri University of Science and Technology, Rolla, MO 65401, USA
Email: *mmck6@mst.edu and crow@mst.edu*

Abstract **- Recent emphasis on transportation electrification, coupled with technological advancements and federal support has led to a new era in commercialization of Plug-in Hybrid Electric Vehicles (PHEVs). PHEVs are being proclaimed as low C-fingerprint, greener sources of energy with a huge potential for grid support (ancillary services, storage in Smart Grids, etc.). Given a high penetration of these vehicles, the impending question of grid health has surfaced in face of the present technological bottlenecks. A major concern is controlling the load or plug-in time of the vehicles which is almost entirely user/owner driven, unless an aggregator is granted centralized control. Charger-type, plug-in time, state of charge, time available before next trip, penetration level and time of use structures are few parameters that directly impact load due to PHEVs. We aim at studying the impacts of these parameters stochastically using Monte-Carlo simulation technique on a test system (California ISO) with driving cycles obtained from the National Household Travel Survey data (2009). Utility-Consumer cost analysis has been performed to gauge the effect of soaring peaks under different scenarios. The open end question of scheduling this variable load has also been addressed. The aim of this poster is to demonstrate the effect of the aforementioned key players on the daily load profiles in the presence of PHEV loads. Further, these results have been analyzed and interpreted to devise charging strategies to minimize these effects.**

HOUSE ID	END TIME	START TIME	VEHICLE ID	TRIP MILES	VEHICLE TYPE	MAX MILES	BATTERY SIZE	CALCULATED SOC	CHARGER TYPE	TIME OF CONNECTION
20000231	20.13	945	1	21	1	80	18	4.725	1	22
20000521	16.35	1330	1	10	1	30	11	3.666666667	2	18
20000521	21	1330	2	24	1	40	16	9.6	1	22
20002570	17.54	650	1	52	1	100	24	12.48	1	19
20002888	11	815	1	8	1	30	11	2.933333333	2	12
20004480	22.02	515	2	52	1	70	16	11.88571429	2	24
20004837	17.1	735	1	58	1	70	16	13.25714286	2	19
20004837	20.2	530	2	72	1	80	18	16.2	2	22
20006381	21.2	820	1	28	1	70	16	6.4	1	23
20006381	15.34	445	2	4	1	80	18	0.9	1	17
20007641	17.2	1556	2	5.11111	1	80	18	1.15	1	19
20008684	22	810	2	51	1	70	16	11.65714286	2	23
20010016	14.3	1020	1	31	1	80	18	6.975	1	16
20010016	20.45	2030	3	2.22222	1	40	16	0.888888889	1	22

Table 1.1 NHTS data and resultant driving cycles

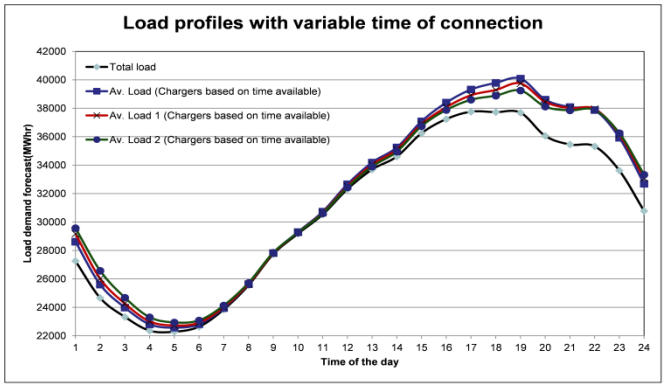

Figure 1.1 Variation of load profiles under various charging scenarios.

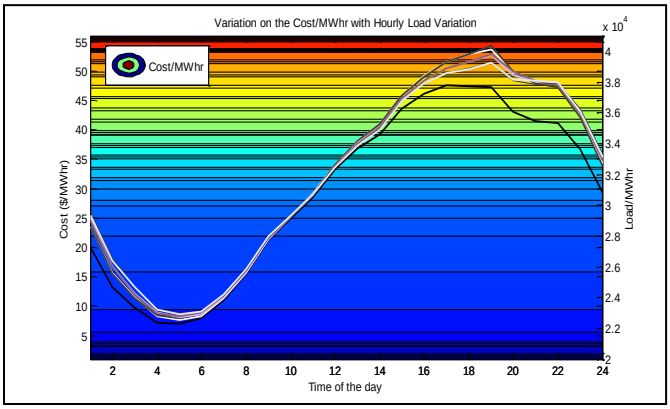

Fig 1.2 Variation in Cost/MWhr with hourly load variations under different charging scenarios.

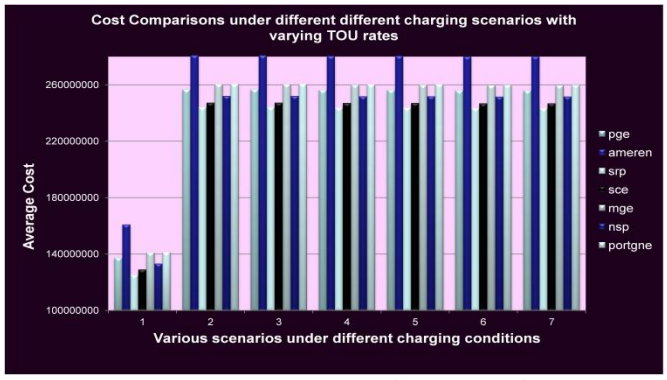

Figure 1.3 Cost comparisons under different Time–of-Use rate structures